UNIVERSITÀ DEGLI STUDI DI SALERNO

UNIVERSITÀ DEGLI STUDI DI SALERNO
Dipartimento di Farmacia

Ph.D. Program
in **Drug Discovery and Development**
XXXIV Cycle — Academic Year 2021/2022

Ph.D. Thesis in

Development of analytical strategies for phytochemical investigation of «superfoods», with particular attention to Botanicals.

Candidate

Ciro Cannavacciuolo

Supervisor

Prof. *Sonia Piacente*

Ph.D. Program Coordinator: Prof. *Gianluca Sbardella*

Table of contents

Introduction

The consumption of healthy foods is the focal point of the rising "culture of wellness and prevention". The increasing request for antioxidants, antimicrobials, natural sources of vitamins or dietary fatty acids that possess functional activities or nutritional properties stimulate the marketing diffusion of endearing and detailed labels suggesting the customers to purchase the products characterized by beneficial effects. The claim "superfoods" is used to emphasize the beneficial properties of foodstuffs due to both high content of essential nutrients and "phytochemicals", bioactive specialized plant metabolites. Moreover, the progress in food technology drives the wide diffusion on the globalized market of botanicals, preparations made from plants in the form of food supplements available in various formulations as juices, tablets and capsules. In this view, the interest to find new food sources with beneficial effects determines a large consumption of wellness-promoting products. The research for innovative and healthy foodstuffs allows a large exchange of products between continents to enhance species with a high functional profile but fallen into disuse in the daily diet, and species appreciated in traditional medicine or food habits of Oriental regions. Sometimes, plants employed in traditional diet or medicine are used for presumed benefits but few studies support the knowledge of chemical content and bioactivity profile.

The present research project is addressed to the investigation of species, currently used in European or foreign areas, to determine their chemical profile as a starting point for the definition of the bioactivity profile. In particular, attention has been paid to *Portulaca oleracea* L., *Raphanus sativus* L., *Abelmoschus esculentus* L. and *Garcinia mangostana* L.

Portulaca oleracea L., is a succulent plant wildly found as a weed in field crops and lawns. Commonly known as purslane, it is widely distributed around the globe

and is popular as a potherb in many areas of Europe, Asia, and the Mediterranean

region. This plant possesses mucilaginous substances which are of medicinal importance. Due to its environmental capacity to spontaneously reproduce in different conditions of climates, it is considered as "weed" by farmers. The plant was used as traditional food in Asian and Mediterranean diets. Actually, its use as food is considered only by a restricted group of consumers, despite the healthy properties reported for the species.[1] There is a growing interest in the reevaluation in horticulture of this spontaneous plant as a promising low-cost source of nutritional components as polyunsaturated fatty acids (PUFAs), vitamins and antioxidants.[2] Recently, farmhouses and restaurants promoting high-quality "slow food" are reproducing traditional dishes of the Mediterranean diet. Among other traditional products, they propose appertizers with in oil portulaca and dishes based on portulaca pesto and salads. The recovery of old-fashioned food habits is a promising success for the novel cuisine promoters and more and more restaurants of the traditional Mediterranean diet are offering reworked dishes mixing ingredients of the past and innovation.

The cotyledons of *Raphanus sativus* L., better known as daikon sprouts, are used in typical Asian dishes. Sprouts are a source of essential nutrients as vitamins,

minerals and dietary fibers but also antioxidants.[3] In addition to the high nutritional value, one of the main advantages is the easy production of sprouts in controlled conditions as the hydroponic cultivation technique. This crop production allows controlling the environmental features as nutritional feeding, temperature, humidity and light exposure to ensure the best growing conditions of the sprouts.

Daikon is one of the most used species in Asian food known by the name of "kaiware daikon"; it is eaten for the particular taste and crispy texture, in sushi rolls, salads and tempures. The increasing success of Asian restaurants in Occidental countries allowed the export of this species to the European market. The occurrence of polyphenols and glucosinolates reported for China, Japan and Korean varieties[4] is the starting point to evaluate the chemical profile and related bioactivity of the increasing production of Italian cultivar of sprouts.


Abelmoschus esculentus L. is a typical fruit of African countries, where it is commonly known as okra. It is considered the "fruit of long life" because of its natural occurrence of vitamins as ascorbic acid and organic acids. In traditional medicine, it is used to reduce blood glucose and in the case of nutritional deficiencies. Due to its large consumptions and benefits in the original tradition, it is imported in the European market. Several studies report the high nutritional values of the current species.[5] The interesting occurrence of antioxidants, essential nutrients and dietary fibers encourages its promising diffusion in the large globalized market.

Mangosteen fruit (*Garcinia mangostana* L.) is commonly called "the queen of fruits" in the tropical regions of Polynesia. It is a source of sugars, amino acids and bioactive secondary metabolites reported by extensively phytochemical and biological investigations.[6,7] Based on proven health benefits, it is used in several functional products available on market as juices, tablets, capsules and other nutraceutical formulations. The effects on human wellness are related both to qualitative and quantitative aspects. The occurrence of phytochemicals of mostly

brand products containing mangosteen, sold with the claim superfood, reflects the qualitative integrity. On the other hand, the quantitative aspects to prove the labeled benefits of the products are sometimes neglected. An analytical approach for the quantitative analysis of bioactive constituents in "eco-friendly" extracts and commercially available products could be useful for the quality control of several food products.

Some of the selected foodstuffs are not only extensively used in the local gastronomy of originary regions but also represent a good economic source in the globalized market. The high importance of these products is evident, considering the rising sales in the food industry of the products labeled as"superfoods". Export and import exchanges of food plants or fruits allow the diffusion in all the world of species with high benefits for the maintenance of healthy care and prevention.

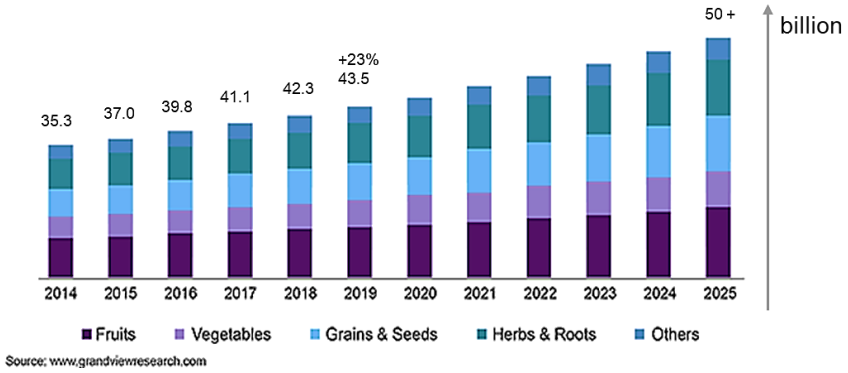

Even if the nutritive features of these products are well known, in some cases very little is known about their metabolome. A deeper insight on the chemical composition of selected food has the purpose to promote rural and agricultural activity, helping producers to obtain a premium price for their authentic products, and to guarantee to the customers the quality of products in terms of nutritional value and functional activity. In particular, the attention has been focused on products with different considerations and relevance in the food industry.

The edible parts of portulaca result in waste products for the farmers of the industrially cultivated fields. Its reevaluation as a food product could reduce the cost of treatments with herbicides, hard manual labor to eradicate it and polluting agricultural vehicles. In this view, it could represent a low-cost food plant for the companies.

Daikon sprouts are a consolidated economic source for the Asiatic food market and it could be a promising product in Occidental food production due to its easily controlling conditions and the rising widespread diffusion of Asian cuisine.

Okra fruit is overproduced in African countries but to date, it is diffusing on the global market. Along with primary products as cereals, corn, grains, pistachios, saffron and other spices peculiarly produced in Africa, the reevaluation of this product could strengthen the commercial exchanges of the continent.

Mangosteen is produced in tropical regions of Asia and Polynesia where it is a solid source for agricultural production. Its consumption in tablets and capsules or in energy drinks and juices is growing. To guarantee the correct information to the consumers, quality control of products is necessary.

The aim of the present Ph.D. project has been the definition of the metabolome of selected foodstuffs and related biological activity; particular attention has been paid to the study of products as potential sources of bioactive molecules, in order to highlight the occurrence of phytochemicals to use as functional ingredients in food products or for nutraceutical, herbal and cosmetic formulations.

Specifically, the objectives achieved during Ph.D. are the following:

- definition of the chemical profile of the different parts of the selected species *Portulaca oleracea* L., *Raphanus sativus* L., *Abelmoschus esculentus* L. and *Garcinia mangostana* L;
- development of methods for the qualitative and quantitative analysis of extracts obtained from the different parts of the selected plants;

- definition of the antioxidant activity and preliminary *in vitro* evaluation of the anti-inflammatory activity of phytocomplexes.

General experimental plan

Extraction of the selected parts of plant.

The specialized metabolism of plants, characterized by the expression of different enzymatic pathways in specific tissues, can be considered as a complex laboratory for the production of several bioactive molecules. In order to define the constituents of phytocomplexes, the chemical investigation of extracts obtained with solvents of different polarity in different conditions is required. The choice of a solvent is extremely important for the achievement of reliable results because it needs to be adequate for the target metabolites and the analytical method. For this reason, a specific extraction protocol has been developed for each plant raw material; in some cases, extraction procedures described by Official Pharmacopoeia have been used.

Analysis for chemical profiling

The extracts obtained from the different parts of the selected plants have been analyzed by high resolution techniques like liquid chromatography coupled to mass spectrometry (LC-HRMS) and NMR. Generally, an untargeted metabolomics approach is based on a preliminary LC-HRMS profile, a very useful tool in phytochemistry and food chemistry, allowing to determine in a single analysis a large number of different molecules. Along with the determination of retention time, the utilization of high-resolution fragmentation experiments is useful to obtain information about the structures of the compounds. In particular, LC coupled with electrospray multicollisional Ion trap (IT) mass spectrometry LC-ESI-

(LTQOrbitrap)MS^n, due to its capacity to rapidly separate, fragment and detect a broad range of small molecules, can be considered a powerful approach for structural characterization in metabolite fingerprinting. Spectrometer with an ion trap analyzer allows running experiments of tandem mass spectrometry and MS^n, increasing the number of information obtained by a single LC-MS experiment.

Moreover, the LC-HRMS profile drives the isolation procedures by carrying out sequential fractionating steps with the aid of different chromatographic semi-preparative techniques. High-pressure Liquid Chromatography (HPLC) is the main chromatographic tool for metabolite isolation. The separation of compounds in a complex mixture depends on the physical-chemical properties of the extracts and the compounds to isolate. With the aim to unambiguously characterize the compounds, structural determination of isolated compounds has been performed by the integration of data obtained by1D-(^{1}H and ^{13}C), 2D- NMR experiments, HRMS flow injection analysis of pure compounds and spectroscopic methods like CD, UV, IR. The NMR structural assignment of metabolites has been obtained by 1D-(^{1}H and ^{13}C) and 2D-NMR (DQF-COSY, HSQC, HMBC, TOCSY, ROESY).

In particular, the NMR structural assignment of plant metabolites has been carried out by acquiring scalar coupling homonuclear spectra (1D-TOCSY, 2D-TOCSY, COSY) for the determination of the molecule spin-systems, heteronuclear spectra (HSQC, HMBC) for the identification of the substitution pattern and for the assembly of the molecule moieties, dipolar coupling homonuclear spectra (NOESY, ROESY) for a further assessment of the substructures contained in the molecule and for the definition of the configurational orientations particularly in those cases with well-defined conformational properties.

In some cases, qualitative profiling of the extracts has been followed by quantitative analyses based on selective techniques. In particular, a mass spectrometry targeted approach by LC-ESI/QqQ/MS/MS by a very sensitive and selective mass tandem

experiment using Multiple Reaction Monitoring (MRM) scan type, or the "non-destructive" targeted approach by quantitative NMR.

Radical scavenging activity, in situ and in vitro assays for the evaluation of the biological activity of the phytocomplexes

Based on the chemical composition of the phytocomplexes, preliminary spectrophotometric assays to determine the antioxidant activity have been carried out. Therefore, the total phenolic content was determined at first, by performing the Folin-Ciocalteu assay. Successively, on the basis of the obtained results, radical scavenging activity was evaluated by performing $DPPH^{\bullet}$ and $ABTS^{\bullet+}$ assays. In line with previous studies in literature or traditional uses related to the species, the interaction with enzymatic targets was evaluated by biochemical assays such as alpha-glucosidase and acetylcholinesterase inhibition assays. As the final step aimed at evaluating cellular tolerance to the phytocomplexes, and the screening of the biological activity against several targets, the gene reporter assays were carried out to determine the transactivation activity of Nrf2 (Nuclear factor erythroid 2-related factor 2), NF-kB (Nuclear Factor kappa-light-chain-enhancer of activated B cells) and PPAR-ɣ (Peroxisome proliferator-activated receptor gamma).

References

1. Milad Iranshahya, Behjat Javadib, Mehrdad Iranshahia, Seyedeh Pardis Jahanbakhshc, Saman Mahyaric, Faezeh Vahdati Hassanid, Gholamreza Karimid. A review of traditional uses, phytochemistry and pharmacology of Portulaca oleracea L. *Journal of Ethnopharmacology*, 2017, **205**, 158–172

2. Zhou, Y-X., Xin, H-L., Rahman, K., Wang, S.J., Peng, C., and Zhang, H. *Portulaca oleracea* L.: A Review of Phytochemistry and Pharmacological Effects. *BioMed Research International*, 2014, **2015**, 1-11

3. Barillari, J., Cervellati, R., Paolini, M., Tatiboue, A., Rollin, P., and Iori, R. Isolation of 4-Methylthio-3-butenyl Glucosinolate from *Raphanus sativus* Sprouts (Kaiware Daikon) and Its Redox Properties. *J. Agric. Food Chem*., 2005, **53**, 9890-9896.

4. Takaya, Y., Kondo, Y., Furukawa, T., and Niwa, M. Antioxidant Constituents of Radish Sprout (Kaiware-daikon), *Raphanus sativus* L. *J. Agric. Food Chem.***,** 2003, ***51,*** 8061-8066.

5. H. Ying, H. Y. Jiang, H. Liu, F. J. Chen and Q. Z. Du, Ethyl acetate-n-butanol gradient solvent system for high-speed countercurrent chromatography to screen bioactive substances in okra, *J Chromatogr A*, 2014, **1359**, 117-123.

6. J. Wittenauer, S. Falk, U. Schweiggert-Weisz, R. Carle, Characterisation and quantification of xanthones from the aril and pericarp of mangosteens (*Garcinia mangostana* L.) and a mangosteen containing functional beverage by HPLC-DAD-MSn. *Food Chem*., 2012, **134**, 445-452.

7. D. Obolskiy, I. Pischel, N. Siriwatanametanon, M. Heinrich, Garcinia mangostana L.: A Phytochemical and Pharmacological Review, *Phytother. Res*., 2009, **23**, 1047-1065.

Chapter 1

Portulaca oleracea L. aerial parts: polar lipids and polyphenolic alkaloids with biological acivity

State of the art

Portulaca oleracea L. is an herbaceous annual plant with succulent edible parts. Leaves are obovate and dark green colored while reddish stems could reach 15 cm. Apical yellow flowers and capsuated seeds characterize the mature satage of growth. Commonly known as purslane, it is a warm-climate plant belonging to the Portulacaceae family. Its capacity of adaptation allows a wide distribution in the tropical and subtropical areas of the world including many parts of the United States, Asia and Australia. It is listed by the World Health Organization as one of the most used medicinal plants, and it has been given the term "Global Panacea".[1] In Traditional Chinese Medicine it is used as a "vegetable for long life" [2,3] for the wide range of pharmacological effects, including antibacterial, antiulcerogenic, anti-inflammatory, antioxidant, and wound-healing properties.[4] Despite the medicinal use, portulaca is particularly appreciated as food, added to soups and salads in the Mediterranean and tropical Asian countries.[5,8] It provides healthy benefits due to high content of essential nutrients and bioactive phytochemicals. In fact, it is rich in omega-3 fatty acids[5] usually occurring in fish oils but not normally found in plants. In addition, the content of vitamins is considerable in the leaves of this plant. It contains a high content of vitamin A which is a natural antioxidant playing an important role in vision, maintaining membranes and protecting against lung and oral cavity cancers. The plant also contains ascorbic acid, α- tocopherol, and B-complex vitamins, as niacin, pyridoxine, and riboflavin.[6] Furthermore, it is rich in minerals like phosphorus, manganese, iron, calcium, selenium[7], and the amino acids isoleucine, proline, leucine, lysine, phenylalanine, methionine, cystine, valine, threonine, thriptophan and tyrosine.[8]

Many specialized metabolites of *P. oleracea* have been isolated, including flavonoids, alkaloids and terpenoids. Among the main classes of metabolites, alkaloids including DOPA, dopamine, noradrenalin and cyclo-DOPA alkaloids (oleraceins A, B, C, D, and E) were isolated from this plant.[9]

Reports on *P. oleracea* focused the attention on Asiatic and North-African varieties; in order to achieve a deepest knowledge of the chemical composition of an Italian variety of *P. oleracea* harvested in Campania region, the edible parts, stems and leaves, were investigated to highlight differences in their chemical composition. The LC-HRMS profile of the methanol extract of both parts showed a large area of signals attributable to many classes of polar lipids (particularly abundant in stems) and other chromatographic peaks related to polyphenolic alkaloids (data not shown).

The following chapter describes the analysis of both polar lipids and polyphenolic alkaloids using different analytical approaches through multi-step chromatography and high-resolution techniques. Finally, *in situ* and *in vitro* tests provides the basis for further deep studies aimed at defining the bioactivity of this plant.

1.1 Multi-class complex polar lipids profiling by LC-ESI/LTQOrbitrap/MS/MS^n analysis and evaluation of their bioactivity

Overview on complex polar lipidst and purposes

The consolidation, typical of the new millennium, of personalized eating habits such as ideological nutrition, vegetarian diet, intolerances and other food necessities, suggests the need to propose innovative sources of essential nutrients. Polyunsaturated fatty acids (PUFAs) rightly fall into this category and it is well known that their daily intake in the diet is necessary for the maintenance of wellness. Omega-3 fatty acids play an important role in the enhancement of immune function[10], prevention and treatment of hypertension, coronary artery disease, cancer, and other inflammatory disorders.[11] They include α-linolenic acid and linoleic acid, which are essential for normal growth, health promotion, and disease prevention in humans. Usually, fish, vegetable oils or plant matrices such as seeds are considerable sources of PUFAs. Notwithstanding this, the use in the modern diet of food sources containing α-linolenic acid (ALA) is almost scant.[12] Furthermore, limited information on fatty acids and multiclass polar lipids from plant sources is available.[13,14]

In this view, *Portulaca oleracea* L. is a food studied for its content of lipids. Previous studies have reported in its leaves an amount of ALA five times higher than in spinach and lettuce[15], along with good content of long-chain PUFAs, eicosapentaenoic acid (EPA) (20:5, ω-3) and docosahexaenoic acid (DHA) (22:6, ω-3). Nevertheless, in literature there is no comprehensive report about the polar lipid composition of *P. oleracea* aerial parts whose diet intake is generally associated with significant biological activities.[16] Thereby, with the aim to fill this gap and to highlight any lipid differences between purslane leaves and stems, the analysis of both edible parts obtained from a wild Italian *P. oleracea* cultivar was carried out by using liquid chromatography coupled to electrospray ionization and

multiple-stage linear ion-trap and orbitrap high-resolution mass spectrometry (LC-ESI/LTQOrbitrap/MS/MSn). By considering mass spectrometric data, chromatographic behavior and literature data, this methodological approach allowed us to ascertain the occurrence in both purslane leaves and stems of different classes of complex polar lipids including glycolipids, phospholipids, oxylipins, and cerebrosides. Furthermore, considering several studies reporting anti-inflammatory activity for dietary sources containing the detected lipid classes[16,17,18], the evaluation of the ability of extracts and lipid-enriched fractions of purslane edible parts to influence the activity of the transcription factors NF-kB, Nrf2 and PPAR-ɣ has been carried out.

Multi-class complex polar lipids in vegetal cells

Polar lipids have a structural and functional role in the plant cells where they are involved in photosynthesis. Chloroplasts/plastids are the major sites for fatty acid synthesis in plant cells.[19] Defined as "complex" relating to the presence of heteroatoms, the polar lipids occurring in plants are classified on the basis of the behavior of the polar group (**Figure 1.1**).

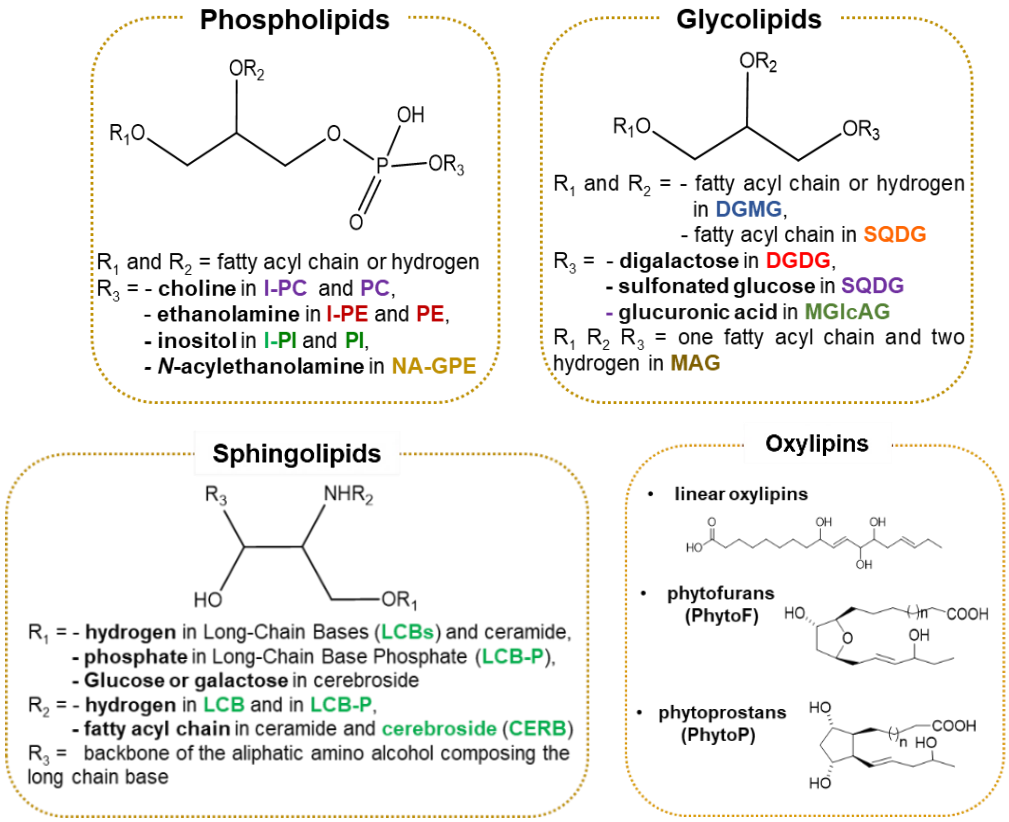

Figure 1.1 Complex polar lipids occurring in plants.

Legend: (**DGMG)**DiGalactosylMonoacylGlycerol; (**MGMG)**MonoGalactosylMonoacylGlycerol; (**DGDG**) DiGalactosilDiacylGlycerol; (**TGDG**) TriGalactosylDiacylGlycerol; (**MGlcDG**) MonoGlucuronosylDiacylGlycerol;; (**SQDG**) SulfoQuinovosylDiacylGlycerol; (**SQMG**) SulfoQinovosylMonoacylGlycerol; (**PI**) PhosfatidylInositol; (**PA**) Phosfatidic Acid(**PG**) PhosphatidylGlycerol

Biosynthesis of lipids in chloroplasts

Approximately 95% of fatty acids in the plant cell are produced by the plastidial fatty acid synthase (FAS). Mitochondria produce only minor amounts of fatty acids, mostly octanoic acid (8:0) as a precursor for lipoic acid, the cofactor for oxidative decarboxylation reactions. Chloroplast FAS enzymes belong to the type I FAS represented by individual polypeptides, as found in prokaryotes, in the pathway of de novo synthesis depicted in **Figure 1.2**.[19]

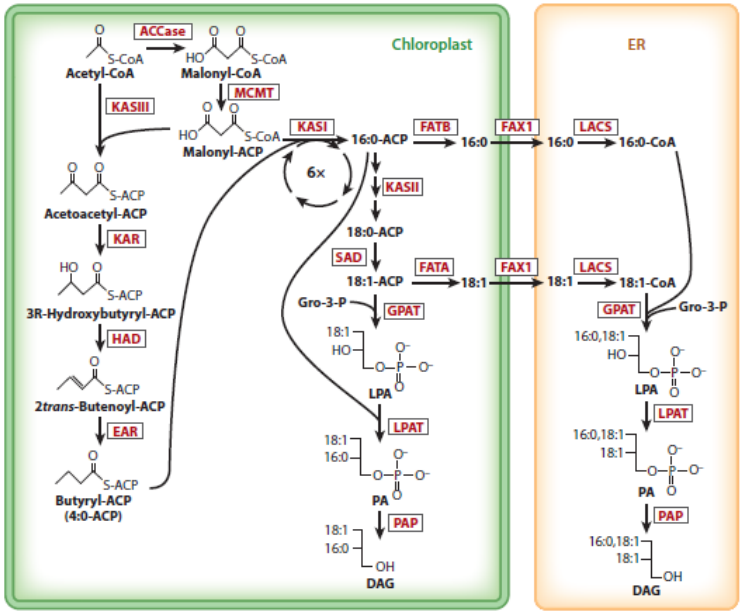

Figure 1.2 De novo synthesis of fatty acids and assembly of DAG backbone. Abbreviations: ACCase, acetyl–coenzyme A carboxylase; ACP, acyl carrier protein; CoA, coenzyme A; DAG, diacylglycerol; EAR, enoyl-ACP reductase; ER, endoplasmic reticulum; FATB, fatty acyl-ACP thioesterase B; FAX, fatty acid exporter; GPAT, glycerol-3-phosphate acyltransferase; Gro, glycerol; HAD, hydroxyacyl-ACP dehydratase; KAR, 3-ketoacyl–acyl carrier protein reductase; KAS, 3-ketoacyl–acyl carrier protein synthase; LACS, long-chain acyl–coenzyme A synthetase; LPA, lysophosphatidic acid; LPAT, lysophosphatidic acid acyltransferase; MCMT, malonyl–coenzyme A:acyl carrier protein malonyltransferase; PA, phosphatidic acid; PAP, phosphatidic acid phosphatase; SAD, stearoyl–acyl carrier protein d9 desaturase.

The depicted biosynthesis of building blocks phosphatidic acid (PA) and DAG occurre in both chloroplasts and the endoplasmic reticulum (**Figure 1.2**). In particular, fatty acids are exclusively derived from chloroplast FAS, while PA is produced both in chloroplasts and at the ER, depending on the plant species. The obtained scaffold is involved in the biosynthetic patway for the synthesis of galactolipid explained in **Figure 1.3**. Briefly, MGDG is produced in *Arabidopsis* by MGD1 via transfer of galactose from UDP-galactose onto DAG derived from the prokaryotic/plastidial (DAG-18:1,16:0) or eukaryotic/ER(DAG-18:2,18:2) pools. DGD1 converts MGDG and UDP-galactose into DGDG. Different plastidial desaturases (FAD5, FAD6, FAD7, and FAD8) introduce double bonds in MGDG and DGDG. A second pathway involving MGD2/MGD3 and DGD2 is mainly activated under phosphate deprivation. DGDG produced by DGD2 and to some extent by DGD1 is exported under phosphate deprivation to extraplastidial membranes.[19]

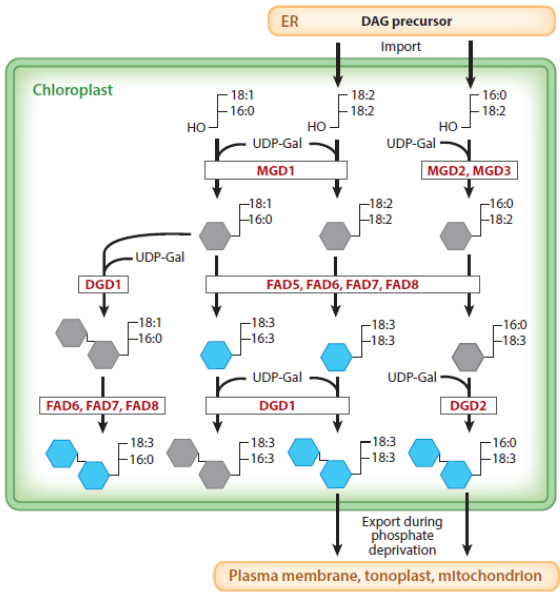

Figure 1.3 Synthesis of galactolipid. Abbreviations: DAG, diacylglycerol; DGD, digalactosyldiacylglycerol synthase; DGDG, digalactosyldiacylglycerol; ER, endoplasmic reticulum; FAD, fatty acid desaturase; Gal, galactose; MGD, monogalactosyldiacylglycerol synthase; MGDG, monogalactosyldiacylglycerol; UDP, uridine diphosphate.

The biosynthesis of SQDG is localized to the chloroplast and comprises several enzymatic steps. First of all, Glucose-1-phosphate is converted into UDP-glucose by a chloroplast UGPase (UGP3). Sulfite is attached to the C6 carbon of glucose by SQD1, and sulfoquinovose is transferred to DAG by SQD2. In the other pathway, the C6 of UDP-glucose (produced by an unknown UGPase different from UGP3) is oxidized to UDP-glucuronic acid by an unknown UGDH. Glucuronic acid is transferred to DAG by SQD2, resulting in the production of GlcADG. 18:1 group in SQDG and GlcADG are desaturated by FAD6, FAD7, and FAD8. DAG for SQDG synthesis can be derived from the prokaryotic pathway (as shown) or the eukaryotic pathway (16:0/18:2,18:2). Then, a galactose is transferred from one MGDG to another in a head group–disproportioning reaction catalyzed by GGGT/SRF2 giving rise to β,β-DGDG and DAG. Subsequent galactose transfer from another MGDG leads to the formation of β,β,β-TGDG. DAG is converted into TAG by an unknown acyltransferase. Acyl transfer via a disproportioning reaction between two MGDG molecules is catalyzed by AGAP1 to form acyl-MGDG. In Arabidopsis, the acyl group of acyl-MGDG can be oxidized to OPDA, giving rise to an arabidopside.[19]

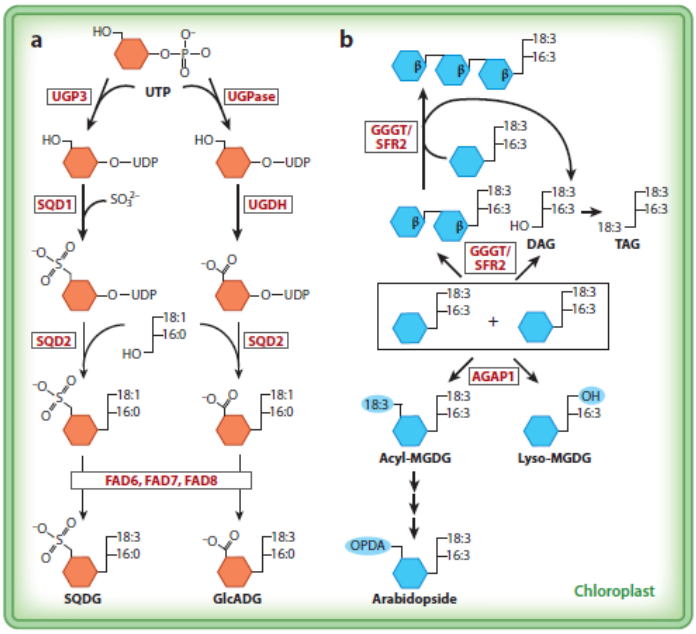

Figure 1.4 Sulfolipid, glucuronosyllipid, and acyl-galactolipid synthesis. Abbreviations: AGAP, acylated galactolipid associated phospholipase; DAG, diacylglycerol; DGDG, digalactosyldiacylglycerol; FAD, fatty acid desaturase; GGGT, galactolipid:galactolipid galactosyltransferase;GlcADG,glucuronosyldiacylglycerol;MGDG, monogalactosyldiacylglycerol; OPDA, 12-oxophytodienoic acid; SFR, sensitive to freezing; SQD1, UDP-sulfoquinovose synthase; SQD2, sulfoquinovosyldiacylglycerol synthase; SQDG, sulfoquinovosyldiacylglycerol; TAG, triacylglycerol; TGDG, trigalactosyldiacylglycerol; UDGH, uridine diphosphate–glucose dehydrogenase; UDP, uridine diphosphate; UGP, uridine diphosphate–glucose pyrophosphorylase; UTP, uridine triphosphate.

Phosphatidylglicerol (PG) is synthesized by the CDP-DAG (activated lipid backbone) pathway in the mitochondrion, ER, and chloroplast (**Figure 1.5**). Briefly, CDP-DAG is produced from PA and CTP by CDS. DAG is transferred onto glycerol-3-phosphate giving rise to PG after dephosphorylation. The trans double bond is introduced into sn2–16:0-PG by FAD4. FAD6, FAD7, and FAD8 convert 18:1 in PG into 18:2 and 18:3. PC is synthesized at the ER from DAG and the activated head group, CDP-choline, by AAPT. CDP-choline is derived from phosphocholine and CTP via the CCT reaction. Phosphocholine can be produced directly by phosphorylation of choline or by successive methylation of phosphoethanolamine. Double bonds are introduced into 18:1 of PC by FAD2 and FAD3. PC, lyso-PC, or PA might be transferred from the ER to the outer chloroplast envelope presumably via contact sites.[19]

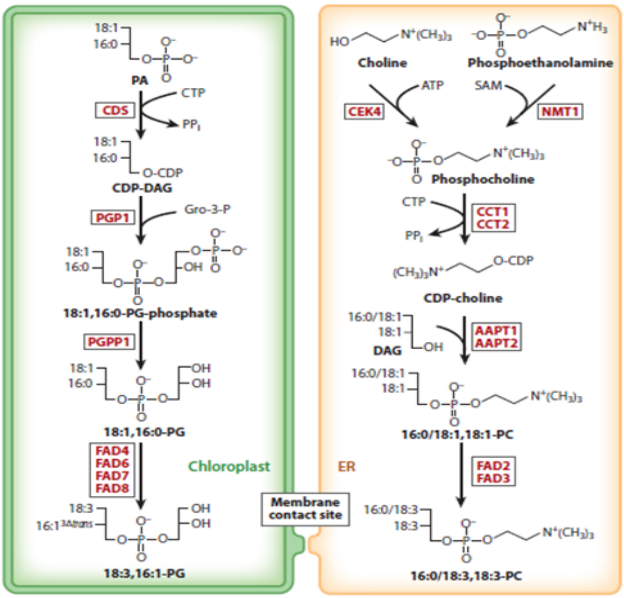

Figure 1.5 PC and PG synthesis. PG is synthesized in chloroplasts following the CDP-DAG pathway. Abbreviations: AAPT, cytidine diphosphate–aminoalcohol:diacylglycerol phosphoaminoalcohol transferase; CCT, cytidine triphosphate:phosphocholine cytidylyltransferase; CDP, cytidine diphosphate; CDS, cytidine diphosphate–diacylglycerol synthase; CEK, choline ethanolamine kinase; CTP, cytidine triphosphate; DAG, diacylglycerol; ER, endoplasmic reticulum; FAD, fatty acid desaturase; NMT, phosphoethanolamine N-methyltransferase; PA, phosphatidic acid; PC, phosphatidylcholine; PG, phosphatidylglycerol; PGP, phosphatidylglycerol-phosphate synthase; PGPP, phosphatidylglycerol–phosphate phosphatase; PPi, diphosphate; SAM, S-adenosyl-methionine.

Lipidomic approach through Mass Spectrometry

Lipid profiling using mass spectrometry is emerging as a strategy allowing the analysis of a broad range of lipid species in a single analysis. Multi-stage high-resolution mass spectrometry ($HRMS^n$) can provide detailed information about lipid composition rapidly and with a small amount of samples; extracts can be analyzed directly and effectively even without pre-separation of the lipids into classes. By using positive or negative electrospray ionization mode, each lipid compound provides singly charged molecular ion, most of the time sufficient on its own to allow unambiguous fatty acyl group identification. In fact, the carbon number/double bond combination is strictly indicative of the nature of fatty acids composing the molecules. When the definition of fatty acids is ambiguous, or lipid species of the same mass (i.e. isobaric species) are contemporary present in the sample, liquid chromatography coupled to tandem mass spectrometry (LC-MS/MS) analysis can be resolutive, since in product ion experiments the head-group can undergo the neutral loss of the common head-group unit or yield a common product ion, in both cases allowing to promptly identify the lipid class.

An example of the determination of lipid classes is the structural delucidation of Phospholipids. Lyso-Phosphatidylcholine (l-PCs) and Phosphatidylcholine (PCs) exhibited in MS/MS spectra acquired in positive ion mode a diagnostic base peak at *m/z* 184, ascribable to the phosphocholine ion, allowing an unambiguous identification of the class (**Figure 1.6**). Similarly, Phosphatidylethanolamines (PEs) showed in their fragmentation spectra in positive ion mode product ions deriving from the loss of the phosphoethanolamine head group (-141 Da) (**Figure 1.6**). Otherwise, Phosphatidylinositoles (PIs) were detected in negative ion mode and were unambiguously identified by the occurrence of two highly diagnostic product ions: the first one was observed at *m/z* 241, and was ascribable to the inositol phosphate ion generated by an initial loss of the sn-2 fatty acyl as ketene; the second

one was the product ion at *m/z* 153 originated by intramolecular cyclization of the glycerol moiety with phosphate, generating a dioxaphosphorinanol oxide moiety (**Figure 1.6**). In negative ion mode also Phosphatidylglicerols (PGs) were observed. This phospholipid class was featured by the occurrence of the typical product ion at *m/z* 171 ascribable to the phosphoglycerol ion, and by the presence in the tandem mass spectrum of product ions formed by neutral loss of 74 Da, corresponding to the dehydrated glycerol moiety (**Figure 1.6**). Once the phospholipid classes were assigned, the identification of the fatty acyl side chains was carried out. PCs, PEs and PGs showed in the MS/MS spectra product ions related to the diacylglycerol moiety, generated by the neutral loss of the head group, preliminarily suggesting a set of possible combinations of acyl side chains. For l-PCs, PCs and PEs the identity of the side chains was unequivocally assessed by the occurrence of the monoacylglycerol moieties, which allowed to determine their length and unsaturation degree. Differently, both PGs and PIs showed MS/MS spectra in which product ions related to monoacylglycerols were not detectable, while acyl side chains were detected as $[\text{fatty acid-H}]^-$ ions (**Figure 1.6**). Unfortunately, even if the achieved information allowed to certainly identify the phospholipid classes and the fatty acyl side chains, it was not possible to determine the sn-1 and sn-2 position on glycerol backbone, as well the unsaturation positions.

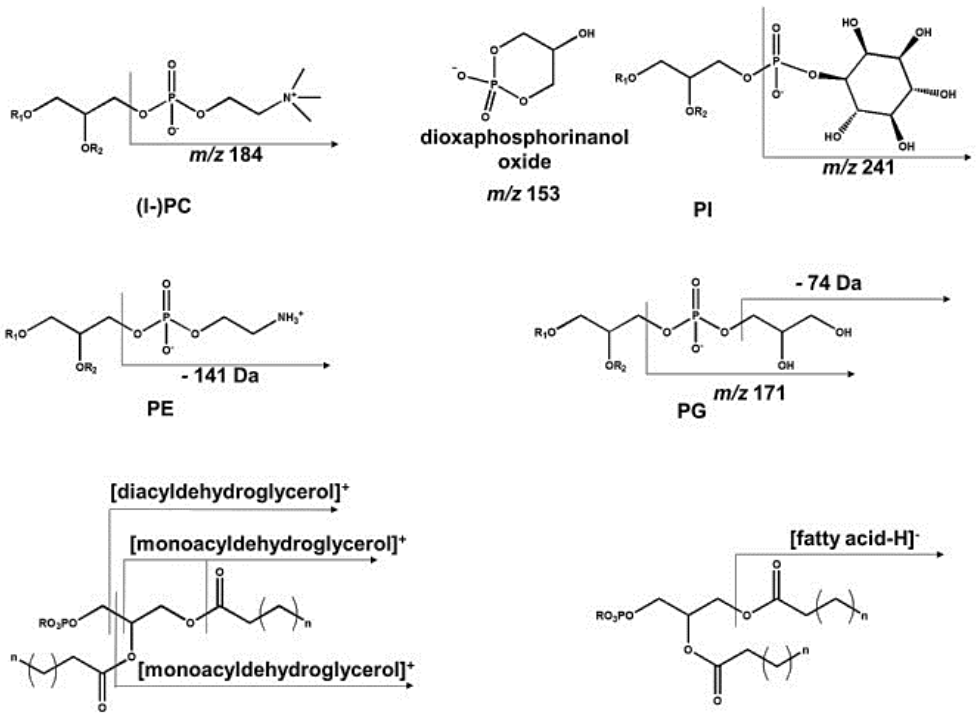

Figure 1.6 Fragmentations observed for pospholipids. R = polar head group. R_1/R_2 = fatty acids side chains, for phospholipids. R_1/R_2= H/fatty acid side chain or fatty acid side chain/H for lysophospholipids.

Each class of polar lipids such as glycolipids, oxylipins, cerebrosides are characterized by their diagnostic fragmentation pattern, as described to discriminate the different classes of phospholipids. The detailed analysis of multistage high-resolution mass spectrometry profile is useful to describe the structure of the different classes. The comparison of their molecular formulas, and the fragmentation patterns produced in LC-HRMS^n experiments with data contained in mass libraries and literature permitted us to putatively identify most of the peaks belonging to the different classes of lipids.

More and more studies describe the biological functions associated with polar lipids, so the interest in innovative sources of polar lipids is growing.

1.1.1 Experimental plan

In order to investigate the occurrence of polar lipids in *P. oleracea*, methanol extracts of both leaves and stems were analyzed by LC-ESI/LTQOrbitrap/MS/MS, using a RP-C18 column for the chromatographic separations. Considering the different class-depending ionization capacity of lipids to produce molecular anions and cations in ESI source, chromatographic profiles were obtained in negative and in positive ionization modes. According to their molecular formula, fragmentation pattern, chromatographic behavior and literature data, different classes of polar lipids could be detected in both *P. oleracea* edible parts, with stems showing a higher crowding of lipid compounds, above all in the final part of the chromatogram.

Thereby, with the aim to obtain lipid enriched fractions, both leaves and stems methanol extracts were submitted to fractionation on a Sep-Pak C-18 cartridge by using step gradients of increasing solvent strength to selectively elute and isolate lipids differing in polarity. In agreement with the LC-MS results acquired for MeOH-POL and MeOH-POS, enriched lipid fractions obtained by using 55% ACN and 100% ACN for the Sep-pak elution were selected to be analyzed by LC-ESI/HRMS/MS^n (**Figure 1.7**). In order to allow early elution and easy separation and detection of lipids occurring in both 100ACN-POL and 100ACN-POS, presumably containing high molecular weight compounds characterized by strong adsorption on RP-18 stationary phase, a RP-C4 column was used along with the RP-C18. This analytical approach allowed to confirm the occurrence in both leaves and stems of *P. oleracea* of polar lipids ranging from hydroxylated linear and cyclic fatty acids to complex polar lipids like glycolipids, phospholipids, and sphingolipids, varying for the nature and the number of the sugar unit and for the unsaturation degree and regiochemistry of acyl chains on *sn-1*/*sn*-2 position of glycerol backbone (**Tables 1.1-1.5**)

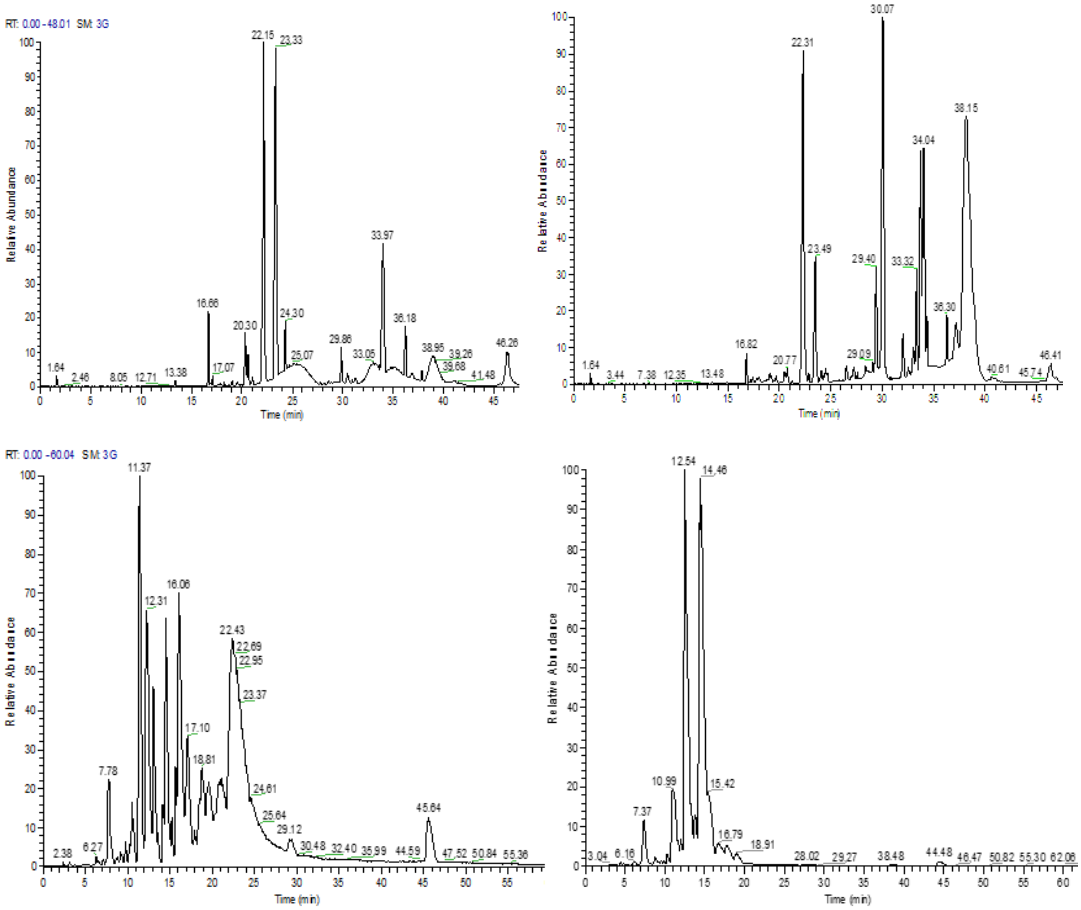

Figure 1.7 LC-HRMS profiles of 55ACN-POL and 55ACN-POS respectively using Luna C-18 column (on the top). LC-HRMS profiles of 100ACN-POL and 100ACN-POS respectively using Symmetry C-4 colum (on the bottom)

In vitro assays

Recently, several studies are reported about the biological activity of complex polar lipids.[16,17,18,41] The activation of Nrf2 (Nuclear factor erythroid 2-related factor 2), along with the inhibition of NF-kB (Nuclear Factor kappa-light-chain-enhancer of activated B cells) contributes to several beneficial bioactivities of natural products, including induction of increased cellular stress resistance and prevention or the resolution of inflammation.[41] With the aim to investigate preliminary the anti-inflammatory activity of the extracts and obtained lipid enriched fractions against different targets, the luciferase gene reporter assays were carried out. It is a sensitive, fast and consolidated *in vitro* assay that allows performing a parallel screening of a large set of samples on several targets. Moreover, the same assays allow the evaluation of both target activity and cell viability. Cell-based assay systems using reporter enzymes are used widely to study promoters, interactions between promoters and transcription factors, signal transduction, and other cellular activities. Among all the reporter genes, luciferases, enzymes that catalyze bioluminescence reactions, are used most frequently because their sensitivity and linear response range are superior to those of typical reporters, including β-galactosidase, chloramphenicol acetyltransferase, β-glucuronidase. The luciferase gene containing the target promoter region of interest in the plasmid is transfected into target cells, then luciferase-expressing cells are lysed and the amount of expressed luciferase protein can be estimated from the *in vitro* light intensity. Bioluminescence is a reaction that is triggered by the addition of luciferin solution and some cofactors, and the equipment for measuring light intensity uses a photomultiplier or a charge-coupled device (CCD) camera; thus, this assay can be applied to high-throughput screening (HTS). All applications of bioluminescence systems are based on the principle of a chemical reaction; that is, the light intensity as the measurable product depends on the amounts of luciferase, luciferin, and

cofactor(s). **Figure 1.8** demonstrates the luciferase reporter assay reported by Bronstein et al., 1996. Transfected cells are previously treated with a fluorescent probe Cell Tracker Green (CTG) to monitor membrane integrity all the experiment long. Then they are exposed to the samples, extracts, positive and vehicle controls, and after cellular lysis both fluorescence and luminescence were measured. Data are expressed as luminescence to fluorescence normalization to correlate the transactivation to the alive cell population. To exclude cytotoxicity, the fold level of fluorescence is 80%. If the fluorescence is less than 80%, the tested compound could be cytotoxic and its fold activation of the pathway is rejected.

The current work delined for the first time the biological activity of the methanol extracts and obtained lipid enriched fractions from edible parts of *P. oleracea* against three targets. In particular, NF-kB a transcription factor recognized as a target in the inflammation processes, Nrf2 a transcription factor promoting the expression of antioxidant proteins as Glutathione S-transferase (GST) and NAD(P)H quinone oxidoreductase 1 (NQO1), and the activation of nuclear receptor PPAR-ɣ involved in metabolic disorders.

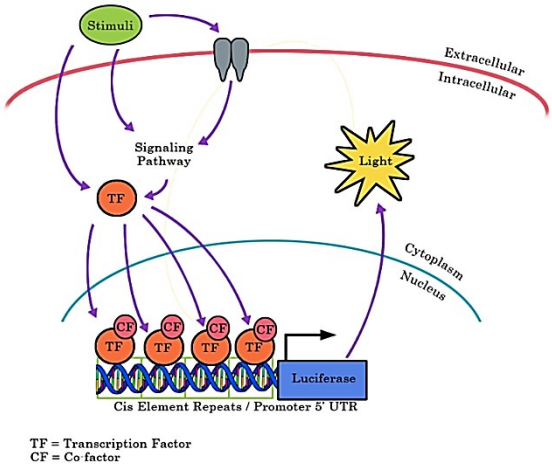

Figure 1.8 Model of *in vitro* luciferase reporter assay

1.1.2 Results and discussion

Characterization of multi-class complex polar lipids of P. oleracea edible parts

- *Glycerolipids*

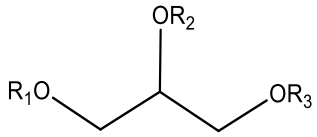

R1 and **R2** = fatty acyl chains in DGDG or hydrogen in DGMG, fatty acyl chains in SQDG; fatty acyl chains or hydrogen in MGlcDG and MGlcMG respectively.
R3 = digalactose in DGMG, sulfonated glucose in SQDG; glucuronic acid MGlcMG and MGlcDG.

The analysis of MS data in negative ionization mode and of chromatographic behavior concurred to identify in both 55ACN-POS and 55ACN-POL different classes of glycolipids, all showing the occurrence of a single fatty acid esterified to the glycerol unit and differing for the nature of the fatty acid and the sugar moiety linked to the *sn*-3 position of the glycerol unit. The presence in the tandem mass spectra of diagnostic product ions, originated by neutral loss of the variable fatty acid and referable to the glycerol unit linked to the sugar portion, allowed to putatively assign the identity of each glycolipid derivative (**Table 1.1**).[16] In particular, tri-, di-, and mono-galactosyl-monoacylglycerols (TGMG, DGMG, and MGMG, respectively) could be identified by the occurrence of the product ions at *m/z* 559, 397, and 253, corresponding to the trigalactosylglycerol and digalactosylglycerol mono-dehydrated units and to the monogalactosylglycerol unit, respectively (**Tables 1.1** and **1.2**, compounds **1**, **2**, **4**, **7**-**16**, **25**-**27**, **29**). The contemporary presence in the tandem mass spectrum of the $RCOO^-$ anion allowed to identify the fatty acid occurring in the glycolipid structure (with indications about the number of double bonds), in some cases attributable to an oxidized fatty acid (**Tables 1.1** and **1.2**). Moreover, a chromatographic trend showed the early elution of the glycolipids made up of oxidized fatty acids respect to the non-oxidized, and of glycolipids containing more sugar units with respect to those having fewer sugar units could be observed. Noteworthy, only 55ACN-POL showed the occurrence of

both ox-DGMGs and ox-MGMGs species. On the contrary, a good number of TGDG, DGDG, and MGDG species showing various degrees of oxidation of one of the two fatty acids esterified at *sn*-1/*sn*-2 positions of the glycerol unit were detectable in both 100ACN-POS and 100ACN-POL (**Table 1.2**; compounds **28**, **30-36**, **39-41**). Overall, in 55ACN-POS a lower number of MGMG and DGMG species could be detected than in 55ACN-POL (**Table 1.1**) while, on the contrary, some more DGDG species could be identified in 100ACN-POS if compared with 100ACN-POL (**Table 1.2**).

The observation of the class-diagnostic product ions at *m/z* 243 and 225 in the tandem mass spectra of compounds **3, 5, 6, 21, 23, 24, 44, 46, 48, 56, 59, 61, 65, 66, 69** and **74**, exhibiting a molecular formula containing a sulfur atom, allowed to identify the occurrence in 55ACN-POS/55ACN-POL and 100ACN-POS/100ACN-POL of sulfoquinovosylmono- and -diacylglycerols (SQMG and SQDG, respectively) (**Tables 1.1** and **1.2**), being the former fragment ion corresponding to the sulfoquinovose unit, and the latter derived from the cleavage of the glycerol-sugar ether linkage of SQMGs, resulting in the formation of an epoxydic bridge between carbon 1 and 2 of the sulfoquinovosylic ring.[16] Once again, the $RCOO^-$ anion accounted for the nature of the fatty acid unit (**Tables 1.1** and **1.2**), allowing to ascertain the occurrence of some ox-SQMG species in both 55ACN-POS and 55ACN-POL (**Table 1.1**, compounds **3**, **5**, and **6**). Finally, both in 55ACN-POS/55ACN-POL and in 100ACN-POS/100ACN-POL a good number of metabolites belonging to mono-glucuronosyl mono- and -diacylglycerols (MGlcMG and MGlcDG, respectively), plant lipid classes recently described, could be detected. They are characterized by the occurrence of glucuronic acid as a sugar unit and yield in tandem mass experiments a characteristic product ion at *m/z* 249, corresponding to the mono-glucuronosyl-glycerol mono-dehydrated anion formed by neutral loss of one or both the fatty acid units occurring in the lipid structure

(**Tables 1.1** and **1.2**; compounds **17-20**, **22**, **50**, **54**, **57**, **60**, **62**, **64**, **67**, **68**, **70**, 71, **73**, **75-77**).[20]

- *Phospholipids*

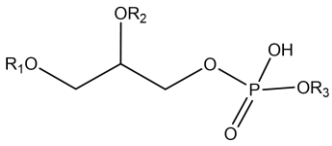

R1 and **R2** = fatty acyl chain or hydrogen in lyso- lipids.
R3 = choline in l-PC and PC, ethanolamine in l-PE and PE, inositol in l-PI and PI; glycerol in l-PG and PG

The analysis of MS data acquired for both 55ACN-POL/55ACN-POS and 100ACN-POL/100ACN/POS lipid enriched fractions allowed us to ascertain the occurrence in both *Portulaca* leaves and stems of metabolites belonging to the phospholipid class, in particular highlighting the occurrence of six different phospholipid subclasses (l-PA/PA, l-PI/PI, l-PE, l-PG/PG, l-PC, and g-l-PE), for which at least one of lyso- or diacylated form could be detected (**Table 1.3**).

The assignment of the detected phospholipid species to the corresponding class could be obtained by observing the occurrence in the relative tandem mass spectrum of class-diagnostic product ions attributable to the specific class-head group: the anion at *m/z* 153, corresponding to the mono-dehydrated form of glycerol phosphatidic acid and detectable in both ox-l-PA and in l-PA, the anion at *m/z* 241, corresponding to the phosphatidylinositol in mono-dehydrated form, the anion at *m/z* 196, corresponding to the mono-dehydrated form of the glycero-phosphatidylethanolamine, the anions at *m/z* 245 and 227, corresponding to the whole and the mono-dehydrated form of the glycerophosphatidylglycerol unit, respectively, and the cation at *m/z* 184, corresponding to the phosphatidylcholine unit (**Table 1.3**).[16] Moreover, the occurrence in negative tandem mass spectrum of product ions originated from the $[M-H]^-$ pseudomolecular ion by neutral loss of 205 Da, 162 Da and 120 Da, corresponding to an aziridine with a hexose unit (43 + 162 Da), to a mono-dehydrated hexose unit and to a fragment of the hexose unit,

respectively, gave information about the occurrence of lyso-form of phosphatidylethanolamine-N-glycoside (g-l-PE), namely a Schiff-PE, a phospholipid chemical class already reported in foods (**Table 1.3**, compounds **86** and **88**).[21] Furthermore, each negative tandem mass spectrum was characterized by the occurrence of one or two $RCOO^-$ fatty acid ions, depending on phospholipid or phospholipid lyso form, allowing to assign the number of double bonds, the oxidation degree and the length of the fatty acid occurring in the molecule (**Table 1.3**). This information was also inferable considering the product anions originated by neutral loss of one fatty acid, as whole or as ketene fatty acyl chain ($[(M-H)-R_xCOOH]^-$ and $[(M-H)-R_x{=}CO]^-$ ions, respectively), from the $[M-H]^-$ ion of the diacylated species (**Table 1.3**).[16] On the basis of MS data, it could be concluded that phospholipids were more represented in portulaca stems than in portulaca leaves. In particular oxidized l-PAs, detected only in 55ACN-POS, and the diacylated PAs species resulted in the most characterizing phospholipids for *portulaca* stems (**Table 1.3**).

- *Oxylipins*

The comparison with literature data of both chromatographic retention times and acquired MS data suggested the occurrence in both 55ACN-POL and 55ACN-POG of another polar lipid class, the oxylipins, i.e. bioactive lipid metabolites derived from the oxidative metabolism of essential PUFA, such as α-linolenic acid (ALA, 18:3ω-3) and linoleic acid (LA, 18:2ω-6). They are composed of fatty acids characterized by a different degree of hydroxylation and unsaturation, arranged in linear or cyclic form, such as in phytofuranes (PhytoF) and phytoprostanes (PhytoP) (**Table 1.4**), metabolites organized in various classes differing for the ring-type and for the structure of the two linear side chains, i.e. the a-chain (*vs* carboxy terminus) and the w-chain (*vs* methyl terminus).[16, 22, 23, 24]

Under tandem mass experiment conditions, the characteristic structural features of these compounds give rise to diagnostic product ions allowing their tentatively identification. So, for example, the occurrence in the relative negative tandem mass spectra of compounds **117** and **116** of diagnostic product ions at *m/z* 171 and 269, respectively, allowed to assign them as PhytoP regioisomers, respectively belonging to the 9 and 16 series of the F1t-PhytoP class (**Table 1.4**), sharing the same dihydroxylated prostanoid-ring and differing only for the position of the third hydroxyl group located, in the case of compound **116**, at C16 on the α-chain and, in the case of compound **117**, at C9 on the a-chain. According to the position of the hydroxyl group on the side chain, different diagnostic product ions can be formed *via* the common backbone fragmentation mechanism known as "a-hydroxy-b-ene-rearrangement", determining the a-cleavage of the bond adjacent to this hydroxyl group on the methyl side, in the case of **117**, and on the carboxyl side, in the case of **116** .[25] Moreover, the additional neutral loss from the product ion at *m/z* 269 of a water molecule or of the carboxyl group yielded the characteristic product ions at *m/z* 251 and 225, respectively (**Table 1.4**).

To the best of our knowledge, this class of polar lipids has been previously reported only in the seeds of *Portulaca* [26], apart from compounds **114**, **115** and **120**, here described for the first time in *Portulaca*. In particular, this analysis allowed to ascertain the occurrence of both linear and cyclic oxylipins in 55ACN-POL but not in 55ACN-POS, this latter in fact did not contain cyclic forms, apart for the 9-L1-PhytoP, **121** (**Table 1.4**).

- *Cerebrosides*

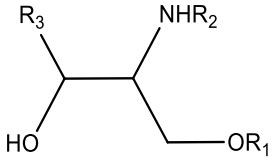

R1 = hydrogen in ceramide, glucose or galactose in cerebroside
R2 = fatty acyl chain in ceramide and cerebroside
R3 = backbone of the aliphatic amino alcohol composing the long chain base.

Finally, the analysis of the 100ACN-POS and 100ACN-POL allowed to highlight the occurrence of nine metabolites belonging to the class of sphingolipids, a ubiquitous class of lipids occurring in eukaryotes and bacteria, representing major components of biological membranes.[16] They are characterized by a considerable structural variation depending on the nature of both the long-chain base (LCB) – i.e. an aminoalcohol usually composed of 18 carbon atoms varying for hydroxylation and unsaturation degree and of the fatty acid, generally made up of 14-26 carbon atoms and usually hydroxylated at C-2, composing these molecules in the structural set-up typical of the so-called ceramides. The further glycosylation of the hydroxyl group located at C1 on the long-chain base with a hexose unit, usually glucose, determines then the formation of cerebrosides. The typical ceramides and cerebrosides fragmentation patterns obtained in negative $MSMS^n$ experiments allowed to determine both the length of the a-hydroxy fatty acid and the hydroxylation and unsaturation degree of the aminoalcohol, according to literature data (**Table 1.5**).[16,27]

So, for example, the occurrence in the MS^2 and MS^3 spectra generated by the cerebroside pseudomolecular anion deprived of the hexose as a mono-dehydrated unit, i.e. the $[(M-H)-162]^-$ ion, of product ions at *m/z* 271, 299, 327, and 355, along with those at *m/z* 270, 298, 326, and 354, corresponding to the $[R_xCOO]^-$ and $[R_xCONH]^-$ ions, respectively, gave information about the occurrence in the molecule of the 16:0h, 18:0h, 20:0h, and 22:0h hydroxyl-fatty acids, respectively (**Table 1.5**). Analogously, the type of long chain base composing the molecule

could be assigned by ascertaining the occurrence of both or at least one of the diagnostic product ions corresponding to the LCB anion as it is or in dehydrogenated form at *m/z* 314 and 312 for the t18:1 LCB, at *m/z* 316 and 314 for the t18:0 LCB, at *m/z* 298 and 296 for d18:1 LCB, and at *m/z* 300 and 298 for the d18:0 LCB, respectively (**Table 1.5**). According to literature data and with the previous nomenclature proposed for detected product ions, further information about the identity of both LCB and hydroxyl-fatty acid could be obtained by the occurrence in the fragmentation pattern of the P and V product ions, respectively, and by the occurrence of the U, T, S, W and X product ions, these latter formed by the fatty acyl chain linked to part of the LCB.[16,27] Noteworthy, unlike 100ACN-POL, 100ACN-POS highlighted the occurrence of all the detected ceramides and cerebrosides (**Table 1.5**).

Table 1.1 Glycolipids putatively identified in 55ACN-POS (stems) and 55ACN-POL (leaves)

n	Compound	R_t (min)	Molecular Formula	$[M-H]^-$	$[(M+FA)-H]^-$	Error (ppm)	Characteristic product ions	L	S
1	Ox-DGMG (18:3 1O)	24.10[a]	C_{33} H_{56} O_{15}	691.3525[a]	737.3580[a]	-1.46[a]	673, 415, 397, 293	+	-
2	Ox-DGMG (18:3-1O)	24.67[a]	C_{33} H_{56} O_{15}	691.3525[a]	737.3583[a]	-1.54[a]	673, 415, 397, 293	+	-
3	Ox-SQMG (18:3-1O)	26.41[b]	C_{27} H_{46} O_{12} S	593.2618[b]		-1.42[b]	299, 293, 225, 207	+	+
4	Ox-MGMG (18:3-1O)	26.77[a]	C_{27} H_{46} O_{10}	529.3003[a]	575.3055[a]	-0.82[a]	511, 293, 253	+	-
5	Ox-SQMG (18:3-1O)	27.24[a]	C_{27} H_{46} O_{12} S	593.2617[a]		-1.52[a]	299, 293, 225, 207	+	+
6	Ox-SQMG (18:3-1O)	27.54[a]	C_{27} H_{46} O_{12} S	593.2618[a]		-1.42[a]	299, 293, 225, 207	+	+
7	TGMG (18:3)	28.37[a]	C_{39} H_{66} O_{19}	837.4099[a]	883.4154[a]	-1.85[a]	577, 559, 415, 397	+	-
8	DGMG (18:3)	28.83[b]	C_{33} H_{56} O_{14}	675.3570[b]	721.3627[b]	-1.71[b]	415, 397, 277, 235	+	+
9	DGMG (18:3)	29.19[b]	C_{33} H_{56} O_{14}	675.3575[b]	721.3630[b]	-1.62[b]	415, 397, 277, 253, 235	+	+
10	DGMG (18:3)	29.81[b]	C_{33} H_{56} O_{14}	675.3578[b]	721.3630[b]	-1.25[b]	415, 397, 277, 253, 235	+	+
11	DGMG (18:2)	31.31[a]	C_{33} H_{58} O_{14}	677.3738[a]	723.3790[a]	-0.65[a]	415, 397, 279	+	-
12	DGMG (18:2)	31.98[a]	C_{33} H_{58} O_{14}	677.3738[a]	723.3790[a]	-0.74[a]	415, 397, 279	+	+
13	DGMG (16:0)	32.60[a]	C_{31} H_{58} O_{14}	653.3736[a]	699.3790[a]	-1.04[a]	415, 397, 255, 235	+	-
14	DGMG (16:0)	33.32[a]	C_{31} H_{58} O_{14}	653.3740[a]	699.3792[a]	-0.40[a]	415, 397, 255, 235	+	+
15	MGMG (18:3)	33.74[a]	C_{27} H_{46} O_9	513.3057[a]	559.3107[a]	-0.15[a]	333, 277, 253	+	+
16	DGMG (18:1)	34.30[a]	C_{33} H_{60} O_{14}	679.3892[a]	725.3946[a]	-1.14[a]	415, 397	+	-
17	MGlcMG (18:3)	34.35[a]	C_{27} H_{44} O_{10}	527.2844[a]		-1.35[a]	509, 277, 249	+	+
18	MGlcMG (18:2)	35.53[a]	C_{27} H_{46} O_{10}	529.3005[a]		-0.46[a]	511, 279, 267, 249	+	+
19	MGlcMG (18:2)	35.89[a]	C_{27} H_{46} O_{10}	529.3004[a]		-0.57[a]	511, 279, 267, 249	+	+
20	MGlcMG (18:2)	36.30[a]	C_{27} H_{46} O_{10}	529.3003[a]		-0.71[a]	511, 279, 267, 249	+	+
21	SQMG (18:3)	37.18[a]	C_{27} H_{46} O_{11} S	577.2671[a]		-1.07[a]	317, 299, 277, 243, 225, 207	+	+
22	MGlcMG (16:0)	37.82[b]	C_{25} H_{46} O_{10}	505.3000[b]		-1.33[b]	487, 267, 255, 249	+	+
23	SQMG (18:3)	38.15[a]	C_{27} H_{46} O_{11} S	577.2670[a]		-1.18[a]	317, 299, 277, 243, 225, 207	+	+

[a] calculated from LC-MS analysis of 55ACN-POL on Luna C-18 column in negative ion mode, [b] calculated from LC-MS analysis of 55ACN-POS on Luna C-18 column in negative ion mode. The 18-carbon oxidized acyl chain is abbreviated, e.g. as 18:3-1O, to indicate three double bonds equivalent and one oxygen atoms beyond the carbonyl group.

Table 1.2 Glycolipids putatively identified in 100ACN-POS e 100ACN-POL

n	Compound	R_t (min)	Molecular Formula	$[M-H]^-$	$[(M+FA)-H]^-$	Error (ppm)	Characteristic product ions	L	S
24	SQMG (16:0)	3.66[a]	$C_{25}H_{48}O_{11}S$	555.2829[a]		-0.83[a]	299, 255, 225	+	+
25	MGMG (18:2)	4.28[a]	$C_{27}H_{48}O_9$	515.3210[a]		-0.81[a]	279, 235	+	-
26	DGMG (18:0)	4.44[a]	$C_{33}H_{62}O_{14}$	681.4047[a]	727.4102[a]	-1.07[a]	415, 397, 283, 235	+	-
27	MGMG (16:0)	4.64[a]	$C_{25}H_{46}O_9$	491.3209[a]	537.3267[a]	-1.09[a]	255, 235	+	-
28	triOx-MGDG (18:3; 18:2-3O)	5.43[a]	$C_{45}H_{76}O_{13}$	823.5196[a]	869.5245[a]	-0.69[a]	563, 545, 513, 327, 309, 277, 253, 235	+	-
29	MGMG (18:0)	5.85[a]	$C_{27}H_{52}O_9$	519.3525[a]	565.3578[a]	-0.54[a]	283, 253	+	+
30	Ox-TGDG (18:3, 18:3-1O)	6.21[a]	$C_{57}H_{94}O_{21}$	1113.6195[a]	1159.6251[a]	-0.79[a]	835, 559, 397, 379	+	+
31	diOx-DGDG (18:3, 18:3-2O)	6.23[a]	$C_{51}H_{84}O_{17}$	967.5615[a]	1013.5671[a]	-0.99[a]	689, 675, 657, 415, 397, 309, 291, 277	+	+
32	diOx-MGDG (18:3; 18:3-2O)	6.58[a]	$C_{45}H_{74}O_{12}$	805.5100[a]	851.5140[a]	0.44[a]	545, 527, 309, 291, 277	+	+
33	Ox-DGDG (18:3; 18:3-1O)	7.42[a]	$C_{51}H_{84}O_{16}$	951.5673[a]	997.5720[a]	-0.32[a]	691, 673, 657, 415, 397, 379, 293, 277	+	+
34	diOx-DGDG (18:3, 18:2-2O)	7.74[a]	$C_{51}H_{84}O_{17}$	967.5619[a]	1013.5668[a]	-0.54[a]	689, 675, 415, 397, 309	+	+
35	Ox-DGDG (18:2; 18:3-1O)	8.36[a]	$C_{51}H_{86}O_{16}$	953.5815[a]	999.5868[a]	-1.82[a]	677, 673, 415, 397, 379, 279, 276	+	+
36	Ox-DGDG (18:3-1O; 16:0)	8.79[a]	$C_{49}H_{86}O_{16}$	929.5820[a]	975.5873[a]	-1.27[a]	911, 673, 653, 635, 415, 397, 293	+	+
37	TGDG (18:3; 18:3)	9.36[a]	$C_{57}H_{94}O_{20}$	1097.6233[a]	1143.6300[a]	-1.99[a]	837, 819, 559, 541, 415, 397; MS3 (819): 559, 541, 379	+	+
38	DGDG (16:3, 18:3)	9.52[a]	$C_{49}H_{80}O_{15}$	907.5401[a]	953.5456[a]	-1.37[a]	675, 657, 647, 629, 415, 397, 379, 277	+	+
39	Ox-MGDG (18:3; 18:3-1O)	10.33[b]	$C_{45}H_{74}O_{11}$	789.5139[b]	835.5200[b]	-1.04[b]	529, 513, 511, 293, 277	+	+
40	diOx-MGDG (18:3; 18:2-2O)	10.59[b]	$C_{45}H_{74}O_{12}$	805.5091[b]	851.5138[b]	-0.70[b]	527, 525, 293, 277	+	+
41	Ox-DGDG (18:0; 18:3-1O)	11.06[b]	$C_{51}H_{90}O_{16}$	957.6127[b]	1003.6182[b]	-1.92[b]	673, 663, 397, 379, 293, 283	+	+
42	DGDG (18:3; 18:3)	11.42[b]	$C_{51}H_{84}O_{15}$	935.5717[b]	981.5770[b]	-1.06[b]	675, 657, 415, 397, 379, 277	+	+
43	DGDG (18:2, 18:3)	12.08[a]	$C_{51}H_{86}O_{15}$	937.5876[a]	983.5923[a]	-0.69[a]	677, 675, 659, 657, 415, 397, 379, 279, 277	+	+
44	SQDG (16:0; 18:3)	12.54[a]	$C_{43}H_{76}O_{12}S$	815.4962[a]		-1.42[a]	559, 537, 277, 255, 243	+	-
45	DGDG (16:0; 18:3)	13.09[b]	$C_{49}H_{86}O_{15}$	913.5882[b]	959.5933[b]	-0.11[b]	675, 657, 653, 635, 415, 397, 379, 277, 255	+	+
46	SQDG (18:3; 18:1)	13.32[a]	$C_{45}H_{78}O_{12}S$	841.5107[a]		-2.71[a]	563, 559, 281, 277, 243	+	-
47	DGDG (18:1; 18:3)	13.56[b]	$C_{51}H_{88}O_{15}$	939.6021[b]	985.6074[b]	-2.02[b]	661, 657, 397, 379, 281, 277	+	+
48	SQDG (18:2; 16:0)	13.82[a]	$C_{43}H_{78}O_{12}S$	817.5108[a]		-2.72[a]	561, 537, 279, 255, 243	+	+
49	DGDG (18:2; 16:0)	14.24[b]	$C_{49}H_{88}O_{15}$	915.6026[b]	961.6089[b]	-1.47[b]	677, 659, 653, 635, 415, 397, 379, 279	-	+
50	MGlcDG (18:3; 18:3)	14.40[b]	$C_{45}H_{71}O_{11}$	787.4995[b]		0.46[b]	527, 509, 277, 249	+	+
51	MGDG (18:3; 18:3)	14.55[b]	$C_{45}H_{74}O_{10}$	773.5192[b]	819.5250[b]	-0.85[b]	513, 495, 277, 253, 235	+	+

52	DGDG (16:0, 16:0)	15.02[b]	$C_{47}H_{88}O_{15}$	891.6027[b]	937.6074[b]	-1.45[b]	653, 635, 415, 397, 379, 255	-	+
53	DGDG (18:3; 18:0)	15.28[b]	$C_{51}H_{90}O_{15}$	941.6182[b]	987.6233[b]	-1.45[b]	681, 675, 663, 657, 415, 397, 379, 283, 277	-	+
54	MGlcDG (18:2; 18:3)	15.75[b]	$C_{45}H_{74}O_{11}$	789.5147[b]		-0.11[b]	529, 527, 511, 509, 279, 277, 249	-	+
55	DGDG (16:0; 18:1)	15.85[b]	$C_{49}H_{90}O_{15}$	917.6179[b]	963.6229[b]	-1.83[b]	661, 635, 397, 379	-	+
56	SQDG (16:0; 16:0)	16.11[b]	$C_{41}H_{78}O_{12}S$	793.5123[b]		-0.88[b]	537, 299, 255, 225	+	+
57	MGlcDG (18:3; 18:2)	16.22[b]	$C_{45}H_{74}O_{11}$	789.5140[b]		-0.89[b]	529, 527, 511, 509, 279, 277, 249	+	+
58	MGDG (18:3; 16:0)	16.43[a]	$C_{43}H_{76}O_{10}$	751.5348[a]		-0.91[a]	513, 495, 491, 277, 255, 235	+	+
59	SQDG (18:0; 18:3)	16.48[b]	$C_{45}H_{80}O_{12}S$	843.5284[b]		-0.28[b]	565, 559, 283, 277	+	+
60	MGlcDG (18:3; 16:0)	16.50[a]	$C_{43}H_{74}O_{11}$	765.5140[a]		-0.91[a]	527, 509, 505, 487, 277, 255, 249	+	+
61	SQDG (16:0; 18:1)	17.10[b]	$C_{43}H_{80}O_{12}S$	819.5269[b]		-2.12[b]	563, 537, 281, 255, 243	+	+
62	MGlcDG (18:2; 18:2)	17.46[b]	$C_{45}H_{76}O_{11}$	791.5301[b]		-0.38[b]	529, 511, 279, 249	+	+
63	MGDG (18:2; 18:2)	17.88[b]	$C_{45}H_{78}O_{10}$	777.5504[b]	823.5551[b]	-0,91[b]	515, 279	+	+
64	MGlcDG (18:2; 18:2)	17.98[b]	$C_{45}H_{76}O_{11}$	791.5285[b]		-2.22[b]	529, 511, 279, 249	+	+
65	SQDG (18:1; 18:1)	18.13[b]	$C_{45}H_{82}O_{12}S$	845.5426[b]		-2.04[b]	563, 281	+	+
66	SQDG (18:0; 18:2)	18.28[b]	$C_{45}H_{82}O_{12}S$	845.5436[b]		-0.88[b]	565, 561, 283, 279	+	+
67	MGlcDG (18:2; 16:0)	18.81[b]	$C_{43}H_{76}O_{11}$	767.5302[b]		-0.23[b]	529, 511, 505, 487, 279, 255, 249	+	+
68	MGDG (18:1; 16:0)	19.22[b]	$C_{43}H_{78}O_{10}$	753.5519[b]	799.5554[b]	1.00[b]	515, 491, 279, 255	+	+
69	SQDG (18:0; 16:0)	19.64[b]	$C_{43}H_{82}O_{12}S$	821.5444[b]		0.06[b]	565, 537, 283, 255, 243	+	+
70	MGlcDG (18:2; 18:1)	19.79[b]	$C_{45}H_{78}O_{11}$	793.5459[b]		-0.18[b]	531, 529, 513, 511, 281, 279, 249	+	+
71	MGlcDG (16:0; 16:0)	20.41[b]	$C_{41}H_{76}O_{11}$	743.5305[b]		0.10[b]	505, 487, 255, 249	+	+
72	MGDG (18:3; 18:0)	20.45[a]	$C_{45}H_{80}O_{10}$	779.5661[a]		-0.87[a]	519, 513, 283, 277, 253, 235	+	+
73	MGlcDG (18:3; 18:0)	20.82[b]	$C_{45}H_{78}O_{11}$	793.5446[b]		-1.88[b]	533, 527, 515, 509, 283, 277, 249	+	+
74	SQDG (18:0; 18:1)	20.93[b]	$C_{45}H_{84}O_{12}S$	847.5598[b]		-0.27[b]	565, 563, 283, 281	+	+
75	MGlcDG (18:1; 16:0)	21.45[b]	$C_{43}H_{78}O_{11}$	769.5457[b]		-0.42[b]	531, 513, 505, 487, 281, 255, 249	+	+
76	MGlcDG (18:1; 18:1)	22.69[b]	$C_{45}H_{80}O_{11}$	795.5604[b]		-1.67[b]	531, 281, 249	+	+
77	MGlcDG (18:2; 18:0)	22.90[b]	$C_{45}H_{80}O_{11}$	795.5613[b]		-0.44[b]	533, 529, 515, 511, 283, 279, 249	+	+

[a] calculated from LC-MS analysis of 100ACN-POL on Symmetry C4 column in negative ion mode,[b] calculated from LC-MS analysis of 100ACN-POS on Symmetry C4 column in negative ion mode. The 18-carbon (or 16-carbon) oxidized acyl chain is abbreviated, e.g., as 18:3-1O and 18:3-2O, to indicate three double bonds equivalent and one or two oxygen atoms beyond the carbonyl group.

Table 1.3 Phospholipids putatively identified in edible parts of *Portulaca oleracea*

n	Compound	R_t (min)	Molecolar formula	$[M-H]^-$	$[(M+FA)-H]^-$	Error (ppm)	$[M+H]^+$	Characteristic product ions	L	S
Phospholipids in 55ACN-POS and 55ACN-POL										
78	l-PI (18:3 1O)	25.34 [a]	$C_{27}H_{47}O_{13}P$	609.2660 [a]		-1.65 [a]		429, 315, 293, 275, 241, 227	+	-
79	l-PI (18:2 1O)	27.29 [b]	$C_{27}H_{49}O_{13}P$	611.2819 [b]		-1.38 [b]		431, 333, 315, 295, 241	-	+
80	l-PA (18:3 1O)	27.76 [b]	$C_{21}H_{37}O_8P$	447.2135 [b]		-1.70 [b]		429, 293, 153	-	+
81	l-PI (18:2 1O)	28.06 [b]	$C_{27}H_{49}O_{13}P$	611.2819 [b]		-1.28 [b]		431, 315, 295, 277, 241	-	+
82	l-PA (18:3 1O)	28.58 [b]	$C_{21}H_{37}O_8P$	447.2133 [b]		-1.97 [b]		293, 153	-	+
83	l-PA (18:2 1O)	30.48 [b]	$C_{21}H_{39}O_8P$	449.2291 [b]		-1.74 [b]		295, 153	-	+
84	l-PE (18:3)	30.64 [a]	$C_{23}H_{42}O_7NP$	474.2609 [a]		-1.38 [a]		277, 196	+	+
85	l-PC (18:3)	30.79 [a]	$C_{26}H_{48}O_7NP$		562.3134 [a]	-0.93 [a]		502, 277	+	+
						-3.10 [c]	518.3225 [c]	500, 184		
86	g-l-PE (18:2)	30.94 [b]	$C_{29}H_{54}O_{12}NP$	638.3288 [b]		-1.86 [b]		620, 548, 518, 476, 433, 279, 214, 196	+	+
87	l-PA (18:2 1O)	31.25 [b]	$C_{21}H_{39}O_8P$	449.2291 [b]		-1.67 [b]		295, 153	-	+
88	g-l-PE (16:0)	32.22 [b]	$C_{27}H_{54}O_{12}NP$	614.3289 [b]		-1.74 [b]		524, 494, 452, 409, 255, 196	-	+
89	l-PE (18:2)	32.43 [b]	$C_{23}H_{44}O_7NP$	476.2763 [b]		-1.73 [b]		279, 196	+	+
90	l-PC (18:2)	32.29 [a]	$C_{26}H_{50}O_7NP$		564.3284 [a]	-2.17 [a]		504, 279	+	+
						-3.49 [c]	520.3379 [c]	502, 184		
91	l-PE (18:2)	32.65 [a]	$C_{23}H_{44}O_7NP$	476.2767 [a]		-0.98 [a]		279, 196	+	-
92	l-PC (18:2)	32.81 [a]	$C_{26}H_{50}O_7NP$		564.3289 [a]			504, 279	+	+
						-3.95 [c]	520.3377 [c]	502, 184		
93	l-PI (18:3)	33.01 [a]	$C_{27}H_{47}O_{12}P$	593.2715 [a]		-1.11 [a]		333, 315, 277, 241, 223	+	+
94	l-PE (16:0)	33.71 [b]	$C_{21}H_{44}O_7NP$	452.2766 [b]		-1.16 [b]		255, 196	+	+
95	l-PC (16:0)	33.96 [c]	$C_{24}H_{50}O_7NP$			-4.08 [c]	496.3377 [c]	478, 184	+	+
96	l-PI (18:3)	33.97 [b]	$C_{27}H_{47}O_{12}P$	593.2713 [b]		-1.41 [b]		413, 315, 277, 241, 223	+	+
97	l-PI (18:2)	36.74 [b]	$C_{27}H_{49}O_{12}P$	595.2867 [b]		-1.76 [b]		333, 315, 279, 241, 223	+	+
98	l-PI (18:2)	40.50 [b]	$C_{27}H_{49}O_{12}P$	595.2869 [b]		-1.54 [b]		415, 315, 279, 241, 223	-	+
99	l-PA (18:3)	41.07 [b]	$C_{21}H_{37}O_7P$	431.2186 [b]		-1.59 [b]		277, 171, 153	+	+
100	l-PI (18:2)	41.84 [b]	$C_{27}H_{49}O_{12}P$	595.2863 [b]		-2.46 [b]		415, 315, 279, 241, 223	-	+

Phospholipids in 100ACN-POS and 100ACN-POL								
101	l-PG (16:0)	4.46 [d]	$C_{22}H_{45}O_9P$	483.2706 [d]	-2.37 [d]	255, 227, 153	+	+
102	l-PA (18:2)	4.49 [e]	$C_{21}H_{39}O_7P$	433.2349 [e]	-0.17 [e]	153	+	+
103	l-PA (16:0)	5.39 [d]	$C_{19}H_{39}O_7P$	409.2344 [d]	-1.43 [d]	153	+	+
104	PI (16:0; 18:3)	11.62 [e]	$C_{43}H_{77}O_{13}P$	831.4998 [e]	-1.95 [e]	669, 593, 575, 571, 553, 391, 277, 255, 241	+	-
105	PG (18:3, 16:1)	14.05 [e]	$C_{40}H_{71}O_{10}P$	741.4693 [e]	-1.75 [e]	667, 505, 487, 481, 463, 277, 253, 245	+	-
106	PG (16:0; 16:1)	16.63 [e]	$C_{38}H_{73}O_{10}P$	719.4850 [e]	-1.07 [e]	483, 481, 465, 463, 391, 255, 253, 245, 227	+	+
107	PA (18:2; 18:3)	19.07 [d]	$C_{39}H_{67}O_8P$	693.4480 [d]	-1.42 [d]	433, 431, 415, 413, 279, 277	+	+
108	PG (16:1; 18:1)	19.48 [d]	$C_{40}H_{75}O_{10}P$	745.5004 [d]	-1.40 [d]	509, 491, 481, 463, 281, 253	+	+
109	PG (16:0; 16:0)	19.64 [d]	$C_{38}H_{75}O_{10}P$	721.5002 [d]	-1.71 [d]	483, 465, 391, 255	-	+
110	PA (18:3; 16:0)	20.36 [d]	$C_{37}H_{67}O_8P$	669.4482 [d]	-1.20 [d]	431, 413, 409, 391, 277, 255	+	+
111	PA (18:2; 18:2)	21.04 [d]	$C_{39}H_{69}O_8P$	695.4633 [d]	-1.89 [d]	433, 415, 279	-	+
112	PA (18:2; 16:0)	22.43 [d]	$C_{37}H_{69}O_8P$	671.4636 [d]	-1.51 [d]	433, 415, 409, 391, 279, 255	-	+
113	PA (18:2; 18:1)	24.14 [d]	$C_{39}H_{71}O_8P$	697.4791 [d]	-1.65 [d]	435, 433, 417, 415, 281, 279	-	+

[a]calculated from LC-MS analysis of 55ACN-POL on Luna C-18 column in negative ion mode, [b]calculated from LC-MS analysis of 55ACN-POS on Luna C-18 column in negative ion mode, [c]calculated from LC-MS analysis of 55ACN-POS on Luna C-18 column in positive ion mode, [d]calculated from LC-MS analysis of 100ACN-POS on Symmetry C4 column in negative ion mode, [e]calculated from LC-MS analysis of 100ACN-POL on Symmetry C4 column in negative ion mode

Table 1.4 Oxylipins putatively identified in 55ACN-POL and 55ACN-POS

n	Compound	R_t (min)	Molecular Formula	$[M-H]^-$	Error (ppm)	Characteristic product ions	POL	POS
112	ent16-9OH-Δ^{14}-10-PhytoF	19.64[a]	$C_{18}H_{32}O_6$	343.2115[a]	-0.16 [a]	325, 307, 289, 285, 209, 201, 199	+	-
113	ent16-13OH-Δ^{14}-9-PhytoF	19.84[a]	$C_{18}H_{32}O_6$	343.2113[a]	-0.63 [a]	325, 307, 289, 285, 257, 229, 201, 171	+	-
114	16-F1-PhytoP	20.15[a]	$C_{18}H_{32}O_5$	327.2166[a]	0.12 [a]	309, 291, 283, 269, 251, 225	+	-
115	9-F1-PhytoP	20.57[a]	$C_{18}H_{32}O_5$	327.2166[a]	-0.06 [a]	309, 291, 283, 273, 171	+	-
116	trihydroxy-octadecadienoic acid	22.15[b]	$C_{18}H_{32}O_5$	327.2170[b]	1.16 [b]	309, 291, 273, 229, 211, 183, 171	+	+
117	trihydroxy-octadecenoic acid	23.33[b]	$C_{18}H_{34}O_5$	329.2326[b]	1.06 [b]	311, 293, 275, 229, 211, 171	+	+
118	Dihydroxy-octadecadienoic acid	26.11[b]	$C_{18}H_{30}O_4$	309.2062[b]	0.47 [b]	291, 273, 251, 237, 171, 137, 97	+	+
119	9-L1-PhytoP	27.24[a]	$C_{18}H_{28}O_4$	307.1905[a]	0.24 [a]	289, 235, 197, 185	+	+

[a] calculated from LC-MS analysis of 55ACN-POL on Luna C-18 column in negative ion mode,
[b] calculated from LC-MS analysis of 55ACN-POS on Luna C-18 column in negative ion mode

Table 1.5 Ceramides and cerebrosides putatively identified in 100ACN-POS and 100ACN-POL

n	Compound	R_t (min)	Molecular formula	$[M-H]^-$	$[(M+FA)-H]^-$	Error (ppm)	Characteristic product ions	L	S
122	GlcCer (t18:1, 16:0h)	10.59 [a]	$C_{40}H_{77}O_{10}N$	730.5460 [a]	776.5513 [a]	-0.48 [a]	568, 550, 326, 271, 253, 225; MS3 (568): 326, 314, 271, 270, 253, 235, 225	+	+
123	GlcCer (t18:0, 16:0h)	11.11 [a]	$C_{40}H_{79}O_{10}N$	732.5615 [a]	778.5667 [a]	-0.77 [a]	570, 552, 326, 280, 271, 255; MS3 (570): 392, 326, 314, 272, 271, 254, 226	-	+
124	GlcCer (d18:1, 16:0 h)	12.31 [a]	$C_{40}H_{77}O_9N$	714.5512 [a]	760.5558 [a]	-0.43 [a]	552, 534, 271 MS3 (552): 534, 314, 298, 296, 280, 271, 270, 253, 225	+	+
125	GlcCer (d18:0, 16:0 h)	12.99 [a]	$C_{40}H_{79}O_9N$	716.5664 [a]	762.5722 [a]	-0.98 [a]	554, 536, 282, 271, 225; MS3 (554): 314, 300, 296, 271, 255, 239, 225	-	+
126	Cer (t18:1, 16:0 h)	13.72 [a]	$C_{34}H_{67}O_5N$	568.4930 [a]		-1.00 [a]	550, 326, 314, 312, 296, 271, 270, 255, 225	-	+
127	GlcCer (d18:1, 18:0 h)	14.29 [a]	$C_{42}H_{81}O_9N$	742.5822 [a]	786.6072 [a]	-0.74 [a]	580, 562, 299; MS3 (580): 323, 299, 298, 290, 281, 253	-	+
128	GlcCer (t18:1, 20:0 h)	14.66 [a]	$C_{44}H_{85}O_{10}N$	786.6080 [a]		-0.58 [a]	624, 606, 382, 327; MS3 (624): 382, 370, 327, 326, 311, 281	-	+
129	Cer (d18:1, 16:0 h)	16.63 [a]	$C_{34}H_{67}O_4N$	552.4976 [a]		-1.84 [a]	534, 326, 314, 312, 298, 296, 271, 270, 255, 253, 225	+	+
130	GlcCer (t18:1; 22:0 h)	17.51 [a]	$C_{46}H_{89}O_{10}N$	814.6390 [a]		-1.59 [a]	652, 634, 410, 355, 309; MS3 (652): 410, 398, 355, 354, 337, 314, 309, 304	-	+

[a] calculated from LC-MS analysis of 100ACN-POS on Symmetry C4 column in negative ion mode. The nomenclature used to name LCBs consists of a first letter that is "d" for dihydroxylated bases or "t" for trihydroxylated ones, followed of two numbers separated by a colon, indicating the number of carbons and double bonds. In GlcCer nomenclature, the 2-hydroxylated fatty acids are indicated by the letter "h" added to their lipid number (i.e., 16:0h).

1.1.3 *In vitro* evaluation of NF-kB, Nrf2 and PPAR-ɣ pathways assessed by reporter gene assays

NF-kB inhibition, Nrf2 and PPAR-ɣ activation by lipids enriched fractions obtained from P. oleracea methanol extracts

The chemical characterization of lipid-enriched fractions revealed the occurrence of several classes of polar lipids, some of which have been previously reported for their anti-inflammatory properties.[16] Therefore, methanol extracts and lipid-enriched fractions of *P. oleracea* leaves and stems were tested for modulation of pro- or anti-inflammatory pathways. In particular, their capacity to inhibit the TNF-α-stimulated NF-kB pathway together with the ability to activate the transcription factor Nrf2 and the nuclear receptor PPAR-ɣ were evaluated in reporter gene assays. Fixed concentrations (20, 10 and 5 µg/ml) of all samples were used in each assay. Results are shown in **Figure 1.9** panels **A-C**. Cell numbers after treatment with the tested extracts and fractions remained in a range of 80-95% of control cells, excluding major cytotoxic effects (data not shown). Regarding NF-kB, the lipid fractions 55ACN-POL, 100ACN-POL and 100ACN-POS (red box of **Figure 1.9A**) showed a concentration-dependent reduction of NF-kB signaling with a reduction by about 30-40% at a concentration of 20 µg/ml. The positive control parthenolide (10 µM) led to a 70% inhibition of the NF-kB-dependent luminescence.

Figure 1.9B depicts the data obtained from the Nrf2 (ARE)-dependent reporter gene assay. The lipid fractions 100ACN-POL and 100ACN-POS (red boxes) elicited a concentration-dependent induction of Nrf2 activity and were at 20 µg/ml more active (7- and 12-fold activation compared to control cells, respectively) than the used positive control (iberin, 3µM; 5-fold activation).

Regarding PPAR-ɣ activation (**Figure 1.9C**), the lipid fraction from stems (100ACN-POS; red box) showed pronounced concentration-dependent activity and turned out to be as active (~ 4.5-fold activation) as pioglitazone (10 µM; used as

reference compound) at a concentration of 20 µg/ml, while the second lipid fraction from leaves (100ACN-POL) appeared to be moderately active with a 2.5 fold activation at the highest concentration tested.

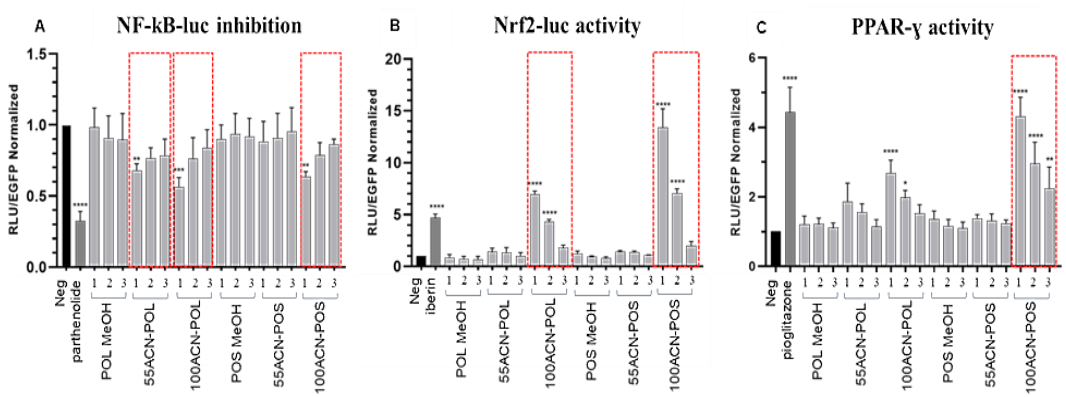

Figure. 1.9. Screening for biological activity of MeOH extracts and lipid-enriched fractions from purslane edible parts

Legend: concentrations of samples: (1) 20 µg/ml; (2) 10 µg/ml; (3) 5 µg/ml; (MeOH-POL) methanol extract of *P. oleracea* leaves; (MeOH-POS) methanol extract of *P.oleracea* stems, (55ACN-POL) lipid fraction 55%ACN of leaves; (55ACN-POS) lipid fraction 55%ACN of stems; (100ACN-POL) lipid fraction 100%ACN of leaves 100ACN-POS lipid fraction 100%ACN of stems.

(**A**) Inhibition of the NF-kB transactivation activity in TNF-α-stimulated HEK-293/NF-KB-luc cells; negative control: DMSO 0.1%; positive control: parthenolide (10 µM); samples were tested at three decreasing concentrations. TNF-α (2 ng/ml) was added after 1 h of pre-treatment with above samples.

(**B**) Activation of the Nrf2 pathway in HepG2-ARE/NRF2-luc cells; negative control: DMSO 0.1%; positive control: iberin (3 µM); samples were tested at three decreasing concentrations.

(**C**) Activation of PPAR-ɣ in HEK293 cells transfected with PPAR-ɣ and a respective luciferase reporter; negative control: DMSO 0.1%; positive control: pioglitazone (10 µM); samples were tested at three decreasing concentrations.

Data are expressed in relative units. Bar charts represents the transactivation activity expressed as mean ± SD of three independent experiments, n=3, ****p<0.0001 (One-way ANOVA with Dunnett's post hoc test vs vehicle control)

1.1.4 Conclusions

The analysis of stems and leaves of *Portulaca oleracea* by the described LC-HRMS/MS^n approach allowed to define the polar lipid profile of this plant, ascertaining the occurrence in both aerial parts of a large number of metabolites, ranging from low mass weight lipids, as linear and cyclic oxylipins, to more complex lipids, as glyco-, phospho- and sphingolipids. Furthermore, some differences in lipid pattern composition between the two analyzed plant parts were highlighted. In fact, albeit in both leaves and stems the glycolipids represented the major lipid components, ox-MGMG and ox-DGMG species were detectable only in 55ACN-POL fraction, and a higher number of MGMG and DGMG species could be appreciated in 55ACN-POL than in 55ACN-POS. On the contrary, 100ACN-POS highlighted a higher occurrence of DGDG species than 100ACN-POL, while the number of detectable oxidized galactolipids in diacylated forms was similar for both and significantly higher than for 55ACN-POL. Analogously, the SQDGs resulted to be more represented in 100% ACN lipid enriched fractions than in 55%, resulting in a number slightly higher in leaves than in stems of *portulaca*. Noteworthy, both parts of *portulaca* showed the occurrence of a good number, higher in 100% ACN lipid enriched fractions, of MGlcMG and MGlcDG species, metabolites belonging to a plant lipid class recently described in higher plants as soya bean leaves and *Arabidopsis* under phosphorus deprivation.[20] To the best of our knowledge, no data reports are available about the occurrence of this class of lipids in *P. oleracea* and other leafy plants. The biochemical pathway for their synthesis is related to phosphorous (P) deficiency conditions of the soil. Normal P level in the ground allows to the enzyme SQD2 to use UDP-SQ as a cofactor for SQDG synthesis, but in the case of P deficiency, the disruption of the SQD2 gene led to the de-regulation of lipid remodeling. In this condition, SQD2 catalyzes not only SQDG but also MGlcDG biosynthesis.[20]

From our analysis, the second more represented polar lipid class in *Portulaca oleracea* stem and leaves is represented by phospholipids, although also in this case some differences could be appreciated in the occurrence of the different phospholipid subclasses in the two plant parts. In fact, if in purslane leaves PAs, in their different forms, were numerically comparable to PIs, in portulaca stems lyso- and diacylated forms of PAs resulted in the most detectable phospholipid subclasses. Moreover, PAs and PIs were the only phospholipids occurring as oxidized-lyso-form species, although differently distributed among *portulaca* stems and leaves, with the ox-l-PA species occurring only in 55ACN-POS. 100ACN-POS fraction showed a higher number of PAs if compared to 100ACN-POL. An analogous trend could be appreciated for ceramides and cerebrosides, mainly detected in 100ACN-POS. On the contrary, oxylipins could be observed mainly in the leaves fractions, with the cyclic forms PhytoPs mainly detectable in 55ACN-POL, and PhytoFs not detectable in *portulaca* stems.

Especially 100ACN-POL and 100ACN-POS showed promising immunomodulatory potential in the performed reporter gene assays. Inhibition of NF-kB, one of the most prominent transcription factors in the regulation of pro-inflammatory gene transcription[28], was still rather moderate (with only 30% inhibition at 20 µg/ml). But the elicited activation of Nrf2, a transcription factor known for triggering cytoprotection against various stressful insults including inflammation[29], and of PPAR-γ, a ligand-dependent transcription factor involved in the regulation of metabolism and inflammation[30], was in the range of or even excelled the values obtained with the positive controls in these assays. Future work may need to focus on the identification of the responsible active principle(s) and their examination in more complex inflammatory test models.

Thus, this study supports a revalued use of portulaca in human nutrition as a source of bioactive polar lipids. Particularly interesting is the identification of glucuronosylglycerols, whose occurrence in higher plants was only recently

established. [20] Moreover, the ripe stems usually considered as waste for their bad appeal, reveal a higher occurrence of sphingolipids than leaves, suggesting possible alternative uses, e.g. as new matrices in skincare formulations with emollient activity. Also, the occurrence of PhytoP and PhytoF, already reported for immunomodulatory capacity[31], has been observed. Promising activity regarding interference with targets involved in inflammation has been highlighted, supporting the need to acquire deeper insights into the bioactivity profile of this plant characterized by a very rich and complex polar lipid profile.

1.2 Polyphenolic alkaloids profiling by LC-ESI/LTQOrbitrap/MS/MS^n, NMR analysis and evaluation of the bioactivity

Overview on polyphenolic alkaloids and purposes

P. oleracea is reported as a medicinal plant in the old manuscript "Le Panedette", a collection of medicinal plants used as fundamentals of the ancient "Schola Medica Salernitana". Over time, a large range of activities have been associated with this species and particular attention has been focused on neuroprotective capacity. Several preclinical trials highlighted the neuroprotective capacity of polar extracts of portulaca.[32,33] Along with polar lipids, the preliminary LC-HRMS profile of the methanol extract of the aerial parts revealed the occurrence of specialized metabolites belonging to the phenolic alkaloids class, peculiarly reported for the species with the name oleraceins. The cyclodopa structure could be related to the occurrence of soluble pigments, betacyanins, able to protect the plant from large exposure to sunlight.

Colored pigments in P. oleracea

Betalains are water-soluble pigments and include red betacyanins [5,6-dihydroxyindoline-2-carboxylic acid (i.e., cyclodopa) connected to betalamic acid, usually glucosylated] and yellow betaxanthins (amino acids connected to betalamic acid). Betalains are used as food colorants and demonstrate beneficial effects on human health, biological effects on the plant itself, and a distinct biosynthetic pathway. Similar to red betacyanins, the yellow water-soluble oleraceins which were discovered in *P. oleracea*[34], contain 5,6-dihydroxyindoline-2-carboxylic acid moieties and are acylated with p-coumaric or ferulic acid. Thus, indoline amide glucosides, along with red betacyanins, are important specialized metabolites of *P. oleracea*.

*Biosynthetic pathway for betalain pigment*s

The biosynthetic pathway consists of several enzymatic reaction steps and spontaneous chemical reaction steps (**Figure 1.10**). DOPA formation is catalyzed by tyrosine hydroxylase (enzyme I in **Figure 1.10**), betalamic acid formation by DOPA 4,5-dioxygenase (DOD; enzyme II), cDOPA formation by plant PPO or DOPA oxidase (enzyme III), conjugation of betalamic acid and amino acid, amine or cDOPA by enzyme VIII, and modification with sugar molecules and aliphatic or aromatic compounds by enzymes IV–VII. The condensation step of betalamic acid and amino acid, amine or cDOPA probably occurs as a spontaneous chemical reaction in vivo, as suggested by feeding experiments.[35]

Similarly, the biosynthesis of oleraceins could occur in the step of condensation between cDOPA to p-coumaroil acids analogues but no accurate evidence is reported.

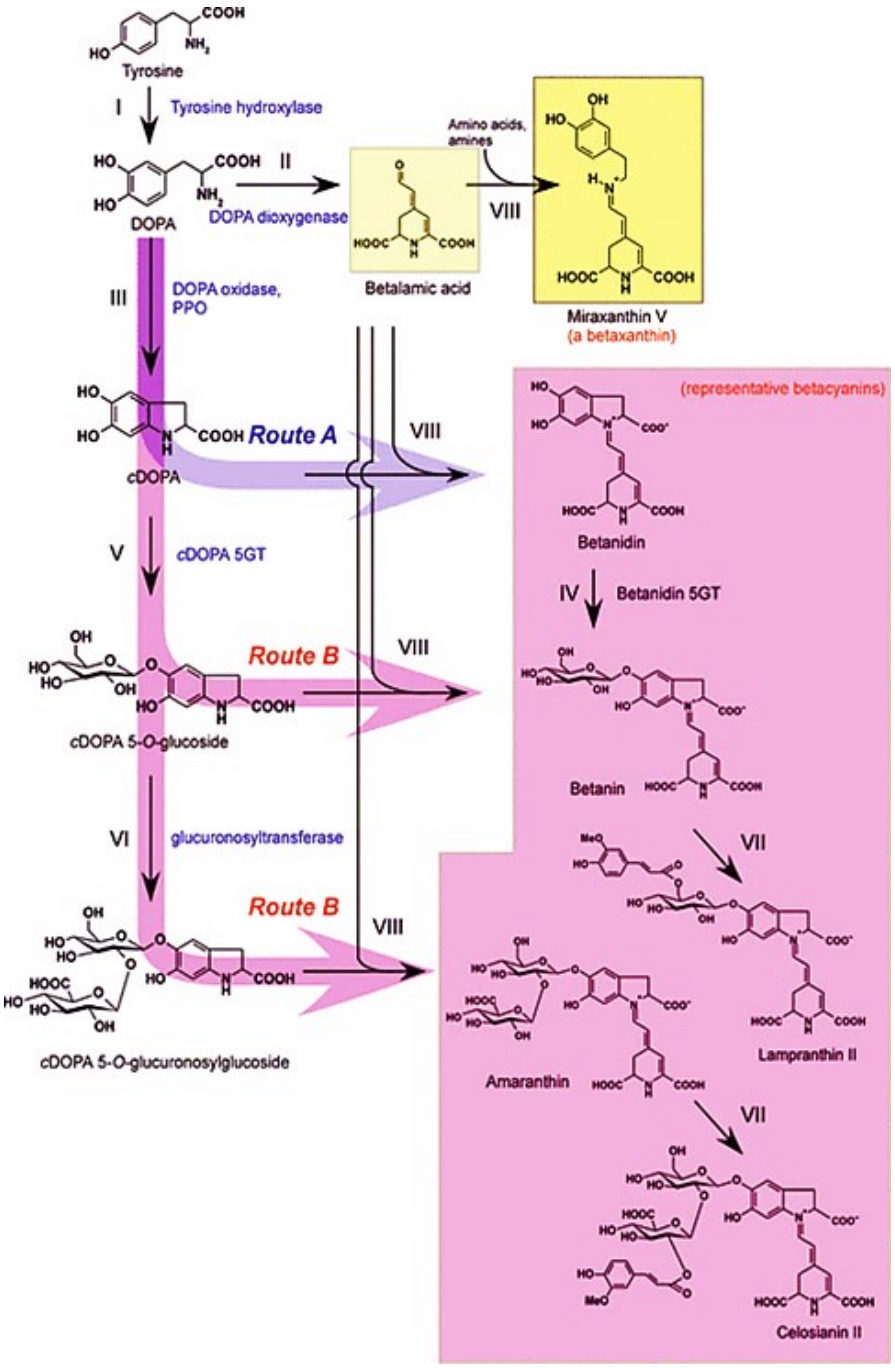

Figure 1.10 Proposed biosynthetic pathway for betalain pigment[35]

1.2.1 Experimental plan

The preliminary LC-HRMS profile of the methanol extract of both stems and leaves revealed the occurrence of polyphenolic alkaloids, known as oleraceins, in a major number in the leaves than in the stems. This observation prompted us to perform the isolation procedure by chromatographic steps, followed by in depth analysis of this class of metabolites, of the leaves extracts.

In order to investigate the effect of different solvents on the extraction efficiency *versus* metabolites occurring in leaves of portulaca plants, 'green' solvents such as ethanol, ethanol/water mixtures (100%, 70% and 50%, *v*/*v*), and water, used for the preparation of infusion, decoction and maceration were employed, obtaining different extraction yields, with the infusion giving the best results.

With the aim to qualitatively estimate the different selectivity shown from the different green extracts *versus* portulaca oleraceins, the (-)ESI/HRMS^n analysis by direct infusion of each extract was undertaken. By this way, the detection of numerous and intense anion peaks showing *m/z* values ascribable to oleraceins on the basis of both molecular formula and fragmentation pattern and literature data, suggested the aqueous solvents, and in particular the infusion, as the more effective to allow a selective extraction of polyphenolic alkaloids, respect to hydro-alcoholic extracts that instead showed poor, in some cases no, selectivity among oleraceins and complex polar lipids.

In line with several trials reported on for the capacity of portulaca extracts to inhibit the neuronal decline related to exposure to neurotoxins[32,33], a preliminary evaluation of several mechanisms involved in the protection and prevention of neuronal damage by testing the activity of polyphenolic alkaloids against different targets was performed. In particular, the radical scavenging activity of the obtained fractions and extracts was measured by the spectrophotometric assays DPPH and ABTS. Moreover, *in situ* inhibition of acetylcholinesterase (AChE) and

butyrylcholinesterase (BChE) were measured. Finally, the screening of the capacity to reduce the neuronal decline of green extract and polyphenolic alkaloids fractions was evaluated by an *in vitro* assay on the transactivation of Nrf2.

1.2.2 Results and Discussion

LC-HRMS profiling of polyphenolic alkaloids

LC-ESI/LTQOrbitrap/MS/MS^n analysis, in negative ionization mode, of the MeOH extracts of *P. oleracea* edible parts allowed us to obtain a preliminary plant metabolite profiling (data not shown), highlighting the occurrence of polyphenolic alkaloids along with the multi-class polar lipids described in the previous paragraph.

With the aim to investigate the effects of different solvents on the extraction efficiency and selectivity for the polyphenolic alkaloid class, "green" solvents like absolute ethanol, ethanol/water mixtures (70% and 50% v/v), and water for the preparation of infusion and decoction were used. The choice of the best extraction method was given by the HR-MS Flow Injection Analysis monitoring of extracts, which showed how the infusion was particularly rich in oleraceins. Furthermore, the highest extraction yield (25%) than other extracts (18-22%) was attributed to the infusion.

The oleraceins were concentrated in a single fraction through SPE chromatography. According to the HPLC gradient and column used for the preliminary LC-HRMS profiling, a C18 cartridge and several mixtures of CH_3CN/H_2O (v/v) in different ratios were employed. All the obtained fractions were monitored through HRMS, allowing to select the fraction eluted with a mixture of 30% ACN as riched in oleraceins. The described steps of selection and concentration of this minoritary class of metabolites resulted in the optimization of signals in the LC-HRMS^n profile (**Figure 1.11**).

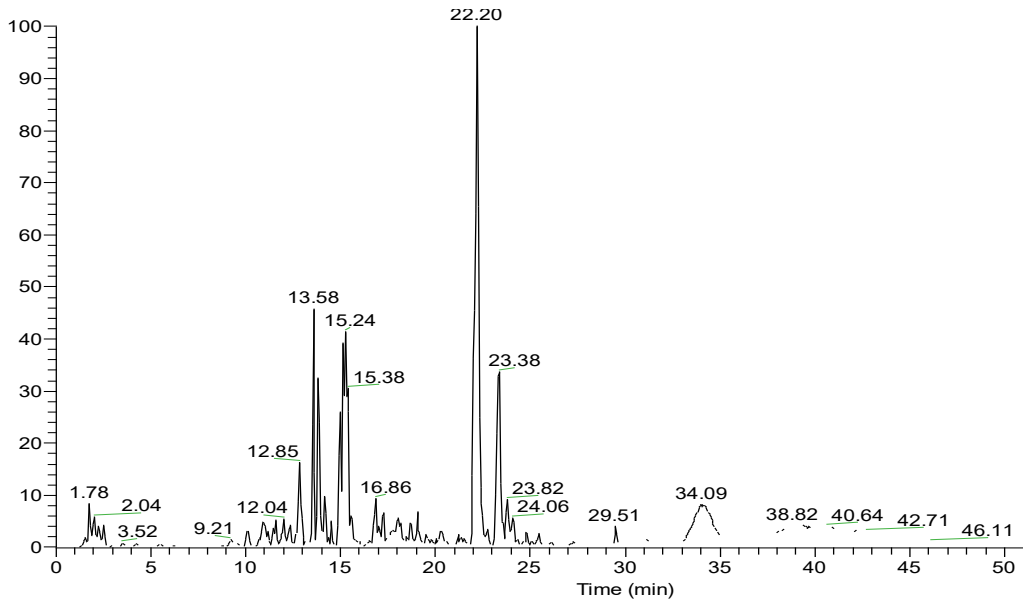

Figure 1.11 LC-HRMS profile, in negative ionization mode, of the oleracein enriched fraction of *P.oleracea* leaves

A detailed analysis of the multistage mass spectra of the main LC-HRMS peaks suggested the presence of phenolic alkaloids (**Table 1.6**). However, the most peculiar secondary metabolites for the species are the oleraceins, metabolites belonging to the class of cyclo-DOPA phenolic alkaloids characterized by a 5,6-dihydroxyindoline-2-carboxylic acid nucleus N-acylated with cinnamic acid derivatives and glycosylated with one or more glucose units.

The analysis of the accurate *m/z* values, allowing the assignment of their molecular formula, and the fragmentation pattern produced in LC-HRMS^n experiments were compared with data contained in mass libraries and literature permitting to putatively identify most of the peaks belonging to the class of polyphenolic alkaloids (compounds **131**, **133-136**, **139-144** of **Table 1.6**). Moreover, the extract ion analysis highlighted the occurrence of minoritary isobar compounds characterized by a different fragmentation pattern. On the basis of of HRMS^n spectra, these compounds were tentatively defined as oleraceins **132, 137-138** (**Table 1.6**). In particular, **Figure 1.12** describes differences in retention times

and multi-stage fragmentation patterns of compounds **131** and **137**, showing the same *m/z* value and, consequently, the same molecular formula.

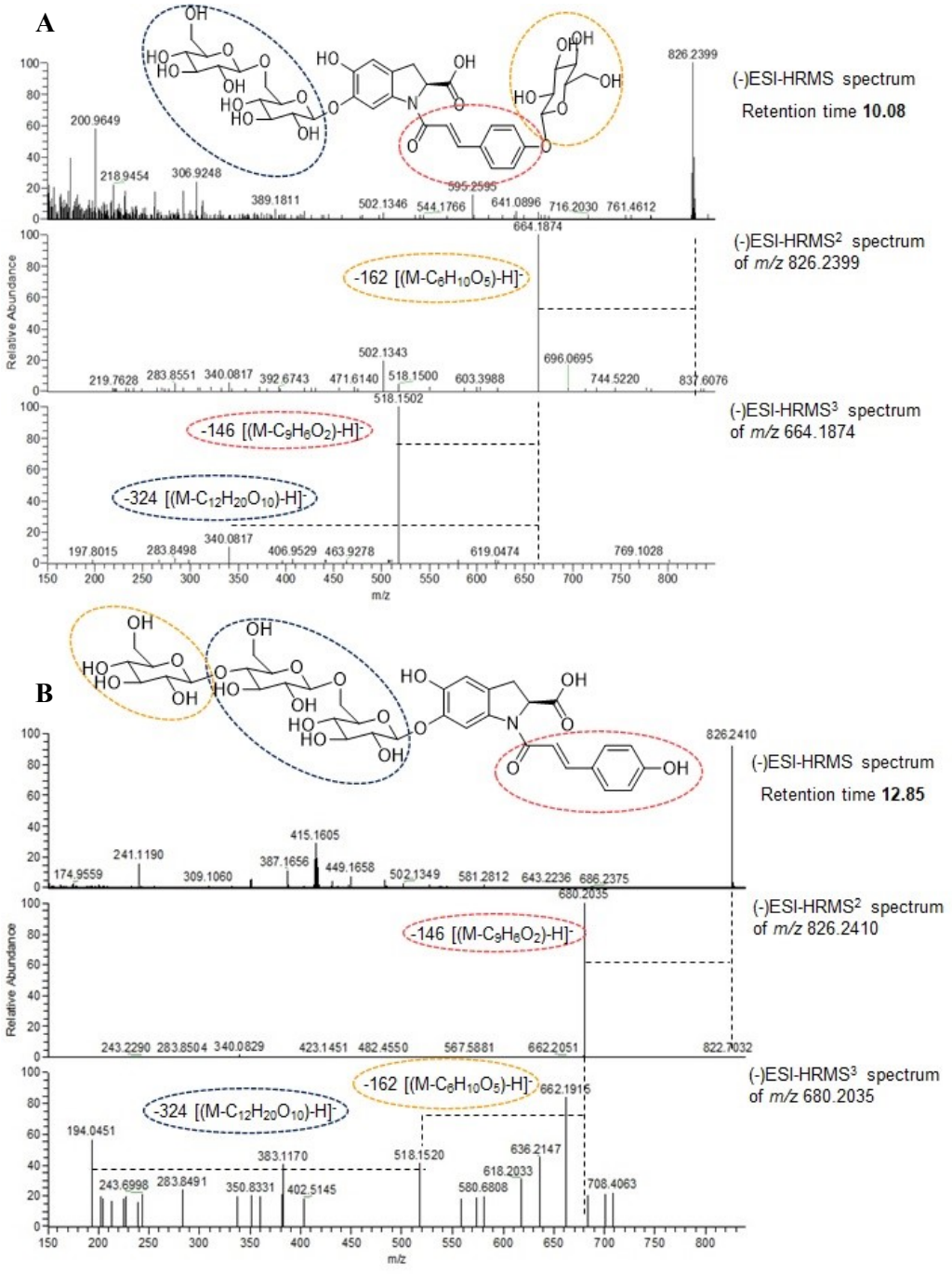

Figure 1.12 HRMS^n spectra of compounds **131** (panel A) and **137** (panel B) respectively

The accurate analysis of tandem mass spectra of compound **131** (*m/z* 826.2419, $C_{36}H_{45}O_{21}N$) highlighted the occurrence of the main product ion at *m/z* 664.1874, corresponding to the molecular formula $C_{30}H_{34}O_{16}N$ and formed by neutral loss of a hexose unit, along with minor product ions at *m/z* 502.1343 ($C_{24}H_{24}O_{11}N$), produced by neutral loss of two hexose units, at *m/z* 340.0817 ($C_{18}H_{14}O_6N$), yielded by neutral loss of three hexose units, and at *m/z* 518.1500 ($C_{21}H_{28}O_{14}N$), formed by neutral loss of a hexose and a coumaroyl unit (**Figure 1.12**, **Table 1.6**). The detection in the $HRMS^3$ spectrum acquired for the product ion at *m/z* 664.1874 of the fragment ions at *m/z* 518.1502 ($C_{21}H_{28}O_{14}N$) and *m/z* 340.0817 ($C_{18}H_{14}O_6N$), and the absence of the product ion formed by neutral loss of a single hexose, allowed to estimate that in **131** one of the three hexose had to be located on the *p*-OH of the coumaroyl unit, in turn *N*-acylated to the cyclo-DOPA scaffold, whereas the two others had to be linked each other, being lost as a whole group of 324 Da, and located at the 6-OH position of the 5,6-dihydroxyindoline-2-carboxylic acid core. Altogether this fragmentation pattern allowed to identify **131** as the already known oleracein P (**Table 1.6**).[45] On the contrary, the tandem mass spectrum of compound **137** showed a unique product ion at *m/z* 680.2035, formed by neutral loss of a ferulic unit and corresponding to the molecular formula $C_{27}H_{38}O_{19}N$ (**Table 1.6**), whose occurrence allowed to estimate that the ferulic unit was not glycosylated. Moreover, the analysis of the $HRMS^3$ spectrum allowed the detection of the product ions at *m/z* 662.1915 ($C_{27}H_{36}O_{18}N$), formed by neutral loss of a water molecule, at *m/z* 636.2147 ($C_{26}H_{38}O_{17}N$), formed by neutral loss of a CO_2 molecule, at *m/z* 518.1520 ($C_{21}H_{28}O_{14}N$), formed by neutral loss of a single hexose unit, and at *m/z* 194.0451 ($C_9H_8O_4N$), corresponding to the 5,6-dihydroxyindoline-2-carboxylate anion and produced by neutral loss of two joint hexose units. This mass spectrometric behaviour gave information about the occurrence in **137** of three hexose units linked each others *via* different interglycosidic linkages, according to which two of them, in agreement with data reported in the literature for other

oleraceins, were lost as a whole neutral group of 324 Da being linked via a 1‴→6″-interglycosidic linkage, and the other one was lost as a single unit, being involved presumably in a 1‴→4‴-interglycosidic linkage, as in oleraceins Y, Z, ZA and ZB.[45] By all these considerations, compound **137** could be tentatively identified as a new oleracein, named oleracein γ (**Figures 1.12** and **1.13**, **Table 1.6**).

Analogously, compounds **133** and **138** showed the same molecular formula but different tandem mass spectra (**Table 1.6**). By analyzing the HRMS/MS of **133**, the occurrence of a main product ion at *m/z* 694.1981 ($C_{31}H_{36}O_{17}N$) formed by neutral loss of a hexose moiety, along with that of a minor product ion at *m/z* 518.1506 ($C_{21}H_{28}O_{14}N$), formed by neutral loss of a hexose and a feruloyl moiety, suggested that this latter moiety had to be glycosylated at the *p*-OH position. Moreover, the detection of a minor product ion at *m/z* 532.1447 ($C_{25}H_{26}O_{12}N$), yielded by neutral loss of two hexose units, along with that at *m/z* 370.0925 ($C_{19}H_{16}O_7N$), obtained by neutral loss of three hexoses, allowed to identify compound **133** as the known oleracein Q (**Table 1.6**).[45] Differently, compound **138** yielded a tandem mass spectrum characterized by a main product ion at *m/z* 680.2013 ($C_{27}H_{38}O_{19}N$) generated by the neutral loss of a feruloyl moiety that, consequently, had to be not glycosylated (**Table 1.6**). Moreover, the detection as minor product ion of only that at *m/z* 370.0915 ($C_{19}H_{16}O_7N$), formed by the neutral loss of three hexose units, and of no product ions formed by neutral loss of one or two hexoses, suggested that, analogously to as deduced for compound **137**, the three sugars had to be glycosylated each other, allowing to suppose that compound **138** was a new oleracein, named oleracein δ (**Figure 1.13, Table 1.6**).

Once again, the analysis of the relative $HRMS^n$ spectra allowed to discriminate among three compounds, **132, 135** and **139**, showing the same molecular formula (**Table 1.6**). In the case of **135**, the check in tandem mass spectrum of a main product ion at *m/z* 502.1349 ($C_{24}H_{24}O_{11}N$), along with a minor one at *m/z* 340.0831($C_{18}H_{14}O_6N$), allowed to identify **135** as the known oleracein C,

structurally characterized by a 5,6-dihydroxyindoline-2-carboxylic acid *N*-acylated with a mono-glycosylated coumaroyl unit and by the occurrence of a second hexose unit at the 6-OH position of the indoline amide scaffold. [45] On the contrary, the analysis of the HRMS/MS spectrum of compound **139** (**Table 1.6**) allowed to ascertain that in this case the coumaroyl unit was not glycosylated, being in fact present in the spectrum the main product ion at *m/z* 518.1500 ($C_{21}H_{28}O_{14}N$) formed by the cleavage of this cinnamic derivative, and that the two hexose units were linked each other, occurring in the spectrum only the product ion formed by their cleavage as a whole group (neutral loss of 324 Da). Altogether this fragmentation pattern allowed to tentatively define **139** as the already known oleracein H.[45] Compound **132** yielded a tandem mass spectrum still different, being characterized by the only main product ion at *m/z* 340.0832 ($C_{18}H_{14}O_6N$), without any product ion formed by neutral loss of single hexose or coumaroyl unit, so allowing to assert that this latter had to be glycosylated and that the two hexose had to be linked each other (**Table 1.6**). By this way, compound **132** could be tentatively identified as a new oleracein, named oleracein α (**Figure 1.13**).

Noteworthy, and differently from the compounds examined so far, **134** and **140** showed both the same molecular formula and the same tandem mass spectrum, characterized by a main product ion at *m/z* 518.1503 ($C_{21}H_{28}O_{14}N$), formed by neutral loss of a ferulic moiety, and by a minor one at *m/z* 370.0927 ($C_{19}H_{16}O_7N$), originated by the neutral loss of two joint hexose units. This fragmentation pattern ascertained the occurrence in both molecules of a ferulic unit not glycosylated and of an indoline amide scaffold diglycosylated at the 6-OH position (**Table 1.6**), as already observed in oleracein I and its isomer.[45]

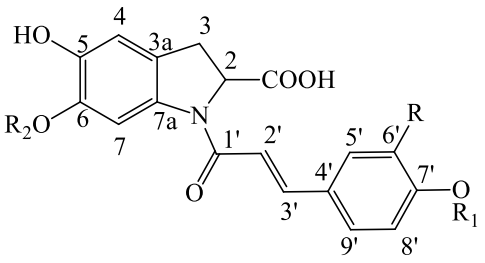

n	compound	R	R_1	R_2
132	Oleracein α	H	Glu-Glu	H
136	Oleracein β	OH	Glu	Glu

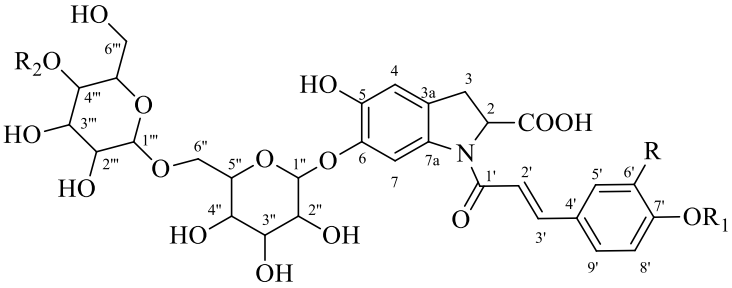

n	compound	R	R_1	R_2
137	Oleracein ɣ	H	H	Glu
138	Oleracein δ	OCH_3	H	Glu

Figure 1.13. Proposed structures of portulaca oleraceins α-δ.

Table 1.6. Compounds identified in the oleracein enriched fraction of *P.oleracea* leaves

n	Compound	R_t (min)	$[M-H]^-$	Molecular formula	Error (ppm)	$HRMS^n$
131	Oleracein P[a]	10.08	826.2399	$C_{36}H_{45}O_{21}N$	-0.20	664.1874 ($C_{30}H_{34}O_{16}N$); 518.1500 ($C_{21}H_{28}O_{14}N$); 502.1343 ($C_{24}H_{24}O_{11}N$); 340.0817 ($C_{18}H_{14}O_6N$). MS^3 (664.1895): 518.1502 ($C_{21}H_{28}O_{14}N$); 340.0817 ($C_{18}H_{14}O_6N$)
132	Oleracein α	10.39	664.1880	$C_{30}H_{35}O_{16}N$	1.26	340.0832 ($C_{18}H_{14}O_6N$)
133	Oleracein Q[a]	11.08	856.2509	$C_{37}H_{47}O_{22}N$	1.65	694.1981 ($C_{31}H_{36}O_{17}N$); 532.1447 ($C_{25}H_{26}O_{12}N$); 518.1506 ($C_{21}H_{28}O_{14}N$); 370.0925 ($C_{19}H_{16}O_7N$)
134	Oleracein I isomer	11.54	694.1981	$C_{31}H_{37}O_{17}N$	0.41	518.1515 ($C_{21}H_{28}O_{14}N$); 370.0939 ($C_{19}H_{16}O_7N$)
135	Oleracein C[a]	11.61	664.1880	$C_{30}H_{35}O_{16}N$	1.17	502.1349 ($C_{24}H_{24}O_{11}N$); 340.0831 ($C_{18}H_{14}O_6N$)
136	Oleracein β	12.32	680.1830	$C_{30}H_{35}O_{17}N$	1.26	518.1296 ($C_{24}H_{26}O_{12}N$); 356.0768 ($C_{18}H_{14}O_7N$). MS^3 (518.1296): 356.0769 ($C_{18}H_{14}O_7N$)
137	Oleracein γ	12.85	826.2410	$C_{36}H_{45}O_{21}N$	1.21	680.2035 ($C_{27}H_{38}O_{19}N$). MS^3(680.2035): 662.1915 ($C_{27}H_{36}O_{18}N$); 636.2147 ($C_{26}H_{38}O_{17}N$); 518.1520 ($C_{21}H_{28}O_{14}N$); 194.0451 ($C_9H_8O_4N$)
138	Oleracein δ	13.12	856.2513	$C_{37}H_{47}O_{22}N$	0.80	680.2013 ($C_{27}H_{38}O_{19}N$); 370.0915 ($C_{19}H_{16}O_7N$)
139	Oleracein H[a]	13.58	664.1885	$C_{30}H_{35}O_{16}N$	1.08	518.1500 ($C_{21}H_{28}O_{14}N$); 340.0820 ($C_{18}H_{14}O_6N$)
140	Oleracein I[a]	13.87	694.1987	$C_{31}H_{37}O_{17}N$	1.38	518.1503 ($C_{21}H_{28}O_{14}N$); 370.0927 ($C_{19}H_{16}O_7N$)
141	Oleracein A[a]	15.12	502.1349	$C_{24}H_{25}O_{11}N$	0.94	356.0984 ($C_{15}H_{18}O_9N$); 340.0822 ($C_{18}H_{14}O_6N$); 296.0922 ($C_{17}H_{14}O_4N$); 194.0454($C_9H_8O_4N$)
142	Oleracein B[a]	15.38	532.1454	$C_{27}H_{27}O_{12}N$	0.94	370.0927 ($C_{19}H_{16}O_7N$); 356.0986 ($C_{15}H_{18}O_9N$); 326.1029 ($C_{18}H_{16}O_5N$);
143	Oleracein N/S	17.49	840.2340	$C_{40}H_{43}O_{19}N$	-0.65	694.1930 ($C_{31}H_{36}O_{17}N$)
144	Oleracein O isomer	17.60	870.2459	$C_{41}H_{45}O_{20}N$	-1.41	694.1999 ($C_{31}H_{36}O_{17}N$)

[a] *Oleraceins isolated and characterized by 1D- and 2D-NMR experiments*

Isolation and characterization of polyphenolic alkaloids

With the aim to unambiguously determine the chemical structure of the main detected constituents, the oleracein enriched fraction of *P. oleracea* was purified by RP-HPLC-UV. On the basis of NMR data reported by Jiao et al., 2014, the structures of the isolated compounds (**131**, **133**, **135**, **139-142**) were elucidated by 1D and 2D homonuclear and heteronuclear NMR experiments (**Figures 1.14-1.20**) and confirmed by HRMS analysis.

As examples, here we describe the structure elucidation of compound **135**.
The molecular formula of compound **135** was deduced as $C_{30}H_{35}O_{16}N$ according to the HRMS parent ion $[M-H]^-$ at *m/z* 664.1871. The chemical structure was unambiguously defined by NMR data (**Figures 1.14-1.17**). In particular, the cyclodopa-type skeleton was deduced from the signals of two aromatic protons at δ 8.26 (1H, s), 6.74 (1H, s), one nitrogen-connected methine proton at δ 5.10 (1H, br s), and two methylene protons at δ 3.50 (1H, m) and 3.22 (1H, m) in the ^{1}H NMR spectrum. Furthermore, the signals at δ 7.59 (2H, d, J = 7.8 Hz) and 7.14 (2H, d, J = 7.8 Hz) and two *trans* olefinic proton signals at δ 7.65 (1H, d, J = 15.0 Hz) and 6.82 (1H, d, J = 15.0 Hz) suggested the occurrence of a *p*-coumaroyl moiety. The presence of two anomeric protons at δ 4.80 (1H, d, J = 7.8 Hz) and 4.91 (1H, d, J = 7.5 Hz) could also be observed. The proton signals were correlated to the corresponding carbon resonances by HSQC experiment (**Figure 1.15**). In this way the occurrence of two β-D-glucopyranosyl units was deduced. HSQC correlations were observed between the proton signals at δ 4.91 and the carbon resonance at δ 101.8 for the *p*-coumaroil linked glucopyranosyl unit, while correlations δH 4.80 and δC for the catechol linked glucopyranosyl unit. Thus, the structure of oleracein C previously reported by Jiao et al., 2014 was deduced. [35]

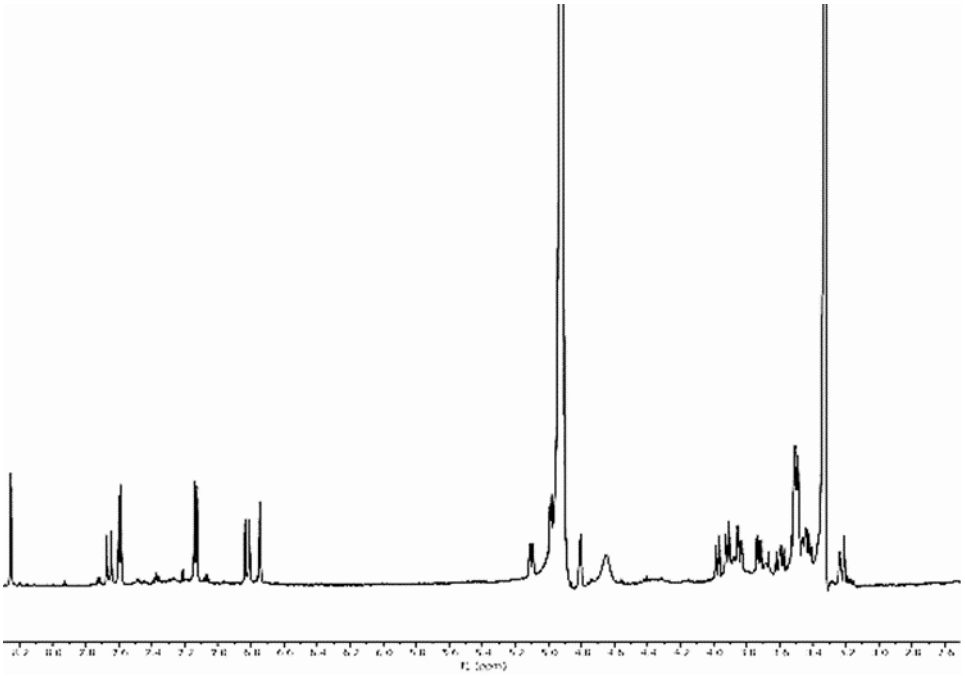

Figure 1.14 ^{1}H NMR spectrum (CD_3OD) of oleracein C (**135**).

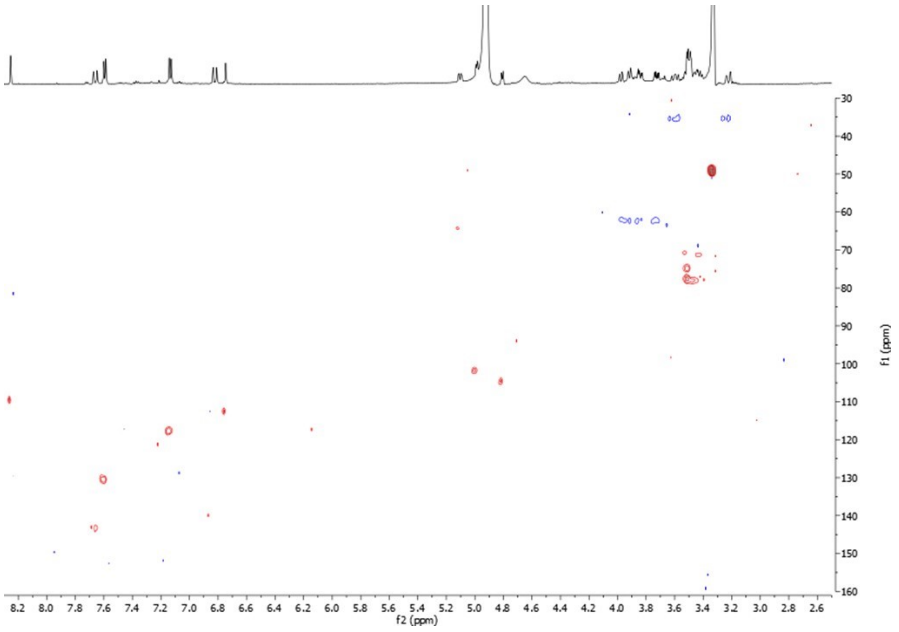

Figure 1.15 HSQC spectrum (CD_3OD) of oleracein C (**135**).

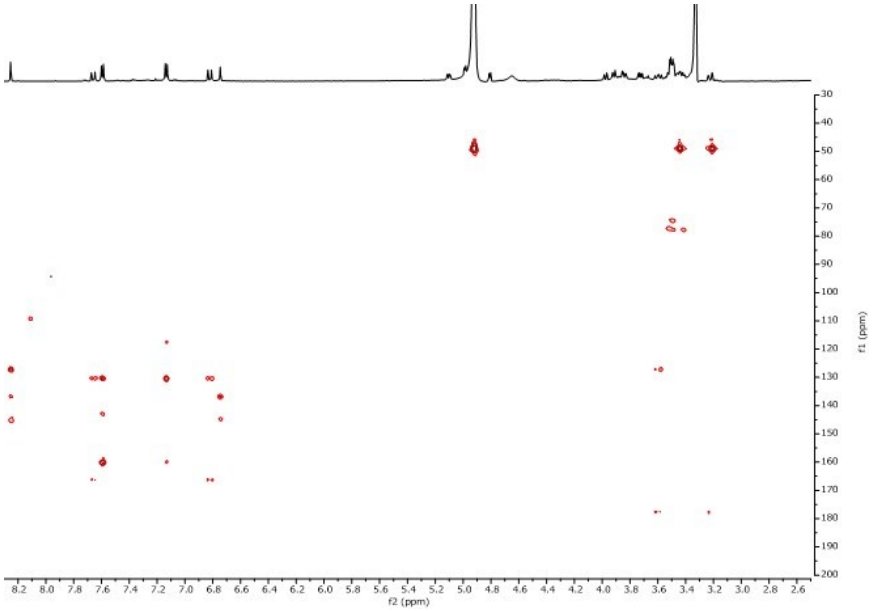

Figure 1.16 HMBC spectrum (CD_3OD) of oleracein C (**135**).

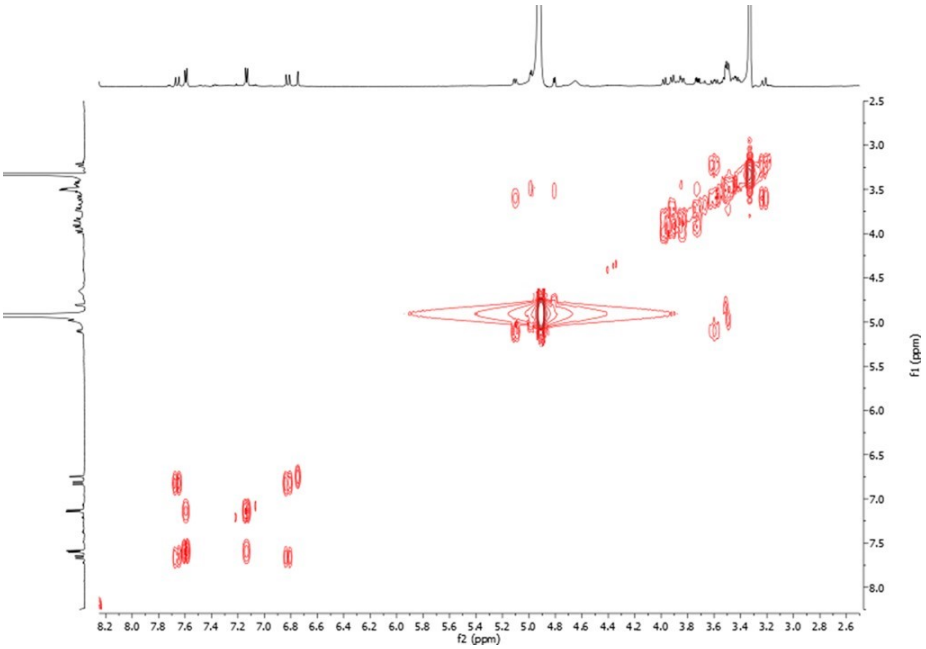

Figure 1.17 COSY spectrum (CD_3OD) of oleracein C (**135**)

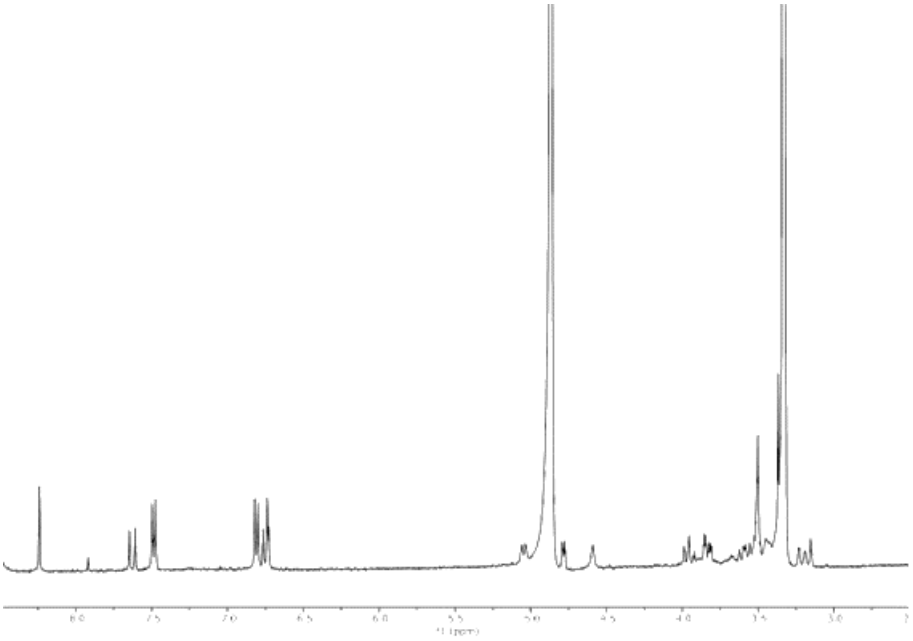

Figure 1.18 ^{1}H NMR spectrum (CD_3OD) of oleracein A (**141**).

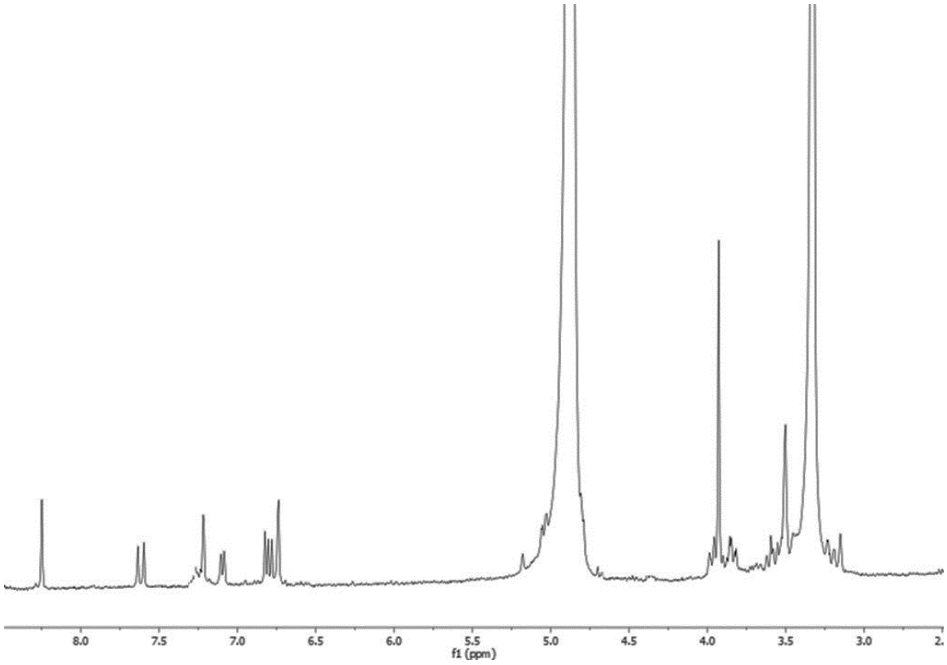

Figure 1.19 ^{1}H NMR spectrum (CD_3OD) of oleracein B (**142**).

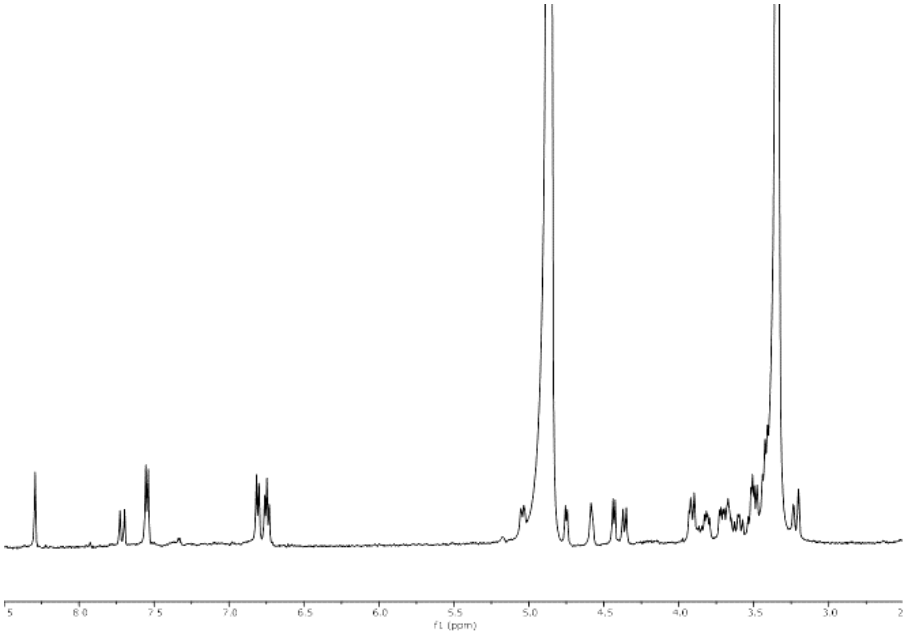

Figure 1.20 ^{1}H NMR spectrum (CD_3OD) of oleracein H (**139**).

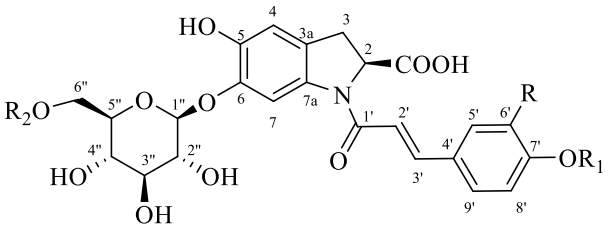

n	compound	R	R_1	R_2
131	Oleracein P	H	Glu	Glu
133	Oleracein Q	OCH_3	Glu	Glu
135	Oleracein C	H	Glu	H
139	Oleracein H	H	H	Glu
140	Oleracein I	OCH_3	H	Glu
141	Oleracein A	H	H	H
142	Oleracein B	OCH_3	H	H

Figure 1.21 Portulaca oleraceins identified by NMR experiments.

1.2.3 Biological activity by multi-target approach

Role of Oxidative Stress in neuronal damage

Neurodegenerative diseases are characterized by progressive damage in neuronal cells and consequently neuronal loss, which leads to the compromised motor or cognitive function. Reactive oxygen species (ROS) are chemically reactive molecules that have been implicated in the pathogenesis of neurodegenerative diseases. They are naturally generated within the biological system, playing important roles in mediating cellular activities such as inflammation, cell survival, and stressor responses as well as many diseases including cardiovascular disorders, muscle dysfunction, allergy, and cancers.[36] Due to their reactivity, high concentrations of ROS can lead to cell death or oxidative stress (OS), which is defined as the disruption of the balance between pro-oxidant and antioxidant levels. The complex pathogeneses of the neurodegenerative diseases remain largely unknown; however, mounting evidence suggests that ROS may play a critical role as high levels of OS are commonly observed in the brain of patients with neurodegenerative conditions.[36]

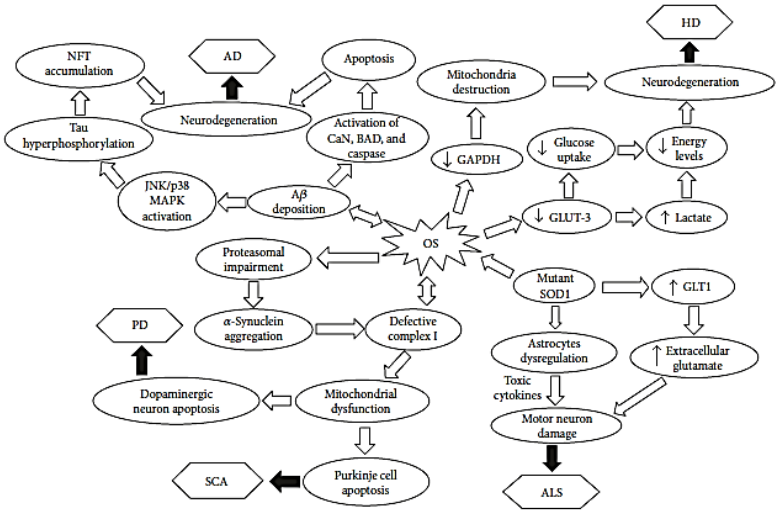

Figure 1.22 Schematic illustration of oxidative stress in neuronal damage and pathologies development

Role of Cholinesterases in neuronal damage

This class of enzymes in superior animals is present in two different isoforms. Acetylcholinesterase (AChE) is involved in the regulation of neurotransmission processes (parasympathetic neurotransmission), being important for (but not limited to) cognition and respiration while Butyrylcholinesterase (BChE) is found in plasma, being responsible for the hydrolysis of different esters. AChE is the enzyme involved in the breakdown of ACh, the parasympathetic neurotransmitter, into choline and acetate, which are reuptake for de novo synthesis of the neurotransmitter

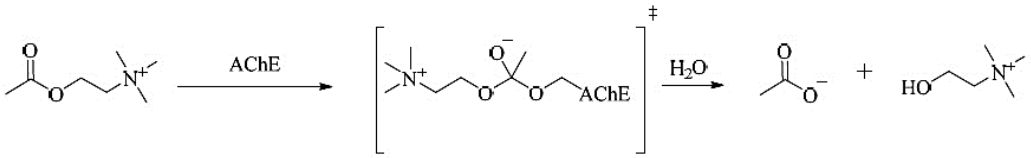

Therefore, AChE is a pharmaceutical target, as its inhibition provokes an increase of neurotransmitter concentration at the post-synaptic cleft, leading to exacerbated cholinergic response over the nerve structures that require parasympathetic stimulation, such as neuromuscular junctions.[37]

Role of Nrf2 pathway in neuronal damage

In various forms of neurodegenerative disease, the connection between Nrf2 and proteostasis is particularly pertinent because these diseases are characterized by abnormal protein aggregation. [40] In humans, APP- injured and tau- injured neurons express increased levels of Nrf2. These findings are consistent with the recently reported role of Nrf2 in upregulating the expression of genes involved in macroautophagy and chaperone-mediated autophagy, two essential mechanisms for clearance of APP, tau and α-synuclein.[40] Upregulation of Nrf2 protected neurons against the toxicity of mutant α- synuclein and leucine-rich repeat kinase 2

(LRRK2), which also leads to neurodegeneration associated with the accumulation of misfolded proteins.[40]

1.2.3.1 Radical scavenging activity of polyphenolic alkaloids of portulaca

The extracts of portulaca leaves were tested for a preliminary antioxidant evaluation by spectrophotometric assays. In the TEAC assay, the oleracein enriched fraction showed an antioxidant activity (TEAC=2.05±0.05) comparable to that observed for quercetin 3-O-gluc (TEAC=1.81±0.21) used as a reference compound. The $DPPH^{\cdot}$ assay revealed that the scavenging activity of the same fraction was 149.3±0.19 µg/mL, using ascorbic acid as a positive control (**Table 1.7**), confirming the better radical scavenging activity of the fraction than other extracts.

Table 1.7 $DPPH^{\cdot}$ and $ABTS^{\cdot+}$ assays of several extracts and oleracein enriched fraction of *P.oleracea*

Extracts/ compounds	**$DPPH^{\cdot}$** (IC_{50}, µg/ml±SD)	**$ABTS^{\cdot+}$** TEAC±SD
MeOH	231.72 ±0 .11	0.56 ± 0.11
Infusion	237.75 ± 0.11	0.59 ± 0.11
Oleracein enriched fraction	149.32 ± 0.19	2.05 ± 0.25
Hydrolyzed fraction	171.21 ± 0.14	0.87 ± 0.11
Acorbic acid	5.43 ± 0.11 µM	-
Quercetin 3-O-gluc	-	1.81 ± 0.21

TEAC: values are expressed as concentration (mM) of standard Trolox solution exerting the same radical scavenging activity of a 1 mg/ml of the tested extract. (SD) standard deviation of three independent experiments.

1.2.3.2 In situ evaluation of AChE and BuChE inhibition

The infusion, the MeOH extract, the oleracein enriched fraction and the hydrolyzed fraction were employed for acetylcholinesterase and butyrylcholinesterase inhibition assay as reported by Ellman, 1961. Galantamine was used as a positive control for both targets. The IC_{50} values of 2.82 ± 0.51 μM for AChE and 66.01 ± 4.78 μM for BChE (**Table 1.8**) observed for galantamine, aligned to data reported in literature[43,44], highlighted the good performances of the assays. Moreover, **Table 1.8** shows the results related to the capacity of inhibition of each sample against both targets which resulted very limited.

Table 1.8 Inhibition of Acetylcholinesterase (AChE) from Electrophorus electricus and butyrylcholinesterase (BuChE) from equine serum. Data expressed as IC_{50} ±SD of three independent experiments.

Extracts / compounds	**AChE inhibition** (IC_{50}, mg/ml±SD)	**BChE inhibition** (IC_{50}, mg/ml±SD)
MeOH	49.72 ± 1.51	-
Infusion	401.43± 1.32	-
Oleracein enriched fraction	83.52 ± 1.11	216.91 ± 6.57
Hydrolyzed fraction	44.74 ± 1.02	66.71 ± 1.48
Galantamine	2.82± 0.31 μM	66.01 ± 4.78 μM

Inhibition of Acetylcholinesterase (AChE) from *Electrophorus electricus* and Butyrylcholinesterase (BuChE) from equine serum. Data expressed as IC_{50}±SD, standard deviation of three independent experiments

1.2.3.3 In vitro evaluation of Nrf2 pathway assessed by a reporter gene assay

Figure 1.23 depicts the data obtained from the Nrf2 (ARE)-dependent reporter gene assay. The oleracein enriched fraction did not show remarkable *in-vitro* activity (fold activation a bit higher than negative control; **Figure 1.23**). To optimize the performances in bioactivity tests increasing the cellular permeability, the oleracein enriched fraction was hydrolyzed using Kiliani reagent HCl:HCOOH:H_2O, to allow the cleavage of sugar moieties.[39] The hydrolyzed fraction showed improved Nrf2 activity at a concentration of 30 µg/ml. Recently, the activation of the defense cellular pathway mediated by Nrf2 transcriptor factor has been reported as a target for preventing neuronal damage, reducing neuronal oxidative stress and protein precipitation of TAU and α-synuclein.[40] Cell numbers after treatment with the tested extracts and fractions remained in a range of 85-98% of control cells, excluding major cytotoxic effects.

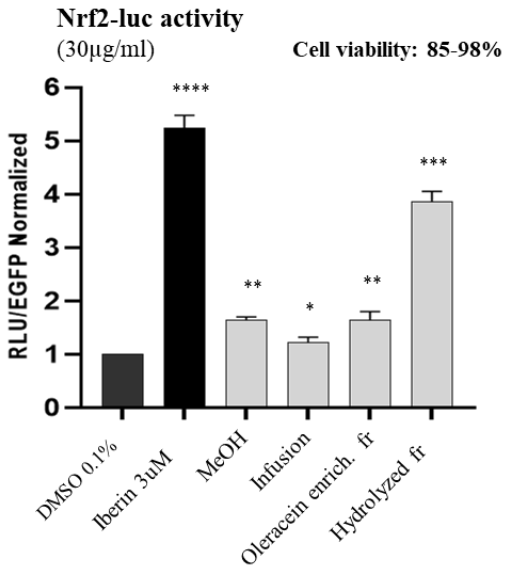

Figure 1.23. Activation of the Nrf2 pathway in HepG2-ARE/NRF2-luc cells, screening for different extracts and oleracein-enriched fractions from purslane leaves. Data are expressed in relative units. Bar charts represents the transactivation activity expressed as mean ± SD of three independent experiments, n=3, ****p<0.0001 (One-way ANOVA with Dunnett's post hoc test vs vehicle control)

1.2.4 Conclusions

The accurate analysis of the LC-HRMS^n spectra acquired for the oleracein enriched fraction of *P. oleracea* leaves allowed the detailed detection of cDOPA alkaloids derivatives. Compounds never reported before were tentatively defined by multi-stage HRMS spectra. The phytochemical investigation of the fraction through isolation and NMR characterization confirmed the structures of the main oleraceins.

The oleracein enriched fraction was characterized by interesting radical scavenging capacity (TEAC value = 2.05 ± 0.25 *versus* 1.81 ± 0.21 μM of quercetin-3-O-glucoside used as positive control) and the fraction obtained by acid hydrolysis exhibited a good capacity to activate *in vitro* the Nrf2 pathway at a concentration of 30 μg/ml, without exerting cytotoxic effects (**Figure 1.23**)

The obtained results on the chemical and bioactivity profile of *P. oleracea* harvested in Campania region of Italy, support the reevaluation of the plant for the employment in daily diet for its potential health benefits and provide the basis for further research on its biological effects on selected targets.

1.3 Experimental section

Plant selection and extraction

The edible parts (leaves and stems) of *P. oleracea* were manually separated and kept at -20°C for 1 night. After freeze-drying, each part (50.0 g) was deprived of chlorophylls by maceration at room temperature with petroleum ether and subsequently with chloroform (500 mL), each one for 3 nights. Finally, the extracted raw material was submitted to a final step of maceration with MeOH at room temperature (500 mL x 3 days x 3 times). The filtered methanol extract obtained from each edible part (named as MeOH-POL for *P. oleracea* leaves and MeOH-POS for *P. oleracea* stems, respectively) was dried under vacuum by rotavapor.

Sample preparation

In order to obtain lipid enriched fractions, 100 mg of each methanol extract was fractionated on a Sep-Pak C-18 cartridge (Strata C18, 100mg from Phenomenex) by using CH_3CN/H_2O (v/v) in the different ratios (10%, 55% and 100% ACN, respectively) as solvent. In particular, the fractions obtained by using 55% ACN (named as 55ACN-POL for P. oleracea leaves and 55ACN-POS for *P. oleracea* stems, respectively) and 100% ACN (named as 100ACN-POL for *P. oleracea* leaves and 100ACN-POS for *P. oleracea* stems, respectively) were selected for further analysis.

The detailed study of polyphenolic alkaloids was performed on the infusion, characterized by the best compromise between selectivity for oleraceins and high extraction yield (25%) than other green extracts as hydroalcoholic mixtures and decoction. On the basis of Official Pharmacopoeia XII, the infusion was carried out in boiling distilled water, using moderate stirring, recovered with aluminum and

protected with plastic parafilm to permit the conservation of a stable temperature and to prevent solvent evaporation and light reaction; then filtered under reduced pressure.

In order to obtain oleracein enriched fraction, 1 g of infusion was fractionated on a Sep-Pak C-18 cartridge (Strata C18, 10 g from Phenomenex) by using CH_3CN/H_2O (v/v) in the different ratios (10%, 30%, 55% and 100% ACN, respectively) as solvent. In particular, the fraction obtained by using 30% ACN was selected for further analysis. The obtained fraction was hydrolyzed by Kiliani reagent HCl:HCOOH:H_2O (in a ratio of 10:35:55 v/v), at the conditions of 2h at 100°C (Mair et al., 2018). Then ethyl acetate/water partition was performed and the ethyl acetate fraction was dried under vacuum and used for further analysis.

LC-ESI/HRMS/MS^n analysis of multi-class complex polar lipids

Both methanol extracts and 55% and 100% ACN lipid enriched fractions obtained from purslane leaves and stems were analyzed by using a system of liquid chromatography coupled to electrospray ionization and high-resolution mass spectrometry (LC-ESI/HRMS) consisting of a quaternary Accela 600 pump and an Accela autosampler coupled to a LTQOrbitrap XL mass spectrometer (ThermoScientific, San Jose, CA), operating in positive and/or negative ionization mode. Depending on the selected ionization, the following experimental conditions for the ESI source were adopted: for negative ion mode sheath gas at 15 (arbitrary units), auxiliary gas at 5 (arbitrary units), capillary temperature at 280 °C, source voltage at 3.5 kV, capillary voltage at -48 V and tube lens at -176.47 V; for positive ion mode, sheath gas at 15 (arbitrary units), auxiliary gas at 10 (arbitrary units), capillary temperature at 280 °C, source voltage at 4.5 kV, capillary voltage at 27 V and tube lens at 105 V. In order to allow MS/MS analysis, data-dependent scan experiments were performed selecting the first and the second most intense ions

from the HRMS scan event and submitted them to collision-induced dissociation (CID) by applying the following conditions: a minimum signal threshold at 250, an isolation width at 2.0, and normalized collision energy at 30%. Data were collected and analyzed using the Xcalibur 2.2 software provided by the manufacturer.

MeOH-POL and MeOH-POS were chromatographically analyzed (data not shown) by using a Luna C-18 column (RP-18, 2.0 x 150 mm, 5 µm; Waters; Millford, MA), a mobile phase consisting of 0.1% formic acid in water (v/v) as solvent A and 0.1% formic acid in acetonitrile (v/v) as solvent B, a flow rate of 0.2 mL/min, and a different gradient according to the used ionization polarity. In fact for LC-(-)ESI/HRMS/MS a linear gradient held at 10% B for 5 min, increased to 59% B in 24 min, to 72% B in 8 min, to 93% B in 7 min, to 100% B in 3 min, and held at 100% B for 5 min was used. For LC-(+)ESI/HRMS/MS a linear gradient held at 10% B for 5 min, increased to 100% B in 35 min, and held at 100% B for 5 min was used. In both cases, the autosampler was set to inject 2 µl of each extract (0.5 mg/ml). For mass spectrometric analysis, a mass range from 150 to 1500 m/z and resolving power of 30000 were used.

Both 55ACN-POL and 55ACN-POS were analyzed by using the same mass spectrometry and chromatographic settings described for MeOH-POL and MeOH-POS except for little changes to the linear gradient used for the LC-(-)ESI/HRMS/MS, because in this case, after to have reached the 59% B in 24 min, the B percentage was increased to 100% B in 8 min and held at 100% B for 5 min. 3 µl of both 55ACN-POL and 55ACN-POS (0.5 mg/ml) were injected.

100ACN-POL and 100ACN-POS were analyzed by LC-(-)ESI/HRMS/MS^n using for the chromatographic separation a Symmetry 300 C-4 column (RP-4, 2.1 x 150 mm, 3.5 µm; Waters; Millford, MA), the same mobile phase and flow rate of the other samples, and the following linear gradient: initial 50% B increased to 65% B in 10 min, held at 65% B for 5 min, increased to 68% B in 6 min and held at this percentage for 10 min, increased to 70% B in 2 min and held at this percentage for

5 min, increased to 75% B in 3 min and held at this percentage for 10 min, and finally increased to 100% B in 9 min. 3 µl of both lipid enriched fractions (0.5 mg/ml) were injected. For mass spectrometric analysis, a mass range from 400 to 1500 m/z and a resolving power of 30000 were used. For data-dependent scan experiments, dynamic exclusion was enabled with a repeated count of 2 and a repeated duration of 5 s, list size 50, with exclusion duration of 10 s. Targeted events consisting of multiple-stage tandem mass experiments (MS^n with n = 3, 4…) on selected product ions were carried out by using a normalized collision energy at 30%.

LC-ESI/HRMS/MS^n analysis of polyphenolic alkaloids fraction

The selected polyphenolic alkaloid enriched fraction was analyzed by using a system of liquid chromatography coupled to electrospray ionization and high-resolution mass spectrometry (LC-ESI/HRMS) consisting of a quaternary Accela 600 pump and an Accela autosampler coupled to a LTQOrbitrap XL mass spectrometer (ThermoScientific, San Jose, CA), operating in positive and/or negative ionization mode. Depending on the selected ionization, the following experimental conditions for the ESI source were adopted: for negative ion mode sheath gas at 15 (arbitrary units), auxiliary gas at 5 (arbitrary units), capillary temperature at 280 °C, source voltage at 3.5 kV, capillary voltage at -48 V and tube lens at -176.47 V; for positive ion mode, sheath gas at 15 (arbitrary units), auxiliary gas at 10 (arbitrary units), capillary temperature at 280 °C, source voltage at 4.5 kV, capillary voltage at 27 V and tube lens at 105 V. In order to allow MS/MS analysis, data-dependent scan experiments were performed selecting the first and the second most intense ions from the HRMS scan event and submitted them to collision-induced dissociation (CID) by applying the following conditions: a minimum signal threshold at 250, an isolation width at 2.0, and normalized collision energy at 30%.

Data were collected and analysed using the Xcalibur 2.2 software provided by the manufacturer.

Selected oleracein enriched fractions were chromatographically analyzed by using a Luna C-18 column (RP-18, 2.0 x 150 mm, 5 µm; Waters; Millford, MA), a mobile phase consisting of 0.1% formic acid in water (v/v) as solvent A and 0.1% formic acid in acetonitrile (v/v) as solvent B, a flow rate of 0.2 mL/min, and a linear gradient held at 10% B for 5 min, increased to 59% B in 24 min, to 72% B in 8 min, to 93% B in 7 min, to 100% B in 3 min, and held at 100% B for 5 min was used. In both cases, the autosampler was set to inject 4 µl of each extract (0.5 mg/ml). For mass spectrometric analysis, a mass range from 150 to 1500 *m/z* and a resolving power of 30000 were used.

Targeted events consisting of multiple-stage tandem mass experiments (MS^n with n =2, 3, 4) on selected product ions were carried out by using a normalized collision energy at 30%.

Isolation and characterization of polyphenolic alkaloids

The polyphenolic alkaloid enriched fractions (100 mg) was purified by semi-preparative HPLC-UV separations, by using a mobile phase consisting of H_2O + 0.1% formic acid, as solvent A, and CH_3CN + 0.1% formic acid, as solvent B. At a flow rate of 2 mL min−1, the following linear gradient program was used: 0–10 min, from 5 to 18% B; 19–21 min an isocratic of 22.5% B; 22–24 min, an isocratic of 23% B, 25–27 min, an isocratic of 24% B, 28–30 min, an isocratic of 25% B, 30–50 min, a linear gradient from 25 to 35% B, up to 60 min to 100% B. 50 µL of sample (100mg/ml) were injected for each run and the analytes were monitored at 330 nm. 7 polyphenolic alkaloids were isolated from 100.0 mg of the selected fraction: compound **1** (1.2 mg Rt = 17.18 min), **3** (0.9 mg Rt = 17.84 min), **5** (1.1

mg Rt = 18.89 min) and **9** (1.2 mg Rt = 23.72 min), **10** (1.1 mg Rt = 24.59 min), **11** (1.3 mg Rt = 29.08 min), **12** (1.4 mg Rt = 30.10 min).

NMR analysis

As reported in general experimental procedures.

Inhibition of the AChE and BuChE activity

The infusion and the fractions therefrom derived were tested for their inhibitory activity toward AChE and BChE by the classical spectrophotometric Ellman's assay (Ellamn et al., 1961). The standardized kit for inhibition assays of AChE from Electrophorus electricus (200 U/mg), and BChE from equine serum (13 U/mg) was purchased by Sigma-Aldrich. Both ChEs were dissolved in Tris-HCL buffer 0.1 M, at pH 7.5. Acetyl-thiocoline iodide was used as substrate (100 mM) and 5,50-dithiobis-2-nitrobenzoic acid (DTNB) as the chromophoric reagent. Galanthamine hydrobromide was used as a positive control. Inhibition assays were carried out on a Thermo Multiscan SkyHigh UV visible spectrophotometer equipped with 96 multiwell plate reader. DMSO/H_2O (35%$_{DMSO}$ v/v) solutions of tested compounds were prepared. AChE inhibitory activity was determined in a 96 well plate containing 45 µL of a solution of AChE (0.4 U/mL), 5 µL of testing compounds and 145 µL solution mix of DTNB and substrate in 0.1 M Tris-HCl (pH 7.4). After incubation for 10 min at 37 °C, the inhibition of AChE-catalyzed hydrolysis was followed by measuring the decrease of absorbance at 412 nm. The concentration of sample determining 50% inhibition of the AChE activity (IC_{50}) was calculated by non-linear regression of the response log (concentration) curve, using Microsoft Excell 2016. Similarly, BuChE inhibitory activity was assessed.

Biological assays

To screen the *in vitro* hits for Nrf2 activation the human liver cancer cell line HepG2, containing a stably integrated firefly luciferase gene under the control of ARE was utilized. They were purchased from Signosis Inc. (Santa Clara, CA, USA). The screening of NF-κB luciferase reporter gene was performed on primary embryonic human kidney cell line HEK293, stably transfected with luciferase gene (Panomics, RC0014), while the in vitro screening of PPAR-ɣ activity was evaluated on HEK293 freshly transfected by plasmids.

- *Cell culture*

Cells were generally grown in 75 cm^2 cell culture flasks as adherent monolayer cultures. Cells were cultured in Dulbecco's Modified Eagle's Medium-high glucose (DMEM) medium supplemented with 10% fetal bovine serum (Invitrogen), 1% penicillin/streptomycin and 2 mM L-glutamine (37°C, 5% CO_2). The flasks containing the cells and growth medium were kept in a HERAcell 150 incubator (Thermo Electron Corporation) at 37 °C with 5 % carbon dioxide (CO_2). Cells were regularly examined under a CKX31 microscope (Olympus) to assess health and growth, and to check for contaminations. Upon reaching 80 % confluence, which occurred between once or twice per week, cells were split and seeded using a laminar flow cabinet. For the splitting process, the growth medium was completely removed. Then, the cells were washed with 10 mL phosphate-buffered saline (PBS). After the removal of PBS, 4 mL of trypsin/ethylenediaminetetraacetic acid (EDTA) were added to the flask, which was then put in the incubator at 37° C with 5 % CO_2 for 3 minutes. Cell detachment was checked under the microscope. The flask was shaken mildly if the detachment was not complete. 11 mL growth medium were added, and the cells were suspended in the medium, which stopped trypsin activity. Using a ViCell XR Cell Viability Analyzer (Beckman Coulter) cell

viability and cell count were measured. An adequate aliquot of cell suspension was subsequently transferred into a new flask and a growth medium was added, as to reach an approximate total volume of 15 mL per flask. After suspension, the flask was once again checked in the microscope and then stored in the incubator.

- *General principle of luciferase reporter assay*

A luciferase reporter gene assay was conducted to determine the test compounds' effect on Nrf2-mediated gene transcription in HepG2-ARE-Luc cells. The same assay was used also to evaluate Nf-kb and PPAR-ɣ targets on relative cell lines, as described in the subsequent paragraphs. Luciferase is an enzyme that produces bioluminescence during the oxidation of its substrate luciferin to oxyluciferin, while using ATP as a co-substrate.

$$\text{Luciferin} + O_2 + \text{ATP} \rightarrow \text{oxyluciferin} + CO_2 + \text{PPi} + \text{AMP} + \text{light}$$

As HepG2-ARE-Luc cells include a stably integrated firefly luciferase gene under the control of ARE, ARE-controlled gene transcription can be detected using this method. Via luminescence measuring the amount of luciferase was quantified. Cells were also treated with a CellTracker™ Green (CTG, Invitrogen AG) solution, allowing for test results to be normalized to fluorescence values and cell numbers.

Inhibition of the NF-kB transactivation activity assessed by reporter gene assay

The assay was essentially performed as described before.[36] The cell culture step of HEK293 cells stably transfected with an NF-κB luciferase reporter gene (Panomics, RC0014), was followed by a staining step for 1 h in serum-free medium supplemented with 2 µM Cell Tracker Green CMFDA (Invitrogen), a fluorescent probe that is retained inside living cells and thus can be used as an indicator for

viable cell number.[40] Cells were then plated in 96-well plates ($4x10^4$ cells/well) overnight. The following morning, cells were pre-treated with samples: positive control (parthenolide, 10 µM; IC50 value: 1.5 µM, 95% CI 1.3–1.8 µM), solvent vehicle control (0.1% DMSO in culture medium) or sample extracts for 1 hour and then stimulated with 2 ng/mL TNF-α for 4 h. Afterward, cells were lysed with a luciferase lysis buffer (Promega; E1531) and the luminescence of the firefly luciferase and the fluorescence of the Cell Tracker Green CMFDA were measured by a Tecan Spark® microplate reader (Männedorf, Switzerland). For quantification of NF-κB activity, the luciferase-derived signal from the NF-κB reporter was normalized by the fluorescence signal derived from Cell Tracker Green CMFDA to account for differences in cell number. Potential differences in viable cell numbers were detected by comparison of the Cell Tracker Green CMFDA fluorescence of the solvent vehicle-treated cells and cells treated with the investigated samples.

Activation of the Nrf2 pathway assessed by reporter gene assay

The luciferase assay was basically performed as reported by Heiss *et al*., 2014. Briefly, stably transfected and Cell Tracker Green stained HepG2-ARE-luc (Signosis, SL-0046-FP) were seeded in a 96-well plate ($2x10^{\wedge 4}$ cells per well). The plates were put in the incubator overnight. The following day, cells were incubated with test samples (dissolved in DMSO). DMSO only (final concentration of 0,1 %) was used as a negative control, and iberin (3 µM) as a positive control. After incubation for 16 hours, cells were lysed and worked up as described in 2.6, in order to obtain fluorescence (indicative for cell number) and luminescence (indicative for Nrf2 activation) readings. Luminescence -to-fluorescence ratios from the sample-treated cells were referred to the negative control which was set at 1.

Activation of PPAR-ɣ transactivation activity assessed by reporter gene assay

The assay was essentially performed as previously described (Resetar *et al*., 2020). Briefly, HEK293 cells were transfected via the calcium phosphate precipitation method with a PPAR-ɣ expression plasmid, the luciferase reporter plasmid tk-PPREx3-luc and the fluorescent protein EGFP (2:2:1 ratio) as an internal control for transfection yield. After 6 hours, cells were washed and treated with the vehicle control (0.1% DMSO), the positive control (pioglitazone, 10 µM), or selected extracts (20, 10 and 5 µg/ml) in a 96 well plate and incubated for 16 h. After cell lysis using the luciferase lysis buffer (Promega; E1531), the luminescence of the firefly luciferase and the fluorescence of the EGFP were measured on a Tecan Spark® microplate reader (Männedorf, Switzerland). For quantification of PPAR-ɣ activity, the luciferase-derived signal was normalized to the fluorescence signal derived from the EGFP protein.

Statistical analysis

Each LC-HRMS experiment was performed in triplicate. The variance (ANOVA) and t-test were applied to estimate differences (considered to be significant at $p \leq 0.05$). Microsoft Excel 2016 was used for statistical analyses.

I*n situ* assays: inhibition tests of AChE and BChE were performed three times in three technical replicates for each extract. The inhibitions of targets were expressed as $IC_{50} \pm$ SD of three independent experiments. The variance (ANOVA) and t-test were evaluated using Microsoft Excel 2016 (considered to be significant at $p \leq 0.05$).

in vitro assays: three independent in vitro assays were performed, each in four technical replicates. The transactivation activity was expressed as mean ± SD of three independent experiments, n=3, ****p<0.0001 (One-way ANOVA with

Dunnett's post hoc test vs vehicle control). Statistics were evaluated using GraphPad Prism 9.2.0.

DPPH radical scavenging activity

Reported in the section: general experimental procedures

TEAC radical scavenging activity

Reported in the section: general experimental procedures.

References

1. Xu, X., Yu, L., and Chen, G. (2006). Determination of flavonoids in *Portulaca oleracea* L. by capillary electrophoresis with electrochemical detection. *Journal of Pharmaceutical and Biomedical Analysis*, (41) **2**, 493–499.

2. Chen, C.-J., Wang, W.-Y. Wang X.-L. Anti-hypoxic activity of the ethanol extract from *Portulaca oleracea* in mice. *Journal of Ethnopharmacology*, 2009, (124) **2**, 246–250.

3. Jin, R., Lin, Z. J., Xue, C. M. and Zhang, B. An improved association- mining research for exploring Chinese herbal property theory: based on data of the Shennong's Classic of Materia Medica. *Journal of integrative medicine*., 2013, (11) **5**, 352–365.

4. Zhou, Y-X., Xin, H-L., Rahman, K., Wang, S.J., Peng, C., and Zhang, H. *Portulaca oleracea* L.: A Review of Phytochemistry and Pharmacological Effects. *BioMed Research International* 2015, **2014**, 1-11.

5. Palaniswamy, U. R. McAvoy, R. J. and Bible, B. B. Stage of harvest and polyunsaturated essential fatty acid concentrations in purslane (*Portulaca oleraceae*) leaves," *Journal of Agricultural and Food Chemistry,* 2001, (49) **7**, 3490–3493.

6. Uddin, M. K., Juraimi, A. S., Hossain, M. S., Nahar, M. A. U., Ali, M. E., and Rahman, M.M. Purslaneweed (*Portulaca oleracea*): a prospective plant source of nutrition, omega-3 fatty acid, and antioxidant attributes. *The Scientific World Journal*, 2014, 1-6.

7. Mohamed A. I. and Hussein, A. S. Chemical composition of purslane (*Portulaca oleracea*). *Plant Foods for Human Nutrition*., 1994, (45) **1**, 1–9.

8. Palaniswamy, U. R., Bible, B. B. and McAvoy, R. J. Effect of nitrate: ammonium nitrogen ratio on oxalate levels of purslane. *Trends in New Crops and New Uses*, 2002, (11) **5**, 453–455.

9. Xiang, L., Xing, D., Wang, W., Wang, R., Ding, Y.and Du, L. "Alkaloids from *Portulaca oleracea* L.," *Phytochemistry*, 2005, (66) **21**, 2595–2601.

10. Abdel Moneim, A. E., Dkhil, M., Al-Quraishy, S. The potential role of *Portulaca oleracea* as a neuroprotective agent in rotenone-induced neurotoxicity and apoptosis in the brain of rats. *Pesticide Biochemistry and Physiology*, 2013, **105**, 203–212.

11. Simopoulos, A. P., Tan, D. X., Manchester, L. C., and Reiter, R. J. Purslane: a plant source of omega-3 fatty acids andmelatonin, *Journal of Pineal Research*, 2005, (39) **3**, 331–332.

12. Venkateshwari, V., Vijayakumar, A., Vijayakumar, A. K., Reddy, L., Prasanna, A., Srinivasan, M., and Rajasekharan, R. Leaf lipidome and transcriptome profiling of *Portulaca oleracea*: characterization of lysophosphatidylcholine acyltransferase. *Planta*, 2018, (2) **248**, 347-367.

13. Ayerza, R. & Coates W. Protein content, oil content and fatty acid profiles as potential criteria to determine the origin of commercially grown chia (*Salvia hispanica* L.). *Ind Crops Prod.*, 2011, (2) **34**,1366–1371.

14. Cumberford, G., Hebard, A. Ahiflower oil: A novel non-GM plant-based omega-3+6 source. *Lipid Technol*., 2015, (9) **27**, 207–210.

15. Simopoulos, A. P., Norman, H. A., Gillaspy, J. E. and Duke, J. A. Common purslane: a source of omega-3 fatty acids and antioxidants. *Journal of the American College of Nutrition*, 1992, (4) **11,** 374-82.

16. Napolitano, A. Cerulli, A., Pizza, C. and Piacente, S. Multi-class polar lipid profiling in fresh and roasted hazelnut (*Corylus avellana* cultivar "Tonda di Giffoni") by LC-ESI/LTQOrbitrap/MS/MSn. *Food Chemistry*, 2018, **269**, 125–135.

17. Rod-in, W., Monmai, C., Shin, I., You, SY. and Park J.W. Neutral Lipids, Glycolipids, and Phospholipids Isolated from Sandfish (*Arctoscopus japonicus*) Eggs, Exhibit Anti-Inflammatory Activity in LPS Stimulated RAW264.7 Cells through NF-κB and MAPKs Pathways. *Mar. Drugs*, 2020, **18**, 480.

18. Yang, Y., Zhang, T., Zhou, G., Jiang, X., Tao, M., Zhang, J., Zeng, X., Wu, Z., Pan, D. and Guo, Y. Prevention of Necrotizing Enterocolitis through Milk Polar Lipids Reducing Intestinal Epithelial Apoptosis. *J. Agric. Food Chem*., 2020, (26) **68**, 7014-7023.

19. Holzl, G.and Dormann, P. Chloroplast Lipids and Their Biosynthesis. Annu. *Rev. Plant Biol*., 2019, **70**, 51–81.

20. Okazaki, Y., Otsuki, H., Narisawa, T., Kobayashi, M., Sawai, S., Kamide, Y., Kusano, M., Aoki, T., Hirai, M. Y. and Saito, K. A new class of plant lipid is essential for protection against phosphorus depletion. *Nat. Commun*, 2013, **4**, 1510.

21. D'Urso, G., Napolitano, A., Cannavacciuolo, C., Masullo, M. and Piacente, S. Okra fruit: LC-ESI/LTQOrbitrap/MS/MSn based deep insight on polar lipids and specialized metabolites with evaluation of anti-oxidant and antihyperglycemic activity. *Food & Function*, 2020, (9) **11**, 7856-7865.

22. Lipan, L., Collado-González, J., Domínguez-Perles R., Corell, M., Bultel-Poncé, V., Galano, J-M., Durand, T., Medina, S., Gil-Izquierdo, A and Carbonell-Barrachina, A. Phytoprostanes and Phytofurans Oxidative Stress and Bioactive Compounds. *J. Agric. Food Chem*., 2020, **68**, 7214−7225.

23. Ruesgas-Ramón, M., Figueroa-Espinoza, M. C., Durand, E., Suárez-Quiroz, M.L., González-Ríos, O., Rocher, A., Reversat, G., Vercauteren, J., Oger, C., Galano, J-M., Durand, T., and Vigor, C. Identification and quantification of phytoprostanes and phytofurans of coffee and cocoa by- and co-products. *Food Funct*., 2019, **10**, 6882.

24. Yonny, M. E., Rodriguez, T. A., Cuyamendous, C., Reversat, G., Oger, C., Galano, J-M., Durand, T., Vigor, C. and Nazareno, M. A. Thermal Stress in Melon Plants: Phytoprostanes and Phytofurans as Oxidative Stress Biomarkers and the Effect of Antioxidant Supplementation. *J. Agric. Food Chem*., 2016, **64**, 8296−8304.

25. Rund, K. M., Ostermann, A. I., Kutzner, L., Galano, J-M., Oger, C., Vigor, C., Wecklein, S., Seiwert, N., Durand, T. and Schebb, N. H. Development of an LC-ESI(-)-MS/MS method for the

simultaneous quantification of 35 isoprostanes and isofurans derived from the major n3- and n6-PUFAs. *Analytica Chimica Acta*, 2018, **1037**, 63-74.

26. Farag, O. M., Abd-Elsalam, R. M., Ogaly, H. A., Ali, S. E., El Badawy, S. A., Alsherbiny, M. A., Li, C. G. and Ahmed, K. A. Metabolomic Profiling and Neuroprotective Effects of Purslane Seeds Extract Against Acrylamide Toxicity in Rat's Brain. *Neurochemical Research*, 2021, **46**, 819–842

27. Napolitano, A., Benavides, A., Pizza, C. and Piacente, S. Qualitative on-line profiling of ceramides and cerebrosides by high performance liquid chromatography coupled with electrospray ionization ion trap tandem mass spectrometry: The case of Dracontium loretense. *Journal of Pharmaceutical and Biomedical Analysis*, 2011, **55**, 23–30.

29. Cuadrado, A., Rojo, A. I., Wells, G., Hayes, J.D., Cousin, S.P., Rumsey, W.L., Attucks, O.C., Franklin, S., Levonen, A.L., Kensler, T.W., and Dinkova- Kostova A.T. Therapeutic targeting of the NRF2 and KEAP1 partnership in chronic diseases. *Drug discovery*, 2019, **18**, 295- 317.

30. Ahmadian, M., Suh, J.M., Hah, N., Liddle, C., Atkins, A.R., Downes, M. and Evans R.M. PPARγ signaling and metabolism: the good, the bad and the future. *Nature Medicine*, 2017, (19) **5**, 557-566.

31. Medina, S., Gil-Izquierdo, A., Durand, T., Ferreres, f. and Domínguez-Perles, R. Structural/Functional Matches and Divergences of Phytoprostanes and Phytofurans with Bioactive Human Oxylipins. *Antioxidants*, 2018, **7**, 165.

32. Abdel Moneim, A. E. The neuroprotective effects of purslane (*Portulaca oleracea*) on rotenone-induced biochemicalchanges and apoptosis in brain of rat," *CNS & Neurological Disorders—Drug Targets*., 2012, (12) **6**, 830–841.

33. Wang, W., Gu, L., Dong, L., Wang, X., Ling, C., and Li, M. Protective effect of *Portulaca oleracea* extracts on hypoxic nerve tissue and its mechanism. *Asia Pac J Clin Nutr*., 2007, (1) **16,** 227-233.

34. Jiao, Z-Z., Yue, S., Sun, H-X., Jin, T-Y., Wang, H-N., Zhu, R-X., and Xiang, L. Indoline Amide Glucosides from *Portulaca oleracea*: Isolation, Structure, and DPPH Radical Scavenging *Activity. J. Nat. Prod*., 2015, **78**, 2588−2597.

35. Tanaka, Y., Sasaki, N., and Ohmiya, A. Biosynthesis of plant pigments: anthocyanins, betalains and carotenoids. *The Plant Journal* 2008, **54**, 733–749.

36. Liu, Z., Zhou, T., Ziegler A. C., Dimitrion, P., and Zuo L. Oxidative Stress in Neurodegenerative Diseases: From Molecular Mechanisms to Clinical Applications. *Oxidative Medicine and Cellular Longevity*, 2017, 1-11.

37. Cavalcante S. F. dA. Simas, A.B.C., Barcellos, M.C., De Oliveira, V.G.M., Sousa R. G., Cabral, P.A. dM., Kuca, K., and França, T. C. C. Acetylcholinesterase: the HUB for neurodegenerative disease and chemical weapon convention. *Biomolecules*, 2020, **10**, 414.

39. Mair, C. E., Grienke, U., Wilhelm, A., Urban, E., Zehl, M., Schmidtke, M., and Rollinger, J. M. Anti-Influenza Triterpene Saponins from the Bark of *Burkea Africana*. *J. Nat. Prod*., 2018, **81**, 515−523.

40. Vogl, S., Atanasov, A. G., Binder, M., Bulusu, M., Zehl, M., Fakhrudin, N., Heiss, E. H., Picker, P., Wawrosch, C., Saukel, J., Reznicek, G., Urban, E., Bochkov, V., Dirsch, V. M. and Kopp, B. Evid. -*Based Complementary Altern. Med*., 2013, **39**, 5316.

41. Heiss, H. E., Tran, T. V. A., Zimmermann, K., Schwaiger, S., Vouk, C., Mayerhofer, B., Malainer C., Atanasov, A. G., Stuppner, H. and Dirsch. V. M. Identification of Chromomoric Acid C-I as an Nrf2 Activator in *Chromolaena odorata*. *J. Nat. Prod*., 2014, **77**, 503−508.

42. Resetar, M., Liu, X., Herdlinger, S., Kunert, O., Pferschy-Wenzig, E-M., Latkolik, S., Steinacher, T., Schuster, D., Bauer, R., and Dirsch, V. M. Polyacetylenes from *Oplopanax horridus* and *Panax ginseng*: Relationship between Structure and PPARγ Activation. *J. Nat. Prod*., 2020, **83**, 918−926.

43. Rakonczay, Z. Potencies and selectivities of inhibitors of acetylcholinesterase and its molecular forms in normal and Alzheimer's disease brain. *Acta Biologica Hungarica*, 2003, **54** (2),183–189.

44. Balkrishna, A., Pokhrel, S., Tomer, M., Verma, S., Kumar A., Nain, P., Gupta, A. and Varshney A. Anti-Acetylcholinesterase Activities of Mono-Herbal Extracts and Exhibited Synergistic Effects of the Phytoconstituents: A Biochemical and Computational Study. *Molecules*, 2019, **24**, 4175.

45. Voynikov, Y., Nedialkov, P., Gevrenova, R., Zheleva-Dimitrova, D., Balabanova, V., Dimitrov, I. UHPLC-Orbitrap-MS Tentative Identification of 51 Oleraceins (Cyclo-Dopa Amides) in *Portulaca oleracea* L. Cluster Analysis and MS2 Filtering by Mass Difference. *Plants,* 2021, **10**, (9), 1921.

46. Jiao, Z., Wang, H., Wang, P., Sun, H., Yue, S., Xiang, L. Detection and quantification of cyclo-dopa amides in Portulaca oleracea L. by HPLC-DAD and HPLC-ESI-MS/MS. *J. Chin. Pharm. Sci*, 2014, **23**, (8), 533-542

Bronstein, I., Martin, C. S., Fortin, J. J., Olenes, C. E. M. and Voyta, S. Chemioluminescence: sensitive detection technology for reporter gene assays. *Clinical chem*., 1996, (42) **9**, 1542-1546.

Castellano, J. M., Guinda, A. Delgado, T. Rada, M. and Cayuela, J.A. Biochemical Basis of the Antidiabetic Activity of Oleanolic Acid and Related Pentacyclic Triterpenes. *Diabetes*, 2013, **62**,1791–1799.

Ellman, G.L., Courtney, K.D., Andres, V., Featherstone, R.M. A new and rapid colorimetric determination of acetylcholinesterase activity. *Biochem Pharmacol*., 1961, **7**, 88–95

Chapter 2

Daikon sprouts (*Raphanus sativus* var. longipinnatus): specialized metabolites and evaluation of the antioxidant activity

State of the art and purposes

The sprouts of *Raphanus sativus* var longipinnatus (Brassicaceae) are commonly known as kaiware daikon in Japanese traditional cuisine. This food product belongs to the category of "microgreens", edible garnishes largely used in gourmet cuisine for visual interest and piquant flavor. Despite the charm as a novel food, microgreens are particularly characterized by healthy promoting effects. A new field of the vegetable industry focuses attention on the production of microgreens to satisfy the rising interest of consumers toward the daily intake of high nutritional values and healthy food sources. Moreover, the rising worldwide expansion of Asiatic foods, along with the easy management of the production of microgreens in controlled conditions as hydroponic cultivations, favored the widespread cultivation and culinary use of this product. [1,2]

The discovery of polyphenolics and glucosinolates from Oriental varieties of the sprouts of *R. sativus*, able to reduce oxidative damages and exert cancer-preventing activity, encouraged the study of the chemical profile of the same species cultivated in Italy as well as the investigation of their biological activity.

A comprehensive phytochemical study based on high-resolution analytical methods was carried out on daikon sprouts aimed at defining the metabolite profile of the polar fraction. A preliminary LC-HRMS analysis of methanol extract of sprouts purchased from Italian producers (Cesena-Italy) highlighted the occurrence of glucosinolates and complex hydroxycinnamic acid derivatives linked to different sugars. The structure of phenolics was delined by accurate NMR analysis of isolated compounds leading to the definition of two structures never reported in the literature. Moreover, the antioxidant capacity of methanol extract was compared to other eco-friendly extracts through $DPPH^{\cdot}$ and $ABTS^{\cdot+}$ radical scavenging assays and *in vitro* evaluation of the activation of Nrf2 pathway.

2.1 Analysis of the polar fraction of the sprouts by LC-ESI/LTQOrbitrap/MS/MS and NMR experiments

Daikon sprouts (Raphanus sativus L., var. longipinnatus)

Belonging to the category of microgreens, sprouts are the young seedling of plants

grown from the seeds of vegetables, herbs, or other plants. They are characterized by two cotyledons made by a pair of true leaves emerging from the stem. Usually, they are harvested within 7 to 10 days after sowing.

2.1.1. Results and discussion

Qualitative analysis of the MeOH extract of R. sativus sprouts

To achieve a preliminary overview of daikon sprouts' chemical composition, the analysis of MeOH extract by LC-HRMS experiment was carried out. The accurate study of the LC-HRMS profile (**Figure 2.1**) suggested the occurrence of multiple classes of metabolites, evidencing the complexity of the analyzed plant matrix. In particular, the occurrence of glucosinolates (blue pointers), poli-hydroxycinnamic acid derivatives (yellow pointers), and oxylipins (green pointers) was highlighted. While a detailed HRMS/MS analysis was enough to define the glucosinolates by the alignment of thousands MS data reported in libraries for Brassicaceae family (**Table 2.1**), the identification of complex polyphenolics required further analyses. In order to unambiguously determine their chemical structure by NMR experiments, the butanol/water repartition of the MeOH extract was carried out to concentrate phenolics in the butanol fraction, then purified by HPLC-UV. The isolated compounds were analyzed by ^{1}H and 2D NMR experiments, and the identity was confirmed by HRMS/MS analysis.

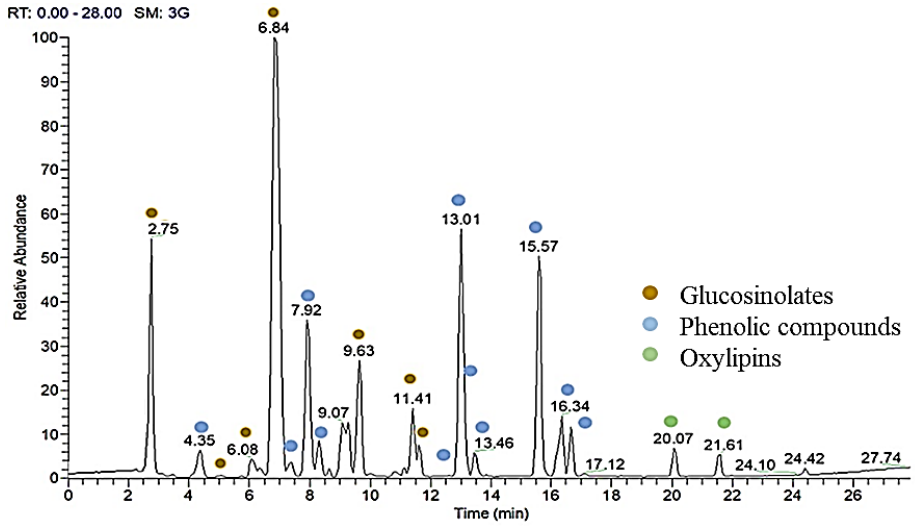

Figure 2.1 LC-HRMSMS profile in negative ionization mode of buthanol faction from MeOH extract of *R. sativus* sprouts

The described analytical workflow led to the identification of a considerable number of methionine glucosinolate derivatives as glucoraphenin, glucoerucin and glucoraphasatin, already reportedy in the species[14], while indolic glucosinolates as hydroxyglucobrassicin and methoxyglucobrassicin were reported for the first time in the species along with phenolic glucosinolates as sinapoylglucoraphanin and benzoylglucoraphanin.

Moreover, glycosylated hydroxycinnamic acid derivatives were defined (**Table 2.1**) namely methylsinapate (**5**), sinapoyl-1-*O*-*β*-D-glucopyranoside (**6**), feruloyl-1-*O*-*β*-D-glucopyranoside (**7**), sinapic acid (**11**), 3-*O*-sinapoyl-6'-*O*-sinapoyl-sucrose (**12**), 1,2-*O*-disinapoyl-β-D-glucopyranoside (**15**), 3,4-*O*-disinapoyl-6'-*O*-sinapoylsucrose (**17**). Among the following compounds already reported by Takaia et al., 2003 in daikon sprouts produced in Japan, the compound 3-*O*-feruloyl-6'-*O*-sinapoylsucrose (**14**) was detected for the first time in the species and 1-*O*-feruloyl-2-*O*-sinapoyl-β-D-glucopyranoside (**16**) was never reported in literature.

Moreover, linear oxylipins 9,12,13-trihydroxioctadeca-10-dienoic acid (**18**) and 9,12,13-trihydroxioctadeca-10-enoic acid (**19**) were identified for the first time in

the species by the detailed analysis of tandem mass spectra and data alignment with data reported in the literature.

Glucosinolates

Glucosinolates (GSLs) are specialized metabolites containing nitrogen and sulfur, mainly found in Brassicaceae. Approximately 200 GSLs are known to exist naturally in plants. GSLs are classified into several groups by the structure of the side chain. According to the modified amino acid content, three main groups exist: aliphatic, indolic, and aromatic. Aliphatic GSLs are derived from methionine, while indolic and aromatic GSLs originate from tryptophan and phenylalanine, respectively.

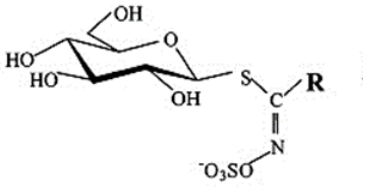

Kang et al., 2020 reported the aliphatic GSL biosynthesis in the Brassicaceae family. It involves three independent phases: (i) chain elongation of precursor amino acids, (ii) core structure synthesis by partial amino acid conversion, and (iii) chain modification of the side amino acids. Major genes involved in GSL biosynthesis have been reported in the Brassicaceae family, including *Raphanus sativus*. Major enzymes and transporters for aliphatic GSL biosynthesis in the Brassicaceae family include branched-chain aminotransferases (BCATs), methylthioalkylmalate synthases (MAMs), isopropylmalate isomerases (IPMIs), isopropylmalate dehydrogenase (IPMDH), bile acid transporter 5 (BAT5), CYP79 cytochrome P450 monooxygenases (CYP79F1), CYP83 cytochrome P450 monooxygenase (CYP83A1), S-alkyl-thiohydroximate lyase (SUR1), UDP-glucosyl transferase 74 (UGT74), sulfotransferases (SOTs) and flavin-monooxygenase glucosinolate S-oxygenases (FMOGS-OXs). MYB28 and MYB29 are transcription factors that regulate the genes involved in aliphatic GSL biosynthesis.[3]

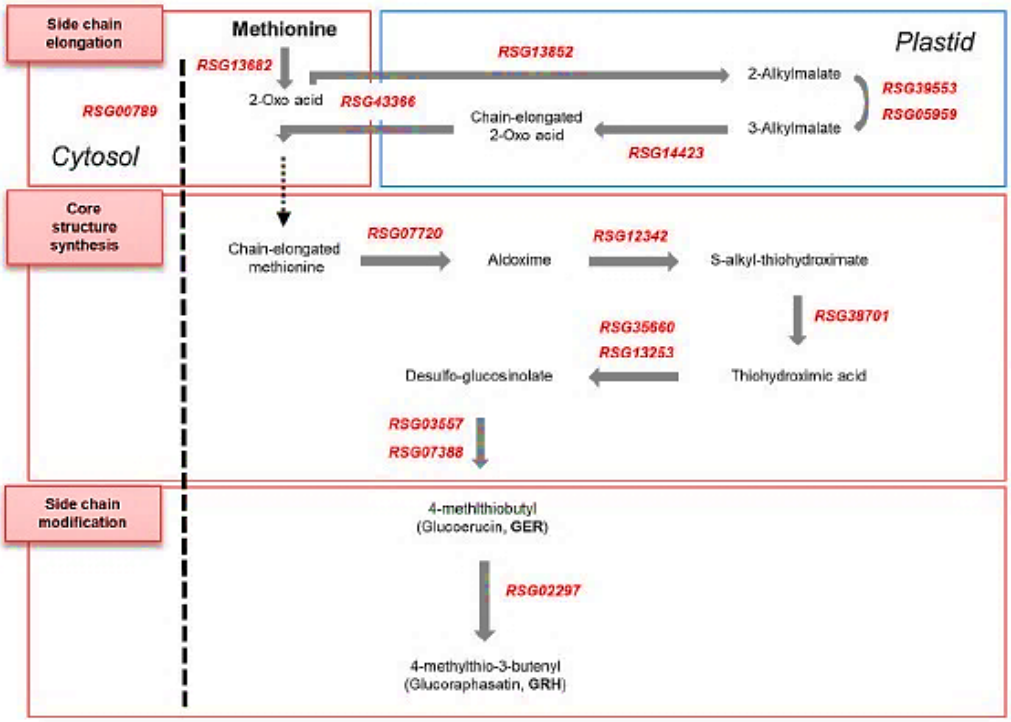

Figure 2.2 Biosynthesis of glucosinolates

The uptake of Cruciferous vegetables on a daily basis is reported to be cancer-preventing.[4] Isothiocyanates (ITCs) are generated as the hydrolyzed product of glucosinolates by the enzyme myrosinase, activated by the plant at the moment of the harvesting, promoting the activation of metabolic phase II enzyme involved in detoxification and antioxidant cellular defense.

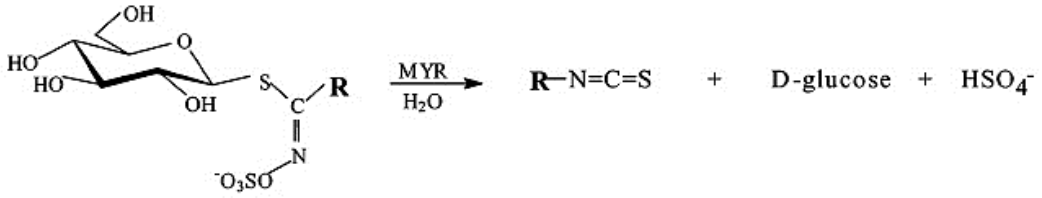

Figure 2.3 Hydrolisis of glucosinolates by myrosinase enzyme

Besides the aliphatic glucosinolates derivated by methionine-like moiety, already reported by Barillari et al., 2005 in daikon sprouts (compounds **1**, **3,** and **4; Table 2.1**), the occurrence of indolic and phenolic glucosinolates was highlighted in LC-HRMS/MS profile of MeOH extract. In particular, the indolic glucosinolates hydroxyglucobrassicin and methoxyglucobrassicin (compounds **2** and **8**), **the** phenolic glucosinolates sinapoylglucoraphanin and benzoylglucoraphenin (compounds **9** and **10,** respectively) were putatively characterized by the detailed analysis of diagnostic fragmentation pattern (**Table 2.1**). To the best of our knowledge, the overmentioned compounds **2**, **8**, **9**, **10** were reported in other Brassicaceae but have been identified in *R. sativus* sprout for the first time in the present work.

Table 2.1 Compounds identified in the buthanol fraction of daikon sprouts

n	t_r	*m/z*	ppm	Molecular formula	MS/MS	Compound
1	**2.75**	434.1692	-0.64	$C_{12}H_{21}O_{10}NS_3$	419, 354, 275, 259, 241, 195	Glucoraphenin[1]
2	**5.05**	463.0468	-1.95	$C_{16}H_{20}O_{10}N_2S_2$	301, 285, 267, 198	Hydroxyglucobrassicin[1]
3	**6.08**	420.1303	-1.26	$C_{12}H_{23}O_9NS_3$	275, 259, 195	Glucoerucin[1]
4	**6.84**	418.0292	-0.40	$C_{12}H_{21}O_9NS_3$	338, 275, 259, 241, 175	Glucoraphasatin[1]
5	**7.28**	237.0758	0.41	$C_{12}H_{14}O_5$	237	Methylsinapate [2]
6	**7.92**	385.1130	0.23	$C_{17}H_{22}O_{10}$	265, 247, 223, 205	1-*O*-Sinapoyl-β-D-glucopyranoside[2]
7	**8.11**	355.1024	0.11	$C_{16}H_{20}O_9$	217, 193, 175	1-*O*-Feruloyl-β-D-glucopyranoside[2]
8	**9.63**	477.0630	-1.91	$C_{17}H_{22}O_{10}N_2S_2$	397, 299, 281, 315, 275, 259, 235, 195	Methoxyglucobrassicin[1]
9	**11.41**	640.1726	-1.08	$C_{23}H_{31}O_{14}NS_3$	625, 465, 434, 325, 283, 223	Sinapoylglucoraphanin[1]
10	**11.53**	538.0502	-0.68	$C_{19}H_{25}O_{11}NS_3$	523, 379, 363	Benzoylglucoraphenin[1]
11	**12.94**	223.0607	2.81	$C_{11}H_{12}O_5$	164	Sinapic acid[2]
12	**13.05**	753.2516	-2.01	$C_{34}H_{42}O_{19}$	547, 529, 365, 325, 223	3-*O*-*S*inapoyl-6'-*O*-sinapoyl-sucrose [2]
13	**13.26**	193.0502	2.51	$C_{10}H_{10}O_4$	149, 134	Ferulic acid[2]
14	**13.37**	723.2121	-1.37	$C_{33}H_{40}O_{18}$	547, 529, 517, 499, 337	3-*O*-*F*eruloyl-6'-*O*-sinapoyl-sucrose [2]
15	**15.48**	591.1705	-0.62	$C_{28}H_{32}O_{14}$	385, 367, 352, 247, 223, 205	1,2-*O*-Disinapoyl-β-D-glucopyranoside [2]
16	**16.04**	561.1598	-1.01	$C_{27}H_{30}O_{13}$	367, 337, 284, 223	1-*O*-Feruloyl-2-*O*-sinapoyl-β-D-glucopyranoside[2]
17	**16.43**	959.2794	-0.91	$C_{45}H_{52}O_{23}$	753, 735, 529, 368	3,4,6'-*O*-Trisinapoylsucrose [2]
18	**20.07**	327.21674	0.43	$C_{18}H_{32}O_5$	309, 291, 229, 211, 171	9,12,13-trihydroxyoctadeca-10-15-dienoic acid[1]
19	**21.61**	329.23227	0.06	$C_{18}H_{34}O_5$	311, 299, 211, 171, 139, 127	9,12,13-trihydroxyoctadeca-10-enoic acid[1]

[1]compounds putatively identified by HRMS/MS analysis, [2]compounds unambiguously identified by isolation and NMR analysis

Poliphenolics

The class of p-hydroxycinnamic acids like sinapic acid (SinA), and its esters (SinE) analogues are present in different plants of Brassicaceae family. This class of specialized metabolites is involved in multiple biological processes in plants. The accumulation of SinA and its derivatives, along with other phenylpropanoids, is believed to favor the adaptation process in plants under environmental stress. Nowadays, these metabolites are increasingly drawing attention due to their bioactivities which include antioxidant, antimicrobial, anticancer, and UV filtering activities. As a result, these metabolites find applications in the pharmaceutical, cosmetic, and food industries.[5]

Sinapic acid and its derivatives are biosynthesized by plants via a set of chemical reactions. The biosynthesis involves the phenylpropanoid pathway via the formation of the shikimate intermediate. This route is composed of three sequential stages: (i) formation of phenylalanine via the shikimate pathway; (ii) non-oxidative deamination of phenylalanine followed by oxygenation to yield activated p-coumaroyl CoA; (iii) further transformations of p-coumaroyl CoA to afford a broad range of SinEs.[5] As an example, the biosynthesis of SinE from erythrose 4-phosphate and phosphoenolpyruvate (PEP) is shown in **Figure 2.4**.

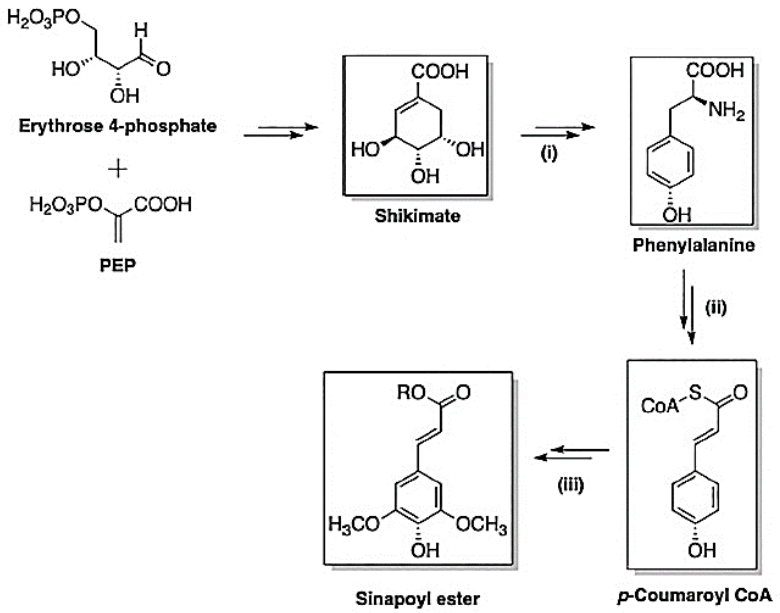

Figure 2.4 Three main stages of sinapic acid derivatives biosynthesis: (i): Formation of Phe; (ii): Formation 4-coumaroyl CoA intermediate; (iii) Formation of sinapoyl esters

Isolation and characterization

The LC-HRMS analysis was not sufficient to unambiguously identify hydroxycinnamic derivatives highlighted in the profile, characterized by sinapoyl or feruloyl moieties linked to different sugars units. The butanol fraction of daikon sprout was purified by RP-HPLC to afford pure compounds, of which the structures were unambiguously elucidated by ^{1}H and 2D NMR experiments (**Figure 2.5**).

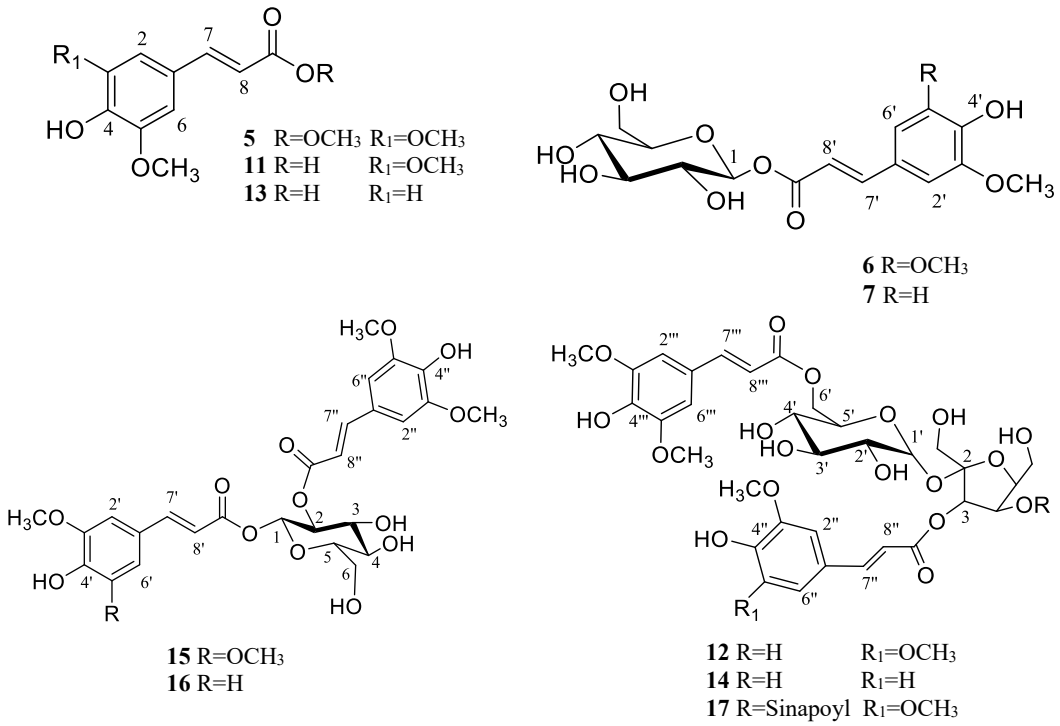

Figure2.5 Structures of compounds isolated from the butanol fraction of MeOH extract of daikon sprouts

The compounds methylsinapate (**5**), sinapoyl-1-*O*-*β*-D-glucopyranoside (**6**), feruloyl-1-*O*-*β*-D-glucopyranoside (**7**), sinapic acid (**11**) 3,6'-*O*-disinapoylsucrose (**12**), ferulic acid (**13**), 1,2-*O*-disinapoyl-β-D-glucopyranoside (**15**), and 3,4,6'-*O*-trisinapoyl-sucrose (**17**) were identified by comparison of their spectroscopic data with those reported in the literature (Takaya et al., 2003). Along with the over mentioned compounds, reported for the antioxidant activity by Takaia et al., 2003, the structure of 3-*O*-feruloyl-6'-*O*-sinapoylsucrose (**14**) was detected for the first time in the species, while 1-*O*-feruloyl-2-*O*-sinapoyl-β-D-glucopiranoside (**16**) was elucidated for the first time by the accurate interpretation of ^{1}H NMR and 2D NMR spectra (**Figures 2.6-2.9**).

The molecular formulae $C_{33}H_{40}O_{12}$ for compound **14** was determined by ^{13}C-NMR analysis, and HR-ESI-MS analysis in the negative ion mode. The HRMS spectrum of **14** showed a parent ion at *m/z* 723.2121 $[M–H]^-$. In the ^{1}H NMR spectrum, the resonances for two sugar units were evident. Furthermore, the ^{1}H NMR (Table 2.2) spectrum showed the presence of the typical proton signals of phenylpropanoid moieties; in particular, signals of two couple of trans olefinic protons at δ 6.46 and 6.47, (each 1H, d, J=15.8 Hz), and at δ 7.71 and 7.63 (each lH, d, J= 15.8 Hz) were observed along with signals of 1,3,4 substituted aromatic system at δ 7.24, (d, J=1.9 Hz), 7.07 (dd, J=1.9, 8.3 Hz), and 6.84 (d, J=8.3 Hz), and with one singlet signal of 1,3,4,5 substituted aromatic system at δ 6.99 (detailed NMR data in Table 2.2). These data confirmed the occurrence of one feruloyl moiety and one sinapoyl moiety.

The assignments of sugar protons were based on the 1D experiments (^{1}H and 1D TOCSY) along with 2D homonuclear (COSY and ROESY) and heteronuclear (HSQC and HMBC) spectra (**Table 2.2**). The 2D-COSY experiment allowed the sequential assignment of most of the resonances for each sugar ring. Indeed, the 2D experiments (**Figures 2.7-2.9**) clearly showed correlation signals for the H-1 to H-6 spin system of sugar residues. Cross peaks observed in the 2D experiments

displayed full coupling information which allowed the identification of proton patterns. Chemical shifts and coupling constants suggested the presence of a sucrose unit. However, the signals attributed to H-3 of fructose and to Ha-6', Hb-6' of glucose were downfield shifted. These values were in agreement with literature data reporting esterification at position C-3 of fructose and at C-6 of glucose. HMBC correlations allowed us to establish the linkage sites between sugars and the feruloyl and sinapoyl moieties. Thus, compound **14** was identified as 3-*O*-feruloyl-6'-*O*-sinapoyl-sucrose.

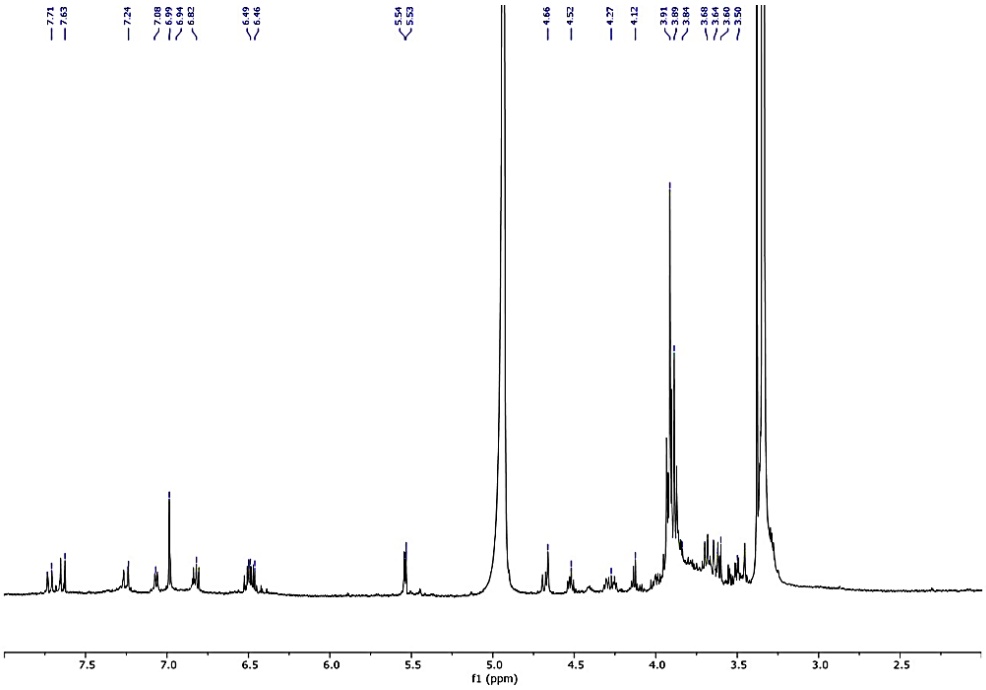

Figure 2.6 ^{1}H NMR spectrum of compound **14**

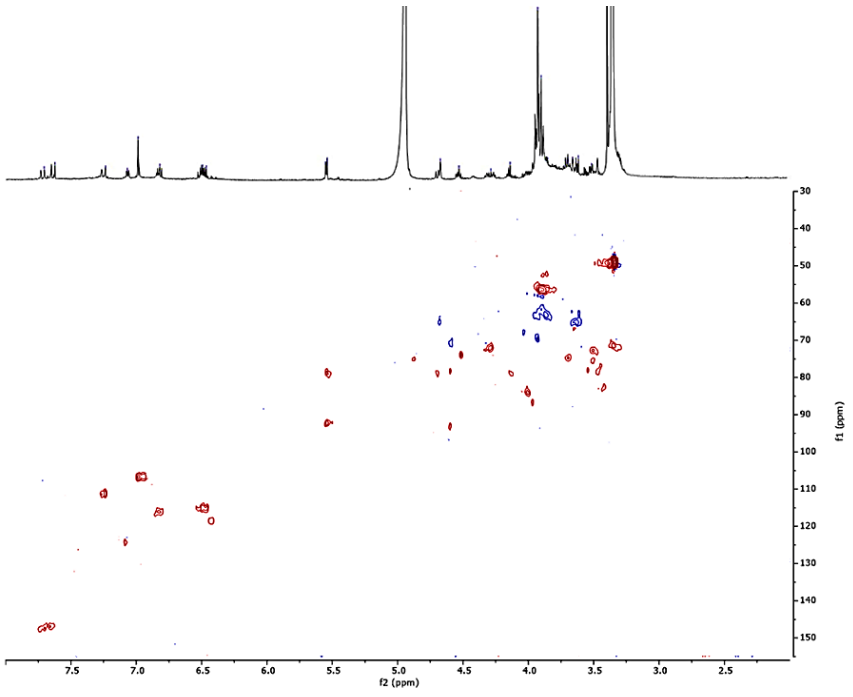

Figure 2.7 HSQC spectrum of compound **14**

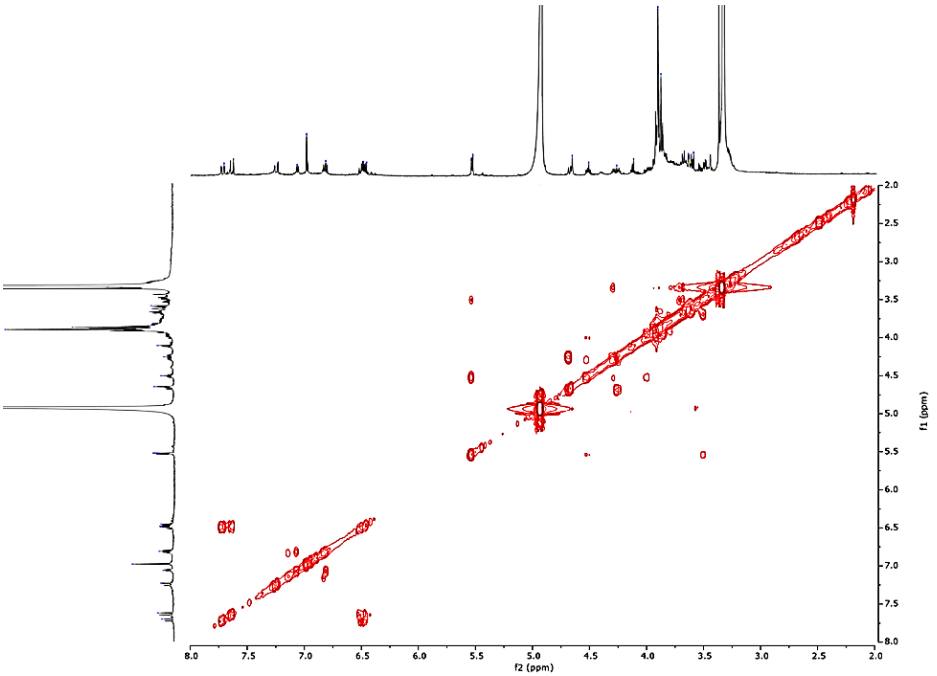

Figure 2.8 COSY spectrum of compound **14**

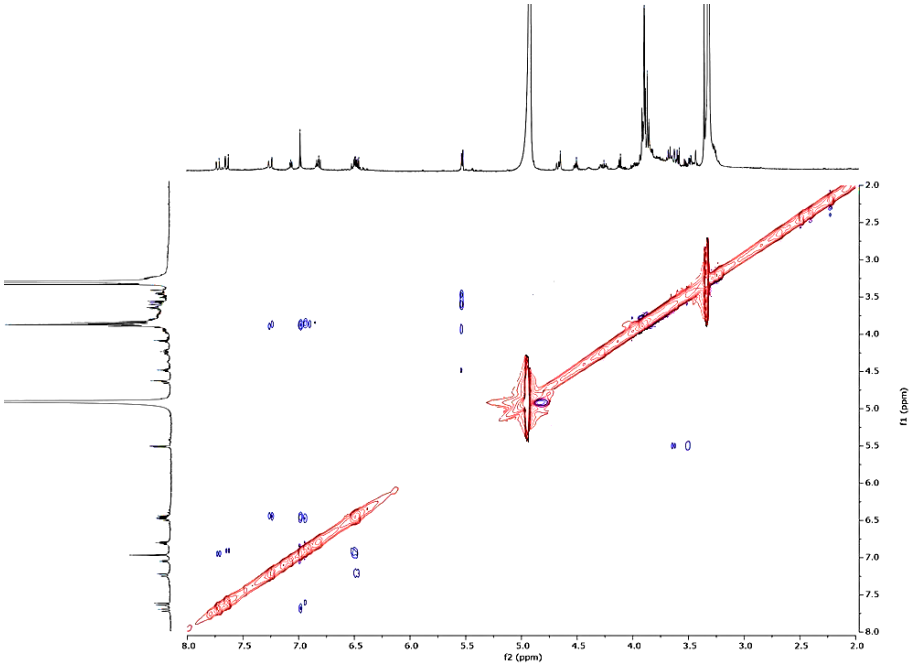

Figure 2.9 ROESY spectrum of compound **14**

The HR-ESI-MS spectrum of **16** (*m/z* 561.1598 $[M-H]^-$, calcd for $C_{27}H_{29}O_{13}$, 561.1588) supported a molecular formula of $C_{27}H_{30}O_{13}$. The MS/MS spectrum of this ion showed fragment ions at *m/z* 367.2461 $[M-H-194]^-$, due to the loss of a feruloyl unit and at *m/z* 337.1253 $[M-H-224]^-$ attributable to a sinapoyl moiety. The ^{13}C NMR spectrum showed 27 carbon signals, of which 21 were assigned to the aglycone moiety and 6 to a sugar portion (**Table 2.2**). The ^1H NMR spectrum displayed the presence of the typical proton signals of two phenylpropanoid derivatives. In particular, signals of two couple of trans olefinic protons at δ 6.34 and 6.42 (each ^1H, d, *J*=15.8 Hz) and at δ 7.69 and 7.64, (each ^1H, d, *J*= 15.8 Hz) were shown. Moreover, signals at δ 7.20 (d, *J*=1.9 Hz), 7.09 (dd, *J*=1.9, 8.3 Hz) and 6.82 (d, *J*=8.3 Hz) confirmed the 1,3,4 substituted aromatic system of a feruloyl moiety along with a singlet signal at δ 6.89 ascribable to 1,3,4,5 substituted aromatic system of a sinapoyl moiety (detailed NMR data in **Table 2.2**). The ^1H NMR spectrum displayed in the sugar region signals corresponding to one anomeric proton at δ 5.83 (d, *J* = 8.0 Hz) assigned to a glucose unit. A detailed analysis of HSQC, COSY, and HMBC experiments allowed us to attribute the signal at δ 5.10 as the H-2glc, downfield shifted for the formation of an ester linkage. An unambiguous determination of the sequence and linkage sites was obtained from the HMBC spectrum, which showed key correlation peaks between the proton signal at δ 5.83 (H-1glc) and the carbon resonance at δ 166.8 (C-9'), the proton signal at δ 5.10 (H-2glc) and the carbon resonance at δ 167.0 (C-9''). On the basis of the above evidence, the structure of compound **16** was established as 1-*O*-feruloyl-2-*O*-sinapoyl-β-D-glucopyranoside.

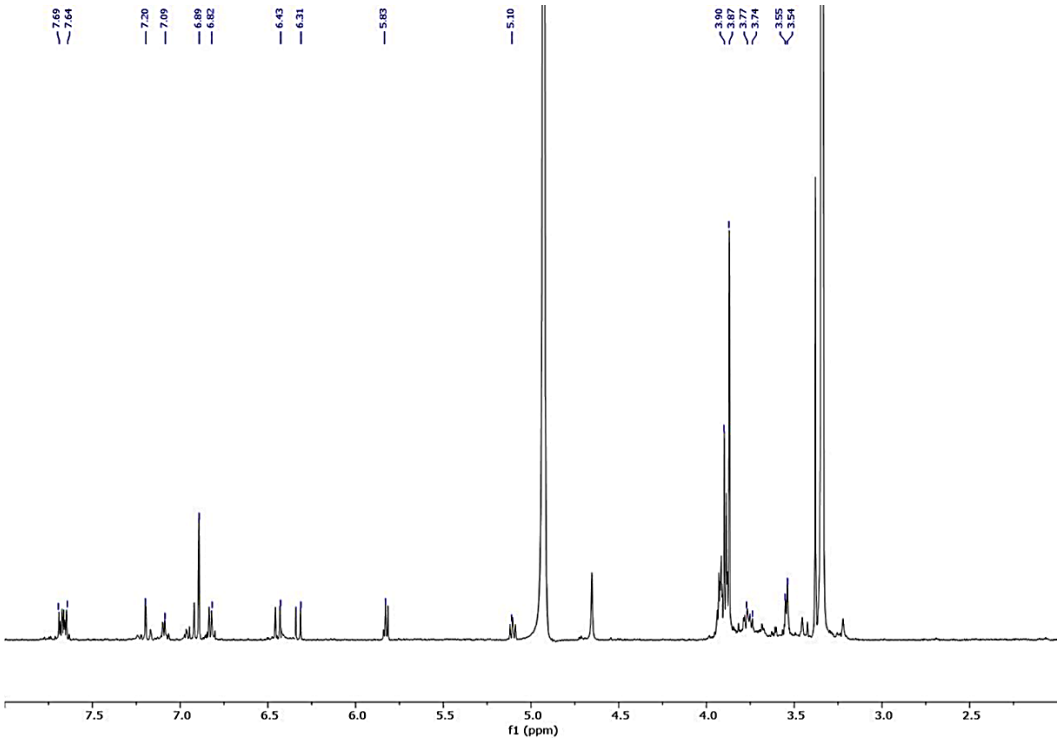

Figure 2.10 ^{1}H NMR spectrum of compound **16**

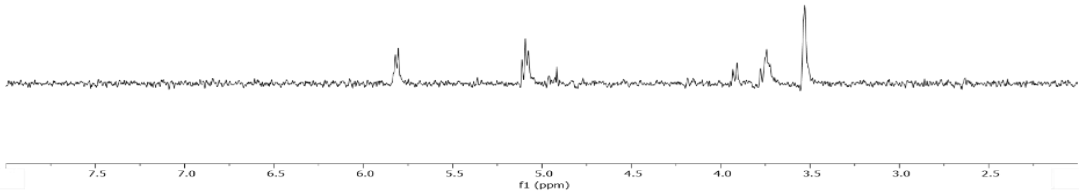

Figure 2.11 1D TOCSY spectrum of compound **16**

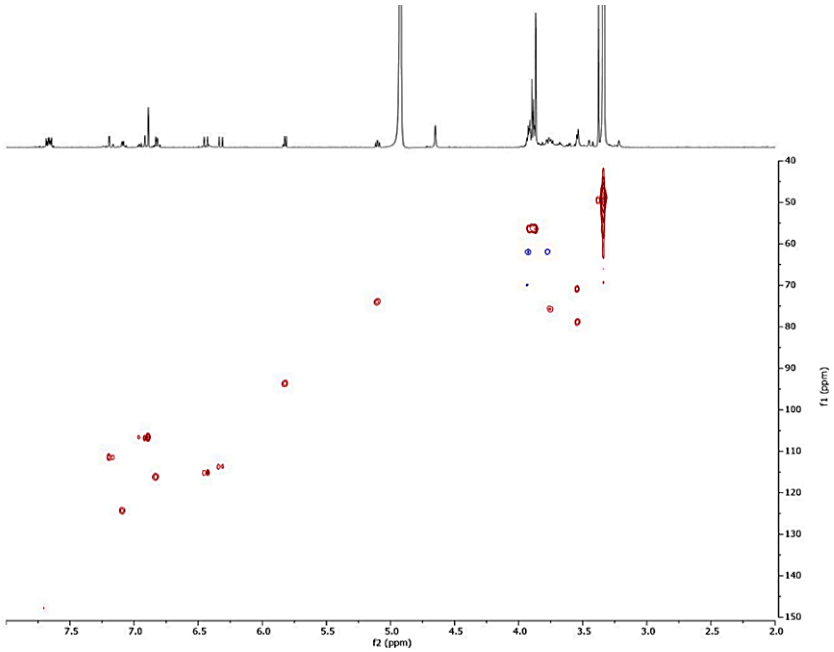

Figure 2.12 HSQC spectrum of compound **16**

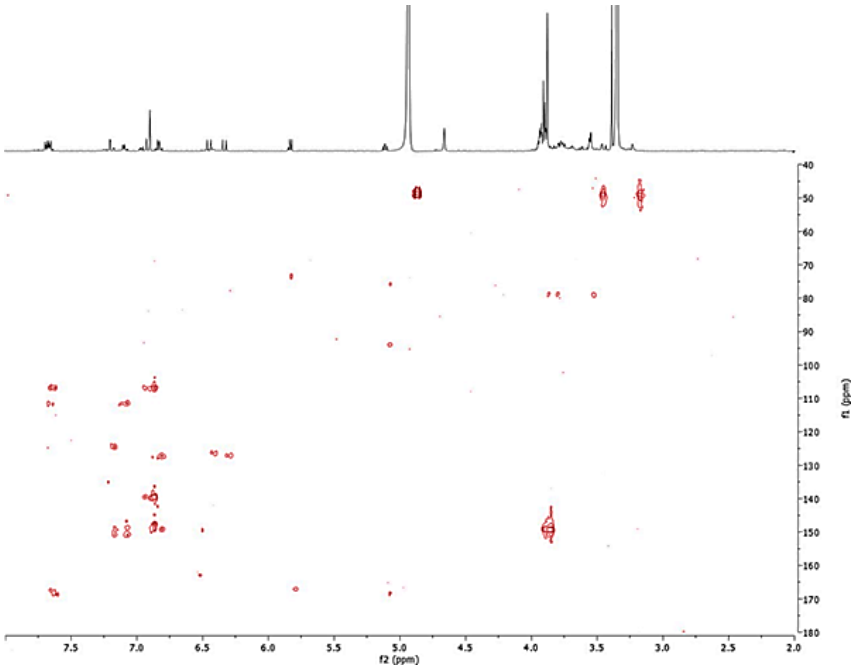

Figure 2.13 HMBC spectrum of compound **16**

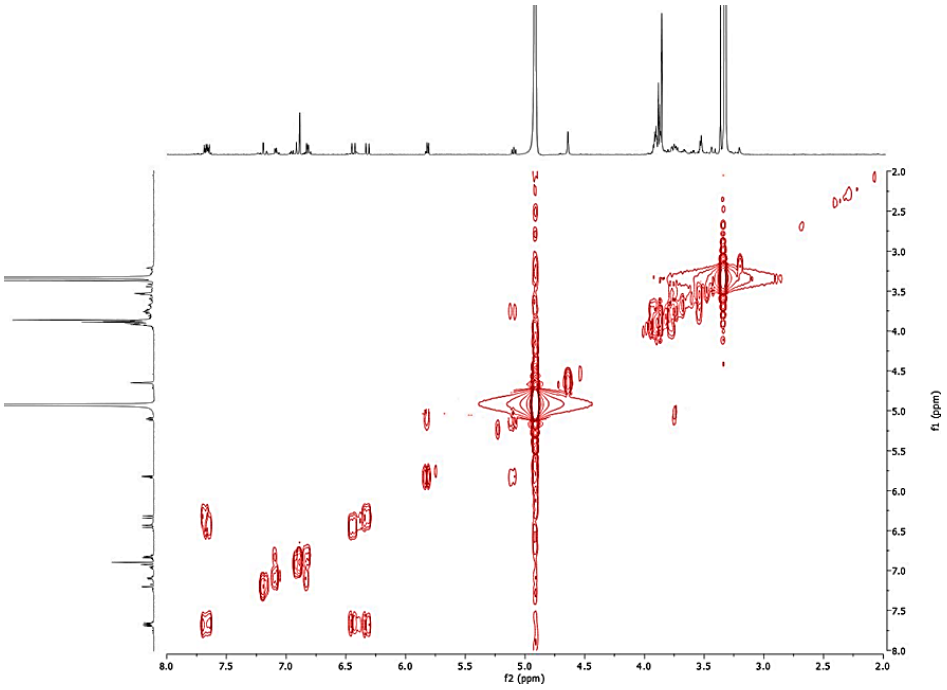

Figure 2.14 COSY spectrum of compound **16**

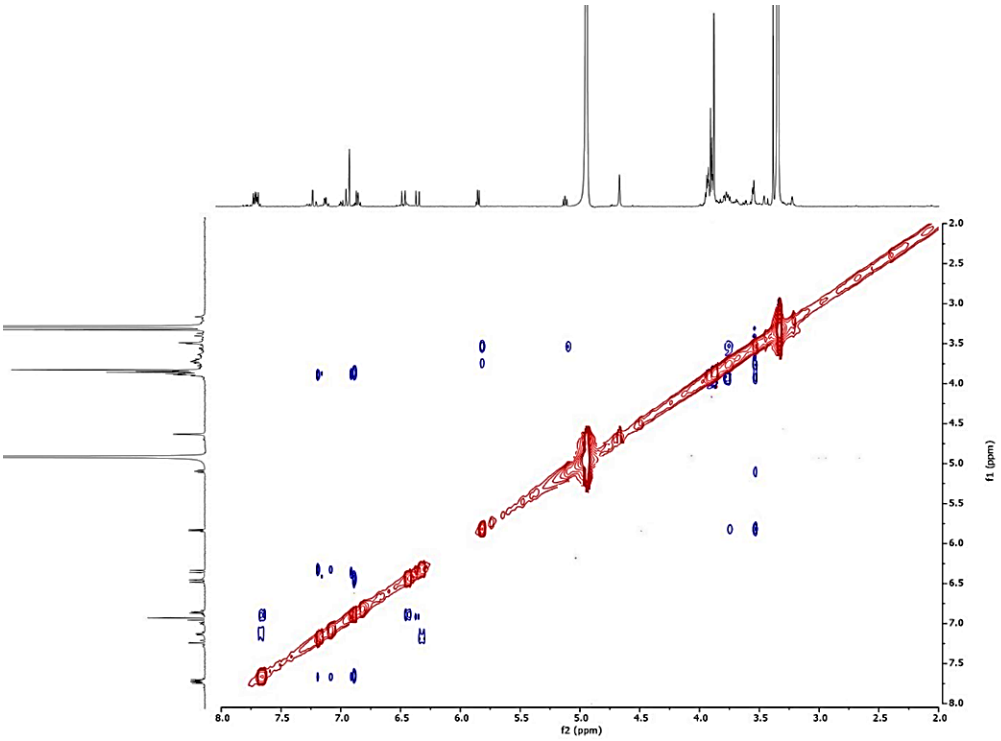

Figure 2.15 ROESY spectrum of compound **16**

Table 2.2 ^{13}C and ^{1}H NMR data of compounds **14** e **16** (600 MHz, δ ppm, in CD_3OD).

	14			**16**	
	δ_C	δ_H (*J* in Hz)		δ_C	δ_H (*J* in Hz)
Fructose				Glucose	
1	65.2	3.60 (d,12.0)	1	93.7	5.82 (d, 8.0)
		3.64 (d,12.0)			
2	104.1		2	74.2	5.10 (dd, 8.0, 9.0)
3	79.1	5.54 (d, 8.0)	3	76.8	3.74 (dd, 9.0, 9.0)
4	73.9	4.52 m	4	71.8	3.54 (dd, 9.0; 9.0)
5	84.0	4.12 m	5	79.0	3.55 (m)
6	63.4	3.84 m	6	62.0	3.93 (dd, 12.0, 2.5)
		3.95 m			3.77 (dd, 12.0, 4.5)
Glucose					
1'	92.3	5.53 (d, 4.0)		-	-
2'	72.0	3.50 (dd, 9.5; 4.0)		-	-
3'	74.2	3.68 (dd, 9.0; 9.0)		-	-
4'	71.5	3.34 (dd, 9.0; 9.0)		-	-
5'	72.0	4.27 (m)		-	-
6'	65.4	4.66 (dd, 12.0; 4.5)		-	-
		4.88 (dd, 12.0; 2.5)		-	-
3-*O*-Feruloyl moiety				1-*O*-Feruloyl moiety	
1"	127.2		1'	127.8	
2"	111.1	7.24 (d, 1.9)	2'	111.7	7.20 (d, 1.9)
3"	149.8		3'	150.1	
4"	147.6		4'	147.6	
5"	116.3	6.82 (d, 8.3)	5'	116.8	6.82 (d, 8.3)
6"	124.2	7.07 (dd, 1.9, 8.3)	6'	124.7	7.09 (dd,1.9; 8.3)
7"	149.1	7.71 (d, 15.8)	7'	149.6	7.69 (d, 15.8)
8"	116.1	6.47 (d, 15.8)	8'	116.3	6.31 (d, 15.8)
9"	166.5		9'	166.8	
OCH_3	56.4	3.89 s	OCH_3	56.7	3.90 s
6'-*O*-Sinapoyl moiety				2-*O*-Sinapoyl moiety	

1'''	125.5		1"	126.2	
2'''	107.5	6.99 s	2"	106.9	6.89 s
3'''	150.0		3"	148.9	
4'''	139.8		4"	139.0	
5'''	150.0		5"	148.9	
6'''	107.5	6.99 s	6"	106.9	6.89 s
7'''	148.2	7.63 (d, 15.8)	7"	148.5	7.64 (d, 15.8)
8'''	115.2	6.46 (d, 15.8)	8"	115.2	6.42 (d, 15.8)
9'''	167.0		9"	167.0	
OCH_3	56.4	3.91 s	OCH_3	56.7	3.87 s

2.2 Evaluation of the antioxidant activity of butanol and "green" extracts of daikon sprouts

2.2.1 Total phenolic content and radical scavenging activity

The preliminary antioxidant activity of the butanol extract in comparison with that exerted by "green" extracts (ethanol-water in different v/v ratios) was evaluated.

Folin-Ciocalteu assay determining the total phenolic content, along with $DPPH^{\cdot}$ and $ABTS^{\bullet+}$ assays for radical scavenging determination were carried out as a preliminary screening of the activity. The green EtOH 70% (v/v) extract showed the highest total phenolic content with a value of 400.95 gallic acid equivalent (**Table 2.3**).

$ABTS^{\bullet+}$ assay was carried out to evaluate the antioxidant properties of the extracts. Standard Trolox solutions were employed to obtain the calibration curve. The extracts were tested, and the obtained results were used to evaluate their antioxidant activity, expressed as TEAC, defined as the concentration (mM) of a standard Trolox solution exerting the same antioxidant activity of a 1 mg/mL solution of the tested extract. The results showed the highest antioxidant activity for EtOH 70% v/v extract with a TEAC value of 1.95. All the other extracts, except the $CHCl_3$ extract, showed good antioxidant activity with TEAC values ranging from 1.02 to 1.70 (**Table 2.3**).

Also the DPPH assay revealed the highest scavenging activity for the EtOH 70% extract (93.97 μg/mL) (**Table 2.3**).

Table 2.3 Total Phenolic Content**,** DPPH$^{\bullet}$and ABTS$^{\bullet+}$ radical scavenging activity of several extracts and green extracts of daikon sprout

Extracts	Total Phenolic Content (GAE[a] ± SD)	DPPH$^{\bullet}$ (IC_{50}, µg/ml ± SD)	ABTS$^{\bullet+}$ (TEAC[b] ± SD)
MEOH	269.36 ± 0.11	216.32 ± 0.12	1.02 ± 0.21
ETOH	283.56 ± 0.13	122.43 ± 0.12	1.70 ± 0.13
ETOH/H_2O (70% V/V)	400.95 ± 0.33	93.97 ± 0.19	1.95 ± 0.14
ETOH/H_2O (50% V/V)	322.40 ± 0.28	119.93 ± 0.18	1.34 ± 0.12
$CHCL_3$	91.12 ± 0.22	313.92 ± 0.12	0.39 ± 0.11
Ascorbic acid	-	4.53±0.01µM	-
Quercetin 3-O-Gluc	-	-	1.81 ± 0.19 mM

[a]Values are expressed as gallic acid equivalent (GAE) mg/g of dried extract. [b]Values are expressed as concentration (mM) of a standard Trolox solution exerting the same antioxidant activity of a 1 mg/mL solution of texted extract.

2.2.2 in vitro evaluation of Nrf2 pathway assessed by a reporter gene assay

The promising preliminary results of the radical scavenging activity of extracts encouraged to further evaluate the antioxidant activity. *In vitro* assay for the activation of Nrf2 pathway, a biological target involved in cellular detoxifying mechanisms, was performed.

The ubiquitously expressed nuclear factor erythroid 2-related factor 2 (Nrf2) is an important mediator of redox regulation, detoxification, protein homeostasis, metabolism, DNA repair, and mitochondrial function. As Nrf2 takes center stage in preserving cellular homeostasis, its activity itself is also tightly regulated. The most prominent and consequently the most investigated negative regulator of Nrf2 is the adapter for ubiquitin ligases Kelch-like-ECH-associated protein 1 (KEAP1). Under basal conditions, a KEAP1 dimer binds Nrf2 in the cytosol of the cell, leading to its polyubiquitylation and subsequent degradation. Upon exposure to oxidative stress or electrophilic xenobiotics, KEAP1 undergoes a Cys-dependent conformational change, causing a disruption of the bond with Nrf2. Consequently, Nrf2 can binds ARE elements of gene promoter (**Figure 2.16**)[29]

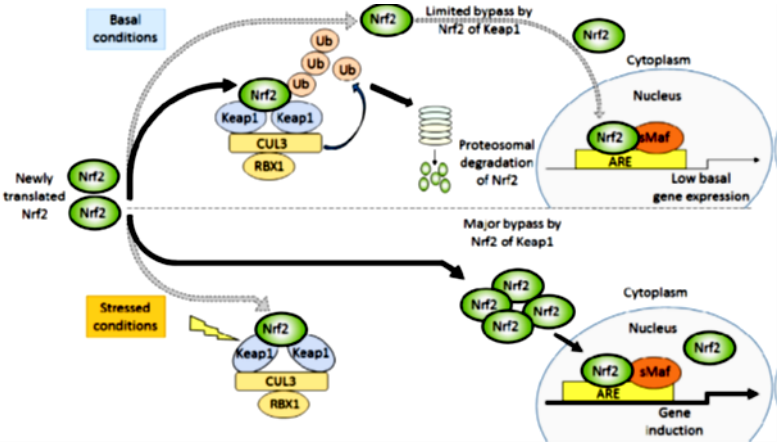

Figure 2.16 Cellular regulation of Nrf2

Due to its beneficial effects, Nrf2 has been established as a promising target for various diseases, including cancer, neurodegenerative diseases, diabetes, and cardiovascular disease.[29]

Cells constantly need to respond and adapt to insults like reactive oxygen species (ROS) and electrophiles that threaten to impede cell functions by damaging DNA and proteins. Since the uncontrolled accumulation of ROS and electrophiles leads to oxidative stress and subsequently to a degeneration of tissues, premature aging, apoptotic cell death, and cancer, cells react to these agents by activating special cellular machinery to protect themselves. Nrf2 plays the most prominent role in the inducible cell defense system. It mediates the expression of defensive genes that promote detoxification of chemicals and ROS and prevent the generation of free radicals. Important target genes of Nrf2 include the phase II enzymes heme oxygenase 1 (HMOX1) and glutamate-cysteine ligase catalytic subunit (GCLC). Further target genes of NRF2 include NAD(P)H dehydrogenase 1 (NQO1), which catalyzes quinone detoxification, and Glutathione S-transferase (GSTs).[6,7]

The methanol and "green" extracts of *R. sativus* sprouts were tested for the modulation of the Nrf2 pathway assessed by gene reporter assay. Fixed concentrations (30, 20, 10 and 5 µg/ml) of all samples were used in the assay. Cells were pre-treated with fluorescent probe CMFDA. After treatment with the tested extracts and fractions, the fluorescence related to alive cells remained in a range of 80-95%, excluding major cytotoxic effects (data not shown). **Figure 2.17** shows the data obtained from the Nrf2 (ARE)-dependent reporter gene assay. Data obtained from the *in vitro* assay were in accordance with the $DPPH^{\cdot}$ and TEAC results of green extracts. In fact, the green extracts EtOH 50% and EtOH 70% elicited a concentration-dependent induction of Nrf2 activity and were at 30 µg/ml more active (6.5- and 10-fold activation compared to control cells, respectively) than the used positive control (iberin, 3µM; 5-fold activation).

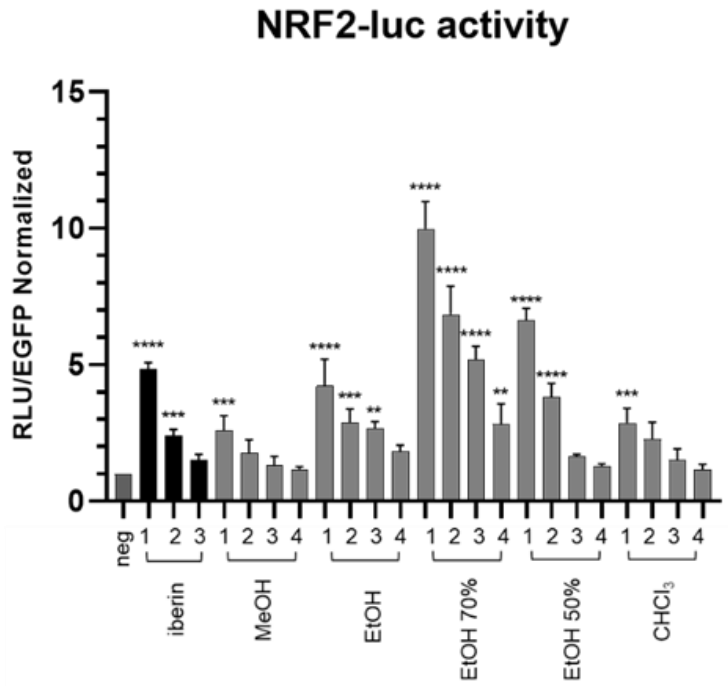

Figure 2.17 Activation of Nrf2 pathway through Nrf2-luc transfected HepG2 cells. Concentrations of iberin used as positive control 3, 1.5, 0.75µM (x values 1-3 respectively). Concentrations of tested compounds 30, 20, 10, 5 µg/ml (x values 1-4 respctively). Cell viability is evaluated in a range of 83-98%. Data are expressed in relative units. Bar charts represent the transactivation activity expressed as mean ± SD of three independent experiments, n=3, ****p<0.0001 (One-way ANOVA with Dunnett's post hoc test vs vehicle control)

2.3 Multivariate data analysis

Several classes of metabolites namely glucosinolates, polyphenols and oxylipins were detailed described by the overmentioned procedures employing high resolution techniques. Moreover, the antioxidant activity of several extracts was evaluated by preliminary radical scavenging and *in vitro* assays. With the aim to visualize a complex set of chemical and biological data reflecting the complex metabolome of the species in the early stage of growth and to correlate the biological activity to specific metabolites, a multivariate analysis by targeted and untargeted approach was carried out. In particular, statistical analysis were carried out. Specifically, an exploratory data analysis was performed by Principal Component Analysis (PCA) and Partial Least Squares-Discriminant Analysis (PLS-DA) methods were applied to discriminate the samples.

Multivariate data analysis has proved over time to be a powerful statistical technique, especially useful in processing large data sets when more than one observation is involved. Due to its effectiveness in making data quick and plain, it is nowadays widely employed for several applications in industrial and scientific fields, like control and optimization processes, quality controls, research and development.[10]

In the present study, the chemical content of daikon sprout was defined by employing different extraction protocols. The prepared extracts were submitted to NMR experiments and the raw data were first filtered by using MestreNova software, and then processed by using SIMCA-P+ software.

Untargeted metabolite profiling of R. sativus (var longipinnatus)

The ^{1}H NMR spectra of extracts of *R. sativus* sprouts obtained with different solvents were compared (**Figure 2.18**). These included solvents commonly known to have a good capacity for the extraction of specialized metabolites like methanol, ethanol, chloroform but also "green" hydroalcoholic mixtures (ethanol/water 70 and 50% v/v). Unsupervised PCA data analysis was performed starting from NMR peak lists obtained from the entire spectrum range (8.5-0.5 ppm) of samples and by measuring the selected peak area in the ^{1}H NMR spectra. Signals corresponding to water and methanol residues were excluded. A matrix was obtained by using these areas (variables), while the columns of the matrix were the different peak areas related to ^{1}H values of each compound detected in the ^{1}H NMR spectra (observations).

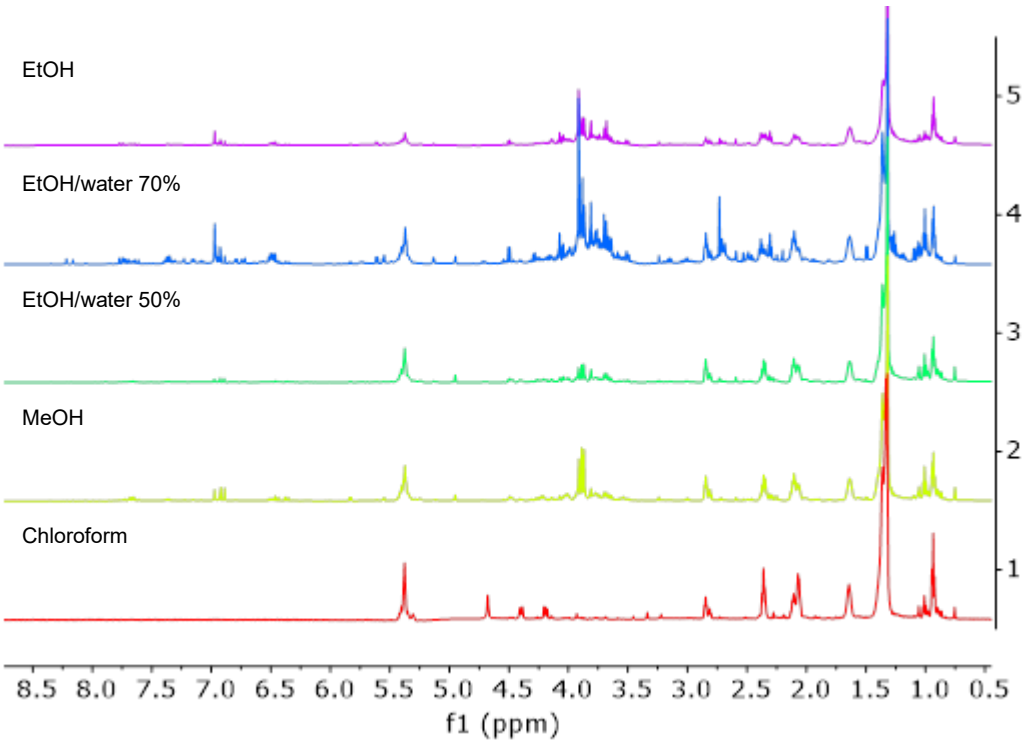

Figure 2.18 ^{1}H NMR spectra of different extracts of *R.sativus* sprouts

The PCA score plot allows visualizing separation of the analyzed samples into clusters, while the loading plot allows identifying the metabolites most influencing the separation.

The first component explained the 73.9% of the variance while the second one the 13.1%. The choice of principal components was established based on the fitting (R2X) and predictive (Q2X) values for the PCA. The untargeted PCA score plot (**Figure 2.19-A**) showed different clusters. Three clusters were observed for the extracts:

1) EtOH of 50% and 70% (E50A1-3 and E50B1-3; E70A1-3 and E70B1-3);

2) EtOH and MeOH extracts (EA1-3 and EB1-3, MA1-3 and MB1-3);

3) $CHCl_3$ extract (CA1-3 and CB1.3).

Therefore, the PCA score scatter plot discriminated the different solvents used for fresh sprouts of *R. sativus*.

The PCA loading plot highlighted the signals responsible for the distribution on the PCA score plot. **Figure 2.19B** shows that the chloroform extracts were characterized by the signals at δ 0.91, 0.95, 1.31, and 1.35 ascribable to the main presence of fatty acids. The signal at δ 2.70, ascribable to glucosinolate compounds (SO-Gls), characterized the EtOH 50% extracts. Moreover, the PCA loading plot showed how several signals were common to the other extracts.

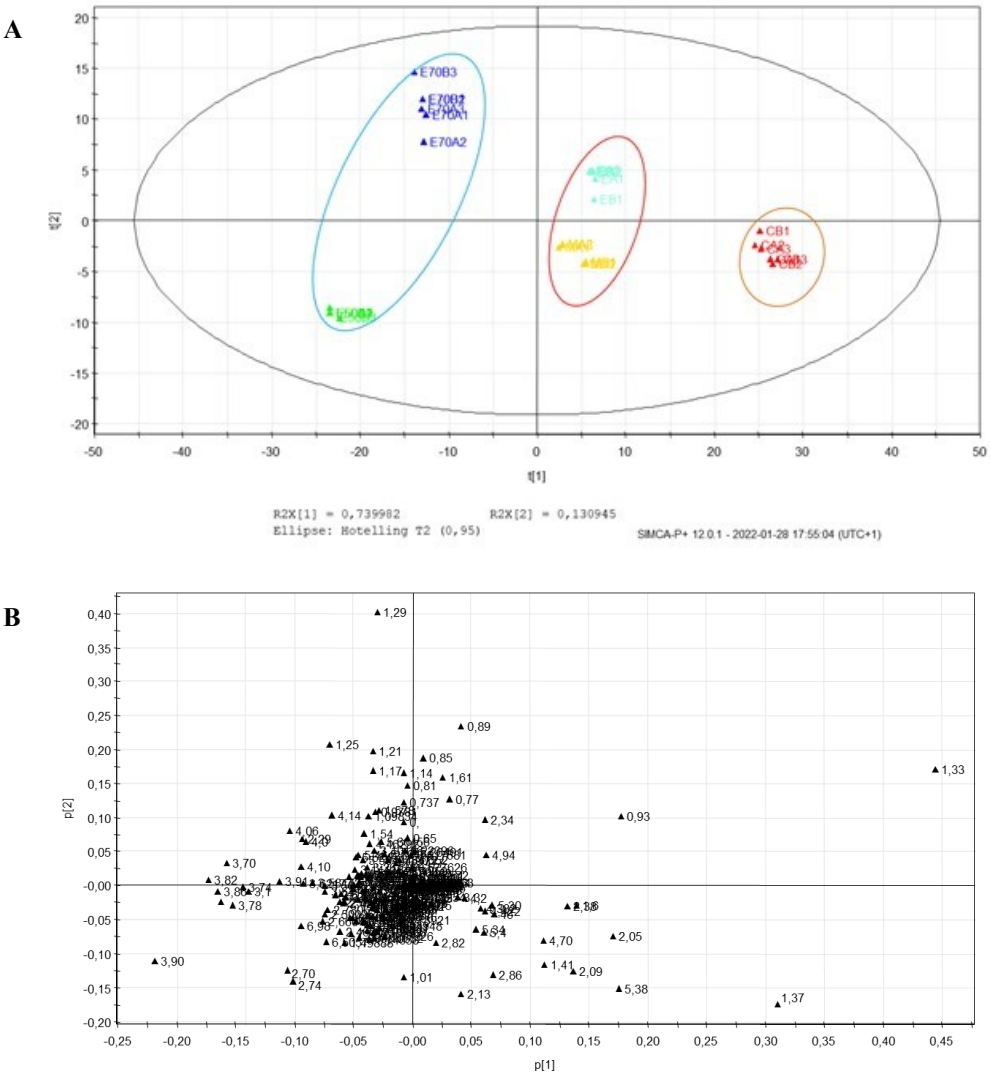

Figure 2.19 Unsupervised multivariate analysis. PCA score scatter plot (panel A), PCA loading plot (panel B)

Targeted Multivariate Statistical Analysis

For PCA, a data matrix was generated by reporting the different employed extraction protocols (observations), and the peak areas of the identified metabolites (variables), obtained from the data deriving from the ^{1}H and 2D NMR experiments. To this extent, PCA was performed by measuring the selected peak area for each identified metabolite in the ^{1}H NMR dataset (**Table 2.4**) and a matrix was obtained by using these areas (variables), while the columns of the matrix were the different "green" extracts obtained through the use of "eco-friendly" procedures (observations). The exploratory principal component analysis (PCA) was employed to acquire a general insight and visualize any relation (trends, outliers) among the observations (samples).

The resulted model, obtained after scaling data by Pareto scaling, showed good fitness and the absence of outliers. PC1 contributed to 84.4% of the variance followed by PC2, which contributed to 8.8%. Hence, the first two PCs exhibited a total variance of 93.6%. Therefore, the extracts were well discriminated against each other. The extracts of the sprouts obtained with the five different solvents (maceration with methanol, ethanol, ethanol/water mixture 70 and 50%, and maceration with chloroform) appeared separated into four clusters. In the PCA model a clear difference between the carried-out extractions was evident, probably due to solvents of different polarity affecting the metabolite content. In **Figure 2.20A**, the extracts obtained with MeOH and EtOH appear located very close in a section of the score plot, far from the other. Specifically, in the PCA model the MeOH, EtOH and $CHCl_3$ (each, two batches in triplicate) were separated by EtOH-H_2O extracts along the first principal component (PC1), showing how the presence of water can affect the extraction process. Moreover, in **Figure 2.20A** the EtOH-H_2O 50 % extracts were separated by EtOH-H_2O 70% extracts along with the second principal component (PC2).

Figure 2.20B shows the loading scatter plot relative to this model. Metabolites in the loading plot that are distant from the origin, can be considered as markers of the extraction procedures as a confirmation of their different distribution in different samples. As observed in the untargeted PCA analysis, fatty acids were responsible for the discrimination of $CHCl_3$ extracts. MeOH and EtOH solvents seem to determine higher concentrations of primary metabolites as PUFA and sucrose. **Figure 2.20B** shows how phytosterols and succinic acid were in higher amounts in the EtOH 70 % with respect to EtOH 50%; for this latter, a higher amount of glucose and isoleucine was also observed. All the investigated compounds were observed in the origin.

Table 2.4 Signal chosen for multivariate data analysis

Compound		^{1}H chemical shifts (multiplicity, in Hz)
PS	Phytosterol	0.69 (m)
Val	Valine	0.98 (d, 7.0)
Ile	Isoleucine	1.01 (s)
FA	Fatty Acids	1.33 (m)
Ala	Alanine	1.49 (d, 7.1)
GABA	gamma-Aminobutyric acid	2.30 (t, 7.3)
SO-Gls	Sulfoxide glucosinolates	2.70 (bt, 7.1)
Asp	Aspartic acid	2.85 (dd, 17.3, 3.7)
5	Compound 5	3.87 (s)
β-glu	β-glucose	4.50 (d, 8.0)
α-glu	α-glucose	5.14 (d, 3.6)
PUFA	Poly unsaturated fatty acids	5.38 (m)
Suc	Sucrose	5.40 (d, 3.8)
15	Compound 15	5.82 (6, 8.3)
Tyr	Tyrosine	6.86 (m)
Ind-Gls	Indolic glucosinoates	2.24 (s)
17	Compound 17	7.50 (d, 15.8)
11	Compound 11	7.54 (d, 15.8)
12, 14	Compound 12 and 14	7.71 (d, 15.8)
6,7	Compound 6 and 7	7.74 (d, 15.8)

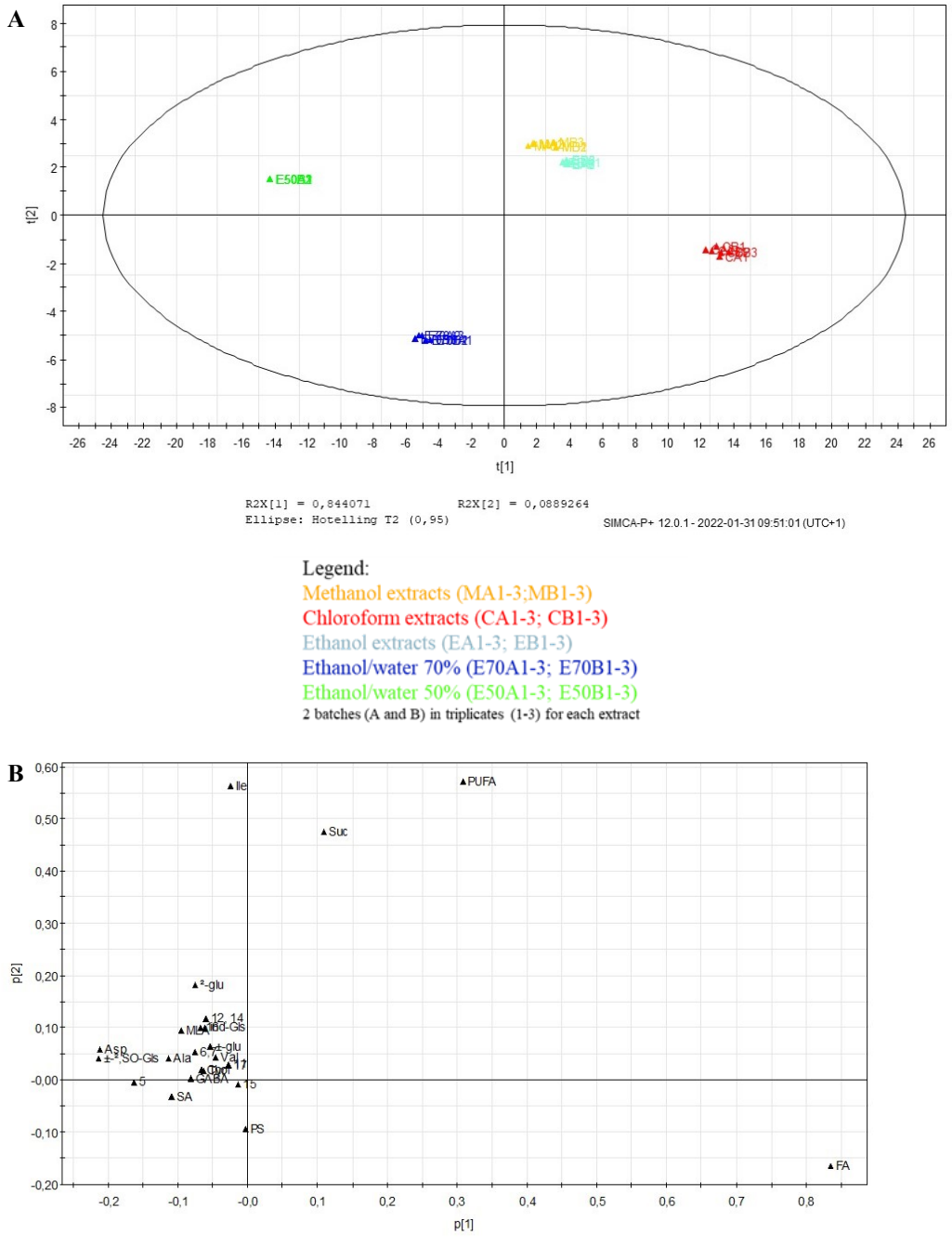

Figure 2.20 Principal component analysis of *R. sativus* extracts. PCA score scatter plot (panel A), PCA loading plot (panel B)

Legend: (PS) phytosterols; (Val) Valine; (Ile) Isoleucine; (FA) Fatty acids; (Ala) Alanine; (GABA); (SA) Succinic acid; (SO-Gls) sulfoxide glucosinolates; (Asp) Aspartica cis; (Chol) choline; (MLA) Malic acid; (α-glu) α-glucose; (β-glu) β-glucose; (PUFA) polyunsaturated fatty acids; (Suc) sucrose; (Tyr) tyrosine, (Ind-Gls) indolic glucosinolates.

Partial Least Square Discriminant Analysis (PLS-DA) (**Figure 2.21A-D**) was performed for the attribution of classes to the different extracts. The classes were attributed based on the different Nrf2 activities, to point out clear differences among the analyzed extracts. Classes attributed were -1, 0 and +1 and specifically -1 to samples EtOH 50% and 70 % (showing higher activity), 0 to EtOH extracts (showing mild activity), +1 to $CHCl_3$ and MeOH extract (showing lower activity).

Figure 2.21 shows the comparative PLS-DA analysis with the PLS-DA score plot with component one explaining 60.8% of the variation and component two accounting for 18.2% of the variation, exhibiting a good separation between these groups. The PLS-DA analysis showed a distinct separation (R2Y, 0.79) and good predictability (Q2, 0.63) and was validated by a permutation test which proved that the model was credible and robust.

PLS-DA showed a good separation among the extracts along the first principal component (PC1). The hydroalcoholic extracts were separated from MeOH, EtOH and $CHCl_3$ extracts by the first principal component (PC1). Moreover, the hydroalcoholic extracts, blue colored (E70A1-3: E70B1- E50A1-3 and E50A1-3) were separated each other in the plot by the second principal component (PC2) but not by PC1 component. In **Figure 2.21B** the loading scatter plot shows potentially significant metabolites based on contributions and reliability to the separation observed in the score scatter plot. As previous described, metabolites in the loading plot that are distant from the origin, can be considered as markers of the extraction procedures as a confirmation of their different distribution in different samples. In addition, the specific contribute of single variables to the principal component 1 (PC1) is reported in **Figure 2.21C**. The metabolites marked below the baseline are present in higher concentrations in the extracts obtained by hydroalcoholic maceration if compared to those obtained by methanol, ethanol and chloroform maceration. Hydroalcoholic maceration protocol determine higher concentrations of primary metabolites as amino acids Valine (Val); Isoleucine (Ile); Alanine (Ala);

Aspartic acid (Asp), tyrosine (Tyr) and sugars (α-glucose, β-glucose) and some of the specialized metabolites as sulfoxide glucosinolates (SO-Gls); indolic glucosinolates (Ind-Dls) and phenolics compounds **5**-**7**, **11**-**12**, **14** along with the afore described compound **16**. It is possible to deduce that metabolites like glucosinolates (SO-Gls and Ind-Gls) and polyphenolic compounds **6**, **7**, **11**, **12**, **14**, **16** and **17** can contribute to the higher Nrf2 activity of the hydroalcoholic extracts.

Along with the occurrence of glucosinolates, reported for the activation of Nrf2 pathway[12,13], PLS-DA analysis highlights the contribution of polyphenolic compounds **6**, **7**, **11**, **12**, **14**, **16** and **17** to the higher activity of the hydroalcoholic extracts in stimulating the activation of the transcriptor factor. In particular, the compounds 1-*O*-feruloyl-2-*O*-sinapoyl-β-D-glucopyranoside (**16**) and 3-*O*-feruloyl-6'-*O*-sinapoyl-sucrose (**14**) are good discriminants for the increased activity as shown in the PLS-DA Score Plot (**Figure 2.21B**)

All the statistical data were in agreement with the ability of EtOH/H_2O mixtures to extract secondary metabolites responsible for *Raphanus sativus* biological properties. Thus, water can play an important role in the swelling of plant material, whereas ethanol is responsible for disrupting the binding between the solutes and plant matrix, thus enabling the better mass transfer of the compounds. The mixtures of EtOH/H_2O, characterized by a main percentage of water, showed a better synergistic effect for the extraction of the compound with health effects.

A

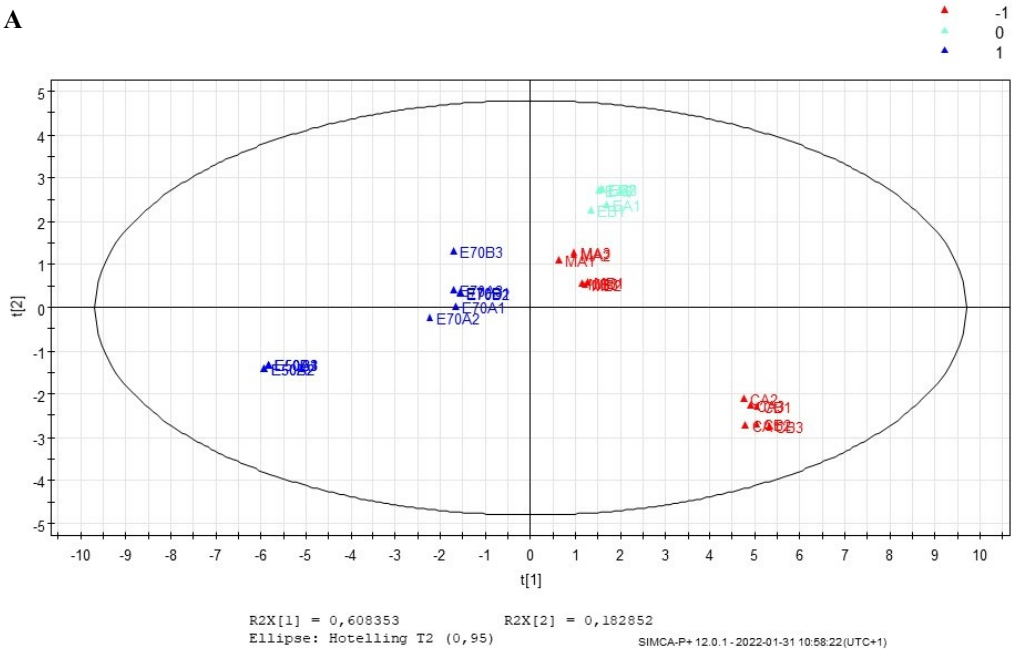
-1
0
1
E70B3
E70A1
E70A2
t[1]
t[2]
R2X[1] = 0,608353
R2X[2] = 0,182852
Ellipse: Hotelling T2 (0,95)
SIMCA-P+ 12.0.1 - 2022-01-31 10:58:22(UTC+1)

B

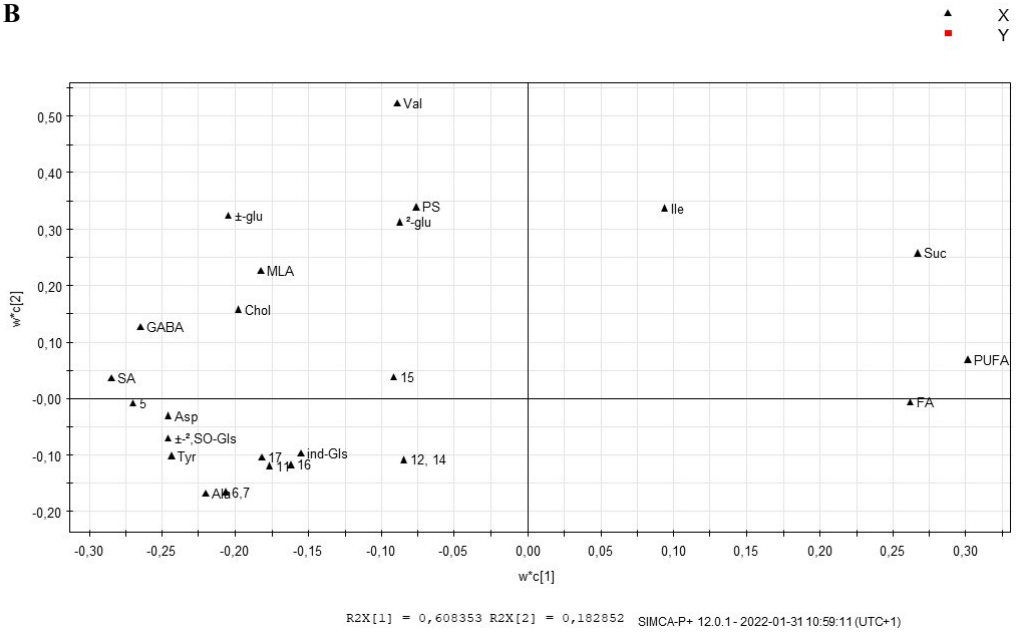
X
Y
Val
PS
±-glu
²-glu
Ile
Suc
MLA
Chol
GABA
PUFA
SA
15
FA
5
Asp
±-²,SO-Gls
Tyr
17
jnd-Gls
16
12, 14
6,7
w*c[1]
w*c[2]
R2X[1] = 0,608353 R2X[2] = 0,182852
SIMCA-P+ 12.0.1 - 2022-01-31 10:59:11 (UTC+1)

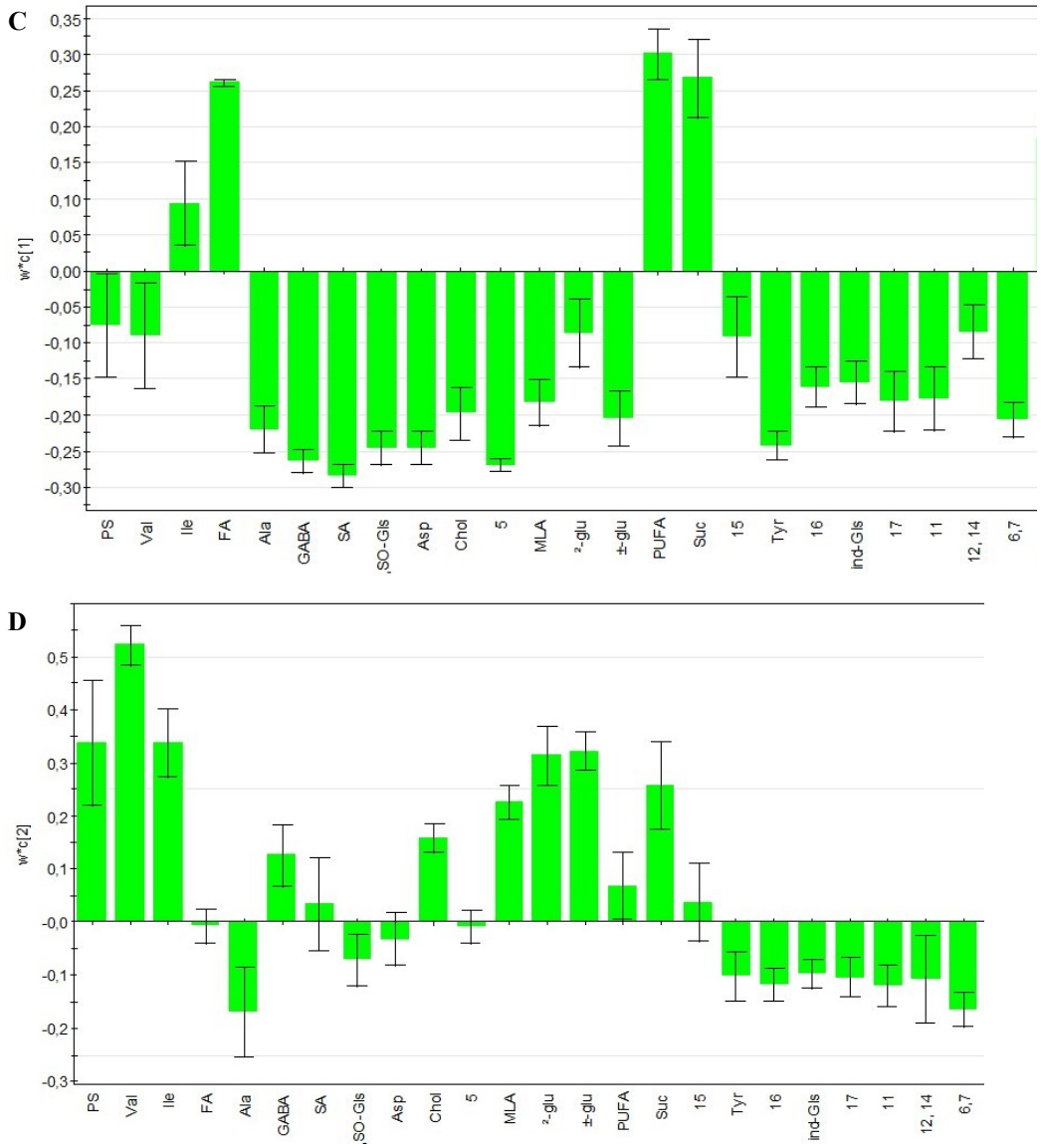

Figure 2.21. (**A**) PLS-DA correlation of ^{1}H NMR data matrix with Nrf2 (measured by a gene reporter assay at 30 µg/ml). (**B**) PLS-DA Score Plot, (**C**) single variables to the principal component 1 (Comp. 1), Y= primary and specialized metabolites. (**D**) single variables to the principal component 2 (Comp. 2), Y= primary and specialized metabolites.
Legend: (PS) phytosterols; (Val) Valine; (Ile) Isoleucine; (FA) Fatty acids; (Ala) Alanine; (GABA); (SA) Succinic acid; (SO-Gls) sulfoxide glucosinolates; (Asp) Aspartica cis; (Chol) choline; (MLA) Malic acid; (α-glu) α-glucose; (β-glu) β-glucose; (PUFA) polyunsaturated fatty acids; (Suc) sucrose; (Tyr) tyrosine, (Ind-Gls) indolic glucosinolates.

2.4. Conclusions

This investigation afforded methionine and indolic glucosinolates derivatives along with linear oxylipins and phenolics. In particular, p-hydroxycinnamic acid derivative 1-*O*-feruloyl-2-*O*-sinapoyl-β-D-glucopyranoside was here described for the first time. "Green" extracts showed antioxidant activity confirmed by both radical scavenging activity and *in vitro* evaluation of the cellular response of detoxifying mechanisms as the activation of the Nrf2 pathway. The biological activity was related to the occurrence of glucosinolates and phenolic compounds as depicted by multivariate analysis. In particular, the new compound 1-*O*-feruloyl-2-*O*-sinapoyl-β-D-glucopyranoside was one of the markers of the PLS-DA model. The absence of cytotoxicity, evaluated on the selected human cancer cell lines at a tested concentration of 30 μg/ml, and the antioxidant activity exerted by the selected phytocomplexes make *R. sativus* sprouts a rich source of phytochemicals with potential health benefits.

2.5. Experimental section

Plant material

Raphanus sativus L. var. *longipinnatus* sprouts were directly purchased by producers in Cesena, Italy in September 2020. A voucher specimen has been deposited in this Department. Suddenly, the sprouts were frozen at -80°C and treated by freeze-drying.

LC-HRMS profiling

Qualitative LC-MS was performed using a Thermo Scientific Accela HPLC system (Thermo Scientific, Germany) equipped with a C_{18} reversed-phase (RP) column at a flow rate of 0.2 µl/min and coupled to a LTQ-Orbitrap XL mass spectrometer. Linear gradient elution was carried out by using water with 0.1% formic acid as eluent A and acetonitrile as B.

The instrument was calibrated using the manufacturer's calibration standards. The scan was collected in the Orbitrap at a resolution of 30 000 in a *m/z* range of 200–1500 amu. The *m/z* of each identified compound was calculated to 4 decimal places and measured with a mass accuracy < 2ppm. The source voltage was -4.0 kV and capillary voltage -35 kV, the tube lens offset -126 V and the capillary temperature was set at 280 °C, the auxiliary gas was set at 20 (arbitrary units) and the sheath gas at 10 (arbitrary units). In full LC-ESI/MS experiments Total Ion Current (TIC) profile was produced by monitoring the intensity of all the ions produced and acquired in every scan during the chromatographic run. In order to get structural information, Data Dependent experiments were performed by acquiring MS^2 spectra of the most intense ions produced during the acquisition.

LC-ESI/LTQOrbitrap/MS/MS gradient for MeOH extract of daikon sprouts. A Luna C-18 column (RP-18, 2.0 x 150 mm, 5 µm; Waters; Millford, MA) was used

for HPLC-ESI-Orbitrap MS analysis. In particular, the HPLC gradient started at 10% (B) and after 25 min the %B was at 50%, then rising until 100% B at 30 minutes.

Extraction and isolation

The sprouts of *R. sativus* (100 g), were dried and extracted at room temperature using MeOH (300 mL for 3 days, three times). After filtration and evaporation of the solvent to dryness in vacuo, 25 g of crude MeOH extract were obtained. The obtained metanolic extract was subjected to *n*-butanol-water repartition to remove free sugars. The final butanolic fraction was dried under vacuum, diluited 100 mg/ml and chromatographed by semipreparative RP-HPLC coupled to UV detector setted at a wavelength of 330 nm. Mobile phases H_2O (0.1% of formic acid) and ACN (0.1% of formic acid) were used with flow rate 2.0 mL/min. The following chromatographyc conditions allowed to isolate compounds **5** (1.2 mg, t_R = 14.5 min), **6** (1.0 mg, t_R = 16.1 min) and **7** (1.1 mg, t_R = 16.6 min), **11** (1.2 mg, t_R = 22.9 min), **12** (2.0 mg, t_R = 25.0 min), **13** (2.0 mg, t_R = 20.2 min), **14** (1.1 mg, t_R = 21.2 min), **15** (1.8 mg, t_R = 21.8 min), **16** (1.8 mg, t_R = 25.8 min), **17** (1.7 mg, t_R = 26.2 min).

*3-O-feruloyl-6'-O-sinapoyl-sucrose (**14**):* Amorphous yellow solid; $C_{33}H_{40}O_{18}$; ^1H and ^{13}C NMR (MeOH-d_4, 600 MHz) data, see **Table 2.2**; ESI/LTQOrbitrap/MS *m/z* 723.2019 $[M-H]^-$ (calcd for $C_{33}H_{39}O_{18}$, 723.2121).

*1-O-feruloyl-2-O-sinapoyl-β-D-glucopyranoside (**16**):* Amorphous yellow solid; $C_{27}H_{30}O_{13}$; ^1H and ^{13}C NMR (MeOH-d_4, 600 MHz) data, see **Table 2.2**; ESI/LTQOrbitrap/MS *m/z* 561.1140 $[M-H]^-$ (calcd for $C_{27}H_{29}O_{13}$, 561.1598).

NMR experiments

As reported in the general experimental procedure.

Nrf2 activation assessed by gene reporter assay

To screen the *in vitro* hits for Nrf2 activation the human liver cancer cell line HepG2, containing a stably integrated firefly luciferase gene under the control of ARE was utilized. They were purchased from Signosis Inc. (Santa Clara, CA, USA).

- *Cell culture*

HepG2-ARE-Luc cells were generally grown in 75 cm^2 cell culture flasks as adherent monolayer cultures. Cells were cultured in Dulbecco's Modified Eagle's Medium-high glucose (DMEM) medium supplemented with 10% fetal bovine serum (Invitrogen), 1% penicillin/streptomycin and 2 mM L-glutamine (37°C, 5% CO_2). The flasks containing the cells and growth medium were kept in a HERAcell 150 incubator (Thermo Electron Corporation) at 37 °C with 5 % carbon dioxide (CO_2). Cells were regularly examined under a CKX31 microscope (Olympus) to assess health and growth, and to check for contaminations. Upon reaching 80 % confluence, which occurred once or twice per week, cells were split and seeded using a laminar flow cabinet. For the splitting process, the growth medium was completely removed. Then, the cells were washed with 10 mL phosphate-buffered saline (PBS). After the removal of PBS, 4 mL of trypsin/ethylenediaminetetraacetic acid (EDTA) were added to the flask, which was then put in the incubator at 37° C with 5 % CO_2 for 3 minutes. Cell detachment was checked under the microscope. The flask was shaken mildly if the detachment was not complete. 11 mL growth medium were added, and the cells were suspended in the medium, which stopped

trypsin activity. Using a ViCell XR Cell Viability Analyzer (Beckman Coulter) cell viability and cell count were measured. An adequate aliquot of cell suspension was subsequently transferred into a new flask and the growth medium was added, as to reach an approximate total volume of 15 mL per flask. After suspension, the flask was once again checked in the microscope and then stored in the incubator.

- *Assay procedure*

For the luciferase assay, HepG2-ARE-Luc cells were seeded in 175 cm2 cell culture flasks instead of the usual 75 cm2 flasks. Upon reaching approximately 80 % confluence, the growth medium was removed, cells were washed with PBS and 15 mL of a 10 µM CTG solution were added to the cells. Subsequently, the flask was put into the incubator for one hour, after which the CTG solution was removed Using a multichannel pipette HepG2-ARE-Luc cells were seeded in a 96-well plate, aiming for 15 000 cells per well. The plates were put in the incubator for 24 hours. The following day, cells were incubated with test compounds in various concentrations. 0,1 % DMSO was used as a negative control, and 25 nM CDDO-imidazole (CDDO-im, Enzo Life Sciences, Switzerland) as a positive control. Testing was always conducted at least in quadruplicates. After incubation for 24 hours, the plates were examined via a microscope. The medium was then completely removed, and after washing all cells with PBS, the plate was frozen at -80 °C.

Before the measurement, the frozen 96-well plate and the assay reagents, Luciferin solution and ATP solution, were taken out of the -80 °C freezer and thawed. The luciferin buffer had to be kept in the dark at all times as it is sensitive to light. Per well 50 µL of freshly prepared lysis buffer were added and the plate underwent vigorous shaking for ten minutes to further disrupt the cells. 40 µL of

the cell lysate were then transferred to a black 96-well plate and shaken for another minute. Immediately after, the plate was measured via TECAN Spark.

- *Measurement and data evaluation*

The TECAN Spark detected fluorescence as a first step of the measurement. The chosen setting "TR Fluorescence Intensity" implied an excitation wavelength of 485 nm and an emission wavelength of 520 nm. To detect luminescence as a next step, the ATP and the luciferin solutions were injected directly into the wells by the TECAN Spark, leading to a reaction of the cell lysate that comprised luciferase and the reagents. The setting "Luminescence" was applied to quantify the reaction.

To evaluate the measurement results, the obtained luminescence was normalized to the number of cells. This was achieved by applying the luminescence to the CTG-mediated fluorescence ratio. To obtain the fold activation of the ARE-dependent gene transcription and to ensure comparability the normalized luminescence value of each TC was divided by the value of DMSO, the solvent control.

Chemometrics by NMR experiments

- *NMR spectroscopy*

All 2D-NMR spectra were acquired in MeOH-d_4 (99.95%). For the sample preparation, 6 mg crude extract was transferred to Eppendorf tube before the addition of the same volume (600 µL) of both MeOH-d_4. The sample was then vortexed and sonicated for 15 min at a controlled temperature. A 500 µL of supernatant was transferred to NMR tube. NMR experiments were performed on a Bruker DRX-600 spectrometer (Bruker BioSpin GmBH, Rheinstetten, Germany) equipped with a Bruker 5 mm TCI CryoProbeat 300 K. The NMR tubes were

labeled and immediately subjected to ^{1}H NMR measurements using a preset setting for all of the samples. The analysis temperature was 24 °C.

Gradient shimming was performed prior to signal acquisition and MeOH-d_4 was used to provide an internal lock. The proton spectra were collected with a 90◦ pulse width of 8.25 μs, a relaxation delay 3 s, 128 scans, 64 K data points and a spectral width of 9 ppm.

A series of 2D experiments, Heteronuclear Single-Quantum Correlation Spectroscopy (HSQC) and Heteronuclear Multiple Bond Correlation (HMBC) were implemented and permitted the assignment of the existing metabolites.

- *Data reduction and spectral alignment*

The spectra were imported into the MestreNOVA 10 software. Phasing, baseline correction, binning (spectral buckets of 0.004 ppm), normalization to the standardized area of the reference compound and removal of unwanted resonances (residual solvent) were performed. Finally, the spectra were aligned and converted to ASCII format.

- *Data analysis*

Spectrum processing is an intermediate step between acquiring the raw spectra and data analysis. It should preserve as much as possible the variance relative to the chemical compounds contained in the NMR spectra while reducing other types of variance induced by different sources of bias such as baseline, noise or misalignment. Generally, spectrum processing steps include baseline correction, noise elimination, alignment, data reduction and normalization prior to multivariate statistical analyses. In the present work, NMR spectra were manually phased and baseline corrected. Identification of metabolites was achieved using chemical shifts known by literature for each compound. Each sample was analyzed in triplicate.

Multivariate data analysis

Chemometric techniques based on projection methods were applied for metabolomics multivariate data analysis. Specifically, exploratory data analysis was performed by principal component analysis (PCA) while a projection to latent structures (PLS-DA) based method was applied to discriminate the samples based on the extraction system. In the protocol here followed, discriminant classification was carried out using partial least squares-discriminant analysis (PLS-DA), a method based on the PLS regression algorithm giving each sample a class based on the extraction method used. Classes attributed were -1, 0 and +1 and specifically -1 to samples obtained with green hydroalcoholic mixtures (EtOH/water 70 and 50%) 0 to samples obtained with ethanol and +1 to samples obtained by methanol and chloroform maceration. Finally, a PLS-DA correlation of data matrix with measured Nrf2 assays was performed (using the measured value as a Y).

Projection methods in multivariate data analysis were performed by using SIMCA-P+ software (Version 12.0, Umetrics, Umeå, Sweden). The entire data matrix, after log transformation and Pareto scaling, was first analyzed by PCA to define a homogeneous cluster of samples (Exploratory data analysis).

Models were validated by cross-validation techniques and permutation tests according to standardized good practice to minimize false discoveries and to obtain robust statistical models. A small number of metabolites changing during the experiment was extracted and the behavior of every single metabolite was studied by a linear mixed-effects model for longitudinal studies. All the different pretreatments provided good discriminant ability in calibration and cross-validation (above 90%).[11]

References

1. Choe, U., Yu, L., and Wang, T. Y. The science behind microgreens as an exciting new food for the 21th century. *J. Agric. Food Chem.,* 2018, (44) **66**, 11519–11530.

2. Xiaoa, Z., Rauscha, S., Luoa, Y., Sunc, J., Yud, L., Wangd, Q., Chenc, P., and Stommele, J. R. Microgreens of Brassicaceae: Genetic Diversity of Phytochemical Concentrations and Antioxidant Capacity. *LWT*, 2018, **101**, 731-737.

3. Kang, J.N., Won, S.Y., Seo, M.-S., Lee, J., Lee, S. M., Kwon, S.-J., and Kim, J. S. Induction of Glucoraphasatin Biosynthesis Genes by MYB29 in Radish (*Raphanus sativus* L.) Roots. *Int. J. Mol. Sci*., 2020, **21**, 5721.

4. Soundararajan, P.and Kim, J. S. Anti-Carcinogenic Glucosinolates in Cruciferous Vegetables and Their Antagonistic Effects on Prevention of Cancers. *Molecules*, 2018, **23**, 2983.

5. Nguyen, V. P. T., Stewart, J. D., Ioannou, I., and Allais, F. Sinapic Acid and Sinapate Esters in Brassica: Innate Accumulation, Biosynthesis, Accessibility via Chemical Synthesis or Recovery From Biomass, and Biological Activities. *Front. Chem*., 2021, **9**, 664602.

6. Itoh K., Chiba T., Takahashi S., Ishii T., Igarashi K. An Nrf2/small Maf heterodimer mediates the induction of phase II detoxifying enzyme genes through antioxidant response elements. *Biochem. Biophys. Res. Commun.*, 1997, **236**, 313-22.

7. Venugopal R. & Jaiswal AK. Nrf1 and Nrf2 positively and c-Fos and Fra1 negatively regulate the human antioxidant response element-mediated expression of NAD(P)H:quinone oxidoreductase1 gene. *Proc. Natl. Acad. Sci. USA*., 1996, **93**, 14960–65.

8. Takaya, Y., Kondo, Y., Furukawa, T., and Niwa, M. Antioxidant Constituents of Radish Sprout (Kaiware-daikon), *Raphanus sativus* L. *J. Agric. Food Chem.*, 2003, **51**, 8061-8066

9. Barillari, J., Cervellati, R., Paolini, M., Tatiboue, A., Rollin, P., and Iori, RIsolation of 4-Methylthio-3-butenyl Glucosinolate from *Raphanus sativus* Sprouts (Kaiware Daikon) and Its Redox Properties. *J. Agric. Food Chem*., 2005, **53**, 9890-9896.

10. D'Urso, G.; Maldini, M.; Pintore, G.; d'Aquino, L.; Montoro, P.; Pizza, C, Characterisation of *Fragaria vesca* fruit from Italy following a metabolomics approach through integrated mass spectrometry techniques *LWT–Food Sci.Technol*. 2016, **74**, 387–395.

11. Westad, F.; Marini, F., Validation of chemometric models - A tutorial. *Anal. Chim. Acta* 2015, ***893***, 14-24.

12. Connolly, E.L., Sim, M, Travica, N., Marx, W., Beasy, G., Lynch, G.S., Bondonno, C.P., Lewis, J.R., Hodgson, J.M. and Blekkenhorst, L.C. Glucosinolates From Cruciferous Vegetables and Their Potential Role in Chronic Disease: Investigating the Preclinical and Clinical Evidence. *Front. Pharmacol*. 2021, **12**, 767975.

13. Kubo, E., Chhunchha, B., Singh, P., Sasaki, H. and Singh, P. D. Sulforaphane reactivates cellular antioxidant defense by inducing Nrf2/ARE/Prdx6 activity during aging and oxidative stress. Scientific Reports. 2017, **7**, 14130.

14. Gamba, M., Asllanaj, E., Raguindin, P. F., Glisic, M., Franco, O. H., Minder, B., Bussler, W., Metzger, B., Kern, H. and Muka T. Nutritional and phytochemical characterization of radish (*Raphanus sativus*): A systematic review. *Trends in Food Science & Technology*. 2021, **113**, 205–218.

Chapter 3

Okra fruit (*Abelmoshus esculentus* L.): polar lipids and specialized metabolites with antioxidant and anti-hyperglycemic activity

State of the art and purposes

Okra plant (*Abelmoschus esculentus* L. Moench., Malvaceae family), also known as "lady's finger", "bhindi" and "gumbo", is very popular in North-Eastern African countries for its edible fruits, consisting of six-chambered green seed pods.[1] It is largely cultivated in tropical, subtropical, and warm temperate regions around the world, from Africa to Asia, Southern Europe, and America; it can be easily found in local European markets as a basic ingredient in many traditional dishes.[2] Okra seeds contain a high lysine level, so they can be used as a supplement to cereal-based diets in which lysine is the first limiting amino acid.[3] The oil extract from okra seeds is gaining great interest for its similarity to cotton and peanut seed oils and for its fatty acid composition, mainly constituted of palmitic, oleic, and linoleic acids, essential for human nutrition.[4]

Moreover, consumption of okra seed oil seems to determine hypocholesterolemic effects.[5] In Turkey, the herbal infusion of roasted okra seeds has long been recognized to attenuate blood glucose levels in diabetes mellitus therapy, in agreement with the promising α-glucosidase inhibitory activity recently reported for isoquercetin and quercetin-3-*O*-glucopyranosyl-glucoside therefrom occurring.[6-7] Several studies have reported the ability of *A. esculentus* fruits and seeds to manage increased blood glucose levels, relating the antidiabetic and anti-hyperglycemic effects to rhamnogalacturonan and flavonoids.[6, 8, 9] Okra fruits present significant antioxidant properties, mostly due to their high content in vitamin C, carotenoids and flavonoids, and anti-proliferative activity, recently reported for bioactive compounds therefrom isolated.[5, 10] Finally, due to their high content in biopolymers (mainly pectins), and bioactive compounds (e.g. ascorbic acid and beta-carotene), extracts from okra fruits are used in food and pharmaceutical industry as emulsifiers, drug tablet formulations or blood plasma replacement.[2] Notwithstanding the extensive use of this vegetable, nowadays no

comprehensive literature information about the okra fruit composition is available. In this study, in order to fill a gap in okra lipid composition and to expand the framework of knowledge to specialized metabolites, the analysis of the n-butanol extract of okra fruits by high-performance liquid chromatography coupled to multiple-stage linear ion-trap and orbitrap high-resolution mass spectrometry in negative electrospray ionization mode (LC-ESI/LTQOrbitrap/MS/MS^n) was carried out. By this analytical approach, several metabolites belonging to different polar lipid classes, such as oxylipins, phospholipids, glycolipids, and sphingolipids, along with specialized metabolites mainly belonging to phenolic acid and flavonoid classes, were identified. These latter metabolites were isolated and their structures unambiguously elucidated by 1D- and 2D-NMR experiments.[11] Moreover, in line with the aforementioned claims, the anti-hyperglycemic potential of okra fruit extract was evaluated in order to investigate its potential as anti-diabetic food.

3.1 Experimental plan

Although its extensive and spread use in traditional medicine and food habits, little information is reported in the literature about its chemical composition. Thereby, inhibition of α-glucosidase activity was assayed, suggesting a good anti-hyperglycemic activity for okra fruit. Thereby, the analysis of the bioactive "green" extract of okra fruits by high-performance liquid chromatography coupled to multiple-stage linear ion-trap and orbitrap high-resolution mass spectrometry in negative electrospray ionization mode (LC-ESI/LTQOrbitrap/MS/MS^n) was carried out. By this approach, 39 metabolites belonging to different polar lipid classes, such as oxylipins, phospholipids, glycolipids, and sphingolipids, were putatively identified for the first time in *A. esculentus*. Moreover, LC-HRMS/MS analyses guided the isolation and characterization by NMR experiments of 19 specialized metabolites belonging to phenolic acid and flavonoid classes, 8 of them never reported before in *A. esculentus*.

3.2. Results and discussion

The edible fruit is a capsule up to 18 centimeters long with a pentagonal cross-section, containing numerous seeds. How about the other parts of the plant, the leaves are 10–20 centimeters long and broad, palmately lobed with 5–7 lobes; the flowers are 4–8 centimeters in diameter, with five white to yellow petals, often with a red or purple spot at the base of each petal while the pollens are spherical shape. This vegetable crop is very popular in North-Eastern African countries for its edible fruits. Nowadays, this species can be easily found in local European markets, as a basic ingredient in many local and traditional dishes.

3.2.1 Preliminary evaluation of the antioxidant and anti-hyperglycemic activity

The traditional use of the fruit as a source of antioxidants and components able to reduce the levels of hematic glucose encouraged a preliminary screening of the activity.

Total phenolic content and radical scavenging activity

The total phenolic content exhibited by okra fruit n-butanol extract (32.8 ± 5.6 mg GAE per g extract; **Table 3.1**), was in substantial agreement with literature reports.[10] Considering that okra fruit is widely used as functional food as well as in traditional medicine to treat diabetes, gastric ulcer, jaundice, andhepatitis,[10,18] the antioxidant activity of the extract was evaluated by TEAC, DPPH and nitric oxide scavenging assay. In the TEAC assay the extract showed a moderate antioxidant activity (TEAC value = 0.33 ± 0.01 mg mL^{-1}) in comparison to that exhibited by quercetin-3-O-glucoside (TEAC value = 0.96 ± 0.02), used as reference compound (**Table 3.1**). The DPPH assay revealed that the antiradical activity of the *n*-butanol extract was 21.9 ± 2.10 μg mL^{-1}, using ascorbic acid as reference compound (5.21± 0.12 μg mL^{-1}) (**Table 3.1**). Additionally, the nitrite radical scavenging assay revealed a good capability of the *n*-butanol extract to quenching the NO radical with IC_{50} values of 23.3 ± 1.20 μg mL^{-1} in comparison with the standard ascorbic acid (25.31 ± 1.50 μg mL^{-1}) (**Table 3.1**), confirming the good antioxidant properties of *A. esculentus*. As nitric oxide has been shown to be directly scavenged by flavonoids and phenolic acids,[19] the results confirmed *A. esculentus* as a natural source of antioxidants.

Evaluation of α-glucosidase inhibition

α-glucosidase is present in the brush border of the human intestine and it is responsible for the breakdown of polysaccharides into absorbable monosaccharide units. Inhibition of this enzymatic activity lowers blood glucose levels by reducing the absorption of carbohydrates and preventing the development of diabetes.[7, 15] As a typical screening method to evaluate the antidiabetic potential of molecules consists in measuring their ability to inhibit this enzyme[7, 15], the okra fruits' extract was subjected to α-glucosidase inhibition assay. Results reported in **Table 3.1** showed potent inhibition of α-glucosidase, with an IC_{50} of 0.27±0.03 mg/mL, a very low value if compared to acarbose (IC_{50} value 3.02±0.02 mg/mL), an antidiabetic drug well known for inhibition of α-glucosidase and α-amylase enzymes, used as the positive control

Table 3.1. Total phenolic content, antioxidant activity and α-glucosidase inhibitory activity of *n*-butanol extract of *A. esculentus* fruits

	Total Phenol Content[a] (mg GAE/g extract)[a]	**DPPH** (IC_{50})	**Nitric Oxide** (IC_{50})	**TEAC**[b]	**Inhibition of α-glucosidase activity**[b] (IC_{50})
A. esculentus	32.8 ± 5.6	21.91 ± 2.10 µg mL−1	23.3 ± 1.20 µg mL−1	0.33 ± 0.01	0.27±0.03 mg/mL
Quercetin-3-O-glu[c]	-	-	-	0.96 ± 0.02	-
Ascorbic Acid[e]	-	5.21 ± 0.12 µg mL−1	25.3 ± 1.50 µg mL−1	-	-
Acarbose[d]	-	-	-	-	3.02±0.02 mg/mL

[a] GAE: gallic acid equivalent. [b] Determined by inhibition assay for α-glucosidase activity. [b]TEAC: values are expressed as concentration (mM) of standard Trolox solution exerting the same radical scavenging activity of a 1 mg/ml of the tested extract [c] Positive control for TEAC assay. [d] Positive control for α-glucosidase inhibition assay. [e] Positive control for DPPH and Nitric oxide scavenging assay

3.3 Complex polar lipids profiling by LC-ESI/LTQOrbitrap/MS/MS^n analysis

To define the polar lipid profile of okra fruit extract, LC-ESI/LTQOrbitrap/MS/MS^n analyses were performed on a RP-C4 column to allow, in a single analytical step, the detection and separation of polar lipids characterized by a wide molecular weight variety (**Figure 3.1**). Chromatographic behavior, accurate mass measurements, fragmentation pattern analyses, and comparison with literature data allowed us to putatively identify 39 lipid compounds belonging to oxylipin, phospholipid, glycolipid, and sphingolipid classes, all of them for the first time described in okra fruits (**Table 3.2**).

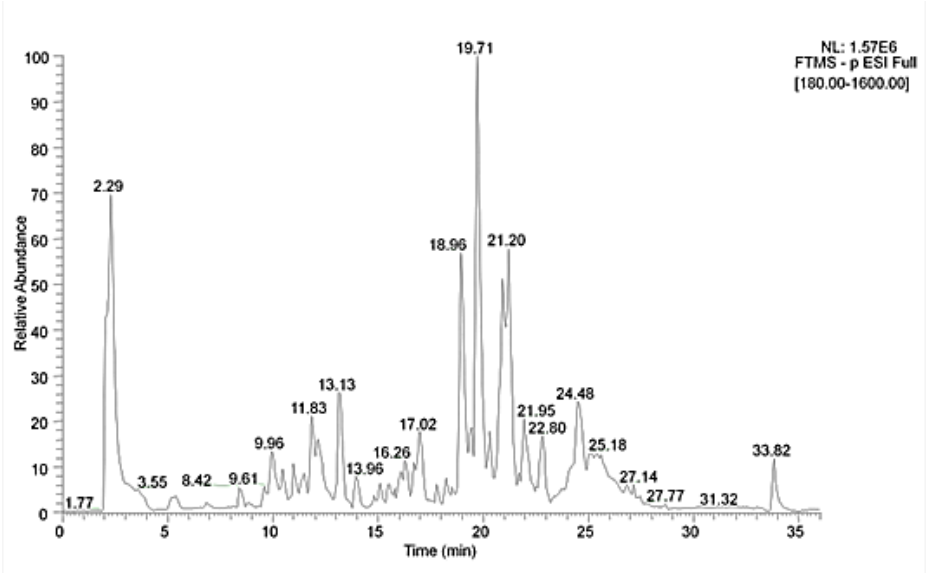

Figure 3.1. LC-ESI/LTQOrbitrap/MS polar lipid profile (negative ion mode) of the n-butanol extract of *A. esculentus* fruit

- *Identification of Oxylipins*

Oxylipins are a family of bioactive secondary metabolites deriving from the oxidative metabolism of essential PUFA, such as α-linolenic acid (ALA, 18:3ω-3) and linoleic acid (LA, 18:2 ω -6).[32] Oxylipins can be synthesized *in vivo* from their precursor fatty acids *via* oxygenase enzymes, or obtained through food or dietary oils. The oxidation of fatty acids in oils is nonenzymatic and is known to be influenced by storage or processing conditions. However, enzymatic oxidation *via* lipoxygenase enzymes occurs during the oil extraction process, when the barrier integrity of the seed is compromised by homogenization. [33]

Oxylipins are reported in several seed oils of higher plants, such as soybean, corn, olive, canola, and ricinus, and in wheat flour. The best known of these metabolites is ricinoleic acid [12-HydroxyOctadec-9-MonoEnoic acid, 12-HOME (9)], which is the main costituent (up to 90%) of castor oil. Moreover, dienoic fatty acids with one hydroxy group [e.g. 9-HydroxyOctadec-10,12-DiEnoic acid, 9-HODE (10,12), and 13-HydroxyOctadec-9,11-DiEnoic acid, 13-HODE (9,11)] and dihydroxy fatty acids [e.g. 9,10-DiHydroxyStearic Acid (DHSA), 9,10-DHSA] have been described in a number of seed oils, and some of them have commercial value.[32,33]

In plants, oxylipins serve as signal molecules in developmental processes (e.g., pollen formation) and in defense mechanisms (e.g., pathogenesis, wounding, and herbivores). Little is known about the role of ALA derived oxylipins in mammals, while LA derived oxylipins have proved to be involved in *in vivo* inflammatory cascades, pain perception, and skin barrier integrity.[33]

The careful study of full and tandem mass spectra acquired by LC-ESI/LTQOrbitrap/MS/MS^n analysis of *Abelmoshus esculentus* MeOH extracts allowed to ascertain the presence of different oxylipin species (**Table 3.2**).

Compounds **1**-**5**, **7**, **24**, **26** and **28** were identified as oxylipins, i.e. hydroxyl fatty acids differing each other by unsaturation degree and number of hydroxyl groups.

In okra LC-MS, an elution order could be noted with oxylipins characterized by more hydroxyl groups eluting before than oxylipins with a higher number of double bonds (i.e. TriHOME>DiHODE) and, for the same number of OH groups, oxylipins with a higher unsaturation degree eluting faster (i.e. DiHODE>DiHOME).[16] Okra oxylipins yielded highly diagnostic MS^2 fragmentation patterns (**Table 3.2**). Product ions generated by one or more consecutive neutral losses of 18 Da allowed to ascertain the number of hydroxyl groups occurring in the oxylipin structure which, by detection of characteristic product ions, such as those at nominal *m/z* 171 ($C_9H_{15}O_3$) and *m/z* 201 ($C_{10}H_{17}O_4$), or those at nominal *m/z* 253 ($C_{15}H_{25}O_3$), 229 ($C_{12}H_{21}O_4$), 223 ($C_{14}H_{23}O_2$) and 199 ($C_{11}H_{19}O_3$), could be located in the head (precisely at C9 and C10 positions) or in the tail of oxylipin (precisely at C12, C13, C15 and C16), respectively.[16] Moreover, along with the molecular formula and the Ring Double Bond equivalent value (RDB), the fragmentation pattern allowed in some case to establish the double bond position. It was the case of compound **1** and **2** differing for 2 Da but showing the same product ion at nominal *m/z* 229, originated by neutral loss of 98 Da and 100 Da from the corresponding molecular ion via rearrangement of the acyl chain end-part by breakdown of the C12-C13 bond, and suggesting the occurrence in **1** of an additional double bond in the end-part of the molecule (**Table 2**). By these considerations, compounds **1**-**4**, **7** and **24** could be putatively defined as reported in **Table 3.2**.[16-18] Compound **5** showed the same molecular formula and *m/z* value of **1** ($C_{18}H_{32}O_5$, *m/z* 327.2169) but a different fragmentation pattern, characterized by product ions at *m/z* 201.1132 and 213.1130 ($C_{11}H_{17}O_4$), suggesting the presence of a double bond at C11, and by one's at *m/z* 171.1026, also present in **1** (**Table 3.2**). By considering both the delayed elution of **5** with respect to **1** and the RDB value of 3.5, indicative of an additional unsaturation, the occurrence of a ketone group in the acyl chain tail could be hypothesized. Thus compound **5** was putatively defined as an oxo-9,10-dihydroxyoctadec-11-enoic acid. Compound **26** (*m/z* 293.2116) showed a MS^2

spectrum characterized by a base peak at *m/z* 249.2217 ($C_{17}H_{29}O$), originated by neutral loss of a CO_2 molecule, and by two product ions at *m/z* 185.1182 ($C_{10}H_{17}O_3$) and 197.1181 ($C_{11}H_{17}O_3$) that, considering their molecular formula and RDB values, could correspond to shortened acyl chain structures in which the head-group retained the carboxylic group under anionic form and the end-group was characterized by an enolic function, in the *m/z* 185.1182 ion, and by a ketone function conjugated to a double bond (ketene), in the *m/z* 197.1181 ion (**Table 3.2**). These considerations and literature data allowed to locate the ketone function at C9 and the double bond at C10, putatively defining **26** as the keto-form of oxylipin **24**.[19] The tandem mass spectrum of **28**, exhibiting the same molecular formula of **24** ($C_{18}H_{32}O_3$) but eluting later, showed as base peak the product ion originated by neutral loss of 44 Da (*m/z* 251.2379) from the $[M-H]^-$ ion (*m/z* 295.2273), allowing to suppose for **28** a ketene structure, along with the product ion at *m/z* 155.1441, corresponding to a negatively charged 1-decen-1-ol ($C_{10}H_{19}O$) originated from the acyl chain' end-part by neutral loss of 96 Da (a heptadiene molecule) from the $[(M-H-44)]^-$ ion. This fragmentation pattern allowed to putatively define **28** as 9-oxo-octadec-7-enoic acid. [20]

.

- *Identification of phospholipids*

Phospholipids (PL) are the main constituents of biological membranes and have important structural and functional properties. They are made up of several distinct moieties with different polar head groups. Each phospholipid class consists of a mixture of many molecular species containing different combinations of fatty acids in the *sn*-1 and *sn*-2 positions on the glycerol backbone.

Phospholipids which are the main constituents of some foods are believed to have a diverse array of beneficial effects in the human body. For example, dietary phosphatidylserine (PS) has emerged as a brain-specific nutrient that ameliorates declining memory, while dietary phosphatidylcholine (PC) has shown to prevent the development of nonalcoholic fatty liver disease in rats fed with a high-fat diet. Moreover, phosphatidylethanolamine (PE) has shown to cause a decrease in serum cholesterol, and phosphatidylinositol (PI) has proved to promote cholesterol transport and excretion in rabbits and to affect cholesterol metabolism and absorption of PI in rats[9].

Dietary phospholipids, known to be metabolized in the gastrointestinal lumen, are hydrolyzed into free fatty acids and lyso-phospholipids (l-PL) by pancreatic phospholipase A_2 (PLA_2) before absorption. l-PL are phospholipids in which only one of *sn*-1/*sn*-2 position of glycerol is fatty acylated; they are recognized as important cellular signaling molecules and are involved in important processes such as cell proliferation, cell survival, cell migration, diabetes, angiogenesis, inflammation, and cancer mediated by l-PL-specific G-protein coupled receptors[10].

A challenge in identifying phospholipids by MS-based methods is that species from different structural classes may have the same masses. For example, exact masses of molecular cations of PC and PE may overlap because their heteroatom compositions are the same (NO_8P).

This was the case of any compounds occurring in the LC-ESI/LTQOrbitrap/MS profile of the *A. esculentus* extract and showing a molecular formula with a NO_7P heteroatom composition that could correspond to lyso-forms of both PC and PE phospholipids. Compounds **11**, **18**, and **21** could be defined as lyso-phosphatidylethanolamine (l-PE) derivatives by considering the occurrence in their MS^2 spectrum of product ions at nominal *m/z* 214 ($C_5H_{13}O_6NP$) and 196 ($C_5H_{11}O_5NP$), corresponding to the glycerophosphatidylethanolamine anion and to its mono-dehydrated form, respectively, and of the product ion obtained from the $[M-H]^-$ ion by neutral loss of ethanolamine (61 Da) (**Table 3.2**).[16] The l-PE fatty acid identity could be instead inferred by the main product ion, corresponding to the $[RCOO]^-$ fatty acid ion (**Table 3.2**). The peak **35**, showing a NO_8P heteroatom composition, could be assumed as the phosphatidylethanolamine species (PE) having both glycerol positions acylated, as confirmed by the presence of two $[RCOO]^-$ ions at *m/z* 255.2328 ($C_{16}H_{32}O_2$) and 279.2328 ($C_{18}H_{32}O_2$), whose ion intensity ratio allowed to establish the acyl residue regiospecificity.[16] Compounds **6** and **8** also showed the NO_7P heteroatom composition but a different tandem mass spectrum, displaying a base peak (at *m/z* 402.2406 and 400.2250, respectively)- originated from the $[M-H]^-$ ion by neutral loss of the mono-dehydrated form of the glycerol unit (74 Da)- having a molecular formula ($C_{20}H_{37}O_5NP$ and $C_{20}H_{35}O_5NP$, respectively) ascribable to a phosphorylated N-fatty acid amide ion, typical of N-acyl-glycerophosphatidylethanolamine structures (NA-GPEs) in which the fatty acid is N-acylated on the nitrogen of the ethanolamine head group (**Table 3.2**).[16] The presence of product ions at nominal *m/z* 171 ($C_3H_8O_6P$) and 153 ($C_3H_6O_5P$), corresponding to the glycerophosphate anion and to its mono-dehydrated form, respectively, confirmed this assignment. Noteworthy this is the first report for compound **6**. Compounds **13**, **20** and **22** were characterized by a different fragmentation pattern showing a main peak formed by neutral loss of 60 Da ($C_2H_4O_2$) from the parent ion. This peak, on the basis of the parent ion molecular

formula and of literature evidences about formation in negative ion mode of $[(M+FA)-H]^-$ formic acid adduct for the pseudomolecular ion of phosphatidylcholine (PC) derivatives, could correspond to the $[(M-15)-H]^-$ ion, in which the PC derivative lost a methyl group from the choline head-group to generate formic acid methyl ester (60 Da). This hypothesis was confirmed by the presence in the MS^3 spectrum of the product ion corresponding to the $RCOO^-$ fatty acid anion originated from the class typical neutral loss of 225 Da ($C_7H_{16}O_5NP$) (**Table 3.2**).[16]

Compound **14** showed a $[M-H]^-$ ion at *m/z* 638.3298, supporting the molecular formula $C_{29}H_{54}O_{12}NP$. Its tandem mass spectrum highlighted a main product ion at *m/z* 476.2767 due to neutral loss of a hexose unit (162 Da, $C_6H_{10}O_5$), a product ion at *m/z* 279.2319 corresponding to the $RCOO^-$ anion of an octadecadienoic acid, and two minor product ions at *m/z* 433.2352 ($C_{21}H_{38}O_7P$), formed by neutral loss of 205 Da, and at *m/z* 518.2872 ($C_{25}H_{45}O_8NP$), formed by neutral loss of 120 Da (**Table 3.2**). These data allowed to suppose for **14** a lyso-phospholipid structure in which the head-group was composed of a glycosylamine generated from the nucleophilic addition of the amine of the l-PE to the carbonyl function of a reducing sugar, according to the Maillard reaction leading to glycation of aminophospholipids.[21] So, the neutral loss of 205 Da could be referred to the loss of an aziridine with a hexose unit (43+162 Da), and the neutral loss of 120 Da ($C_4H_8O_4$) to the hexose fragmentation, allowing to distinguish between glycosylamines and the more stable aminoketoses (Amadori compounds);[22] Therefore, **14** could be putatively defined as the lyso-form of phosphatidylethanolamine N-glycoside (g-PE), here described for the first time, namely a Schiff-PE, a chemical class already reported in foods.[23-25]

Compounds **10**, **12**, **29**-**31** and **33** were attributed to lyso-phosphatidylinositol (l-PI) and phosphatidylinositol (PI) classes, on the basis of their molecular formula and mass fragmentation pattern, this latter characterized by the product ion at

nominal *m/z* 241 (**Table 3.2**), corresponding to the mono-dehydrated form of the inositol-phosphate ($C_6H_{10}O_8P$), the $[(M-162)-H]^-$ and $[(M-180)-H]^-$ product ions formed by neutral loss of the inositol moiety, and by $[(M-RxCOOH)-H]^-$, $[(M-Rx=CO)-H]^-$ and $RxCOO^-$ ions, allowing to establish the fatty acid nature and regiospecificity (**Table 3.2**).[16] Interestingly, compounds **28** and **29** could be defined as hydroxylated phosphatidylinositol molecules (OH-PI) in which the sn-1 position on glycerol backbone was esterified with an oxylipin unit.[16]

The fragmentation pattern of **23** and **25** pointed to define them as lyso-phosphatidic acids (l-PA), showing the highly diagnostic product ion at nominal *m/z* 153 corresponding to the mono-dehydrated glycero-phosphate (**Table 3.2**). The same product ion occurred in the MS^2 spectrum of **19**, along with those at *m/z* 227.0326 ($C_6H_{12}O_7P$), corresponding to the mono-dehydrated glycerophosphoglycerol anion, and *m/z* 391.2239 ($C_{19}H_{36}O_6P$), originated by neutral loss of a glycerol unit (92 Da), allowing to identify 19 as a lyso-phosphatidylglycerol (l-PG) lipid. The product ion at *m/z* 391.2245, corresponding to a mono-dehydrated glycerophosphate esterified to a palmitic acid unit, could be observed also in the MS^2 spectrum of compound **36**, putatively identified as dipalmitoylphosphatidylglycerol (PG). By analogous considerations, compounds 37-39 could be defined as phosphatidic acids (PA) differing each other for the fatty acids (**Table 3.2**).[16]

- *Identification of glycolipids*

Among glycolipids, sulfolipids and galactolipids, species containing a sulfonic group and one (or two) galactose molecule(s), respectively, have been regarded as the predominant lipid components of the photosynthetic membrane in plants, algae and various bacteria.[35]

Mono- and digalactosyldiacylglycerols, along with digalactosylmonoacylglycerols (MGDG, DGDG and DGMG) have been observed in significant levels in oat kernels and other seeds.[36] Various studies have shown that galactolipids exhibit specific biological properties including antiviral, antitumor, and anti-inflammatory activities. Additionally, they appear to play a role in the inhibition and promotion of cell growth and in protection against cell death. [37]

The LC-ESI/LTQOrbitrap/MS/MS^n analysis allowed to ascertain the presence of DGMG species in *A. esculentus* (**Table 3.2**).

The MS^2 spectra of $[M-H]^-$ ions from DGMGs showed as principal product ion the $[(M-RCOOH)-H]^-$ ion due to the cleavage of the fatty acid attached to the *sn*-1 or *sn*-2 positions of the glycerol backbone, along with minor product ions corresponding to the $RCOO^-$ ion. The $[(M-RCOOH-162)-H]^-$ product ion originated by the loss of RCOOH and one anhydrous hexose moiety (belonging to the disaccharide unit linked to the *sn*-3 position of the glycerol), and the molecular ion without both the fatty acid and the glycerol moiety, also in the anhydrous form, were detectable (**Table 3.2**).[32] Thus, DGMG species differing in degree of unsaturation and/or regiospecificity of the fatty acyl group were identified. They are here described for the first time in the specie.

Sulfoquinovosyldiacylglycerols (SQDG) are relatively abundant sulfolipids specifically associated with photosynthetic membranes of higher plants, mosses, ferns, algae and most photosynthetic bacteria. [35] Their chemical structure is characterized by two fatty acyl moieies, with various degrees of unsaturation, linked

to the glycerol backbone at *sn*-1 and *sn*-2 positions, and a polar head group represented by a sulfoquinovose molecule. In contrast to most naturally occurring sulfolipids, in which sulfur is involved in an ester linkage, SQDGs bear a sulfonic acid residue. Some SQDGs have been reported to exhibit a remarkable antiviral activity, mainly against the human immunodeficiency virus (HIV-1), and are clinically promising as antitumor and immunosuppressive agents.[35]

The careful study of the full LC-ESI/LTQOrbitrap/MS/MS^n spectra pointed to suggest the presence of SQDGs species in the extract, accordingly with their molecular formula containing a sulfur atom (**Table 3.2**). The analysis of the corresponding MS^2 and MS^3 allowed to define the nature of the corresponding acyl chains. Tandem mass spectrum of SQDG precursor ions clearly demonstrated a remarkable loss of neutral fatty acids from the relative pseudomolecular anion, clearly prevailing over ketene loss and carboxylate anion generation. In particular, in agreement with literature data, the regiochemical characterization of SQDG species could be based on the intensities of the $[(M-R_xCOOH)-H]^-$ product ions (with $[(M-R_1COOH)-H]^- > [(M-R_2COOH)-H]^-$).[35] Additionally, the SQDG identity could be confirmed by the analysis of the MS^3 spectrum generated by the $[(M-R_1COOH)-H]^-$/$[(M-R_2COOH)-H]^-$ ions, characterized by the presence of the well-known fragment ion at *m/z* 225, for which a structure bearing an epoxydic bridge between carbon 1 and 2 of the quinovosylic ring has been recently proposed. [35] Noteworthy, the three SQDGs found in the extract of *A. esculentus* have never been described before in the specie.

The mass spectrometric behavior of compounds **9**, **15-17**, **27** indicated their glyceroglycolipid nature, with hydrophilic carbohydrate groups and hydrophobic fatty acid moieties linking a glycerol moiety.[26] Compounds **9**, **16** and **17** showed in MS^2 spectra a common principal product ion at nominal *m/z* 397, whose molecular formula ($C_{15}H_{25}O_{12}$) and RDB value (3.5) corresponded to the mono-dehydrated form of a diglycosidated glycerol, formed from the $[M-H]^-$ ion by neutral loss of a

fatty acid unit (**Table 3.2**). The presence of a product ion at nominal *m/z* 235, likely formed by neutral loss of a mono-dehydrated hexose from the product ion at nominal *m/z* 397, along with the $RCOO^-$ anion, supported the identification of these compounds as digalactosylmonoacylglycerol (DGMG) species.[16] Analogously, compound **27** was putatively identified as monogalactosylmonoacylglycerol (MGMG) (**Table 3.2**). Compound **15** showed a $[M-H]^-$ ion at *m/z* 555.2834, supporting a molecular formula containing a sulphur atom. MS^2 spectrum of $[M-H]^-$ ion clearly highlighted two main product ions at *m/z* 299.0438 ($C_9H_{15}O_9S$), formed by neutral loss of a palmitic acid unit, and *m/z* 225.0069 ($C_6H_9O_7S$), likely corresponding to a mono-dehydrated sulfoquinovose moiety (**Table 3.2**),[16] identifiying 15 as sulfoquinovosyl-monoacylglycerol (SQMG).[27]

- *Identification of sphingolipids*

Sphingolipids are anubiquitous class of lipids present in a variety of organisms including eukaryotes and bacteria. They are major structural lipids of biological membranes and perform additional essential functions as signalling molecules. Although there is considerable structural variation among the sphingolipids from different species, the basic building block of sphingolipids is an amino alcohol long chain base (LCB), which is composed predominantly of 18 carbon atoms.[34]

The analysis of LC-ESI/LTQOrbitrap/MS/MS spectra of compounds **32** and **34** showed signals $[(M-180)-H]^-$ and $[(M-162)-H]^-$ product ions, originated by neutral loss of whole or mono-dehydrated hexose unit, whose further fragmentation allowed to define them as glycosylceramides (GlcCer).[16, 28] For compound **34**, e.g., the MS^3 spectrum of the $[(M-180)-H]^-$ ion displayed two diagnostic product ions at *m/z* 298.2754 ($C_{18}H_{36}O_2N$), corresponding to the hydroxylated fatty amide anion, and *m/z* 253.2524 ($C_{17}H_{33}O$), corresponding to the shortened acyl chain by cleavage of the C1'-C2' bond, identifying the fatty acid unit as 2-hydroxy-octadecanoic acid

(h18:0) (**Table 3.2**). The presence of the product ion at *m/z* 278.2487 ($C_{18}H_{32}ON$), corresponding to the amino alcohol long chain base (LCB) in form of mono-dehydrated anion, suggested the identity of this latter as a dihydroxylated and di-unsaturated sphingoid base (d18:2). Further confirmation of these assignments was given by the product ions at *m/z* 306.2447 ($C_{19}H_{32}O_2N$), corresponding to the formylated-LCB anion, and at *m/z* 368.3172 ($C_{22}H_{42}O_3N$) and 352.2859 ($C_{21}H_{38}O_3N$), corresponding to product ions containing fatty acyl chain linked to part of LCB and likely formed by cleavages of the C4-C5 and C3-C4 bonds on the LCB moiety (**Table 3.2**)

Table 3.2. Polar lipids putatively identified in the *n*-butanol extract of *A. esculentus* fruits

n°	Compound	R_t (min)	Molecular Formula	$[M-H]^-$	RDB	ppm	Characteristic product ions
1	9,12,13-TriHODE (10,15)	4.4	$C_{18}H_{32}O_5$	327.2172	3.5	1.80	309.2069(*24*)/291.1961(*70*)/273.1856(*5*)/229.1442(*100*)/211.1340(*56*)/171.1026(*34*)
2	9,12,13-TriHOME (10)	5.3	$C_{18}H_{34}O_5$	329.2328	2.5	1.82	311.2223(*45*)/293.2116(*30*)/229.1442(*100*)/211.1339(*61*)/199.1337(*2*)/171.1026(*14*)
3	15,16-DiHODE	8.4	$C_{18}H_{32}O_4$	311.2221	3.5	1.36	293.2118(*99*)/275.2010(*54*)/253.1805(*6*)/235.1699(*24*)/223.1701(*100*)
4	9,10-DiHODE	8.7	$C_{18}H_{32}O_4$	311.2223	3.5	1.94	293.2116(*100*)/275.2010(*47*)/201.1131(*80*)/171.1024(*21*)
5	oxo-9,10-DiHOME (11)	8.8	$C_{18}H_{32}O_5$	327.2169	3.5	1.07	309.2068(*100*)/291.1960(*31*)/273.1855(*15*)/213.1130(*9*)/201.1132(*43*)/171.1026(*85*)
6	NA-GPE (18:3)	9.1	$C_{23}H_{42}O_7NP$	474.2609	4.5	-1.32	400.2250(*100*)/171.0059(*14*)/152.9957(*61*)
7	9,10-DiHOME	9.6	$C_{18}H_{34}O_4$	313.2379	2.5	1.64	295.2272(*51*)/277.2166(*29*)/201.1131(*100*)/171.1025(*17*)
8	NA-GPE (18:2)	9.7	$C_{23}H_{44}O_7NP$	476.2769	3.5	-0.52	402.2406(*100*)/171.0063(*14*)/152.9959(*60*)
9	DGMG (18:3)	9.9	$C_{33}H_{56}O_{14}$	675.3590	6.5	0.56	415.1443(*32*)/397.1338(*100*)/323.0983(*2*)/305.0870(*4*)/277.2165(*3*)/235.0818(*4*)
10	l-PI (18:2)	10.2	$C_{27}H_{49}O_{12}P$	595.2877	4.5	-0.22	415.2228(*60*)/315.0484(*22*)/279.2321(*100*)/241.0108(*7*)

11	l-PE (18:3)	10.3	$C_{23}H_{42}O_7NP$	474.2611	4.5	-0.86	413.2081(*2*)/277.2166(*100*)/214.0481(*2*)/196.0377(*2*)
12	l-PI (16:0)	10.4	$C_{25}H_{49}O_{12}P$	571.2893	2.5	2.66	409.2356(*45*)/391.2254(*60*)/315.0495(*35*)/255.2331(*100*)/241.0121(*25*)
13	l-PC (18:3)	10.5	$C_{26}H_{48}O_7NP$	562.3141 $[(M+FA)-H]^-$	4.5	0.26	502.2925(*100*); MS^3(502.2925): 277.2165(*100*)
14	*g*-l-PE (18:2)	10.6	$C_{29}H_{54}O_{12}NP$	638.3298	4.5	-0.25	620.3186(*6*)/548.2981(*3*)/518.2872(*17*)/476.2767(*100*)/433.2352(*3*)/279.2319(*11*)
15	SQMG (16:0)	10.9	$C_{25}H_{48}O_{11}S$	555.2834	2.5	0.16	299.0438(*97*)/255.2322(*10*)/225.0069(*100*)
16	DGMG (18:2)	10.9	$C_{33}H_{58}O_{14}$	677.3748	5.5	0.71	415.1447(*30*)/397.1342(*100*)/323.0966(*2*)/305.0871(*5*)/279.2318(*3*)/235.0817(*4*)
17	DGMG (16:0)	11.1	$C_{31}H_{58}O_{14}$	653.3745	3.5	0.35	415.1443(*30*)/397.1337(*100*)/323.0976(*1*)/305.0869(*5*)/235.0816(*3*)
18	l-PE (18:2)	11.2	$C_{23}H_{44}O_7NP$	476.2773	3.5	0.37	415.2243(*2*)/279.2322(*100*)/214.0481(*1*)/196.0377(*2*)
19	l-PG (16:0)	11.3	$C_{22}H_{45}O_9P$	483.2719	1.5	0.28	391.2239(*5*)/255.2324(*100*)/227.0326(*4*)/152.9955(*3*)
20	l-PC (18:2)	11.5	$C_{26}H_{50}O_7NP$	564.3295 $[(M+FA)-H]^-$	3.5	-0.12	504.3081(*100*); MS^3(504.3081): 279.2320(*100*)
21	l-PE (16:0)	11.5	$C_{21}H_{44}O_7NP$	452.2773	1.5	0.39	255.2322(*100*)/214.0483(*1*)/196.0378(*2*)
22	l-PC (16:0)	11.7	$C_{24}H_{50}O_7NP$	540.3294 $[(M+FA)-H]^-$	1.5	-0.45	480.3081(*100*);

							MS^3(480.3081):255.2323(*100*)/242.0810(*1*)/224.0677(*3*)
23	l-PA (18:2)	12.2	$C_{21}H_{39}O_7P$	433.2362	3.5	2.80	152.9958(100)
24	9-HODE (10,12)	12.3	$C_{18}H_{32}O_3$	295.2270	3.5	0.84	277.2169(*100*)/195.1389(*2*)/171.1026(*70*)
25	l-PA (16:0)	12.7	$C_{19}H_{39}O_7P$	409.2361	1.5	2.7	152.9957(100)
26	9-KODE (10,12)	13.2	$C_{18}H_{30}O_3$	293.2116	4.5	1.67	275.2011(*40*)/249.2217(*100*)/197.1181(*35*)/185.1182(*80*)
27	MGMG (18:3)	13.5	$C_{27}H_{46}O_9$	513.3058	5.5	0.55	277.2169(*100*)/253.0923(*9*)
28	9-KOME (7)	13.9	$C_{18}H_{32}O_3$	295.2273	3.5	1.89	277.2166(*35*)/251.2379(*100*)/155.1441(*40*)/141.1286(*4*)
29	PI (18:2-1*O*; 16:0)	16.7	$C_{43}H_{79}O_{14}P$	849.5144	5.5	2.39	553.2798(*100*)/391.2258(*40*)/295.2290(*30*)/ 241.0109(*15*)
30	PI (18:2-2*O*; 16:0)	16.9	$C_{43}H_{79}O_{15}P$	865.5092	5.5	2.17	847.4987(*100*)/553.2804(*15*)/391.2256(*10*)
31	PI (16:0; 18:3)	19.0	$C_{43}H_{77}O_{13}P$	831.5036	6.5	2.16	575.2659(*21*)/571.2886(*19*)/553.2783(*100*)/391.2259(*60*)/277.2176(*15*)/255.2324(*35*)
32	GlcCer (d18:2; h16:0)	19.5	$C_{40}H_{75}O_9N$	712.5374	4.5	2.25	550.4847(*41*)/532.4738(*100*); MS^3(532.4738): 324.2556(*97*)/306.2423(*100*)
33	PI (16:0;18:2)	19.7	$C_{43}H_{79}O_{13}P$	833.5191	5.5	1.97	595.2850(*2*)/577.2785(*21*)/571.2898(*17*)/553.2785(*100*)/415.2252(*7*)/391.2259(*60*)/279.2329(*20*)/255.2329(*35*)
34	GlcCer (d18:2; h18:0)	21.1	$C_{42}H_{79}O_9N$	740.5690	4.5	2.59	578.5150(*50*)/560.5045(*100*)/299.2591(*8*); MS^3(560.5045): 542.4962(*22*)/368.3172(*37*)/352.2859(*100*)/306.2447(*75*)/298.2754(11)/278.2487(42)/253.2524(*26*)

35	PE (16:0; 18:2)	21.9	$C_{39}H_{74}O_8NP$	714.5084	4.5	2.14	452.2774(*25*)/279.2328(*100*)/255.2328(*30*)
36	PG (16:0; 16:0)	22.8	$C_{38}H_{75}O_{10}P$	721.5034	2.5	2.70	483.2732(*17*)/465.2649(*10*)/391.2245(*25*)/255.2326(*100*)
37	PA (18:2; 18:3)	23.6	$C_{39}H_{67}O_8P$	693.4509	7.5	2.81	433.2349(*17*)/415.2254(*100*)/413.2104(*99*)/279.2329(*74*)/277.2189(*16*)
38	PA (18:2; 18:2)	24.1	$C_{39}H_{69}O_8P$	695.4664	6.5	2.59	433.2358(*60*)/415.2252(*100*)/279.2326(*80*)
39	PA (16:0; 18:2)	25.3	$C_{37}H_{69}O_8P$	671.4667	4.5	3.03	415.2255(*20*)/409.2359(*60*)/391.2256(*100*)/279.2329(*30*)/255.2326(*60*)

Relative intensities are reported in round brackets. The 18-carbon hydroxylated acyl chain of OH-PI is abbreviated, as 18:2-1*O* and 18:2-2*O*, to indicate two double bond equivalent s and one or two oxygen atoms beyond the carbonyl group. In GlcCer nomenclature, the 2-hydroxylated fatty acids are indicated by the letter “h” added to their lipid number (i.e., h16:0). The nomenclature used to name LCBs consists of the letter “d” to indicate di-hydroxylated bases followed of two numbers separated by a colon, indicating the number of carbons and double bonds.

3.4 LC-HRMS profile and NMR analysis of okra specialized metabolites

The LC-ESI/LTQOrbitrap/MS profile (**Figure 3.2**) performed on a RP-C18 column showed 19 main ion peaks which, on the basis of molecular formula, mass fragmentation behavior, and literature data,[29, 30] could be defined as phenolic acids, distinguishable into benzoic acid (**40**-**42**, **44**-**45**, **47**-**49**) and hydroxycinnamic acid derivatives (**43**, **46**, **50**-**52**), and flavonoids (**53**-**58**), namely quercetin and myricetin glycosides (**Table 3.3**, **Figure 3.2**).

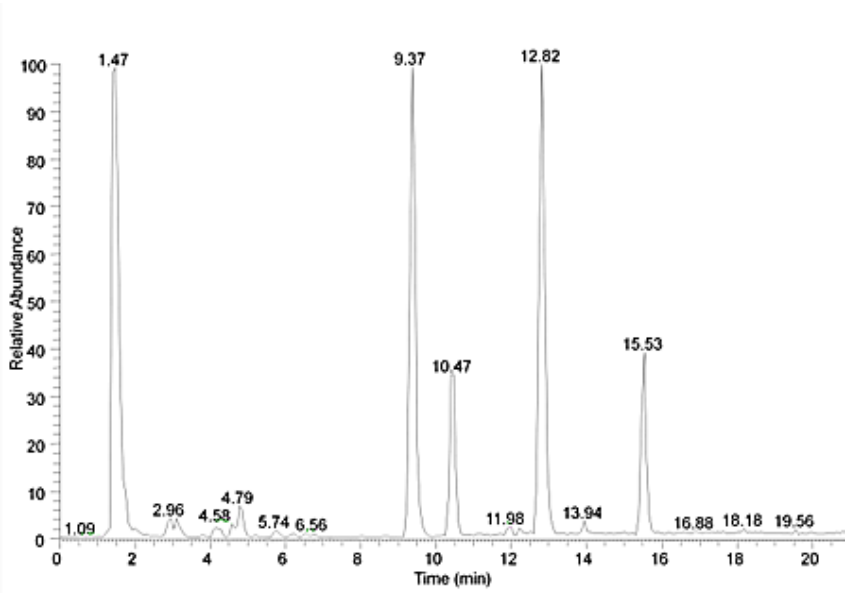

Figure 3.2. LC-ESI/LTQOrbitrap/MS profile (negative ion mode) of the *n*-butanol extract of *A. esculentus* fruits

The fragmentation pattern analysis allowed to ascertain the presence in most compounds of sugar units linked via different combinations to the aglycone moiety, determining characteristic neutral losses from precursor ions of 162 and 132 Da, precisely corresponding to the mono-dehydrated form of hexose and pentose sugars, respectively (**Table 3.3**). Moreover, product ions originated by neutral loss of 44 Da (CO_2) from the pseudomolecular $[M-H]^-$ ions of **47**, **50**, and **58** indicated

a free carboxylic group in their structure but the structure of the current compounds was not clear by only HRMS experiments. With the purpose to achieve an in-depth knowledge of the phenolic constituents of the fruit and to unambiguously attribute the main peaks observed in LC-HRMS profile, a phytochemical investigation of the n-butanol fraction was performed. The current fraction was fractionated by RP-HPLC to afford pure compounds of which the structures were elucidated bu 1D and 2D NMR experiments.

Isolation and characterization

After their isolation, the structural identification of compounds **40-58** was confirmed by 1D- and 2D-NMR experiments, allowing to unambiguously define both the sugar identity and the glycosylation site (**Table 3.3**). By this analytical approach, compounds **43**, **46**, and **50-51** were identified as the hydroxycinnamic derivatives: ferulic acid 4-*O*-β-D-glucopyranoside (**43**), coumaric acid (**46**), ferulic acid (**50**), and sinapic acid (**51**), while compounds **53-58** were identified as the flavonoids: quercetin-3-*O*-β-D-glucopyranosyl-(1→6)-β-D-glucopyranoside (**53**), myricetin-3-*O*-β-D-glucopyranoside (**54**), quercetin-3-*O*-β-D-xylopyranosyl-(1→2)-β-D-glucopyranoside (**55**), rutin (**56**), quercetin-3-*O*-β-D-glucopyranoside (**57**) and quercetin-3-*O*-β-D-(6-malonyl) glucopyranoside (**58**). [3, 10, 31] Compound **40** was identified by Li, 2011 as the known compound 4-hydroxybenzoic acid 1-*O*-β-D-glucopyranosyl ester, already isolated from the flowers of *Abelmoshus manihot* L. The following polar metabolites were here reported for the first time in *A. esculentus*: benzoic acid β-D-glucopyranosyl ester (**41**), benzyl alcohol β-D-xylopyranosyl-(1→6)-β-D-glucopyranoside (**42**), 4-hydroxybenzoic acid (**44**), 3-methoxybenzoic acid (**45**), 3,4-dimethoxybenzoic acid (**47**), benzoic acid β-D-xylopyranosyl-(1→6)-β-D-glucopyranosyl ester (**48**), tecomin (**49**), and 4-hydroxycinnamic acid β-D-glucopyranosyl ester (**52**).

Table 3.3. Specialized metabolites identified in the *n*-butanol extract of *A. esculentus* fruits

n°	Compound	R_t (min)	Molecular formula	$[M-H]^-$	RDB	ppm	Characteristic product ions
40	4-hydroxybenzoic acid 1-O-β-D-glucopyranosyl ester	2.9	$C_{13}H_{16}O_8$	299.0760	6.5	-0.60	137.0247(100)
41	benzoic acid β-D-glucopyranosyl ester	4.1	$C_{13}H_{16}O_7$	283.0671	6.5	4.00	121.0289(100)
42	benzyl alcohol β-D-xylopyranosyl-(1→6)-β-D-glucopyranoside	4.2	$C_{18}H_{26}O_{10}$	401.1444	6.5	0.53	269.1021(100)/161.0453(15)
43	ferulic acid 4-O-β-D-glucopyranoside	4.8	$C_{16}H_{20}O_9$	355.1020	7.5	-1.12	193.0504(100)
44	4-hydroxybenzoic acid	5.0	$C_7H_6O_3$	137.0240	5.5	2.18	-
45	3-methoxybenzoic acid	5.5	$C_8H_8O_4$	167.0347	5.5	5.00	-
46	coumaric acid	6.7	$C_9H_8O_3$	163.0393	5.5	4.70	-
47	3,4-dimethoxybenzoic acid	6.8	$C_9H_{10}O_4$	181.0050	5.5	-1.20	137.0611(100)
48	benzoic acid β-D-xylopyranosyl-(1→6)-β-D-glucopyranosyl ester	6.8	$C_{19}H_{28}O_{10}$	415.1598	6.5	-0.05	283.1190(100)
49	tecomin	6.9	$C_{15}H_{20}O_9$	343.1024	6.5	0.17	181.0500(100)
50	ferulic acid	7.3	$C_{10}H_{10}O_4$	193.0504	6.5	3.10	149.0609(100)
51	sinapic acid	8.7	$C_{11}H_{12}O_5$	223.0604	6.5	1.50	205.0479(100)/163.0375(20)

52	4-hydroxycinnamic acid β-D-glucopyranosyl ester	8.9	$C_{15}H_{18}O_8$	325.0919	7.5	0.20	163.0395(100)
53	quercetin-3-O-β-D-glucopyranosyl-(1→6)-β-D-glucopyranoside	9.3	$C_{27}H_{30}O_{17}$	625.1396	13.5	-0.44	301.0343(100)/463.0878(10)
54	myricetin-3-O-β-D-glucopyranoside	9.9	$C_{21}H_{20}O_{13}$	479.0813	12.5	-1.40	317.0304(100)
55	quercetin-3-O-β-D-xylopyranosyl-(1→2)-β-D-glucopyranoside	10.4	$C_{26}H_{28}O_{16}$	595.1295	13.5	0.26	301.0342(100)/445.0757(25)/463.0878(15)
56	rutin	11.9	$C_{27}H_{30}O_{16}$	609.1447	13.5	-0.58	301.0350(100)
57	quercetin-3-O-β-D-glucopyranoside	12.8	$C_{21}H_{20}O_{12}$	463.0873	12.5	0.38	301.0345(100)
58	quercetin-3-O-β-D-(6-malonyl)-glucopyranoside	15.5	$C_{24}H_{22}O_{15}$	549.0879	14.5	0.70	505.0970(100)/301.0348(15)

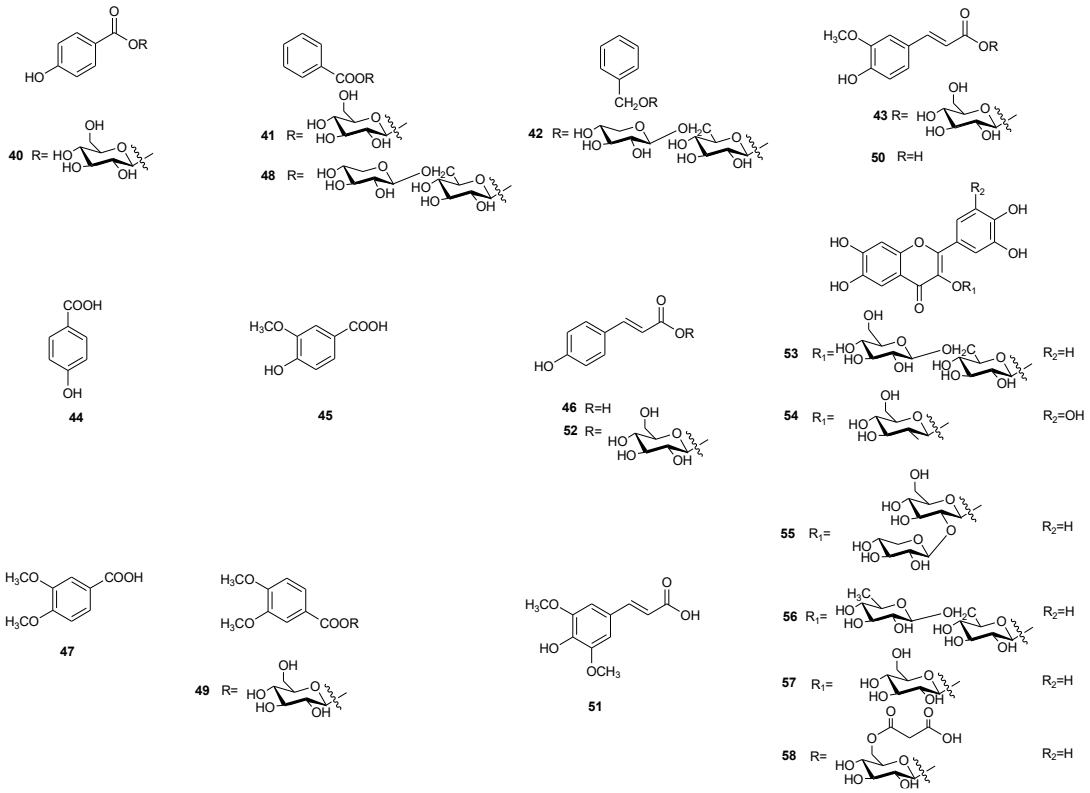

Figure 3.3 Specialized secondary metabolite (**40**-**58**) in *n*-butanol extract of *A. esculentus* fruits

3.5 Conclusions

In the present study, detailed information about the polar lipid composition of *A. esculentus* fruit was provided for the first time, with the identification of 39 compounds mainly belonging to oxylipin, phospholipid, glycolipid and sphingolipid classes, contributing to fill a gap in the literature concerning a fruit largely distributed and with an interesting range of nutritional and nutraceutical properties. The phytochemical investigation guided by LC-HRMS/MS analyses led to the isolation and characterization via combined NMR and ESI/HRMS experiments of 19 compounds, 8 of them never reported before in okra fruit. The antioxidant activity of the extract has been evaluated confirming *A. esculentus* as a good source of natural antioxidants. In addition, the antihyperglycemic activity has been tested by α-glucosidase inhibitory assay, defining okra fruit as an effective source of α-glucosidase inhibitors. In particular, this activity could be due to a synergistic effect, considering that rutin **56** and quercetin-3-O-β-D-glucopyranoside **57** have been already reported to exhibit this bioactivity.[39] The results obtained confirm the ethnomedicinal use of okra for the treatment of diabetes, suggesting the potential use of this fruit as a functional food with anti-hyperglycemic effects and as a natural antioxidants source.

3.6 Experimental section

Plant material and sample preparation

Okra (*A. esculentus* L. Moench.) fruits (1 kg) were purchased from local market in Tunis in June 2016. They were freeze dried, grinded in a thin powder and extracted with a solution of ethanol and water (7:3, v/v) (400 mL×3 days×3 times) at room temperature. The filtrate extract was concentrated under vacuum until elimination of solvent to obtain a crude extract (30 g), that was subjected to n-butanol-water partition to remove free sugars. 3.7 g of n-butanol extract were obtained.

Isolation and characterization

HPLC-RI separations were carried out on a Waters 590 system equipped with a Waters R401 refractive index detector, a Rheodyne injector, and a Waters Symmetry C18 Prep (300 × 7.8 mm; 7 μm) column. HPLC-UV separations were carried out on an Agilent 1260 Infinity system (Agilent Technologies, Palo Alto, CA, USA), equipped with a binary pump (G-1312C), an UV detector (G-1314B), and a Phenomenex C18 Synergi-Hydro-RP (250×10 mm; 10 μm) column. LC-ESI/HRMS/MS^n experiments were performed using a Thermo Scientific liquid chromatography system constituted of a quaternary Accela 600 pump and an Accela autosampler, connected to a linear ion-trap-Orbitrap hybrid mass spectrometer (LTQOrbitrap XL) equipped with an electrospray ion (ESI) source (Thermo Fisher Scientific, Bremen, Germany).

NMR experiments were acquired in methanol-d4 (99.95%, Sigma-Aldrich) on a Bruker DRX-600 spectrometer (Bruker BioSpin GmBH, Rheinstetten, Germany) equipped with a Bruker 5 mm TCI CryoProbe at 300 K. Data processing were carried out with Topspin 3.2 software.

Determination of total phenolic content

As reported in general experimental section.

Trolox Equivalent Antioxidant Capacity (TEAC) assay

As reported in general experimental section.

Inhibition Assay for α-Glucosidase Activity

The α-glucosidase inhibitory activity was determined by following protocols reported in literature[14] with slight modifications. n-butanol extract was dissolved in methanol and 4 concentrations were prepared (250 µg, 500 µg, 700 µg and 1000 µg); 20 µL of each concentration and 30 µL of α-glucosidase from *Saccharomyces cerevisiae* (Sigma-Aldrich, Milan, Italy) (2 U/mL, 0.1 M potassium phosphate buffer, pH 6.8) were mixed in 650 µL of 0.1 M potassium phosphate buffer (pH 6.8). After 5 min of incubation at 37.0 °C, 150 µL of p-NPG (10 mM) as substrate was added to the mixture, and the solution was incubated at 37.0 °C for further 10 min. Then, 650 µL of Na_2CO_3 (1 M) was added to stop the reaction. The absorbance of generated *p*-nitrophenol was measured at 405 nm using an UV spectrometer. Acarbose (range of tested concentration 0.2-5 mg/mL) was used as positive control. For negative control, the sample was substituted with 20 µL of MeOH. The inhibition assay was performed in triplicate and the concentration that inhibited 50% α-glucosidase activity was calculated as the IC_{50} (mg/mL) value.

LC-ESI/LTQOrbitrap/MS/MS^n analysis of n-butanol extracts of A. esculentus

The polar lipid and specialized metabolite profiles of the *n*-butanol okra extract were achieved by LC-ESI/LTQOrbitrap/MS, in negative ion mode. For polar lipid analysis, a chromatographic separation was performed on a Waters Symmetry

300^{TM} C4 (2.1x150 mm; 3.5 µm) column. The mobile phase consisted of H_2O + 0.1% formic acid (A) and CH_3CN + 0.1% formic acid (B). A linear gradient program at a flow rate of 0.2 mL/min was used: 0-30 min, from 30 to 100% (B); then 5 minutes to 100% (B) and back to 30% (B) for 5 min.

For specialized metabolite analysis, a chromatographic separation was performed on a Phenomenex Kinetex EVO C18 (100 x 2.1mm; 5 µm) column. The mobile phase was the same as above described. A linear gradient program at a flow rate of 0.2 mL/min was used: 0-15 min, from 10 to 20% (B), and then 5 min from 20 to 30% (B).

The autosampler was set to inject 10 µl of okra *n*-butanol extract (1 mg/ml). ESI source parameters were as follows: capillary voltage -48 V; tube lens voltage -176.47 V; capillary temperature 280 °C; sheath and auxiliary gas flow (N_2) 15 and 5 (arbitrary units), respectively; source voltage 3.5 kV. MS spectra were acquired by full range acquisition covering *m/z* 180-1600 with a resolving power of 30000. In order to obtain their HRMS/MS and HRMS^3 product ions, a data-dependent scan experiment was performed, in which the first and the second most intense ion from both the HRMS and the HRMS/MS scan event were selected to be submitted to collision induced dissociation (CID). For the experiment, a normalization collision energy at 30%, a minimum signal threshold at 300, an isolation width at 2.0, and a resolving power of 30000 in MS/MS scan mode and 7500 in MS^3 scan mode were used. For specialized metabolite analysis, the autosampler was set to inject 6 µl of okra *n*-butanol extract (1 mg/ml). ESI source parameters were as above reported. MS spectra were acquired by full range acquisition covering *m/z* 120-1600. For fragmentation studies, a data-dependent scan experiment was performed, selecting the three most intense precursor ions of the HRMS scan event to be submitted to CID. For the experiment, collision energy, minimum signal threshold and isolation width were the same as for lipid analysis; resolving power of 30000 in full scan and 7500 in MS/MS were used. For the ESI/HRMS analysis of isolated compounds

(concentration of 0.01 μg/mL), direct infusion was performed by a syringe pump, at a flow rate of 10 μL/min. Xcalibur software version 2.1 was used for instrument control, data acquisition and data analysis.

References

1. I. Molfetta, L. Ceccarini, M. Macchia, G. Flamini and P. L. Cioni, *Abelmoschus esculentus* (L.) Moench. and *Abelmoschus moschatus* Medik: Seeds production and analysis of the volatile compounds, *Food Chem*, 2013, **141**, 34-40.

2. S. Petropoulos, A. Fernandes, L. Barros and I. C. F. R. Ferreira, Chemical composition, nutritional value and antioxidant properties of Mediterranean okra genotypes in relation to harvest stage, *Food Chem*, 2018, **242**, 466-474.

3. P. Arapitsas, Identification and quantification of polyphenolic compounds from okra seeds and skins, *Food Chem*, 2008, **110**, 1041-1045.

4. R. L. Jarret, M. L. Wang and I. J. Levy, Seed Oil and Fatty Acid Content in Okra (*Abelmoschus esculentus*) and Related Species, *J Agr Food Chem*, 2011, **59**, 4019-4024.

5. H. F. R. Gemede, Negussie; Haki, Gulelat Desse; Woldegiorgis, Ashagrie Z.; Beyene, Fekadu, Nutritional quality and health benefits of okra (*Abelmoschus esculentus*): a review, *Journal of Food Processing & Technology*, 2015, **6**, 458/451-458/456.

6. A. Roy, Lal Shrivastava, S., Mandal, S. M., Functional properties of Okra *Abelmoschus esculentus* L. (Moench): traditional claims and scientific evidences *Plant Science Today,* 2014, **1**, 121-130.

7. W. Thanakosai and P. Phuwapraisirisan, First Identification of alpha-Glucosidase Inhibitors from Okra (*Abelmoschus esculentus*) Seeds, *Nat Prod Commun*, 2013, **8**, 1085-1088.

8. J. Liu, Y. P. Zhao, Q. X. Wu, A. John, Y. M. Jiang, J. L. Yang, H. L. Liu and B. Yang, Structure characterisation of polysaccharides in vegetable "okra" and evaluation of hypoglycemic activity, *Food Chem*, 2018, **242**, 211-216.

9. P. T. Nguekouo, D. Kuate, A. P. N. Kengne, C. Y. Woumbo, F. A. Tekou and J. E. Oben, Effect of boiling and roasting on the antidiabetic activity of *Abelmoschus esculentus* (Okra) fruits and seeds in type 2 diabetic rats, *J Food Biochem*, 2018, **42**.

10. H. Ying, H. Y. Jiang, H. Liu, F. J. Chen and Q. Z. Du, Ethyl acetate-n-butanol gradient solvent system for high-speed countercurrent chromatography to screen bioactive substances in okra, *J Chromatogr A*, 2014, **1359**, 117-123.

11. A. Shakeri, M. Masullo, G. D'Urso, M. Iranshahi, P. Montoro, C. Pizza and S. Piacente, In depth chemical investigation of *Glycyrrhiza triphylla* Fisch roots guided by a preliminary HPLC-ESIMSn profiling, *Food Chem*, 2018, **248**, 128-136.

12. A. Cerulli, M. Masullo, P. Montoro, J. Hosek, C. Pizza and S. Piacente, Metabolite profiling of "green" extracts of *Corylus avellana* leaves by H-1 NMR spectroscopy and multivariate statistical analysis, *J Pharmaceut Biomed*, 2018, **160**, 168-178.

13. A. Cerulli, A. Napolitano, M. Masullo, C. Pizza and S. Piacente, LC-ESI/LTQOrbitrap/MS/MSn Analysis Reveals Diarylheptanoids and Flavonol O-glycosides in Fresh and Roasted Hazelnut (*Corylus avellana* cultivar "Tonda di Giffoni"), *Nat Prod Commun*, 2018, **13**, 1123-1126.

14. N. Cardullo, V. Muccilli, R. Saletti, S. Giovando and C. Tringali, A mass spectrometry and (1)H NMR study of hypoglycemic and antioxidant principles from a *Castanea sativa* tannin employed in oenology, *Food Chem*, 2018, **268**, 585-593.

15. J. L. Perez, G. K. Jayaprakasha and B. S. Patil, Metabolite profiling and in vitro biological activities of two commercial bitter melon (*Momordica charantia* Linn.) cultivars, *Food Chem*, 2019, **288**, 178-186.

16. A. Napolitano, A. Cerulli, C. Pizza and S. Piacente, Multi-class polar lipid profiling in fresh and roasted hazelnut (*Corylus avellana* cultivar "Tonda di Giffoni") by LC-ESI/LTQOrbitrap/MS/MSn, *Food Chem*, 2018, **269**, 125-135.

17. C. E. Richardson, M. Hennebelle, Y. Otoki, D. Zamora, J. Yang, B. D. Hammock and A. Y. Taha, Lipidomic Analysis of Oxidized Fatty Acids in Plant and Algae Oils, *J Agr Food Chem*, 2017, **65**, 1941-1951.

18. K. M. Rund, A. I. Ostermann, L. Kutzner, J. M. Galano, C. Oger, C. Vigor, S. Wecklein, N. Seiwert, T. Durand and N. H. Schebb, Development of an LC-ESI(-)-MS/MS method for the

simultaneous quantification of 35 isoprostanes and isofurans derived from the major n3-and n6-PUFAs, *Anal Chim Acta*, 2018, **1037**, 63-74.

19. E. H. Oliw, U. Garscha, T. Nilsson and M. Cristea, Payne rearrangement during analysis of epoxyalcohols of linoleic and alpha-linolenic acids by normal phase liquid chromatography with tandem mass spectrometry, *Anal Biochem*, 2006, **354**, 111-126.

20. M. A. Trapp, M. Kai, A. Mithofer and E. Rodrigues, Antibiotic oxylipins from Alternanthera brasiliana and its endophytic bacteria, *Phytochemistry*, 2015, **110**, 72-82.

21. C. Simoes, V. Simoes, A. Reis, P. Domingues and M. R. M. Domingues, Oxidation of glycated phosphatidylethanolamines: evidence of oxidation in glycated polar head identified by LC-MS/MS, *Anal Bioanal Chem*, 2010, **397**, 2417-2427.

22. C. M. Breitling-Utzmann, A. Unger, D. A. Friedl and M. O. Lederer, Identification and quantification of phosphatidylethanolamine-derived glucosylamines and aminoketoses from human erythrocytes - Influence of glycation products on lipid peroxidation, *Arch Biochem Biophys*, 2001, **391**, 245-254.

23. T. Goldberg, W. J. Cai, M. Peppa, V. Dardaine, B. S. Baliga, J. Uribarri and H. Vlassara, Advanced glycoxidation end products in commonly consumed foods, *J Am Diet Assoc*, 2004, **104**, 1287-1291.

24. A. Kodate, Y. Otoki, N. Shimizu, J. Ito, S. Kato, N. Umetsu, T. Miyazawa and K. Nakagawa, Development of quantitation method for glycated aminophospholipids at the molecular species level in powdered milk and powdered buttermilk, *Sci Rep-Uk*, 2018, **8**.

25. J. H. Oak, K. Nakagawa and T. Miyazawa, UV analysis of Amadori-glycated phosphatidylethanolamine in foods and biological samples, *J Lipid Res*, 2002, **43**, 523-529.

26. A. Napolitano, V. Carbone, P. Saggese, K. Takagaki and C. Pizza, Novel galactolipids from the leaves of *Ipomoea batatas* L.: Characterization by liquid chromatography coupled with electrospray ionization-quadrupole time-of-flight tandem mass spectrometry, *J Agr Food Chem*, 2007, **55**, 10289-10297.

27. L. L. Fu, H. Ding, L. F. Han, L. Jia, W. Z. Yang, C. X. Zhang, Y. Hu, T. T. Zuo, X. M. Gao and D. A. Guo, Simultaneously targeted and untargeted multicomponent characterization of Erzhi Pill by offline two-dimensional liquid chromatography/quadrupole-Orbitrap mass spectrometry, *J Chromatogr A*, 2019, **1584**, 87-96.

28. A. Napolitano, A. Benavides, C. Pizza and S. Piacente, Qualitative on-line profiling of ceramides and cerebrosides by high performance liquid chromatography coupled with electrospray ionization ion trap tandem mass spectrometry: The case of *Dracontium loretense*, *J Pharmaceut Biomed*, 2011, **55**, 23-30.

29. V. C. da Silva, A. Napolitano, D. Eletto, C. M. Rodrigues, C. Pizza and W. Vilegas, Characterization of gallotannins from Astronium species by flow injection analysis-electrospray ionization-ion trap-tandem mass spectrometry and matrix-assisted laser desorption/ionization time-of-flight mass spectrometry, *Eur J Mass Spectrom*, 2011, **17**, 365-375.

30. M. Masullo, A. Mari, A. Cerulli, A. Bottone, B. Kontek, B. Olas, C. Pizza and S. Piacente, Quali-quantitative analysis of the phenolic fraction of the flowers of *Corylus avellana*, source of the Italian PGI product "Nocciola di Giffoni": Isolation of antioxidant diarylheptanoids, *Phytochemistry*, 2016, **130**, 273-281.

31. N. Jiang, C. Q. Liu, D. J. Li, Z. Y. Zhang, C. J. Liu, D. Wang, L. Y. Niu and M. Zhang, Evaluation of freeze drying combined with microwave vacuum drying for functional okra snacks: Antioxidant properties, sensory quality, and energy consumption, *Lwt-Food Sci Technol*, 2017, **82**, 216-226.

32. Geng, F.; Huang, X.; Majumder, K.; Zhu, Z.; Cai, Z.; Ma, M., Mass Spectrometry and Two-Dimensional Electrophoresis To Characterize the Glycosylation of Hen Egg White Ovomacroglobulin. *J. Agric. Food Chem.* **2015,** *63*, 8209-8215.

33. Richardson, C. E.; Hennebelle, M.; Otoki, Y.; Zamora, D.; Yang, J.; Hammock, B. D.; Taha, A. Y., Lipidomic Analysis of Oxidized Fatty Acids in Plant and *Algae* Oils. *J. Agric. Food Chem.* **2017,** *65*, 1941-1951.

34. Napolitano, A.; Benavides, A.; Pizza, C.; Piacente, S., Qualitative on-line profiling of ceramides and cerebrosides by high performance liquid chromatography coupled with electrospray

ionization ion trap tandem mass spectrometry: The case of *Dracontium loretense*. *J. Pharm. Biomed. Anal.* **2011,** *55*, 23-30.

35. Zianni, R.; Bianco, G.; Lelario, F.; Losito, I.; Palmisano, F.; Cataldi, T. R. I., Fatty acid neutral losses observed in tandem mass spectrometry with collision-induced dissociation allows regiochemical assignment of sulfoquinovosyl-diacylglycerols. *J. Mass Spectrom.* **2013,** *48*, 205-215.

36. Moreau, R. A.; Doehlert, D. C.; Welti, R.; Isaac, G.; Roth, M.; Tamura, P.; Nunez, A., The Identification of Mono-, Di-, Tri-, and Tetragalactosyl-diacylglycerols and their Natural Estolides in Oat Kernels. *Lipids* **2008,** *43*, 533-548.

37. Napolitano, A.; Carbone, V.; Saggese, P.; Takagaki, K.; Pizza, C., Novel galactolipids from the leaves of *Ipomoea batatas* L.: characterization by liquid chromatography coupled with electrospray ionization-quadrupole time-of-flight tandem mass spectrometry. *J. Agric. Food Chem.* **2007,** *55*, 10289-10297.

Chapter 4

Mangosteen fruit (*Garcinia mangostana* L.), quantitative NMR analysys of “green” extracts and commercially available food supplemets

State of the art and purposes

The genus Garcinia (Guttifereae), a large genus of polygamous trees or shrubs commonly encountered in tropical Asia, Africa, and Polynesia, has been investigated extensively from the phytochemical and biological points of view [1,2]. *Garcinia mangostana* L. is an evergreen tree native of Malaysia, of which the fruit, mangosteen, known as "the queen of fruits", is one of the most praised tropical fruit due to its delicious taste [3].

G. mangostana fruit shows a colored shell that changes from yellowish-white to reddish-purple depending on levels of maturity, a white, soft, and juicy pericarp containing 8-10 aril segments of different widths and many kernels inside. In the ripening stage, mangosteen pericarp can be easily opened manually at the equator, revealing the edible aril segments. [4]

Mangosteen is mainly eaten fresh but it is also employed for the production of wine, preserve, jam and puree. In Thailand, the pericarp of G. mangostana is used in traditional medicine to treat catarrh, cystitis, diarrhea, fever, skin infections, inflammation, and wounds[4]. In literature, several investigations were reported aimed at highlighting the health benefits of mangosteen.[5]

Due to their biological properties, many phytochemical investigations have been carried out on mangosteen pericarp and shells resulting in the identification of specialized metabolites belonging to the classes of xanthones, benzophenones, flavonoids, condensed tannins, and anthocyanins.[5] Prenylated and oxygenated xanthones are the main constituents responsible for the various bioactivities of G. mangostana, including antioxidant, anti-inflammatory, and cytotoxic activities.[6]

Mangosteen ranks among the so-called ''super fruits'', a marketing claim to identify fruits and vegetables able to confer beneficial health effects. Thus, in the last years, its use in functional products has been increasing, mainly in food

beverages but also in tablets and capsule formulations, widely distributed not only in the drug stores but also in the online market.

These dietary supplements, all promising an enhancement of health, especially related to antioxidant effects, are generally sold at a higher price than similar foods not marketed with the label "super fruits", but often the purported health benefits and effects are not supported by scientific data.

A range of analytical methods including HPLC–PDA and HPLC–DAD have been developed to quantify xanthones in Garcinia mangostana focusing on the determination of the few constituents of the extracts of the fruits or the fruit rinds and highlighting the main xanthones as α-mangostin and γ-mangostin.[3,4,7-13] Recently, α-mangostin, β-mangostin, γ-mangostin were quantified by UHPLC–PDA method in the hexane, chloroform, ethyl acetate, and methanol extracts of 8 Garcinia species fruit rinds[14], and a UHPLC analysis coupled with mass spectrometry was also carried out.[15] Near-infrared spectroscopy (NIR) was applied to the quantitative analysis of the concentration of α-mangostin in mangosteen pericarp.[16]

Quantitative NMR analysis

^{1}H NMR is a powerful analytical tool in the field of quality evaluation of various food and medicinal plants since it is a non-destructive technique, and is characterized by simple sample preparation and rapid analysis.[17] For the last 30

years, NMR spectroscopy has increasingly been used for the quality assessment of drugs and excipients, either qualitatively or quantitatively.[18-20] Furthermore, ^{1}H NMR can provide comprehensive characteristic fingerprints of herbal products.[21] More recently, quantitative Nuclear Magnetic Resonance (qNMR) has attracted considerable attention as an effective quantitative analytical method, which has been widely used in many scientific areas due to its ability to analyze essentially all types of molecules and provide rich and fast qualitative and quantitative information.[22] qNMR has been frequently employed to determine the content of natural products in plant extracts, drugs, foods, and drinks.[23]

4.1 Experimental plan

In this work, in a first step a phytochemical investigation of mangosteen aril and shell extracts was performed affording xanthone derivatives (**1**-**12**) and oligandrol (**13**), a natural compound belonging to the benzopyran class, which were unambiguously elucidated by NMR analysis.

Considering the traditional use of the whole ripe fruit in the producing countries and their increasing use in functional beverages and food supplements, in the first step, this investigation was aimed at performing a quali-quantitative analysis of G. mangostana extracts of arils and shells. Herein, the chloroform and methanol extracts were investigated. Furthermore, ethanol and ethanol/water extracts, "eco-friendly" solvents mainly used for the preparation of functional ingredients, were explored. [24-27]

The content of xanthone derivatives, oligandrol, as well as some primary metabolites occurring in the chloroform, methanol, ethanol, and EtOH:H_2O (7:3) extracts of mangosteen arils and shells was determined for the first time by quantitative Nuclear Magnetic Resonance (qNMR), a rapid and accurate method for the simultaneous quantification of metabolites.

Moreover, the amount of xanthones in these extracts was compared with that occurring in four selected commercial food supplements, among which two fruit juices, tablets, and capsules based on mangosteen fruits.

4.2. Results and discussion

Isolation of compounds in G. mangostana extracts

In a first step, aimed to recognize the main constituents of the fruit, the extraction of the matrix using solvents with different polarity was performed. Pure compounds were isolated from arils and shells of mangosteen, to compare their ^{1}H NMR spectra with ^{1}H NMR spectra of extracts and food derived supplements and to unambiguously identify the compounds occurring in extracts, fruit juices, tablets, and capsules. The MeOH and $CHCl_3$ extracts of mangosteen shells and arils were subjected to chromatographic separation by HPLC-UV. Following this analytical approach, compounds **1**-**13** were isolated and further characterized by 1D- and 2D-NMR experiments along with ESI-HRMS/MS^n analysis. In particular, compounds **1**-**12** were determined as prenylated xanthones: 1,7-dihydroxy-3-methoxy-2-(3-methylbut-2-enyl)-xanthen-9-one (**1**)[29], gudraxanthone (**2**)[30], 1,3,7-trihydroxy-2,8-bis-(3-methyl-2-buten-1-yl)-9H-xanthen-9-one (**3**)[4], γ-mangostin (**4**)[31], α-mangostin (**5**)[31], β-mangostin (**6**)[30], demethylcalabaxanthone (**7**)[32], mangostanin (**8**)[32], 8-deoxygartanin (**9**)[4], garcinone E (**10**) [4], garcinone D (**11**)[30], mangostanol (**12**)[30]; moreover oligandrol (**13**)[33], a benzopyran compound never isolated before from mangosteen was identified (**Figure 4.1**).

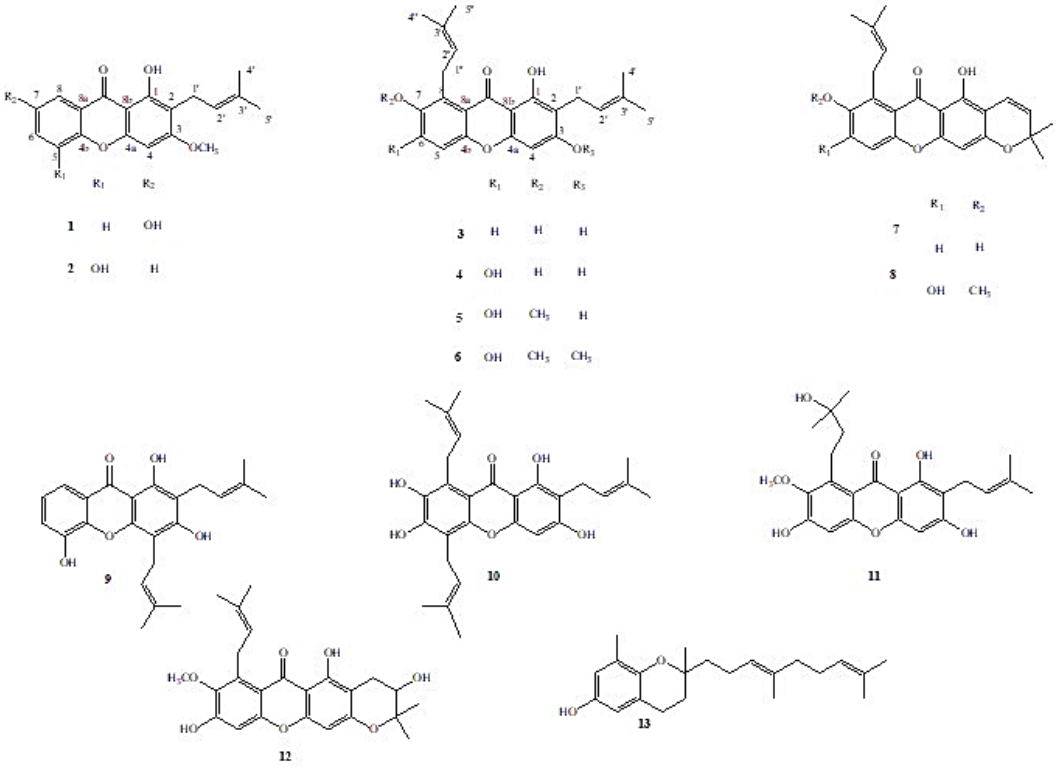

Figure 4.1. Specialized metabolites identified in extracts of *G. mangostana* arils and shells.

Identification of chemical constituents in Garcinia mangostana extracts by ^{1}H NMR analysis

The identification of chemical constituents in *G. mangostana* extracts and commercial preparations has been achieved by analysis of their ^{1}H NMR spectra. The protonic signals of the identified components in the extract have been assigned by analysis of their mono and bidimensional NMR spectra as well as by comparison with the ^{1}H NMR spectra of pure isolated compounds (**Figures 4.2-4.5**). The assignment of the protonic signals of each compound is shown in **Table 4.1**.

Table 4.1. Characteristic ^{1}H NMR peaks used to identify the compounds in *G. mangostana* extracts

	compound	^{1}H chemical shifts (multiplicity, J)
1	1,7-dihydroxy-3-methoxy-2-(3-methylbut-2-enyl)-xanthen-9-one	7.54* (d, 2.8), 7.45 d (8.2)
2	gudraxanthone	7.71* (dd, 2.8, 8.2), 7.29, dd (1.6, 8.2)
3	1,3,7-trihydroxy-2,8-bis(3-methyl-2-buten-1-yl)-9H-xanthen-9-one	7.20* (d, 8.2), 6.31 s
4	γ-mangostin	6.71* s, 6.27 s
5	α-mangostin	3.79* s, 6.76, s
6	β-Mangostin	3.95* s, 6.81 s
7	demethylcalabaxanthone	5.69* (d, 10.2), 7.27 d (8.2)
8	mangostanin	5.67* (d, 10.2), 6.78 s
9	8-deoxygartanin	5.33* (d, 6.8), 7.67 d (8.2)
10	garcinone E	3.60* (d, 6.8), 6.34 s
11	garcinone D	3.45* (d, 6.8), 6.76 s
12	mangostanol	2.57* (dd 6.2, 16.4), 2.92 (dd 6.2, 16.4), 6.36 s
13	oligandrol	6.44* (d, 2.2), 6.35 d (2.2)
	sucrose	5.42* (d, 3.8), 4.13 (d, 8.7),
	α-glucose	5.14* (d, 3.6)
	β-glucose	4.50* (d, 7.9)
	GABA	2.3* (t, 7.5)

*Signal chosen for qNMR analysis.

The ^{1}H NMR spectra of *G. mangostana* extracts and food derived supplements showed crowded areas, with several overlapping signals (**Figure 4.15**). Therefore, accurate analysis of the proton spectra has been carried out to select unambiguously a key signal characteristic of each metabolite.

The ^{1}H NMR spectra (**Figures 4.2-4.14**) displayed NMR values corresponding to specialized metabolites, mainly xanthones, and primary metabolites. In particular, xanthones displayed characteristic proton signals which could be divided into three regions of the spectrum. A first region ranging from δ 7.72 to δ 6.27, characterized by the presence of the phenolic protons, a second region ranging from δ 5.33 to δ 3.33, including signals ascribable to isoprenyl functions and methoxy groups and finally a third region in the upper field consisting of signals corresponding to methyl and methylene groups. To avoid overlapped signals, for compounds **1-4** signals in the aromatic region were selected, specifically the signals at δ 7.54, 7.71, 7.20, 6.71, respectively (**Table 4.1**, **Figures 4.2-4.5**). Proton signals corresponding to isoprenyl functions were selected for compounds **7-11** (**Table 4.1, Figures 4.8-4.12**); in detail, proton signals at δ 5.69, 5.67, 5.33, 3.60, 3.45, respectively were considered, while for compounds **5** and **6** key-signals at δ 3.79 and 3.95 respectively, ascribable to methoxy groups, were chosen (**Table 4.1, Figures 4.5-4.6**). In the case of compound **12**, being several proton signals overlapped, the peaks at δ 2.52 and δ 2.97(**Figure 4.13**), relative to the methylene group, were selected as typical signals.

For oligandrol (**13**), a natural compound belonging to the benzopyran class, the signal at δ 6.44, falling in a region free from xanthone signals, was chosen (**Table 4.1, Figure 4.14**).

The ^{1}H NMR spectra of some extracts displayed some peaks relative to primary metabolites. In particular, signals ascribable to sucrose at δ 5.42 (d, J = 3.8 Hz), and to two anomeric protons related to β-glucose at δ 4.50 ppm (d, J = 7.9 Hz) and α-

glucose at δ 5.14 (d, J = 3.6 Hz) were evident. A typical signal at δ 2.30 (t, J = 7.5) corresponding to γ-aminobutyric acid (GABA) was observed (**Table 4.15**).[17,21]

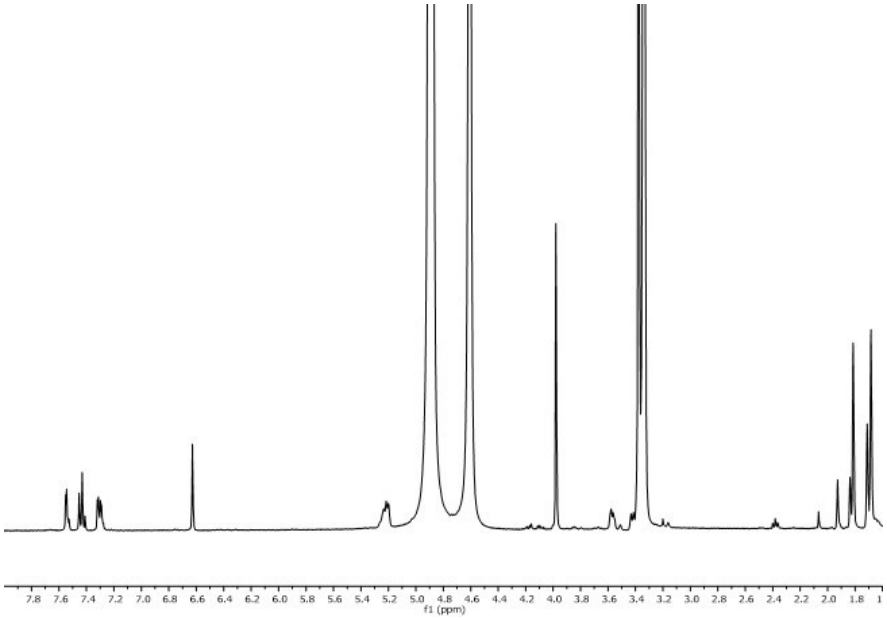

Figure 4.2. ^{1}H NMR Spectrum (600 MHz, CD_3OD) of MeOH extract of compound **1**

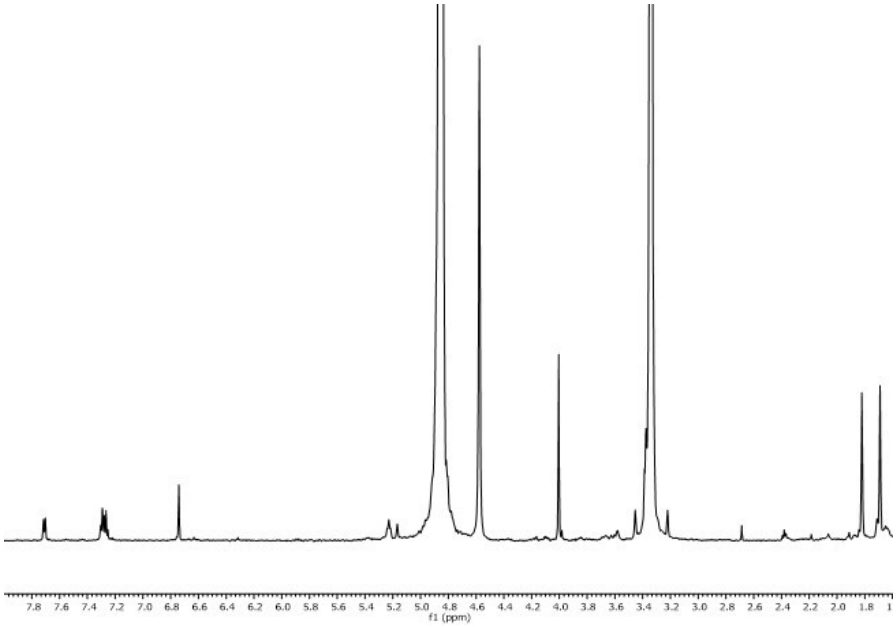

Figure 4.3. ^{1}H NMR Spectrum (600 MHz, CD_3OD) of MeOH extract of compound **2**

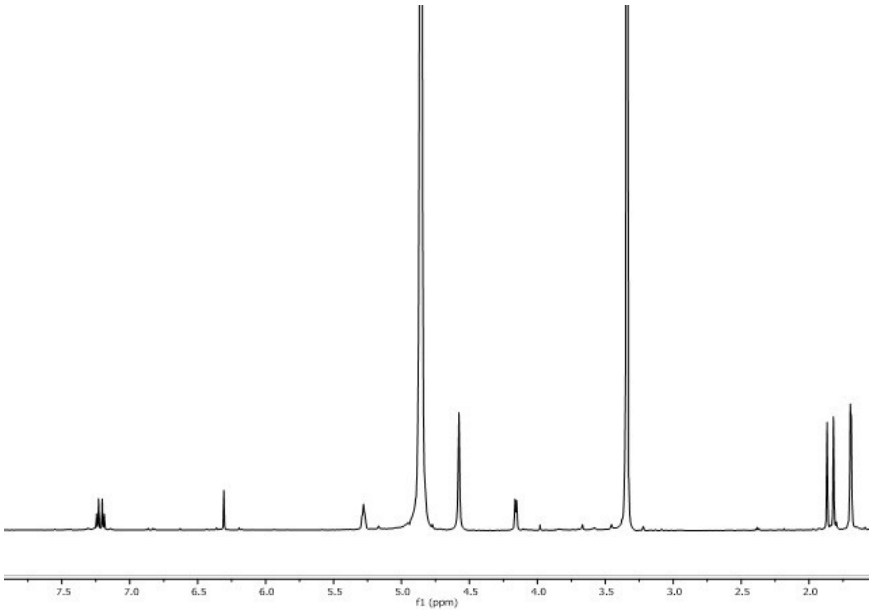

Figure 4.4. ^{1}H NMR Spectrum (600 MHz, CD_3OD) of MeOH extract of compound **3**

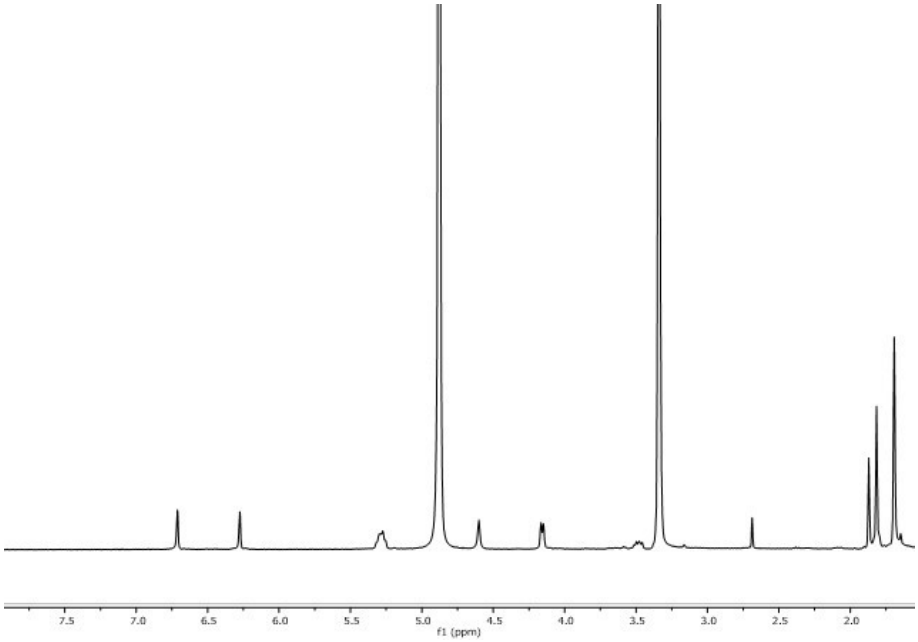

Figure 4.5. ^{1}H NMR Spectrum (600 MHz, CD_3OD) of MeOH extract of compound **4**

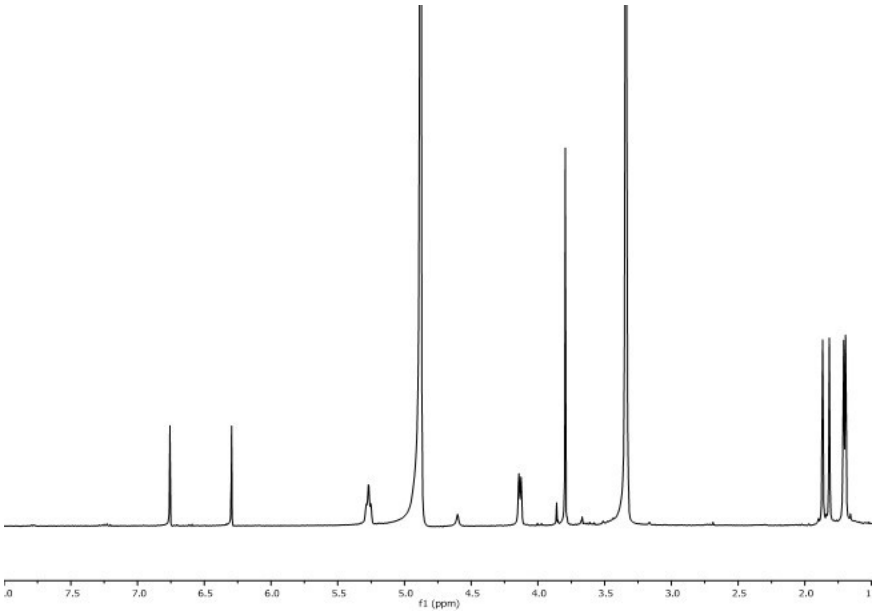

Figure 4.6. ^{1}H NMR Spectrum (600 MHz, CD_3OD) of MeOH extract of compound **5**

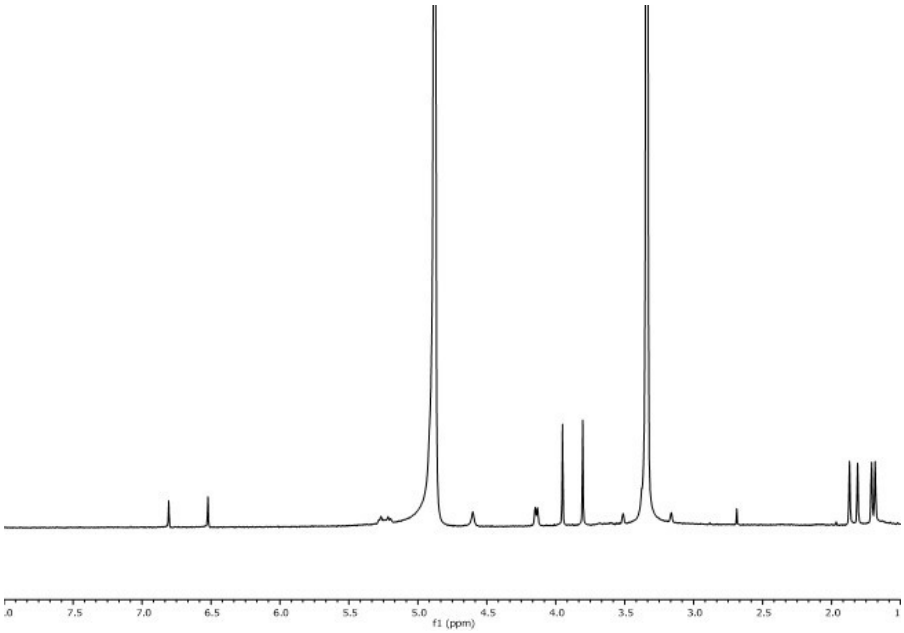

Figure 4.7. ^{1}H NMR Spectrum (600 MHz, CD_3OD) of MeOH extract of compound **6**

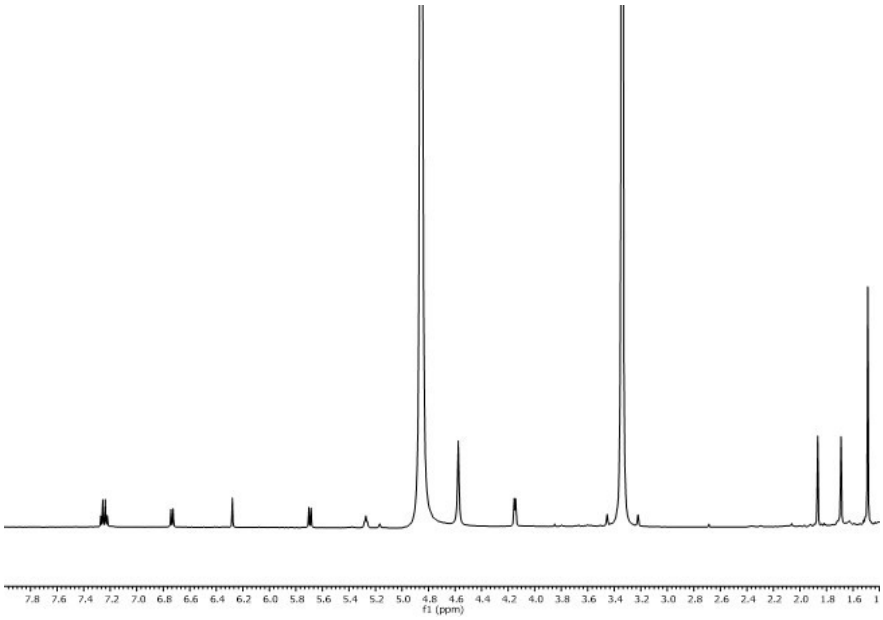

Figure 4.8. ^{1}H NMR Spectrum (600 MHz, CD_3OD) of MeOH extract of compound **7**

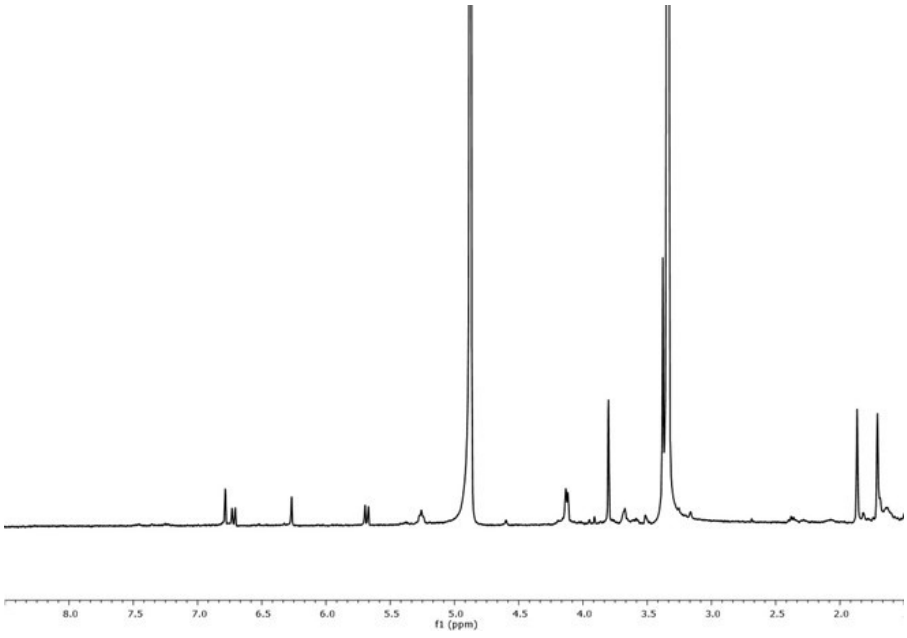

Figure 4.9. ^{1}H NMR Spectrum (600 MHz, CD_3OD) of MeOH extract of compound **8**

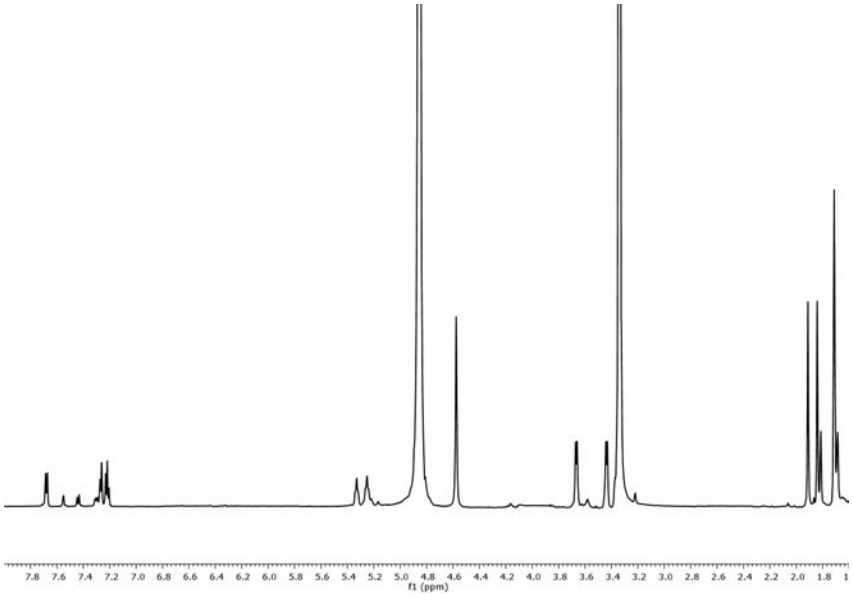

Figure 4.10. ^{1}H NMR Spectrum (600 MHz, CD_3OD) of MeOH extract of compound **9**

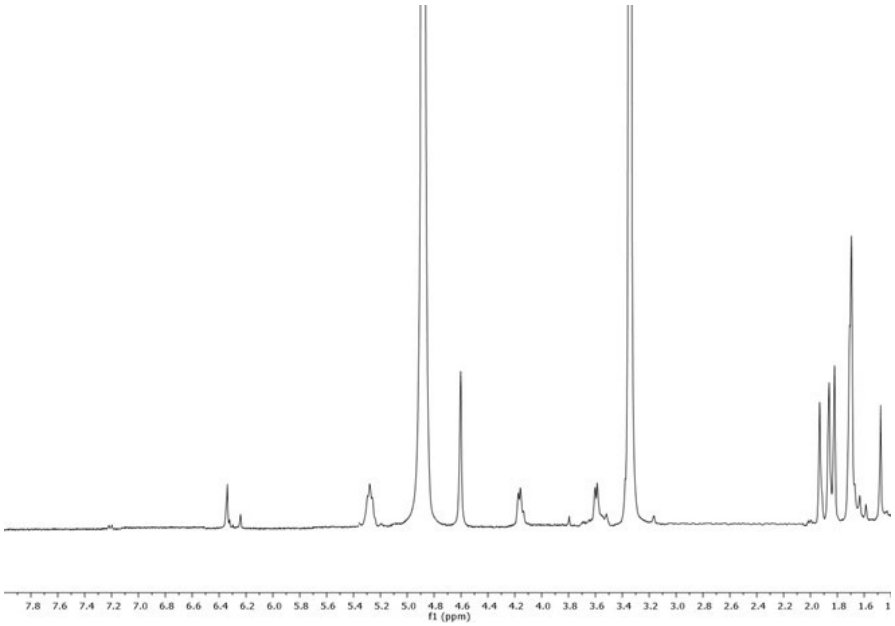

Figure 4.11. ^{1}H NMR Spectrum (600 MHz, CD_3OD) of MeOH extract of compound **10**

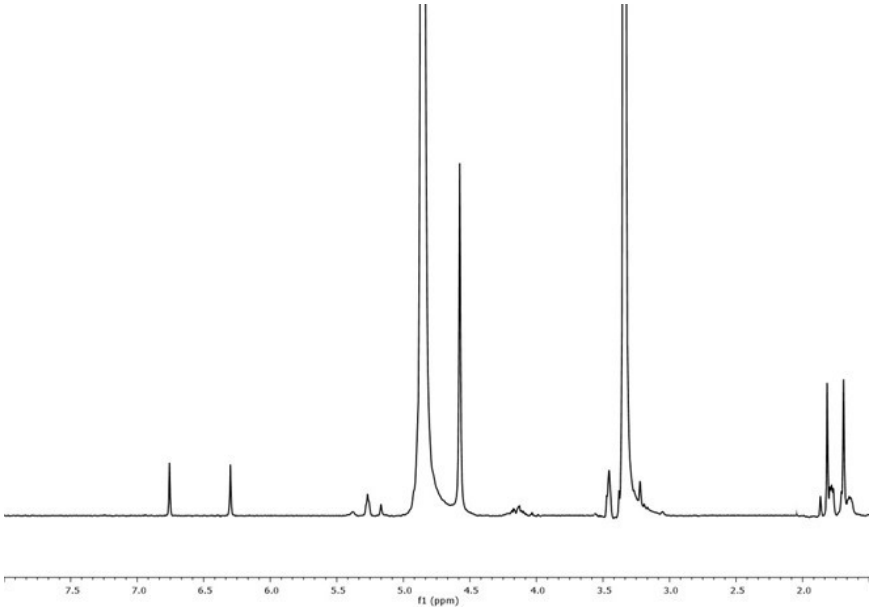

Figure 4.12. ^{1}H NMR Spectrum (600 MHz, CD_3OD) of MeOH extract of compound **11**

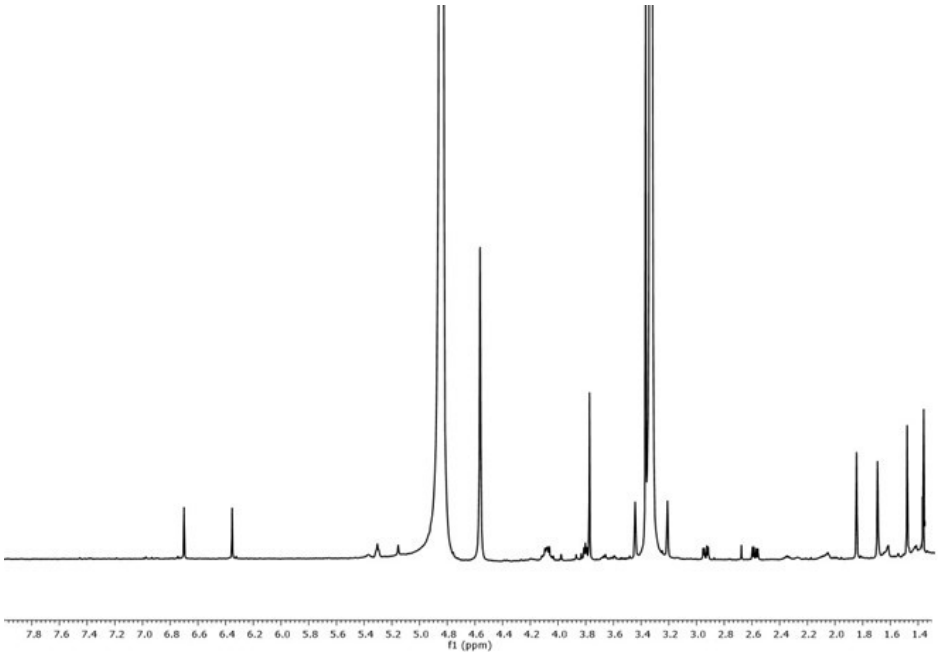

Figure 4.13. ^{1}H NMR Spectrum (600 MHz, CD_3OD) of MeOH extract of compound **12**

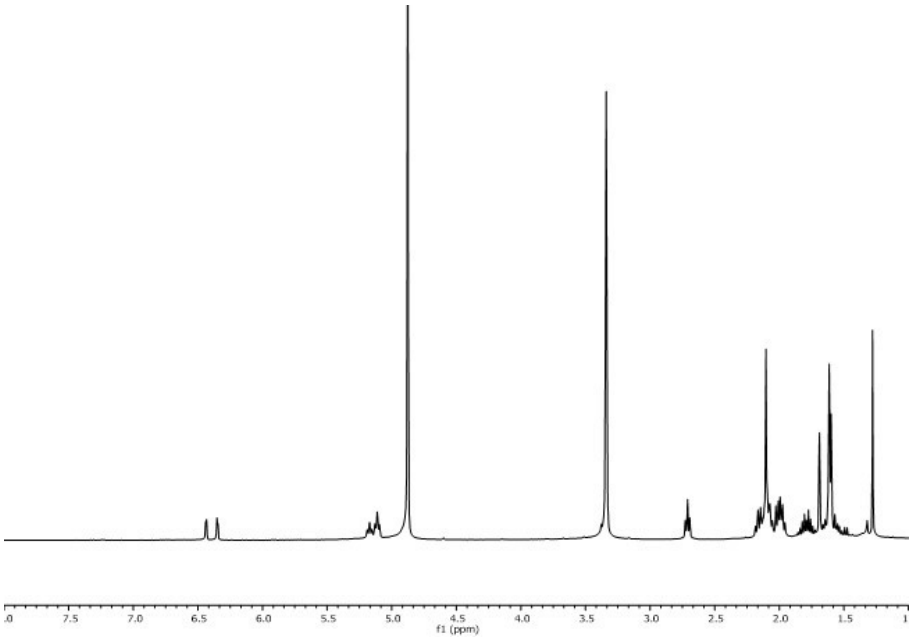

Figure 4.14. ^{1}H NMR Spectrum (600 MHz, CD_3OD) of MeOH extract of compound **13**

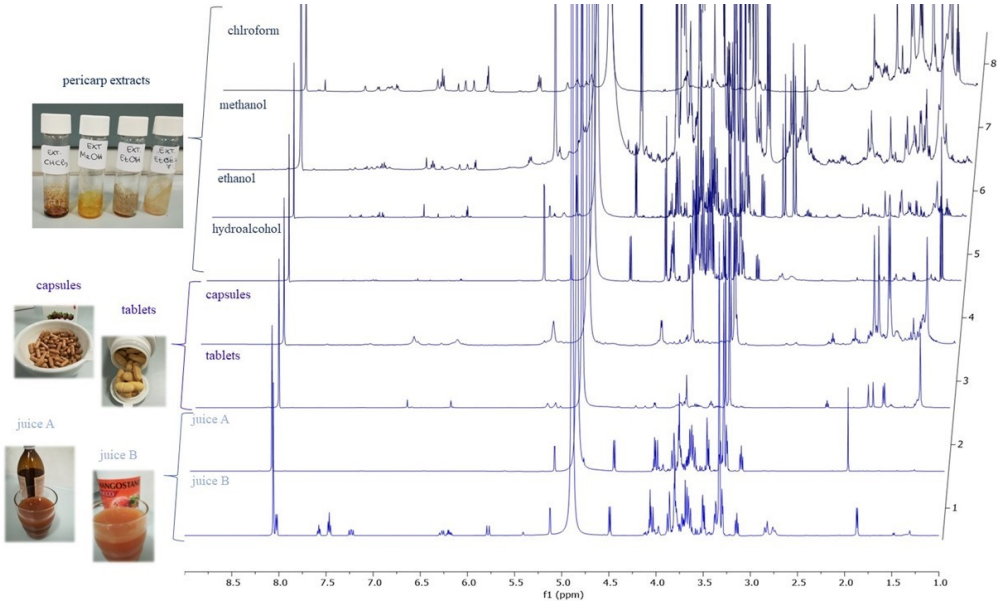

Figure 4.15. Comparison between ^{1}H NMR of aril extracts of mangosteen and related food supplements.

Optimization of qNMR parameters

Terephthalic acid was selected as an internal standard for quantitation because it owns a single peak at δ 8.08 (4H, s) which was not overlapped with the signals of primary metabolites and specialized metabolites, in particular xanthones, occurring in *G. mangostana* extracts.

The value of relaxation delay (T1) represents an important parameter for quantitative NMR. To determine T1 of each external standard the inversion-recovery pulse sequence (t1ir), acquiring 10 recovery delays between 0.001 and 15 s, has been carried out (**Table 4.2**).

Generally, high precision in qNMR spectrum can be achieved when the pulse delay time (d1) is greater than the quintuple T1. To obtain an optimal d1 value, the ^{1}H NMR spectra using different d1 (10, 15, 20, and 25 s) have been carried out. When d1 was longer than 15 s, the integral area ratio (I_X/I_{IS}) became invariant. Therefore, the value of d1 was set as 15 s for all measurements. Another important role in the optimation of qNMR method is played by the number of scans since it influences the signal-noise ratio (S/N). The growth of the scanning numbers is helpful to improve the S/N ratio, which has a potent effect on the integral value. Generally, an S/N of more than 250-folds is satisfied with the quantitative NMR. [33] In the present study, ^{1}H NMR experiments using different numbers of scans (NS = 4, 8, 16, 32, 64, 128, and 256) were carried out. The results highlight that the S/Ns of the selected standards were more than 250-folds after 64 scans in the ^{1}H NMR spectra.

Table 4.2 T_1 value of external standards (**1**-**13**).

compounds	T_1
1,7-Dihydroxy-3-methoxy-2-(3-methylbut-2-enyl)xanthen-9-one (**1**)	4.058 s
gudraxanthone (**2**)	3.245 s
1,3,7-Trihydroxy-2,8-bis(3-methyl-2-buten-1-yl)-9H-xanthen-9-one (**3**)	913.238 ms
γ-mangostin (**4**)	337.641 ms
α-mangostin (**5**)	1.100 s
β-mangostin (**6**)	985.384 ms
demethylcalabaxanthone (**7**)	1.352 s
6-hydroxycalabaxanthone (**8**)	524.597 ms
8-deoxygartanin (**9**)	1.989 s
garcinone E (**10**)	827.524 ms
garcinone D (**11**)	160.273 ms
mangostanol (**12**)	421.223 ms
oligandrol (**13**)	3.206 s
terephthalic acid	2.627s

4.2.1 Quantitative analysis of "green" extracts of pulp and shells

In recent years, quantitative Nuclear Magnetic Resonance (qNMR) has been widely used for the analysis of different compounds in complex mixtures of plant extracts.[33,34] qNMR methods provide rapid, accurate, highly repeatable, and reproducible quantification of several components together with their unambiguous identification. After the accurate analysis of NMR spectra for the characterization of isolated compounds and the optimization of parameters, a second analytical step was implemented based on the overmentioned quantative approach.

The quantitative results highlight the great variability of the analyzed samples relative to the xanthones. The extracts of the shells displayed an amount of γ-mangostin (**4**) and α-mangostin (**5**) higher than the arils. On the other hand, α-mangostin (**6**), demethylcalabaxanthone (**7**), mangostanin (**8**), 8-deoxygartanin (**9**) occurred in a higher amount in the extracts of arils. As evident in **Tables 4.3A** and **B**, oligandrol (**13**) was detected only in the arils while gudraxanthone (**2**) and mangostanol (**12**) were detected only in the shells.

$CHCl_3$ and MeOH extracts were compared with extracts obtained by using EtOH and EtOH/H_2O (7:3) solvents, considered suitable for eco-friendly extraction procedures. Regarding the arils, the xanthones occurring in the highest amount in the "green" extracts or at least in one of them were 1,3,7-trihydroxy-2,8-bis-(3-methyl-2-buten-1-yl)-9H-xanthen-9-one (**3**), *α*-mangostin (**5**), demethylcalabaxanthone (**7**), mangostanin (**8**).

α-mangostin (**5**) represented the more abundant compound in all the shell extracts. *γ*-mangostin (**4**) and *α*-mangostin (**5**) showed the highest amount in the chloroform extracts of the shells with a value of 324.70 mg/g extract and 438.91 mg/ g extract, respectively; the amount of *α*-mangostin (**5**) was also remarkable in the green extract EtOH:H_2O with a value of 283.19 mg/ g extract. Considering the above results and the biological activities of *α*-mangostin, the "eco-friendly"

procedures represent suitable extraction methods to obtain nutraceutical formulations with high content of this xanthone. The remaining xanthones, except oligandrol (**13**), occurred in the extracts in a wide range of concentrations

Moreover, the ^{1}H NMR spectra of different extracts of mangosteen displayed signals of primary metabolites ascribable to *γ*-aminobutyric (GABA) acid, sucrose, *α*-glucose, and *β*-glucose; the quantitative analysis of primary metabolites showed in arils extracts the highest concentrations of sugars (**Table 4.3A** and **B**.

Table 4.3A Results of quantitative analysis of primary and specialized metabolites occurring in the extracts *of G. mangostana* arils (mg/g extract)

COMPOUNDS	**ARILS**			
	$CHCl_3$	MeOH	EtOH	EtOH:H_2O
1,7-Dihydroxy-3-methoxy-2-(3-methylbut-2-enyl)-xanthen-9-one (**1**)	10.41 ± 0.16	16.20 ± 0.92	10.68 ± 0.17	2.55 ± 0.21
gudraxanthone (**2**)	N.D.[b]	N.D.[b]	N.D.[b]	N.D.[b]
1,3,7-Trihydroxy-2,8-bis(3-methyl-2-buten-1-yl)-9H-xanthen-9-one (**3**)	15.52 ± 0.15	28.96 ± 1.45	21.30 ± 1.04	7.17 ± 0.24
γ-mangostin (**4**)	N.D.[b]	11.53 ± 0.75	1.95 ± 0.20	1.76 ± 0.13
α-mangostin (**5**)	67.68 ± 2.20	67.89 ± 2.45	45.25 ± 0.72	2.85 ± 0.04
β-mangostin (**6**)	39.29 ± 0.14	N.D.[b]	ND[b]	N.D.[b]
demethylcalabaxanthone (**7**)	109.87 ± 0.87	6.93 ± 0.49	28.60 ± 0.83	21.21 ± 0.57
mangostanin (**8**)	120.34 ± 0.75	7.00 ± 0.15	30.61 ± 0.78	28.34 ± 0.26
8-deoxygartanin (**9**)	111.97 ± 6.07	2.08 ± 0.22	N.D.[b]	N.D.[b]
garcinone E (**10**)	N.D.[b]	8.00 ± 0.18	N.D.[b]	N.D.[b]
garcinone D (**11**)	4.68 ± 0.08	206.44 ± 5.73	37.16 ± 0.39	332.70 ±3.41
mangostanol (**12**)	N.D.[b]	N.D.[b]	N.D.[b]	N.D.[b]
oligandrol (**13**)	59.42 ± 0.30	17.98 ± 1.36	17.09 ± 0.18	9.66± 0.47
sucrose	N.D.[b]	297.45 ± 8.65	147.98 ± 2.45	822.57 ± 17.34
α-glucose	N.D.[b]	188.85± 10.07	254.84 ± 3.21	155.00 ± 5.11
β-glucose	N.D.[b]	171.74 ± 3.44	202.99 ± 1.95	106.74 ± 7.73
GABA	28.82 ± 0.15	N.D.[b]	N.D.[b]	N.D.[b]

Table 4.3B Results of quantitative analysis of primary and specialized metabolites occurring in the extracts *of G. mangostana* shells (mg/g extract)

COMPOUNDS	SHELLS			
	$CHCl_3$	MeOH	EtOH	EtOH:H_2O
1,7-Dihydroxy-3-methoxy-2-(3-methylbut-2-enyl)-xanthen-9-one (**1**)	N.D.b	6.99 ± 1.06	11.98 ± 0.04	5.85 ± 0.24
gudraxanthone (**2**)	3.10 ± 0.17	N.D.b	N.D.b	N.D.b
1,3,7-Trihydroxy-2,8-bis(3-methyl-2-buten-1-yl)-9H-xanthen-9-one (**3**)	15.36 ± 0.35	7.68 ± 0.92	11.17 ± 0.60	17.98 ± 0.25
γ-mangostin (**4**)	324.70±1.17	219.54±13.14	60.89 ± 0.84	2.14± 0.26
α-mangostin (**5**)	438.91±6.22	411.91±8.70	342.00 ± 8.07	283.19±2.66
β-mangostin (**6**)	2.05 ± 0.01	N.D.b	2.50 ± 0.05	N.D.b
demethylcalabaxanthone (**7**)	7.53 ± 0.53	N.D.b	N.D.b	N.D.b
mangostanin (**8**)	53.99 ± 0.75	6.87 ± 0.21	11.12 ± 0.11	0.95± 0.13
8-deoxygartanin (**9**)	11.41 ± 1.01	44.57 ± 3.31	5.00 ± 0.21	22.88 ± 0.25
garcinone E (**10**)	27.79 ± 0.12	27.21 ± 1.61	13.64 ± 0.82	47.97±3.21
garcinone D (**11**)	7.47 ± 0.52	25.89 ± 0.63	N.D.b	24.48± 0.14
mangostanol (**12**)	21.92 ± 0.78	13.04 ± 2.26	33.27 ± 0.39	52.26± 0.28
oligandrol (**13**)	N.D.b	N.D.b	N.D.b	N.D.b
sucrose	N.D.b	N.D.b	8.38 ± 0.17	15.09 ± 0.89
α-glucose	N.D.b	32.63 ± 0.43	21.07 ± 0.19	50.28±0.80
β-glucose	N.D.b	38.16 ± 0.67	30.06 ± 0.09	105.45±0.54
GABA	N.D.b	N.D.b	3.41 ± 0.03	9.29± 0.33

4.2.2 Quantitative analysis of commercially available products

On the market, mangosteen is available in different commercial preparations. To identify the xanthones in some of the above-mentioned preparations, qNMR analysis of different commercial products has been carried out. In particular, tablets, capsules, and two different juices have been submitted to qNMR analysis. The amounts of specialized and primary metabolites in commercial preparations of *G. mangostana* are reported in **Table 4.4**.

For the capsules and tablets, the amount is expressed as mg/capsule and mg/tablet, respectively. For the two juices, the amount is expressed as mg/100 ml for juice A and juice B. The analyzed preparation showed that few xanthones were evident in these preparations.

Analyzing the results obtained from the qNMR of tablets and capsules is evident how γ-mangostin (**4**) and *α*-mangostin (**5**) were the most abundant compounds in both preparations, in agreement with literature data.[4] The amount of *α*-mangostin (**5**) was comparable in tablets and capsules with values of 41.22 mg/ tablet and 56.76 mg/ capsule while the content of γ-mangostin (**4**) was higher in capsules (19.41 mg/ capsule) than tablets (3.57 mg/ tablet). Noteworthy, the results obtained using this method were in agreement with those reported by the producer's information on the amount of α-mangostin per tablet. Mangostanin (**8**) was also quantified in tablets and capsules, while 1,7-dihydroxy-3-methoxy-2-(3-methylbut-2-enyl)-xanthen-9-one (**1**) and 8-deoxygartanin (**9**) were quantified only in tablets and in capsules, respectively.

Moreover, a high amount of α-glucose was evident in the capsules (120.55 mg/capsule).

The analysis of the juices showed that they contained a high amount of sugars. Regarding the xanthones, both juices showed variability of the content of γ-mangostin (**4**) and α-mangostin (**5**); in detail, while juice A showed a high amount

of γ-mangostin (**4**) (106.22 mg/100 ml) and α-mangostin (**5**) (168.79 mg/100 ml). In juice A, the amount of garcinone D (**11**) (80.76 mg/100 ml) was also remarkable. The juice B was characterized by a lower amount of γ-mangostin (**4**) and α-mangostin (**5**) and along with these molecules, gudraxanthone (**2**) (8.27 mg/100 ml), demethylcalabaxanthone (**7**) (14.61 mg/100 ml), and mangostanin (**8**) (40.72 mg/100 ml) could be determined. The other xanthones resulted below the limit of detection.

Table 4.4 Content of primary and specialized metabolites in commercial preparations based on *G. mangostana* fruit

Compounds	Tablets[b]	Capsules[c]	Juice A[d]	Juice B[d]
1,7-Dihydroxy-3-methoxy-2-(3-methylbut-2-enyl)-xanthen-9-one (**1**)	1.21 ± 0.05	N.D.[e]	N.D.[e]	N.D.[e]
gudraxanthone (**2**)	N.D.[e]	N.D.[e]	N.D.[e]	8.27 ± 0.01
γ-mangostin (**4**)	3.57 ± 0.03	19.41 ± 0.53	106.22 ± 14.81	4.02 ± 0.01
α-mangostin (**5**)	41.22 ± 0.39	56.76 ± 0.38	168.79 ± 14.83	2.08 ± 0.15
demethylcalabaxanthone (**7**)	N.D.[e]	N.D.[e]	N.D.[e]	14.61± 0.68
mangostanin (**8**)	3.76 ± 0.32	3.12 ± 0.01	N.D.[e]	40.72 ± 0.01
8-deoxygartanin (**9**)	N.D.[e]	32.16 ± 0.17	N.D.[e]	N.D.[e]
garcinone D (**11**)	N.D.[e]	N.D.[e]	80.76 ± 0.01	N.D.[e]
sucrose	N.D.[e]	N.D.[e]	499.29 ± 29.82	361.57 ± 25.05
α-glucose	13.78 ± 0.69	120.55 ± 0.27	3469.47 ± 4.81	1568.08 ± 32.29
β-glucose	4.84 ± 0.37	N.D.[e]	4519.49 ± 48.06	1674.65 ± 65.59
GABA	3.25 ± 0.04	10.30 ± 0.03	N.D.[e]	N.D.[e]

[a]The amount of compounds **3**, **6**, **7**, **10**, **12** and **13** was below the LOD of the applied method.
[b]Amount of xanthones expressed as mg/tablet, each tablet (1.0 g) included 0.1 g of extract.
[c]Amount of xanthones expressed as mg/capsule, each capsule contained 0.5 g of extract.
[d]Amount of xanthones expressed as mg/100 ml, for juice A and B.
[e] Not detected: the amount of these compounds was below the LOD of the applied method

4.3 Conclusions

The growing interest in foods with healthy effects led to the commercialization of a large variety of supplements not only in the drug stores but also in the online market. The claims of these products are generally focused on the health benefits such as antioxidant activity and other appealing properties. Mangosteen is considered a super fruit for its biological activities, tested in several biological investigations and correlated to the content of active specialized metabolites, mainly xanthones. They represent a class of polyphenols that is synthesized by a small group of higher plants. Xanthones are well-known for their biological activities including hepato-protective, antioxidant, anticancer, antithrombotic. [4,35] Biological activities of these specialized plant metabolites are related to their scaffold but vary depending on the nature and position of substituents.[36] γ-mangostin and α-mangostin are the main bioactive xanthones occurring in the arils and shells of mangosteen, reported to have pharmacological activities, including anti-inflammatory, antioxidant, anticancer, antibacterial, and cardioprotective activities.[5] Considering the large interest in these molecules, several analytical methods have been developed to quantify their amount in the mangosteen extracts. To achieve deep insight into the bioactive constituents occurring in the different parts of the fruit, for the first time a qNMR-based analytical method has been developed. This approach allowed us to easily recognize the compounds in the samples and to determine their amount. The results highlighted how the "green" extracts of the shells represent a good source of xanthones, in particular of α-mangostin. This is an interesting result because it reveals how the green extracts are suitable for employment in nutraceutical formulations.

Although the quantitative analyses are referred to extracts, they give information on the occurrence of xanthones in the arils and highlight how also consuming fresh fruits, the biologically active xanthones are present in good amounts.

Moreover, this study has provided information on the xanthone content in food supplements. The obtained results on the food supplements should take into account their suggested daily dosage (2 tablets, 2-4 capsules, 30 ml for juice A and 120 ml for juice B). In this context, formulations as the analyzed capsules represent a good source of specialized metabolites with a remarkable amount of biologically active xanthones (i.e. γ-mangostin and α-mangostin, **Figure 4.16**); the analyzed tablets represent a good source of α-mangostin with a very low content of γ-mangostin; the juices displayed a considerable amount of sugars as expected, but while in juice A the content of xanthones was appreciable for both γ-mangostin, α-mangostin, and garcinone D, juice B showed a very low amount of biologically active xanthones. These aspects are very important to protect the consumers, attracted by the claims of the market and guide them to the choice of the right products.

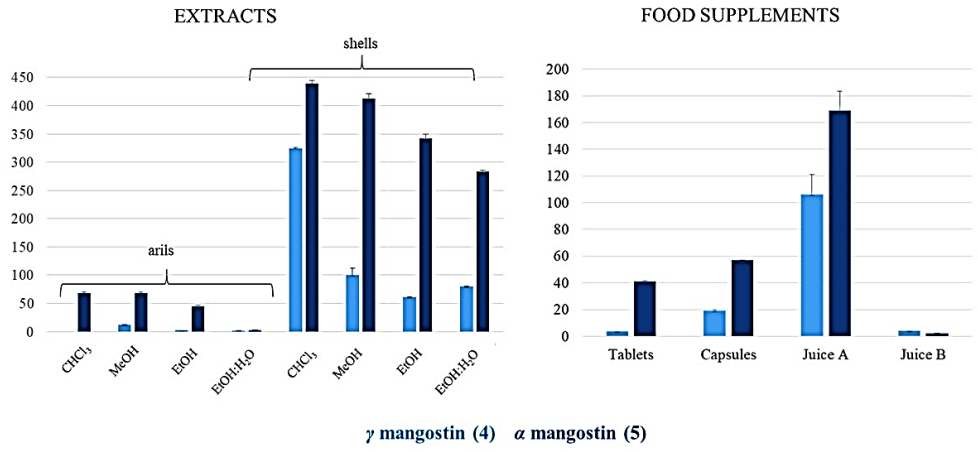

Figure 4.16 Quantitative content of γ-mangostin (**4**) and α-mangostin (**5**) in mangosteen arils and shells extracts and in food supplements.

4.4 Experimental section

Chemicals

Solvents used for extractions were purchased from VWR (Milano, Italy). NMR solvent MeOH-d_4 (99.95%) and terephthalic acid (98%) were purchased from Sigma-Aldrich (Germany).

Herbal material and food supplements

The fruits of *Garcinia mangostana* were purchased from the online market in April 2019 and identified by V. De Feo (Department of Pharmacy, University of Salerno, Italy). A voucher specimen (N. 150) has been deposited in the Department of Pharmacy, University of Salerno, Italy. Tablets, capsules, and juices were purchased directly from a pharmacy in Salerno, Italy, and through online shopping. According to the producer's information, each tablet (1000 mg) is reported to contain 100 mg of *G. mangostana* dried extract standardized at 40 % of α-mangostin, each capsule containing 500 mg of pure mangosteen. Moreover, the two juices A and B are reported to contain 100 % and 95% of *G. mangostana* whole fruit juice, respectively.

Extraction and isolation procedures

Mangosteen shells were separated manually from arils and each part was crushed.

G. mangostana arils (250.0 g) were stored in the freezer at a temperature of -5 C°, after some days the fruits were submitted to lyophilization to obtain 51.63 g; the dried arils were extracted using solvents of increasing polarity such as

petroleum ether (300 mL for 3 days, three times), $CHCl_3$ (300 mL for 3 days, three times), and MeOH (300 mL × 3 days × 3 times). After filtration and evaporation of the solvent to dryness in vacuo, 0.42 g and 18.15 g of crude extracts of $CHCl_3$ and MeOH were obtained, respectively. In addition, 22.04 g of lyophilized *G. mangostana* arils were extracted with EtOH (65 ml× 3 days × 3 times) and EtOH:H_2O (7:3) (65 ml× 3 days × 3 times) to obtain 1.75 and 9.09 g of extract, respectively.

G. mangostana shells (490 g) were dried and extracted at room temperature with petroleum ether (1500 mL for 3 days, three times), $CHCl_3$ (1500 mL × 3 days × 3 times), and MeOH at room temperature (1500 mL × 3 days × 3 times). The filtrates were concentrated under reduced pressure until the elimination of $CHCl_3$ and MeOH to obtain 15.71 g and 70.13 g of crude extracts, respectively. Moreover, 75.0 g of *G. mangostana* shells were treated in the same way to be extracted with EtOH (235 ml× 3 days × 3 times) and EtOH:H_2O (7:3) (235 ml× 3 days × 3 times) to obtain 12.21 and 12.64 g of extracts, respectively.

The $CHCl_3$ and MeOH extracts of *G. mangostana* fruits were analyzed by an RP-HPLC-UV system on an Agilent 1260 Infinity system (Agilent Technologies, Palo Alto, CA, USA), equipped with a binary pump (G-1312C), and a UV detector (G-1314B). with a Phenomenex C_{18} Synergi-Hydro-RP (250 mm × 10 mm, 10 μm) column; the elution gradient was executed by using water with 0.1% formic acid as eluent A and acetonitrile with 0.1% formic acid as B at a flow rate of 2.0 mL/min. In particular, the HPLC gradient started at 5% B, after 5 min % B was at 50%, after 15 min at 80%, after 10 min at 87%. % B remained at 87% for 20 min and finally, after 10 min it reached 100% and so remained for 20 min.

In detail, the chloroform extract (injection of 2.5 mg for twenty time) of mangosteen yielded 1,7-dihydroxy-3-methoxy-2-(3-methylbut-2-enyl)-xanthen-9-one (**1**) (2.3 mg, t_R = 30.0 min), 1,3,7-trihydroxy-2,8-bis-(3-methyl-2-buten-1-yl)-9H-xanthen-9-one (**3**) (1.5 mg, t_R = 33.3 min), *α*-mangostin (**5**) (2.9 mg, t_R = 35.0

min), *β*-mangostin (**6**) (1.0 mg, t_R 49.8 min), demethylcalabaxanthone (**7**) (1.1 mg, t_R = 43.5 min), mangostanin (**8**) (3.2 mg, t_R = 47.5 min), 8-deoxygartanin (**9**) (1.1 mg, t_R = 32.0 min), garcinone D (**11**) (1.2 mg, t_R = 24.0 min), and oligandrol (**13**) (1.4 mg, t_R = 68.0 min). Moreover, 1,7-dihydroxy-3-methoxy-2-(3-methylbut-2-enyl)-xanthen-9-one (**1**) 1,3,7-trihydroxy-2,8-bis(3-methyl-2-buten-1-yl)-9H-xanthen-9-one (**3**), *α*-mangostin (**5**), demethylcalabaxanthone (**7**), mangostanin (**8**), garcinone D (**11**), and oligandrol (**13**) were isolated also from MeOH extract of *G. mangostana* arils; from this extract also *γ*-mangostin (**4**) (1.3 mg, t_R = 20.0 min) was isolated.

The $CHCl_3$ and MeOH extracts of *G. mangostana* shells were analyzed by RP-HPLC-UV. For the above mentioned extracts the same HPLC conditions applied to *G. mangostana* aril extracts were used. In this way from the chloroform extract of *G. mangostana* shells, gudraxanthone (**2**) (1.2 mg, t_R = 31.0 min), 1,3,7-trihydroxy-2,8-bis-(3-methyl-2-buten-1-yl)-9H-xanthen-9-one (**3**) (1.3 mg, t_R = 33.3 min), *γ*-mangostin (**4**) (2.0 mg, t_R = 20. min), *α*-mangostin (**5**) (5.2 mg, t_R = 35.0 min), *β*-mangostin (**6**) (2.0 mg, t_R 49.7 min), demethylcalabaxanthone (**7**) (1.6 mg, t_R = 43.8 min), mangostanin (**8**) (2.1 mg, t_R = 47.5 min), 8-deoxygartanin (**9**) (2.2 mg, t_R = 32.0 min), garcinone E (**10**) (2.1 mg, t_R = 36.0 min), garcinone D (**11**) (2.3 mg, t_R = 24.0 min), and mangostanol (**12**) (1.8 mg, t_R = 35.0 min) were isolated. Furthermore, 1,3,7-trihydroxy-2,8-bis (3-methyl-2-buten-1-yl)-9H-xanthen-9-one (**3**), *γ*-mangostin (**4**), *α*-mangostin (**5**), *β*-mangostin (**6**), mangostanin (**8**), 8-deoxygartanin (**9**), garcinone D (**11**), and mangostanol (**12**) were isolated from the MeOH extract of *G. mangostana* shells.

Sample preparation for quantitative analysis

For quantitative analysis, the extracts (15 mg), two juices, tablets, capsules, and pure compounds were dissolved in MeOH-d_4 (550 µL) containing 0.8 mg/mL

terephthalic acid [internal standard (IS)]. All the samples were used for ^{1}H NMR analysis.

For the sample preparation of crude extracts, tablets, and capsules, 15 mg were prepared in the vial before the addition of MeOH-d_4 (550 µL) and the obtained solution was transferred to an NMR tube. Juices A and B were concentrated under reduced pressure to obtain 5 mg of dried juice. The above-mentioned quantity of dried juices was prepared in a vial before the addition of MeOH-d_4 (550 µL) and the obtained solution was transferred to an NMR tube.

1D and 2D NMR experiments

NMR experiments were performed on a Bruker DRX-600 spectrometer (Bruker BioSpin GmBH, Rheinstetten, Germany) equipped with a Bruker 5 mm TCI CryoProbeat 300 K. ^{1}H NMR spectra were acquired using Bruker pulse program with the following settings: flip angle of 90° relaxation delay (d1) = 15 s, size of fid (TD) = 64k, number of scans (NS) = 64, spectral width (SW) = 14.0237 ppm, acquisition time (AQ) = 3.8928385, requested probe temperature (TE) = 298.0 K. The NMR data were processed using TOPSPIN3.2 software. The NMR tubes were labeled and immediately subjected to ^{1}H NMR measurements using a preset setting for all the samples. The analysis temperature was 24 °C.

A series of 2D-NMR experiments, including Homonuclear Correlation Spectroscopy (DQF-COSY), Heteronuclear Single-Quantum Correlation Spectroscopy (HSQC), and Heteronuclear Multiple Bond Correlation (HMBC) were acquired permitting the assignment of the existing metabolites.

NMR Data processing

The spectra were imported into the MestreNOVA 9 software. All spectra were manually corrected for phase and baseline. Spectra were referenced using the solvent signal at 3.34 as the chemical shift standard, obtaining good peak alignment. Bucketing was performed within 0.5–8 ppm region (spectral buckets of 0.004 ppm). The obtained data set was normalized.

Determination of contents

The contents of different external standards (*x*) in *G. mangostana* arils and shells were calculated by the equation as follows:

$$C_x = \frac{I_X}{I_{std}} \; x \; \frac{N_{std}}{N_X} x \frac{M_X}{M_{std}} \; x \; C_{std}$$

where I_x and I_{std} are the integrals of the selected signals of external and internal standard, respectively; N_x and N_{std} are the numbers of proton atoms of the selected signals of external and internal standard, respectively; M_x and M_{std} are the molecular weights (g/mol) of the external and internal standard; C_x and C_{std} are the concentrations (mg/mL) external and internal standard in NMR tubes, respectively.[28]

Quantitative ^1H NMR method validation

qNMR method was validated by calibration curves, precision, accuracy, repeatability, stability, limit of detection (LOD) and limit of quantitation (LOQ) assays.

The calibration curve for each compound using the ratio of the peak area of the compound and the internal standards were determined in the range of 0.05-1.0 mg/mL by subsequent dilution of the stock solutions using MeOH to evaluate the accuracy of this method at different concentrations the regressive calibration curves, limits of detection (LODs) and limits of quantitation (LOQs) (**Table 4.5**). LOD has defined as the lowest concentration of an analyte that can be detected, typically, it is evaluated at a signal-to-noise (S/N) ratio of 3, while LOQ is defined as the lowest concentration of an analyte that can be accurately and precisely quantified; it was evaluated at an S/N value of 10. Repeatability was determined by comparing results from multiple spectra acquisition of the same sample in 24 h. All samples were investigated in consecutive days for estimating the stability. The results of precision, stability, and repeatability experiments were expressed as relative standard deviation (RSD%).

Table 4.5. Quantitative data of *G. mangostana* extract. Seven-points calibration with standards **1**-**9**, **11** and **13**. Limits of detection (LODs), limits of quantification (LOQs) in mg/mL.

Compound name	R^2	Regression line	LOD	LOQ
1,7-Dihydroxy-3-methoxy-2-(3-methylbut-2-enyl)xanthen-9-one (**1**)	0.986	y = 297.34x-24.16	0.091	0.115
gudraxanthone (**2**)	0.990	y = 32.47x-9.47	0.384	0.600
1,3,7-Trihydroxy-2,8-bis(3-methyl-2-buten-1-yl)-9H-xanthen-9-one (**3**)	0.991	y = 56.52x-0.96	0.063	0.183
γ-mangostin (**4**)	0.999	y = 401.8x-2.02	0.0024	0.0198
α-mangostin (**5**)	0.999	y = 938.35-1.89	0.0028	0.0127
6-hydroxycalabaxanthone (**8**)	0.987	y = 93.72x-21.66	0.091	0.151
8-deoxygartanin (**9**)	0.999	y = 70.3x-18.80	0.310	0.410
garcinone D (**11**)	0.999	y = 219.73x+5.85	0.036	0.066
oligandrol (**13**)	0.996	y = 107.38x-4.54	0.070	0.135

References

1. M. Masullo, C. Bassarello, G. Bifulco, S. Piacente, Polyisoprenylated benzophenone derivatives from the fruits of Garcinia cambogia and their absolute configuration by quantum chemical circular dichroism calculations, *Tetrahedron*, 2010, **66**, 139-145.

2. M. Masullo, M. Menegazzi, S. Di Micco, P. Beffy, G. Bifulco, M. Dal Bosco, M. Novelli, C. Pizza, P. Masiello, S. Piacente, Direct Interaction of Garcinol and Related Polyisoprenylated Benzophenones of *Garcinia cambogia* Fruits with the Transcription Factor STAT-1 as a Likely Mechanism of Their Inhibitory Effect on Cytokine Signaling Pathways, *J. Nat. Prod*., 2014, **77**, 543-549.

3. U.M. Acuña, K. Dastmalchi, M.J. Basile, E.J. Kennelly, Quantitative high-performance liquid chromatography photo-diode array (HPLC-PDA) analysis of benzophenones and biflavonoids in eight Garcinia species, *J. Food Compos. Anal*., 2012, **25,** 215-220.

4. J. Wittenauer, S. Falk, U. Schweiggert-Weisz, R. Carle, Characterisation and quantification of xanthones from the aril and pericarp of mangosteens (*Garcinia mangostana* L.) and a mangosteen containing functional beverage by HPLC-DAD-MSn, *Food Chem*., 2012, **134,** 445-452.

5. D. Obolskiy, I. Pischel, N. Siriwatanametanon, M. Heinrich, *Garcinia mangostana* L.: A Phytochemical and Pharmacological Review, *Phytother. Res*., 2009, **23,** 1047-1065.

6. S. Di Micco, M. Masullo, A.F. Bandak, J.M. Berger, R. Riccio, S. Piacente, G. Bifulco, Garcinol and Related Polyisoprenylated Benzophenones as Topoisomerase II Inhibitors: Biochemical and Molecular Modeling Studies, *J. Nat. Prod*., 2019, **82,** 2768-2779.

7. A. Aisha, K. Abu-Salah, M. Siddiqui, Z. Ismail, A.A. Majid, Quantification of α-, β-and γ-mangostin in *Garcinia mangostana* fruit rind extracts by a reverse phase high performance liquid chromatography, *J. Med. Plants Res*., 2012, **6,** 4526-4534.

8. X. Ji, B. Avula, I.A. Khan, Quantitative and qualitative determination of six xanthones in *Garcinia mangostana* L. by LC–PDA and LC–ESI-MS, *J. Pharm. Biomed. Anal*., 2007, **43,** 1270-1276.

9. U. Sukatta, M. Takenaka, H. Ono, H. Okadome, I. Sotome, K. Nanayama, W. Thanapase, S. Isobe, Distribution of major xanthones in the pericarp, aril, and yellow gum of mangosteen (*Garcinia mangostana* linn.) fruit and their contribution to antioxidative activity, *Biosci. Biotechnol. Biochem.*, 2013, **77**, 984-987.

10. A. Chaivisuthangkura, Y. Malaikaew, A. Chaovanalikit, A. Jaratrungtawee, P. Panseeta, P. Ratananukul, S. Suksamrarn, Prenylated Xanthone Composition of *Garcinia mangostana* (Mangosteen) Fruit Hull, *Chromatographia*, 2009, **69,** 315-318.

11. S. Yodhnu, A. Sirikatitham, C. Wattanapiromsakul, Validation of LC for the determination of alpha-mangostin in mangosteen peel extract: a tool for quality assessment of *Garcinia mangostana* L, *J. Chromatogr. Sci*., 2009, **47,** 185-189.

12. M. Muchtaridi, N.A. Puteri, T. Milanda, I. Musfiroh, Validation analysis methods of α-mangostin, Y-mangostin and gartanin mixture in mangosteen (*Garcinia mangostana* L.) fruit rind extract from West Java with HPLC, *J. Appl. Pharm. Sci*., 2017, **7,** 125-130.

13. E.P. Tejamukti, W. Setyaningsih, Irnawati, B. Yasir, G. Alam, A. Rohman, Application of FTIR spectroscopy and HPLC combined with multivariate calibration for analysis of xanthones in mangosteen extracts, *Sci. Pharm*., 2020, **88,** 35.

14. A.A. Kureshi, C. Dholakiya, T. Hussain, A. Mirgal, S.P. Salvi, P.C. Barua, M. Talukdar, C. Beena, A. Kar, T.J. Zachariah, P. Kumari, T. Dhanani, R. Singh, S. Kumar, Simultaneous identification and quantification of three biologically active xanthones in Garcinia species using a rapid UHPLC-PDA method, *Acta Chromatogr*., 2020, **32,** 179-188.

15. R. Pandey, P. Chandra, B. Kumar, M. Srivastva, A.P. Anu Aravind, P.S. Shameer, K.B. Rameshkumar, Simultaneous determination of multi-class bioactive constituents for quality

assessment of Garcinia species using UHPLC-QqQLIT-MS/MS, *Ind. Crops Prod*., 2015, **77**, 861-872.

16. J. Peerapattana, K. Otsuka, M. Otsuka, Application of NIR spectroscopy for the quality control of mangosteen pericarp powder: quantitative analysis of alpha-mangostin in mangosteen pericarp powder and capsule, *J. Nat. Med*., 2013, **67,** 452-459.

17. A. Cerulli, M. Masullo, P. Montoro, J. Hosek, C. Pizza, S. Piacente, Metabolite profiling of "green" extracts of *Corylus avellana* leaves by 1H NMR spectroscopy and multivariate statistical analysis, *J. Pharm. Biomed. Anal*., 2018, **160,** 168-178.

18. E.S.C. Oliveira, F.L.D. Pontes, L.D.R. Acho, A.S. do Rosário, B.J.P. da Silva, J. de A. Bezerra, F.R. Campos, E.S. Lima, M.B. Machado, qNMR quantification of phenolic compounds in dry extract of Myrcia multiflora leaves and its antioxidant, anti-AGE, and enzymatic inhibition activities, *J. Pharm. Biomed. Anal*., 2021, **201,** 114109.

19. B. Diehl, U. Holzgrabe, Y. Monakhova, T. Schönberger, Quo Vadis qNMR, *J. Pharm. Biomed. Anal*., 2020, **177,** 112847.

20. M. Weber, C. Hellriegel, A. Rueck, J. Wuethrich, P. Jenks, Using high-performance 1H NMR (HP-qNMR) for the certification of organic reference materials under accreditation guidelines—Describing the overall process with focus on homogeneity and stability assessment, *J. Pharm. Biomed. Anal*., 2014, **93**, 102-110.

21. A. Cerulli, M. Masullo, S. Piacente, Metabolite Profiling of *Helichrysum italicum* Derived Food Supplements by 1H-NMR-Based Metabolomics, *Molecules*, 2021, **26,** 6619.

22. X. Chen, Y. Guo, Y. Hu, B. Yu, J. Qi, Quantitative analysis of highly similar salvianolic acids with 1H qNMR for quality control of traditional Chinese medicinal preparation Salvianolate Lyophilized Injection, *J. Pharm. Biomed. Anal*., 2016, **124,** 281-287.

23. J. Zhao, M. Wang, S.G. Saroja, I.A. Khan, NMR technique and methodology in botanical health product analysis and quality control, *J. Pharm. Biomed. Anal*., 2022, **207**, 114376.

24. A. Bottone, P. Montoro, M. Masullo, C. Pizza, S. Piacente, Metabolomics and antioxidant activity of the leaves of *Prunus dulcis* Mill. (Italian cvs. Toritto and Avola), *J. Pharm. Biomed. Anal*., 2018, **158,** 54-65.

25. A. Bottone, M. Masullo, P. Montoro, C. Pizza, S. Piacente, HR-LC-ESI-Orbitrap-MS based metabolite profiling of *Prunus dulcis* Mill. (Italian cultivars Toritto and Avola) husks and evaluation of antioxidant activity, *Phytochem. Anal.*, 2019, **30,** 415-423.

26. A. Bottone, P. Montoro, M. Masullo, C. Pizza, S. Piacente, Metabolite profiling and antioxidant activity of the polar fraction of Italian almonds (Toritto and Avola): Analysis of seeds, skins, and blanching water, *J. Pharm. Biomed. Anal*., 2020, **190,** 113518.

27. A. Cerulli, A. Napolitano, M. Masullo, J. Hosek, C. Pizza, S. Piacente, Chestnut shells (Italian cultivar "Marrone di Roccadaspide" PGI): Antioxidant activity and chemical investigation with in depth LC-HRMS/MSn rationalization of tannins, *Food Res. Int*., 2020, **129**, 108787.

28. J. Staneva, P. Denkova, M. Todorova, L. Evstatieva, Quantitative analysis of sesquiterpene lactones in extract of *Arnica montana* L. by 1H NMR spectroscopy, *J. Pharm. Biomed. Anal*., 2011, **54**, 94-99.

29. K. Matsumoto, Y. Akao, E. Kobayashi, K. Ohguchi, T. Ito, T. Tanaka, M. Iinuma, Y. Nozawa, Induction of Apoptosis by Xanthones from Mangosteen in Human Leukemia Cell Lines, *J. Nat. Prod*., 2003, **66**, 1124-1127.

30. H.W. Ryu, J.K. Cho, M.J. Curtis-Long, H.J. Yuk, Y.S. Kim, S. Jung, Y.S. Kim, B.W. Lee, K.H. Park, α-Glucosidase inhibition and antihyperglycemic activity of prenylated xanthones from *Garcinia mangostana*, *Phytochemistry,* 2011, **72**, 2148-2154.

31. L. Yu, M. Zhao, B. Yang, Q. Zhao, Y. Jiang, Phenolics from hull of *Garcinia mangostana* fruit and their antioxidant activities, *Food Chem*., 2007, **104**, 176-181.

32. S. Suksamrarn, O. Komutiban, P. Ratananukul, N. Chimnoi, N. Lartpornmatulee, A. Suksamrarn, Cytotoxic prenylated xanthones om the young uit of *Garcinia mangostana*. *Chem. Pharm. Bull.*, 2006, **54**, 301-305.

33. J.-W. Dong, X.-J. Li, L. Cai, J.-Y. Shi, Y.-F. Li, C. Yang, Z.-J. Li, Simultaneous determination of alkaloids dicentrine and sinomenine in Stephania epigeae by 1H NMR spectroscopy, *J. Pharm. Biomed. Anal*., 2018, **160**, 330-335.

34. E.R. Samuels, T. Wang, Quantitative 1H NMR analysis of a difficult drug substance and its exo-isomer as hydrochloride salts using alkaline deuterated methanol*, J. Pharm. Biomed. Anal*., 2020, **187**, 113338.

35. H.-A. Jung, B.-N. Su, W.J. Keller, R.G. Mehta, A.D. Kinghorn, Antioxidant Xanthones from the Pericarp of *Garcinia mangostana* (Mangosteen), *J. Agric. Food Chem*., 2006, **54**, 2077-2082.

36. K.M. Moon, C.Y. Kim, J.Y. Ma, B. Lee, Xanthone-related compounds as an anti-browning and antioxidant food additive, *Food Chem*., 2019, **274**, 345-350.

General experimental procedures

Chromatographic method

Analytical Thin-layer chromatography (TLC) in direct phase was performed with sheets of silica gel laminated on glass 60 F254 of 0.25 mm (Merck). The revelation was carried out both with UV light at 254 and 366 nm and with the following detector electrospray: saturated solution of cerium sulphate in 65% sulfuric acid, followed by heating at 120 degrees for 15 minutes.

For Molecular Exclusion Chromatography, was used a resin of Sephadex LH-20 (25-100 mm Pharmacia), eluting with MeOH a constant flow of 1.2 mL / min. The size of the column used is 100x5 cm.

HPLC separations were carried out on a Waters 590 system equipped with a Waters R401 refractive index detector, a Waters XTerra Prep MSC18 column (300 x 7.8 mm i.d.), and a Rheodyne injector.

Chemical fisics method

Nuclear magnetic resonance spectroscopy (NMR). NMR experiments were performed on a Bruker DRX-600 spectrometer (Bruker BioSpin GmBH, Rheinstetten, Germany) equipped with a Bruker 5 mm TCI CryoProbe at 300 K. All 2D-NMR spectra were acquired in MeOH-d_4 (99.95%,) and standard pulse sequences and phase cycling were used for Double Quantum Filter Homonuclear Correlation Spectroscopy (DQF-COSY), Heteronuclear Single-Quantum Correlation Spectroscopy (HSQC), and the Heteronuclear Multiple Bond Correlation (HMBC) spectra. The NMR data were processed using TOPSPIN 3.2 software. The Rotating-frame Overhauser Spectroscopy (ROESY) spectra were acquired with t_{mix} = 400 ms.

High Resolution Electrospray Ionisation Mass Spectrometry (HRESIMS).

HRESIMS spectra were carried out using a Thermo Scientific Accela HPLC system (Thermo Scientific, Germany) equipped coupled to a LTQ-Orbitrap XL mass spectrometer. operating in negative and positive ion mode. The Orbitrap mass analyzer was calibrated according to the manufacturer's directions using a mixture of caffeine, methionine-arginine-phenylalanine-alanine-acetate (MRFA), sodium dodecyl sulfate, sodium taurocholate and Ultramark 1621. Data were collected and analyzed using the software provided by the manufacturer. In full LC-ESI/LTQOrbitrap/MS experiments Total Ion Current (TIC) profile was produced by monitoring the intensity of all the ions produced and acquired in every scan during the chromatographic run. In order to get structural information, Data Dependent experiments were performed. For the data-dependent scan, the first and the second most intense ions from the HRMS scan event were selected, in order to offer their tandem mass (MS^2) product ions with a normalization collision energy at 30%, a minimum signal threshold at 250, and an isolation width at 2.0; multiple-stage tandem mass (MS^n with n = 3, 4…) experiments on selected product ions were carried out by the same collision energy.

Determination of total phenolic content

MeOH extracts have been analyzed according to the Folin-Ciocalteu (FC) colorimetric method. The extracts have been dissolved in MeOH to obtain a concentration of 0.5 mg/mL. Folin-Ciocalteu phenol reagent (0.5 mL) has been added to centrifuge tubes containing 0.5 mL of the extract. The content has been mixed, and 1 mL of a saturated sodium carbonate solution has been added to each tube, followed by adjusting the volume to 10 mL with distilled water. The content

in the tubes has been thoroughly mixed by vortex and kept at room temperature for 45 min (until the characteristic blue color developed) and then centrifuged at 3000 rpm for 5 min. Absorbance of the clear supernatant has been measured at 517 nm on a UV-visible spectrophotometer (Evolution 201, Thermo Fisher Scientific, Milan, Italy). A control without FC reagent and a blank with MeOH instead of sample have been included in the assay. The total polyphenol content has been expressed as gallic acid equivalents (GAE μmol/mg extract, means ± SD of three determinations) calculated by calibration curves ($y=0.0027x+0.0982$ $R^2 = 0.9929$).

Determination of DPPH Radical Scavenging Activity

The antiradical activity of extracts and vitamin C (positive control) has been determined using the stable 1,1-diphenyl-2-picrylhydrazyl radical ($DPPH^{\bullet}$). An aliquot (37.5μL) of the MeOH solution containing different amounts of the extract or vitamin C has been added to 1.5 mL of daily prepared $DPPH^{\bullet}$ solution (0.025 g/L in MeOH); the highest concentration employed was 75 μg/mL. An equal volume (37.5 μL) of the vehicle alone has been added to the control tubes. Absorbance at 517 nm has been measured on a UV-visible spectrophotometer (Evolution 201, Thermo Fisher Scientific, Milan, Italy) 10 min after starting the reaction. The $DPPH^{\bullet}$ concentration in the reaction medium has been calculated from a calibration curve (range = 5−36 μg/mL) analyzed by linear regression ($y = 0.2129x + 40.776$, $R_2= 0.95$). All experiments were carried out in triplicate.

Determination of TEAC Radical Scavenging Activity

The antioxidant activity of the extracts and of the isolated compounds was determined by the Trolox Equivalent Antioxidant Capacity (TEAC) assay as previously reported. The TEAC value is based on the ability of the antioxidant to

scavenge the radical cation 2,2′-azinobis(3-ethylbenzothiazoline-6-sulfonate) $ABTS^{\bullet+}$ by spectrophotometric analysis.

The extracts have been diluted with MeOH to produce solutions of 250, 500, 750, 1.00 μg/mL; the isolated compounds were diluted with MeOH to produce solutions of 0.3, 0.5, 1, and 1.5 mM. The reaction has been initiated by the addition of 1.5 mL of diluted ABTS to 15 μL of each sample solution. Determinations have been repeated three times for each extract. The inhibition percentage of absorbance at 734 nm has been calculated for each concentration relative to a blank absorbance (MeOH) and has been plotted as a function of concentration of compound or standard 6-hydroxy-2,5,7,8-tetramethylchroman-2-carboxylic acid (Trolox). The TEAC value is defined as the concentration of a standard Trolox solution with the same antioxidant capacity as a 1 mg/mL of the tested extract.

Conclusion

This project has been addressed to the definition of the chemical profile of selected food products (*P. oleracea, R. sativus* var longipinnatus*, A. esculentus* and *G. mangostana)* used in typical cuisine and traditional medicine of different regions of the World. The interesting aim is to diffuse the culinary use in the everyday diet of these products characterized by benefits in disease prevention. Some of these foods are employed in nutraceutical products with large diffusion. In the field of marketing claims, the correlation of the presence of phytochemicals with healthy benefits between food and industrial products is necessary to satisfy the correct information of customers. Moreover, this work highlights the phytochemicals contained in selected foods are responsible for properties attributed to the plants as "healthy food".

The phytochemical investigation of *P. oleracea* allowed us to characterize in detail the profile of beneficial polar lipids, not typical in leafy plants and related biological activities but also to define polyphenolic alkaloids, known in literature as oleraceins but never reported with clear biological activity before.

A detailed characterization of the lipids occurring in portulaca was performed by multi-stage LC-ESI/LTQOrbitrap/MS analysis showing a wide range of compounds from oxylipins and phospholipids to sphingolipids, and glycolipids. The lipid enriched fractions were tested by *in vitro* gene reporter assay highlighting interesting activity against three different biological targets Nrf2, PPAR-ɣ and NF-kB.

The polyphenolic alkaloids were isolated and characterized by 1D and 2D NMR experiments, 4 molecules were tentatively defined for the first time by multi-stage LC-ESI/LTQOrbitrap/MS analysis along with the NMR unambiguously elucidation of 7 known compounds reported in portulaca harvested in Asiatic regions, confirming this class of molecules as chemical markers of the specie. The

oleracein enriched fractions displayed the ability to prevent oxidative damages induced by radicals $DPPH^{\cdot}$ and $ABTS^{+\cdot}$. Moreover, *in vitro* assay confirmed a good tolerace of the chemical class and the activity against Nrf2.

With the aim to achieve deeper insight into the chemical composition of *Raphanus sativus* L. the phytochemical investigation of the sprouts has been carried out; the phenolic compounds isolated were described by 1D and 2D NMR experiments. Moreover, the ability of several extracts to activate Nrf2 pathway has been investigated. Finally, the correlation between the chemicals contained in the extracts and the biological activity was evaluated by multivariate analysis.

The overmentioned biological tests for the screening of obtained extracts and selective metabolite containing fractions against several targets were performed during the Ph.D. stage at the University of Vienna in the Division of Pharmacognosy of the department of Pharmaceutical Sciences.

Preliminary tests to evaluate the ability of *A. esculentus* extracts to inhibit reactive radicals $DPPH^{\cdot}$ and $ABTS^{+}$ along with the *in situ* inhibition of intestinal α-glucosidase have been carried out. To explain the strong antioxidant activity of the green extract of *A. esculentus* fruit, its metabolite profile by LC-ESI/LTQOrbitrap/MS/MS^n was carried out. LC-MS led to the identification of a wide range of compounds belonging to different chemical classes such as flavonoids, p-hydroxycinnamic acid derivatives and benzoyl acid derivatives. All the phenolic compounds described in the LC-HRMS profile were isolated and characterized by NMR.

The quantitative Nuclear Magnetic Resonance (qNMR) analysis, a rapid and accurate method used for simultaneous quantification of plant metabolites, was here employed to determine the amount of bioactive xanthones in the extracts of *G. mangostana* arils and shells obtained by using solvent of increasing polarity along with "eco-friendly" solvents like ethanol and ethanol/water. The content of xanthones was compared with that occurring in four selected commercial food

supplements, among which tablets and capsules, and two fruit juices, based on mangosteen. Quantitative results highlighted a great variability: the extracts of the shells displayed a higher amount of bioactive xanthones than those of the arils, in particular, of γ-mangostin and α-mangostin, while β-mangostin, demethylcalabaxanthone, mangostanin, 8-deoxygartanin occurred in higher amounts in arils. Regarding commercial food supplements, a certain variability in the amount of biologically active xanthones (i.e. α-mangostin and ɣ-mangostin) could be observed.

The obtained results can be useful to enhance the use of selected food products that represent a large business in the globalized market, to protect the reputation of the regional foods and to promote rural and agricultural activity. Moreover, this work highlights that often only MS information is not sufficient to determine the complete profile of plant constituents and reinforces the notion that the combination of LC-MS and NMR analysis is a powerful tool to achieve the truly chemical structure of naturally occurring molecules in food plants.

Publication list

Gilda D'Urso, Assunta Napolitano, Ciro Cannavacciuolo, Milena Masullo, Sonia Piacente. Okra fruit: LC ESI/LTQOrbitrap/MS/MSn based deep insight on polar lipids and specialized metabolites with evaluation of anti-oxidant and antihyperglycemic activity. Food & Function (2020) 11, (9), 7856-7865.

Ciro Cannavacciuolo, Assunta Napolitano, Helke Heiss, Verena M. Dirsch, Sonia Piacente. Portulaca oleracea, a rich source of polar lipids: chemical profile by LC-ESI/LTQOrbitrap/MS/MSn and in vitro preliminary anti-inflammatory activity. Submitted.

Milena Masullo, Antonietta Cerulli, Ciro Cannavacciuolo, Hilal Kılınç, Cosimo Pizza and Sonia Piacente. Garcinia mangostana L. fruits and derived food supplements: identification and quantitative determination of bioactive xanthones by NMR analysis. Submitted.

Ciro Cannavacciuolo, Assunta Napolitano, Milena Masullo, Sonia Piacente. Analysis by high-resolution mass spectrometry of the polyphenolic alkaloids fraction from *Portulaca oleracea* L. Submitted

Ciro Cannavacciuolo, Antonietta Cerulli, Milena Masullo, Sonia Piacente. Daikon (*Raphanus sativus*) sprouts polar extracts: LC-ESI/LTQOrbitrap/MS/MS profile, isolation of hydroxycinnamic acid derivatives glycoside esters and preliminary antioxidant activity. Submitted